

PERFORMANCE AND DESIGN OF STEEL PIPE PILE TO CONCRETE CAP
CONNECTIONS SUBJECT TO SEISMIC OR
HIGH TRANSVERSE LOADING

by

Lenci Robert Kappes

A dissertation submitted in partial fulfillment
of the requirements for the degree

of

Doctor of Philosophy

in

Civil Engineering

MONTANA STATE UNIVERSITY
Bozeman, Montana

June, 2016

ProQuest Number: 10146332

All rights reserved

INFORMATION TO ALL USERS

The quality of this reproduction is dependent upon the quality of the copy submitted.

In the unlikely event that the author did not send a complete manuscript and there are missing pages, these will be noted. Also, if material had to be removed, a note will indicate the deletion.



ProQuest 10146332

Published by ProQuest LLC (2016). Copyright of the Dissertation is held by the Author.

All rights reserved.

This work is protected against unauthorized copying under Title 17, United States Code
Microform Edition © ProQuest LLC.

ProQuest LLC.
789 East Eisenhower Parkway
P.O. Box 1346
Ann Arbor, MI 48106 - 1346

©COPYRIGHT

by

Lenci Robert Kappes

2016

All Rights Reserved

ACKNOWLEDGEMENTS

I would like to express sincere gratitude and many thanks to my advisor, mentor, and friend, Dr. Michael Berry, who directed me in my research and course work at Montana State University. Mike has helped me grow as both a person, and as an engineer, and I will be forever thankful for his support. Similarly, the guidance provided by Dr. Jerry Stephens, whose sound judgement, voice of reason, and passion for engineering was welcomed and appreciated at every turn. I would also like to extend recognition to the other members of my committee, Dr. Ed Adams, and Dr. Ladean McKittrick, for their continued contribution to my studies.

An additional note of gratitude goes to the Montana Department of Transportation for making this research possible. I am very thankful for the opportunity to study such a fascinating engineering topic, and appreciate the knowledgeable and ambitious technical panel members that we have had the pleasure to work with on this project.

Finally, I would like to acknowledge all of my family and friends that have been such a big part of my life, studies, work, and success; especially my wife, Bethany, and Westie, Willa.

TABLE OF CONTENTS

1. INTRODUCTION TO DISSERTATION	1
Background	1
Dissertation Overview	4
References	7
2. CONCRETE FILLED STEEL TUBE PILES TO CONCRETE PILE-CAP CONNECTIONS	8
Contribution of Authors and Co-Authors	8
Manuscript Information Page	9
Abstract	10
Introduction	11
Experimental Design	13
Experimental Results	18
Discussion of Results	21
Summary and Conclusions	23
Acknowledgements	24
References	25
3. SEISMIC PERFORMANCE OF CONCRETE FILLED STEEL TUBE TO CONCRETE PILE-CAP CONNECTIONS	26
Contribution of Authors and Co-Authors	26
Manuscript Information Page	27
Abstract	28
Introduction	28
Phase I Research	33
Phase II Research	36
Experimental Program	36
Test Setup and Instrumentation	40
Loading Schemes	43
Results	44
Discussion of Results	51
Cyclic Test Series	57
Proposed Design Methodology	60
Determining Plastic-Moment Capacity of CFT	60
Embedment Length	61
U-Bar Size and Configuration	64
Transverse Reinforcement	64
Discussion	65

TABLE OF CONTENTS – CONTINUED

Summary and Conclusions	66
Acknowledgements	68
References	69
4. ANALYSIS METHODOLOGY FOR CONCRETE-FILLED STEEL PIPE PILES TO CONCRETE CAP CONNECTIONS	71
Contribution of Authors and Co-Authors	71
Manuscript Information Page	72
Abstract	73
Introduction	73
Proposed Analysis Methodology	77
Compatibility Relationships	78
Constitutive Relationships	80
Forces and Equilibrium	82
Radial Concrete and Friction Forces	83
U-Bar Reinforcement Forces	86
Interface Shear Force	87
Equilibrium	88
Calibration and Evaluation of Proposed Methodology	89
Experimental Dataset	89
Application of Modeling Strategy to Dataset and Parameter Calibration	92
Application to VT2	93
Summary and Conclusions	97
References	100
REFERENCES CITED	104
APPENDIX A: Performance of Steel Pipe Pile-To-Concrete Bent Cap Connections Subject to Seismic or High Transverse Loading: Phase II	107

LIST OF TABLES

Table	Page
1. Experimental Parameters and Material Properties.....	16
2. Experimental Parameters and Material Properties.....	18
3. Test Results.....	19
4. Phase I experimental parameters and material properties.....	34
5. Phase II experimental parameters and material properties	38
6. Summary of test results.....	45
7. MSU testing summary of pile-to-pile cap connections.....	94
8. Measured and predicted ultimate capacities	95

LIST OF FIGURES

Figure	Page
1. Typical concrete-filled steel pile and concrete pile cap bridge substructure support system (Kappes, 2012)	1
2. Typical bridge bent with reinforcing steel	3
3. MDT Bridge Support System under Lateral Load.....	13
4. Test Frame with Pile Cap Specimen	14
5. Typical Pile Cap Reinforcing Cage	16
6. Typical Failure Mechanism seen in PC-1 through PC-3a	20
7. Force-Drift Response for PC-2	20
8. Force-Drift Response for VT1	22
9. Typical bridge bent	30
10. Subsection of bent tested in this research	30
11. Typical failure mechanism observed in Phase I effort.....	35
12. Reinforcing cage from Phase I PC4.....	35
13. Typical reinforcing cage	38
14. Typical connection detail.....	38
15. U-bar configuration: (a) CT1 U-bar configuration; (b) CT2 U-bar configuration	40
16. Test setup	41
17. Cyclic-loading history for CT1 and CT2	44
18. Force-deflection responses of test specimens: (a) VT1; (b) VT2; (c)VT2.5; (d) VT3; (e) CT1; (f) CT2.....	46

LIST OF FIGURES - CONTINUED

Figure	Page
19. VT1 test: (a) at maximum drift; (b) plastic-hinge region	50
20. Typical cap at failure	51
21. Pushover moment-drift responses: (a) VT1; (b) VT2; (c) VT2.5; (d) VT3... ..	53
22. Response comparison between VT2 and CT1	58
23. Cyclic envelopes	59
24. Simplified mechanics in pile cap	62
25. Typical bridge bent with U-bar reinforcing steel.....	76
26. Imposed rotation and resultant internal stresses	78
27. Pile rotation, displacements, and radial strain distribution	80
28. Assumed concrete material model (Mander et al., 1988)	81
29. Assumed stress-strain response of U-bar.....	82
30. Effective areas and dimensions.....	84
31. Internal force components.....	86
32. External loads and assumed inflection point	89
33. CFT piles and concrete pile cap.....	90
34. Typical test specimen.....	91
35. 3D representation of internal forces in VT2 at Moment = 145ft-kip.....	95
36. Summary of forces at each layer along embedment depth at various applied moments – VT2	97

ABSTRACT

This research investigated the seismic behavior of the connection between concrete-filled steel tube (CFT) piles and concrete pile caps. This connection is an important component of an accelerated bridge construction technique, which involves driving steel piles to a finished elevation just below the design deck level, forming a pile cap around the ends of the driven piles, reinforcing this cap, and then filling the piles and the cap formwork with concrete. This cap then serves as the support for the superstructure of the bridge. Conventional configurations of the CFT to pile cap connection often involve congested and complex reinforcing schemes, which can limit the use of this bridge support system. The research discussed herein evaluated the performance of a new detailing scheme that significantly reduces congestion and construction issues, and developed a mechanics-based analysis tool to predict load carrying capacity of this type of connection. This new reinforcing scheme uses U-shaped reinforcing bars to encircle the tip of the embedded CFT pile within the cap, which act to confine the concrete immediately around the pile and transfer the loads throughout the cap.

In this research, six connection specimens with various details were tested under lateral loads until failure while monitoring applied loads and lateral displacements. As intended, five specimens experienced failure in the concrete cap, with the remaining specimen failing through plastic hinging in the CFT at the face of the cap. The focus of this test program was on characterizing the failure behavior of the concrete cap; typically, this behavior was observed to consist of crushing of the concrete adjacent to the pile near the face of the cap and at the tip of embedment, followed by yielding of the longitudinal reinforcement, and concluding with yielding of the transverse reinforcement and the formation of diagonal cracks extending from the embedded pile to the edge of the cap. Based on the results of this and a previous investigation, an analysis methodology (similar to moment-curvature analysis) was developed and evaluated. This methodology proved to be an effective means for predicting the ultimate capacity of CFT to concrete pile cap connections.

CHAPTER ONE - INTRODUCTION TO DISSERTATION

Background

A series of concrete-filled steel pipe piles embedded in a concrete pile cap can be a desirable solution for supporting small to medium-span bridges. This system is fast and efficient to construct and, with proper design, improves the ductile response and overall strength of the structure. A typical bent constructed using this system is shown in Figure 1, which in this case specifically consists of seven concrete-filled steel piles joined by a concrete pile cap.



Figure 1. Typical concrete-filled steel pile and concrete pile cap bridge substructure support system (Kappes, 2012)

The structural benefits of a concrete-filled steel tube (CFT) are well known. In the case of the concrete-filled steel pile, the flexural capacity and ductility of the steel tube when subjected to lateral loads (e.g., during a seismic event) is enhanced by the concrete. The concrete inside the tube not only adds stiffness and strength to the cross section, it also delays the onset of buckling of the steel tube. Further, the compression strength of the concrete is also enhanced by the confinement provided by the steel tube. The basic ductility provided by the steel tube may be very beneficial to the overall response of the structure if sufficient strength is provided by the concrete pile cap, to ensure the formation of a plastic hinge in the CFT. This failure mechanism is preferable to failure of the concrete cap, due to its enhanced energy-dissipating characteristics (i.e. more robust hysteresis response under lateral loads). Thus, proper design of the cap and, notably the connection to the CFT, is essential to ensure the design loads can be carried by these elements without failure.

While a significant amount of research has been focused on the structural performance of CFTs, fewer projects have focused on the details of their connection to reinforced concrete elements, i.e. pile caps; thus, the need for more research in this area. Furthermore, many of the CFT to pile cap connection details currently used in practice are extremely congested and difficult to construct, and their performance, specifically during seismic events, may be somewhat uncertain. In an attempt to expand the state of practice, research was conducted on this connection at Montana State University (MSU) several years ago under the sponsorship of the Montana Department of Transportation (MDT). Data collected during this effort was subsequently used by MDT to formulate a

design guide for their typical concrete-filled steel pipe-to-pile cap connections (Stephens & McKittrick, 2005). The basic connection configuration used by MDT is shown in Figure 2.

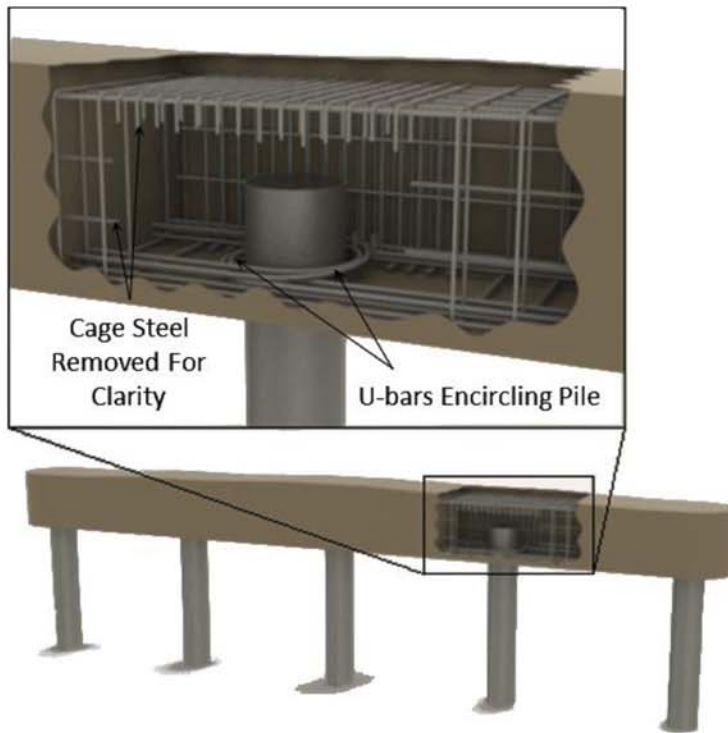


Figure 2. Typical bridge bent with reinforcing steel

Based on engineering principles and the results of the various physical tests completed by Stephens and McKittrick (2005) at MSU, the reinforcing configurations used in the MDT design guide were not specifically tested, which made it imperative to further examine typical connections produced following this design guide, to verify their performance. The additional suite of laboratory testing is described in its entirety in the final report entitled: *Performance of Steel Pipe Pile-to-Concrete Pile Cap Connections Subject to Seismic or High Transverse Loading: Phase III Confirmation of Connection*

Performance (Kappes, Berry, & Stephens, 2013), published through MDT and reproduced in Appendix A of this dissertation.

Dissertation Overview

The testing completed through this recent study, coupled with further analysis of the earlier test program, is the basis for this dissertation, in which the fundamental behaviors of pile-to-pile cap connections are further clarified and a refined design algorithm is developed that effectively specifies an efficient reinforcing scheme for the concrete cap, ensuring that the structural system performs desirably under high lateral loads.

Chapter Two provides an overview of the suite of nine CFT to concrete pile-cap connections tested at MSU to evaluate their performance under seismic loads; five tests were conducted by Stephens and McKittrick (2005), and four further monotonic tests were conducted by Kappes and his colleagues. Variables differing between tests included concrete and pile strength, embedment depth, and reinforcing configuration. The specimens were loaded with a constant axial load, and were subjected to monotonically increasing lateral load until failure. The specimens were then cycled to determine their post-peak energy dissipation characteristics. A general review of the test results reveals the importance of a) embedment depth and b) reinforcing scheme – notably, use of U-shaped reinforcing bars encircling the embedded pile (see Figure 2) – on connection capacity and behavior. Additionally, two follow-up tests evaluating the cyclic loading response of the connection are outlined. (Note, as previously commented, the total of six laboratory tests conducted by Kappes, et al. as part of this dissertation

research are described and discussed in detail in the technical report presented in Appendix A of this document.)

Chapter Three offers a more detailed description and discussion of the progressive failure states observed during the connection tests, including the results of the cyclic tests completed by Kappes, et al. Four key limit states are identified: (1) formation of a plastic hinge in the CFT, (2) interior and exterior crushing of the concrete in the cap, (3) yielding of the longitudinal reinforcement in the cap, and (4) splitting of the concrete cap. The focus of this work is on the latter three limit states, which result in loss of fixity of the connection, resulting in reduced energy dissipation. A preliminary design guide for the connection is developed that determines the required embedment length, as well as the necessary U-bar size and configuration, so that these connections will not fail due to premature damage of the concrete caps.

Building on all of the previous information and analyses, an innovative mechanics based model of the connection behavior was developed, and it is presented in Chapter 4. This model employs a multi-dimensional moment-rotation approach to determine the internal force distribution on the connection elements, utilizing nonlinear material models to estimate the ultimate capacity of the connection. The model resembles classical moment curvature analyses, using the principles of equilibrium of internal and external forces, compatibility between deformations and strain, and constitutive relationships representing the unique material behaviors, to analytically replicate connection behavior and predict ultimate capacity. This methodology was found to well represent the results of all the physical models tested to-date, and an algorithm was developed for its use as a

design tool. In light of its development using well established principles of mechanics, it is expected to offer robust design solutions within and beyond connections physically tested thus far.

While this dissertation presents considerable work moving forward the design of concrete pile cap to steel pile connections, remaining work may include exercising the algorithm with more tests consisting of embedded piles in concrete caps, and investigating the relationship between the strain function and the physical rotation of the test specimens. This research is expected to lead to calibration of the behavior for a single layer of confined concrete in the cap connection region, accounting for specific connection details, to be modeled by a single non-linear spring. This would provide for a series of calibrated nonlinear springs to represent the strength provided by the interaction of components in the connection region, analogous to p-y springs for modeling soil in L-Pile. Additionally, utilizing the backbone curve of the moment-rotation response for the algorithm presented herein, it may be useful to investigate the connection represented by a nonlinear torsional spring for a system-level, seismic bridge analysis. Finally, an examination of connections with lateral forces, transverse to the cap (bridge longitudinal direction), caused by thermal effects or seismic demands, would benefit from the output of the moment-rotation analysis presented in this research for the subject connection.

References

- Kappes, B. *Photo of Pryor Creek Intermediate Bent*. Montana Department of Transportation, Huntley, MT.
- Kappes, L., Berry, M., & Stephens, J. (2013). *Performance of Steel Pipe Pile-to-Concrete Pile Cap Connections Subject to Seismic or High Transverse Loading: Phase III Confirmation of Connection Performance*. Helena: Montana Department of Transportation.
- Stephens, J., & McKittrick, L. R. (2005). *Performance of Steel Pipe Pile-To-Concrete Bent Cap Connections Subject to Seismic or High Transverse Loading: Phase II*. Bozeman: Civil Engineering Department, Montana State University.

CHAPTER TWO - CONCRETE FILLED STEEL TUBE PILES TO CONCRETE PILE-
CAP CONNECTIONS

Contribution of Authors and Co-Authors

Manuscript in Chapter 2

Author: Lenci Kappes

Contributions: Designed and built laboratory test specimens. Conducted load testing of model pile-to-pile cap connections, including the collection and analysis of test data. Wrote the first draft of the manuscript.

Co-Author: Dr. Michael Berry

Contributions: Assisted in concept development for the laboratory test series. Provided technical expertise on data analysis. Provided feedback on early drafts of the manuscript.

Co-Author: Dr. Jerry Stephens

Contributions: Assisted in concept development for the laboratory test series. Provided technical expertise on data analysis. Provided feedback on early drafts of the manuscript.

Co-Author: Dr. Ladean McKittrick

Contributions: Assisted in concept development for the laboratory test series. Provided technical expertise on data analysis. Provided feedback on early drafts of the manuscript.

Manuscript Information Page

Lenci Kappes, Michael Berry, Jerry Stephens, Ladean
McKittrick Structures Congress 2012

Status of Manuscript:

Prepared for submission to a peer-reviewed journal

Officially submitted to a peer-review journal

Accepted by a peer-reviewed journal

Published in a peer-reviewed journal

Published by American Society Of Civil Engineers
Structures Congress 2012: pp. 581-590

Abstract

This paper describes preliminary findings from a Montana Department of Transportation (MDT) funded project focused on testing the seismic performance of concrete filled steel tube (CFT) pile to concrete pile-cap connections. These connections are common/critical components of the support structure for highway bridges in Montana and across the country, and it is essential for these connections to perform well during seismic events. Despite their widespread use, the design and expected performance of these connections are not necessarily well understood. The preferred failure mechanism for this connection is for the pile cap to possess sufficient capacity to force the connection failure into the more ductile CFT piles. Traditional design methods for this connection often lead to congested and complex reinforcing schemes, and this complexity can obscure the true behavior/effectiveness of the elements within the connection. In this research effort, nine half-scale connections were tested under a monotonic pushover load until failure. The piles were then cycled through several load reversals. As a result of this research effort, a new reinforcing scheme was developed that greatly simplifies the design and construction of the connection while increasing the capacity of the cap. This newly developed reinforcing scheme includes U-shaped reinforcing bars that encircle the embedded CFT piles within the cap that counteract the moment related demands introduced by the embedded pile.

In particular, this paper presents the details and results of the nine specimens tested during this research effort. Data collected during these tests includes load, deformations, and strains. The structural efficiency of the newly developed reinforcing

scheme is discussed and contrasted with conventional reinforcing schemes. Additionally, future directions of this research effort are presented.

Introduction

The advantages of using concrete filled steel tubes (CFTs) in structural applications are numerous. CFTs are very efficient, and offer large capacities and increased ductility over typical reinforced concrete elements. With respect to efficiency, the steel tubes act as the formwork for the concrete and eliminates the need for traditional reinforcing steel, accelerating construction time and reducing material costs. In regards to structural advantages of CFTs, the steel pipe acts to confine the concrete fill, which subsequently increases the ultimate capacity and ductility of the concrete. The confined concrete, in turn, acts to increase the overall stiffness and flexural capacity of the CFT, and restrain buckling of the steel pipe walls. Despite these obvious advantages, the use of CFTs is often limited due to the inherent difficulty of connecting them to other structural elements. This issue has been the focus of several recent research efforts (Roeder & Lehman, 2008; Kingsley, Williams, Lehman, & Roeder, 2005; Silva & Seible, 2001), and is the primary focus of the research presented herein. In particular, this research focuses on improving a CFT-pile to concrete pile-cap connection commonly used by the Montana Department of Transportation (MDT), and developing a design methodology for such connections.

A common bridge support system used by MDT consists of a linear array of concrete filled steel pipe piles connected at the top by a concrete pile cap (Figure 3). This bridge support system is popular because of its low initial cost, short construction time,

low maintenance requirements, and long service life. To simplify construction and maintain a positive connection between the CFT piles and the pile cap, the CFT piles are typically extended up into the reinforced concrete cap. Conventional structural design methodologies, however, do not explicitly address the situation of a large rigid CFT element embedded in a conventionally reinforced concrete structure. While these methodologies can confidently be extended to predict the capacity of such a connection to carry in-service gravity loads, the direction to follow in determining the capacity of such a connection under extreme lateral loads (say, of seismic origin) is much less clear. Therefore, MDT initiated a research project to investigate the behavior of the CFT to pile-cap connection under lateral loads. This investigation consisted of a combination of experimental and analytical work. This paper presents the results of the experimental work, which consisted of laterally loading nine models of a typical connection to failure. The primary objective of these tests was to generally characterize the behavior of the connection and to assist in validating the performance of analytical model of this behavior.

This paper first presents the experimental design used for these tests (e.g., model dimensions, steel configurations, loading scheme), and then proceeds to present the results from these tests. The then concludes with a discussion of results and conclusions, and provides suggestions for future work.

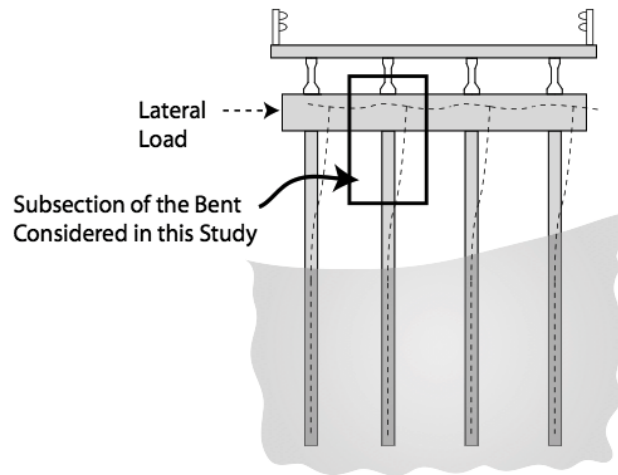


Figure 3. MDT Bridge Support System under Lateral Load

Experimental Design

The test specimens used in this study were approximately half-size models of a subsection of a typical bridge bent constructed with CFT piles joined by a reinforced concrete pile cap. The models were designed to represent an interior section of such a bent, centerline-to-centerline between pile supports (see Figure 3). Thus, each model consisted of a single pile and an attendant length of pile cap. The CFT pile-to-pile cap connections were tested so as to generate the deflected shape expected in this subsection of a full-size bent subjected to a lateral load, as shown in Figure 3. The frame used to test the models is shown in Figure 4. Note that for convenience, the model was tested in the horizontal plane, rather than in the vertical plane of an actual bridge.

Each model was subjected to a slowly increasing lateral load applied to the tip of the pile, while the pile cap was held stationary. Coincident with the lateral load, a constant axial force was applied to represent gravity load effects. While some preliminary tests were conducted on the models at elastic load levels, in the primary load

event for each model, the lateral load was monotonically increased until the lateral capacity of the connection was achieved. In some cases, the model was subsequently subjected to reversed load cycles, to assess the residual strength and energy dissipation characteristics of the connection. During each test, the load and displacement response of the connection was measured and recorded. Measurements were also made of the strains in the CFT pile and in the cap concrete. In selected tests, strains in various bars in the reinforcing cage were also measured.

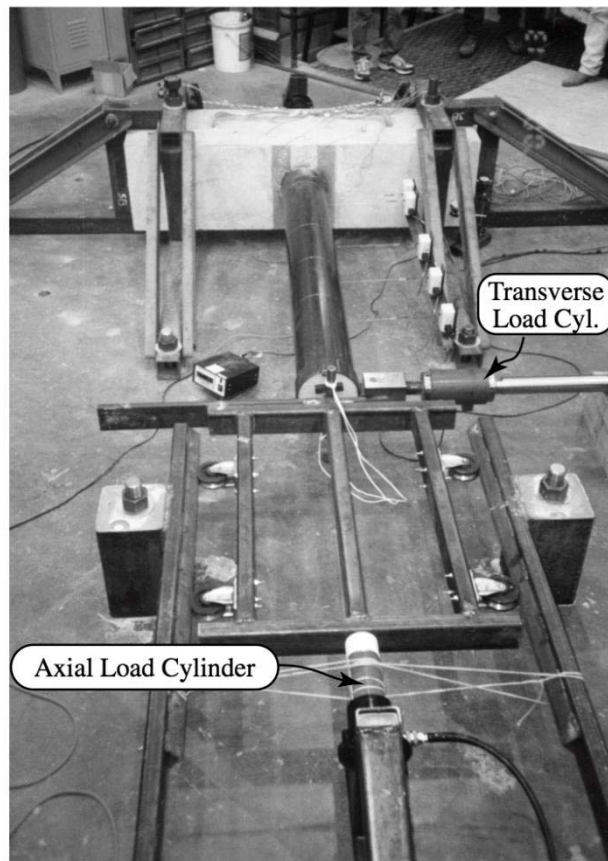


Figure 4. Test Frame with Pile Cap Specimen

This research effort consisted of two phases. The first phase (Stephens & McKittrick, 2005) consisted of a total of five tests, and the second phase (Kappes, 2012)

tested four additional connections. In the first phase, the baseline configuration of the models was intended to represent a typical connection configuration used by MDT prior to this research effort. All specimens in this effort used the same basic reinforcing scheme (Figure 5) in the pile cap. The intended variable between the tests was the specific amount and placement of this reinforcement in the pile cap, although in the final program the strength of the steel pipe pile and of the concrete also varied in some tests. Table 1 provides the experimental parameters and material properties for this initial phase of testing. In this table, the longitudinal steel ratio was calculated for a cross section extending from the bottom face of the cap (pile side) to the embedded tip of the CFT pile. This parameter was defined in this manner because the embedded pile would impose localized load demands in this region, and, therefore, the amount of longitudinal steel in this region is an important parameter. The transverse steel ratio was calculated as the area of two legs of the transverse stirrups divided by an area of concrete with a width of the transverse steel spacing and a height equal to the height of the cap. As the project advanced, the configuration of each successive model was adjusted based on the results of the preceding test. In general, the amount of reinforcement in the cap was increased in each test, starting with a model depicting current practice, up to a model with 7 times the original amount of longitudinal and transverse reinforcing steel. In addition to the amount of reinforcement increasing with each test, the configuration of the reinforcing steel also varied, with the final test using a combination of spirals and u-shaped bars to confine the embedded pile.

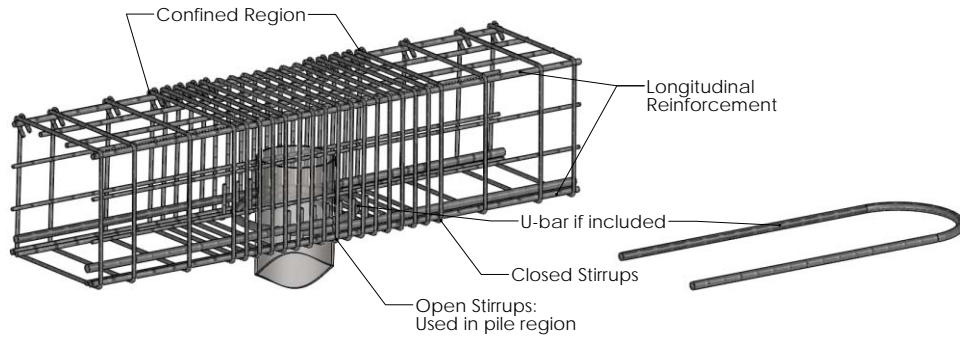


Figure 5. Typical Pile Cap Reinforcing Cage

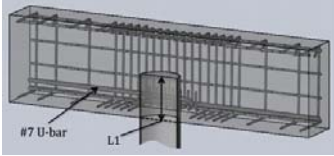
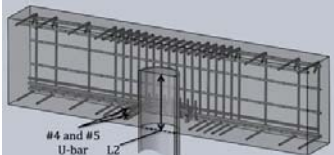
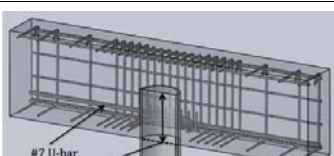
Table 1. Experimental Parameters and Material Properties

Test	Pile Wall Thickness, (mm)	Embedment Length, (mm)	Long Steel (%)	Trans Steel (%)	Concrete Strength, (MPa)	Reinforcement Layout
PC1	8.1	228.6	0.41	0.09	33.3	
PC2	6.35	228.6	0.41	0.09	36.7	
PC3	6.35	228.6	1.09	0.41	21.7	
PC3a	6.35	228.6	2.11	0.65	27.2	
PC4	6.35	228.6	2.83	0.70	32.2	

The second phase of testing consisted of a total of four specimen tests. In this phase of testing, the amount and configuration of the reinforcing steel was investigated further.

Table 2 provides the experimental parameters and material properties for this phase of testing. In general, in this phase of testing, the amount of longitudinal reinforcement was reduced and the reinforcing configuration was changed from the final layout used in the in the previous phase of tests (PC-4). That is, this test series used significantly less longitudinal reinforcing steel, and incorporated u-shaped reinforcing bars and no spiral reinforcing directly around the embedded pile. The remaining tests in this series varied the longitudinal reinforcement slightly, with the primary difference between tests in this series being the embedment depth. Also, it should be noted that VT2, VT2.5, and VT3 used CFT piles with wall thicknesses significantly larger than those used in the previous tests. It was decided to use an oversized pile in these tests to ensure that the ultimate capacity of the cap could be attained, although in practice a smaller CFT pile would be used. The oversized pile essentially became part of the testing apparatus, with the test focus being on the performance of the cap.

Table 2. Experimental Parameters and Material Properties

Test	Pile Wall Thickness (mm)	Embedment Length (mm)	Long Steel (%)	Trans Steel (%)	Concrete Strength (MPa)	Reinforcement Layout
VT1	6.35	L1 = 228.6	1.5	0.70	43.1	
VT2	12.7	L2 = 298.5	1.38	0.70	26.2	
VT2.5	12.7	L1 = 228.6	1.5	0.70	43.1	
VT3	12.7	L3 = 263.5	1.5	0.70	28.3	

Experimental Results

The CFT to pile cap connections described in the previous section were all loaded with a monotonically increasing lateral load until failure, and then in some cases cycled to evaluate the post-peak energy dissipation characteristics of the specimen.

Table 3 summarizes the results from both testing phases, including the observed failure mechanism and maximum moment observed in each test.

Table 3. Test Results

Test	Failure Mechanism	Maximum Moment (kN-m)
PC-1	cracking of concrete cap	111
PC-2	cracking of concrete cap	100
PC-3	cracking of concrete cap	106
PC-3a	cracking of concrete cap	137
PC-4	plastic hinge in CFT Pile	164
VT1	plastic hinge in CFT Pile	148
VT2	cracking of concrete cap	224
VT2.5	cracking of concrete cap	180
VT3	cracking of concrete cap	199

In the first phase of testing, all of the specimens, with the exception of PC-4, failed due to crushing of the pile cap directly behind the pile and the formation of large cracks apparently along two compression struts (Figure 6) extending outward from the pile (in the direction of the applied load) to the faces of the cap. A typical pinched force/drift response from these initial tests is shown in Figure 7. As can be seen in this figure, the initial push until failure exhibits a somewhat ductile response. That is, a significant amount of lateral deformation is observed after initial yielding and before failure. However, the cyclic response beyond this initial failure is considerably pinched and degraded. Therefore, as previously mentioned, this failure mechanism should be avoided. As can be seen in Table 1 and Table 3, the capacity of the caps generally increased with increasing amounts of longitudinal and transverse reinforcing steel. Of these specimens, PC-4 was the only to achieve the desired failure mechanism (the formation of a plastic hinge in the CFT pile).



Figure 6. Typical Failure Mechanism seen in PC-1 through PC-3a

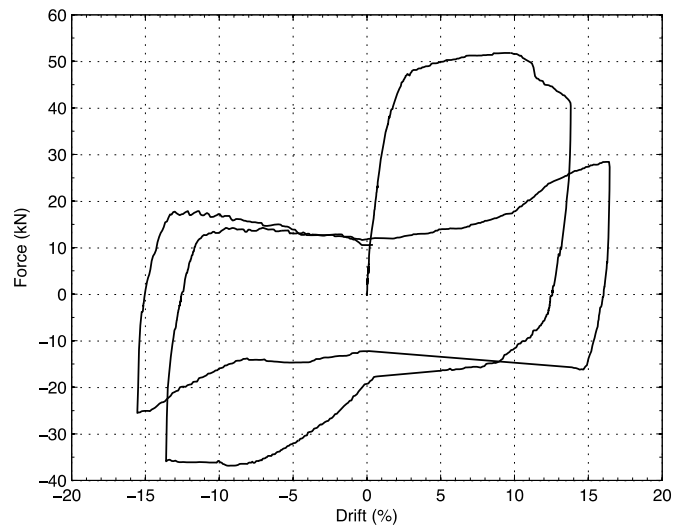


Figure 7. Force-Drift Response for PC-2

In regards to the second test series, a plastic hinge formed in the first test in this series (VT1) prior to the cap failing. The force/drift response for this specimen is provided in Figure 8. In contrast to the pinched response in Figure 7, this response is significantly more robust. After VT1, as explained previously, the CFT pile wall

thickness was increased in the remaining cap tests to ensure that the actual cap capacity could be attained, although a smaller pile wall thickness would actually be used in practice. An identical configuration to VT1 was also tested with this oversized pile (VT2.5) to attain the actual cap capacity of this configuration. As expected, the remaining test specimens in this series ultimately failed in a manner very similar to the failures in the initial test series: crushing of the concrete and the formation of two large cracks along two compression struts. However, these caps had significantly higher capacities than those from the original test series. Another observation can be made from this second phase of tests regarding the effect of embedment depth; generally speaking, as the embedment depth increased the capacities of the caps also increased.

Discussion of Results

In the original test series, the cap capacities increased with increasing reinforcing steel for all five test specimens. Only one specimen from the original test series was able to provide enough cap capacity to achieve the desired failure mechanism of a plastic hinge in the CFT pile. This was achieved by including a significantly congested reinforcing scheme that included a large amount of longitudinal and transverse reinforcement (7 times that of the original specimen), and spirals and u-shaped bars around embedded pile. Although this specimen was able to achieve the desired capacity, the actual ultimate capacity of this heavily reinforced cap and the attendant absolute effect of the reinforcing scheme on cap capacity could not be determined, as the pile failed before the cap capacity was reached. The second test series in this research was

intended to investigate the mechanics of this connection further and to simplify the successful connection detail from the previous test series.

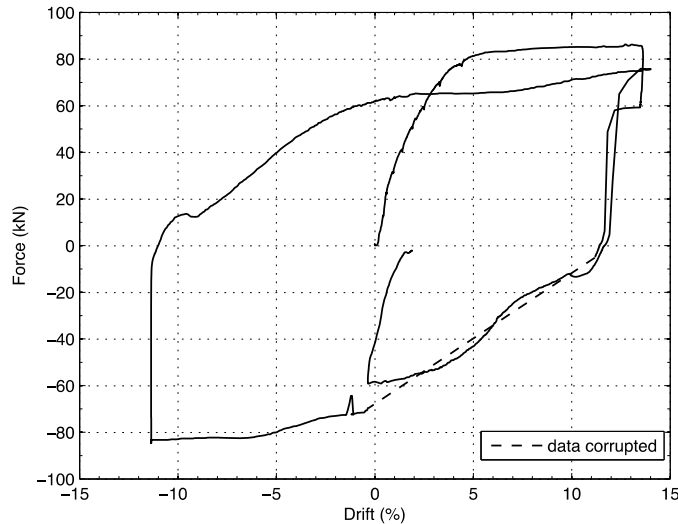


Figure 8. Force-Drift Response for VT1

A total of four specimens were tested in the second test series, with the primary difference between tests in this series being the embedment depth. In these tests, the cap capacities increased with increasing embedment depth, highlighting the importance of this parameter. In general, the caps from the second test series performed significantly better than those from the original series, providing increased strength while having significantly less longitudinal reinforcing steel. These increased capacities are most likely attributed to the combination of two features of the specimens in this test series: an increased embedment depth, and a more effective reinforcement configuration. Two of the three specimens tested until cap failure in the second test series had embedment depths greater than the embedment depths in the original test series. Furthermore, all of the specimens from the second test series used u-shaped bars (Figure 5) to confine the

concrete immediately around the embedded pile. Only one specimen from the original series used these u-bars (PC4), and this was the only specimen to achieve the desired cap capacity. Progressing from this test, caps with desired capacities were achieved in the second test series by also using u-bars, coupled with a significantly less congested total reinforcing configuration compared to that of PC4.

Summary and Conclusions

A total of nine CFT to concrete pile-cap connections were tested to evaluate their performance under seismic loads. The specimens were loaded with a constant axial load, and were subjected to monotonically increasing lateral load until failure. The specimens were then cycled to determine their post-peak energy dissipation characteristics. As a result of this research effort, the mechanics governing the behavior of this connection are better understood, and a new reinforcing scheme has been developed that offers several advantages over previous connection configurations with respect to design and detailing. This newly developed reinforcing scheme includes u-shaped reinforcing bars that encircle the embedded CFT piles within the cap that counteract the moment related demands introduced by the embedded pile. An analytical study is currently underway to further investigate the mechanics behind the behavior of this connection and to develop an appropriate design methodology. Also, the cyclic performance of this general connection configuration is being investigated further through a series of tests to be completed Spring 2012.

Acknowledgements

The authors gratefully acknowledge the financial support of the Montana Department of Transportation, and the advice and assistance provided by Mr. Kent Barnes and the technical panel at MDT.

References

- Kappes, L. (2012). *Validation of Pile-to-Pile Cap Bridge Connection Design*. Montana State University, Civil Engineering, Bozeman.
- Kingsley, A., Williams, T., Lehman, D., & Roeder, C. (2005). Experimental Investigation of Column-to-Footing Connections for High-Strength Vanadium Steel Concrete Filled Tube Construction. *International Journal of Steel Structures* , 5 (4), 377-387.
- Roeder, C., & Lehman, D. (2008). An Economical and Efficient Foundation Connection for Concrete Filled Steel Tube Piers and Columns . *COMPOSITE Construction in Steel and Concrete VI; Engineering Conferences International* . Devil's Thumb Ranch, Colorado.
- Silva, P., & Seible, F. (2001). Seismic Performance and Evaluation of Cast-in-Steel-Shell (ciss) piles . *ACI Structural Journal* , 98 (1), 36-49.
- Stephens, J., & McKittrick, L. (2005). *Performance of Steel Pipe Pile-to-Concrete Pile Cap Connections Subject to Seismic or High Transverse Loading*. Montana State University, Civil Engineering. Helena: Montana Department of Transportation.

CHAPTER THREE - SEISMIC PERFORMANCE OF CONCRETE-FILLED STEEL
TUBE TO CONCRETE PILE-CAP CONNECTIONS

Contribution of Authors and Co-Authors

Manuscript in Chapter 3

Author: Lenci Kappes

Contributions: Designed and built laboratory test specimens. Conducted load testing of model pile-to-pile cap connections, including the collection and analysis of test data. Developed proposed design methodology. Wrote the first draft of the manuscript.

Co-Author: Dr. Michael Berry

Contributions: Assisted in concept development for the laboratory test series. Provided technical expertise on data analysis and development of proposed design methodology. Provided feedback on early drafts of the manuscript.

Co-Author: Flynn Murray

Contributions: Provided feedback on early drafts of the manuscript.

Co-Author: Dr. Jerry Stephens

Contributions: Assisted in concept development for the laboratory test series. Provided technical expertise on data analysis and development of proposed design methodology. Provided feedback on early drafts of the manuscript.

Co-Author: Kent Barnes

Contributions: Provided technical expertise on the development of proposed design methodology. Provided feedback on early drafts of the manuscript.

Manuscript Information Page

Lenci Kappes, Michael Berry, Flynn Murray, Jerry Stephens, Kent
Barnes ASCE Journal of Bridge Engineering

Status of Manuscript:

- Prepared for submission to a peer-reviewed journal
- Officially submitted to a peer-review journal
- Accepted by a peer-reviewed journal
- Published in a peer-reviewed journal

Published by American Society of Civil Engineers

Abstract

This study investigates the seismic behavior of the connection between concrete-filled steel tube piles and concrete pile caps. This connection is an important component of an accelerated bridge construction technique, which involves driving steel piles to a finished elevation just below the design deck level, forming a pile cap around the ends of the driven piles, reinforcing this cap, and then filling both the piles and formwork with concrete. This cap will then serve as the deck support system. In this research, a total of six connection specimens with various details were tested under lateral loads until failure while monitoring applied loads and lateral displacements. All of the specimens achieved the desired moment capacity, and all but one experienced a typical progression of damage in the concrete cap. This progression initiated with crushing of the concrete (interior and exterior), was followed by yielding of the longitudinal reinforcement, and concluded with yielding of the transverse reinforcement and the formation of diagonal cracks extending from the embedded pile to the edge of the cap. Based on the results of this and a previous investigation, an initial design methodology is proposed.

Introduction

Several state departments of transportation (DOTs) commonly use an accelerated bridge construction (ABC) technique for short and medium span bridges that uses concrete-filled steel tubes (CFTs) as the support system. This system consists of a linear array of circular CFT piles connected at the top by a concrete pile cap, as shown in Figs. 1 and 2. During construction, the steel pipe piles are driven to their required depth, but are not terminated at the grade level, as is typically done. Rather, the steel pipe piles

extend above grade and terminate just below the level of the deck. Formwork for the pile caps is then placed at the ends of the steel piles, and the reinforcing cages for the caps are tied and placed. The steel pipe piles and pile caps are subsequently filled with concrete. To simplify construction and maintain a positive connection between the CFT piles and the pile cap, the steel piles typically extend up into the reinforced concrete cap. This method of construction is accelerated/efficient relative to conventional methodologies, because it takes advantage of some inherent benefits of CFTs. No formwork or reinforcing steel is required in the columns, and it is not necessary to wait for the concrete in the columns to gain strength because the steel tube is adequate for resisting initial gravity loads. The advantages of using CFTs in structural applications go beyond efficiency, because CFTs offer large capacities and increased ductility over typical reinforced concrete elements. However, the use of CFTs to resist lateral/seismic loads in the manner discussed earlier is relatively new, therefore, a reliable design methodology has not been fully developed. In particular, conventional structural design methodologies do not explicitly address the situation of a large CFT element embedded in a conventionally reinforced concrete element. This connection between the CFT and the concrete pile cap in the bridge support system discussed previously is the focus of the research discussed in this paper.



Figure 9. Typical bridge bent

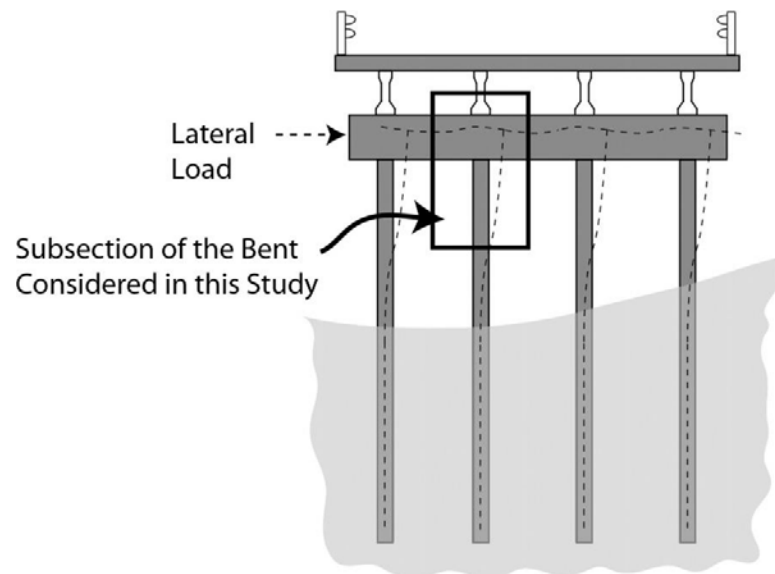


Figure 10. Subsection of bent tested in this research

The behavior of CFT elements alone, and in particular the behavior of circular CFTs, has been the focus of multiple research efforts over the last several decades (Moon

et al. 2012, 2013; Roeder et al. 2010; Bruneau and Marson 2004; McFarlane 2006). This previous research has demonstrated the structural benefits of CFTs and has resulted in several analysis and design methodologies for these elements. However, less is known about the connections of CFTs to other structural elements, and in particular concrete elements. As such, the connection of CFTs to concrete elements has been the focus of recent research (Hsu and Lin 2006; Marson and Bruneau 2004; Silva et al. 1999; Silva and Seible 2001; Rollins and Stenlund 2010; Kingsley 2005; Kingsley et al. 2005; Williams 2007; Lee 2011; O'Neill 2011; Lehman and Roeder 2012; Stephens et al. 2014). For example, Silva et al. (1999) and Silva and Seible (2001) investigated the performance and design of three full-size bridge bents using a connection design that did not embed the CFTs in the concrete elements. These connections performed well under cyclic loading; however, a significant amount of steel was required to span between the CFTs into the concrete beams. Rollins and Stenlund (2010) completed a study focused on characterizing the response of an at-grade CFT pile-to-concrete pile-cap connections in which the end of the CFTs were embedded in the concrete pile caps. Variables in their study included embedment depth and the amount of reinforcement spanning from the cap into the embedded CFT. Their work demonstrated the importance of embedment depth; the connection with the best performance relied solely on its embedment depth with no additional reinforcement provided between the cap and the CFT. A significant amount of research has been conducted at the University of Washington (Seattle, WA) on CFT columns to concrete foundations (Kingsley 2005; Kingsley et al. 2005; Williams 2007; Lee 2011; O'Neill 2011; Lehman and Roeder 2012; Stephens et al. 2014). The

connections in their work consisted of embedded CFTs with annular rings welded to the ends. A total of 19 specimens were tested at the University of Washington, with the objective of evaluating the effects of tube diameter, depth to thickness ratio, yield stress of steel, and embedment depth. As was concluded in other work on embedded connections, their work also demonstrated the importance of embedment depth, with the deeper embedded specimens achieving drift capacities in excess of the maximum seismic design drifts. Their work demonstrated that this annular-ring embedded connection was a practical and effective means for connecting CFT columns to foundations, and a design methodology was developed based on the results of their test series (Lehman and Roeder 2012).

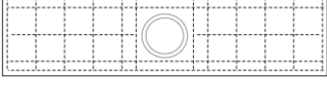
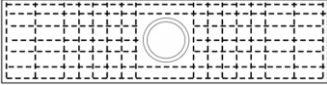
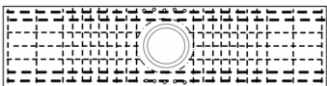
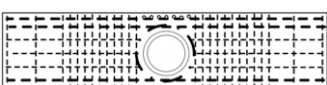
While valuable in understanding the general behavior of CFT to concrete element connections, this previous research does not specifically address connections between CFT columns and above-grade concrete pile caps, as is the case in the ABC bridge support system discussed earlier. In this situation, space may be more limited than in concrete foundation connections. Thus, in the research presented in this paper, a total of 11 CFT to pile-cap connections were experimentally evaluated to determine the performance of this connection under seismic loads and to develop a reliable design methodology for such connections. This research was performed in two phases: five specimens were tested during Phase I and six were tested during Phase II. The Phase I research was primarily focused on determining the minimum amount of reinforcing steel required to develop the full plastic moment of the CFT and to develop a preliminary design methodology. The Phase II investigation was focused on optimizing the

reinforcement and further developing the design methodology. In this paper, the Phase I investigation is discussed briefly, followed by a more detailed discussion of the Phase II investigation. The resulting preliminary design methodology is then presented followed by a summary and conclusions.

Phase I Research

Stephens and McKittrick (2005) tested five half-size embedded CFT to pile-cap connections under lateral loading. All specimens in this series used the same embedment depth and the same basic reinforcing scheme, and the intended variable between the tests was the specific amount and placement of this reinforcement in the pile cap. Table 4 is intended to provide a simple overview of the experimental parameters and material properties used in this research. It should be noted that the test setup used in this series is identical to that used in Phase II, which is discussed in the following section. As the project advanced, the configuration of each successive model was adjusted based on the results of the preceding test. Generally, the amount of reinforcement in the cap was increased in each test, up to a model with seven times the original amount of longitudinal and transverse reinforcing steel. In addition to the amount of reinforcement increasing with each test, the configuration of the reinforcing steel also varied, with the final test using a combination of spirals and U-shaped bars to confine the embedded pile.

Table 4. Phase I experimental parameters and material properties

Test	Pile Wall Thickness, (mm)	Embedment Length, (mm)	Long Steel (%)	Trans Steel (%)	f_c (MPa)	Reinforcement Layout
PC1	8.1	228.6	0.41	0.09	33.3	
PC2	6.35	228.6	0.41	0.09	36.7	
PC3	6.35	228.6	1.09	0.41	21.7	
PC3a	6.35	228.6	2.11	0.65	27.2	
PC4	6.35	228.6	2.83	0.7	32.2	

These CFT to pile-cap connections were all loaded with a monotonically increasing lateral load until failure, and then in some cases cycled to evaluate the postpeak energy dissipation characteristics of the specimen. All of the specimens, with the exception of PC4, failed due to crushing of the pile cap directly behind the pile and the formation of large cracks along two compression struts extending outward from the pile (in the direction of the applied load) to the faces of the cap (Figure 11). The capacity of the caps generally increased with increasing amounts of longitudinal and transverse reinforcing steel. Of these specimens, PC4 (see Figure 10) was the only specimen to achieve the desired failure mechanism (the formation of a plastic hinge in the CFT pile). This was achieved using a large amount of longitudinal and transverse reinforcement (seven times that of the original specimen) with a reinforcing scheme that was fairly congested, which included spirals and U-shaped bars around the embedded pile (Figure 12). Although this specimen was able to achieve the desired capacity, the actual ultimate

capacity of this heavily reinforced cap and the attendant absolute effect of the reinforcing scheme on cap capacity could not be determined, because the CFT yielded before the cap capacity was reached. Further, as can be observed in Figure 12, this connection is fairly congested.



Figure 11. Typical failure mechanism observed in Phase I effort



Figure 12. Reinforcing cage from Phase I PC4

Phase II Research

Based on the results of the Phase I research, a follow-on Phase II investigation was performed to further optimize the reinforcement configuration used in the cap-to-CFT pile connections (to reduce congestion) and to further develop a design guide for such connections.

Experimental Program

A total of six specimens were tested in this phase of the research. The specimens were approximately half-size models from an existing bridge in eastern Montana (Timber Creek Bridge on County Route 38218 in Powder River County, MT) and consisted of a single connection of the overall bridge bent (Fig. 2). Details regarding dimensions, loading, and assumed inflection points can be found in Stephens and McKittrick (2005). In the specimens, the caps were terminated at the inflection points halfway between CFTs, and the CFT was terminated at an assumed inflection point along its length. The specimens were supported and loaded to generate the deflected shape expected in this subsection of the full-size bent (as illustrated by the dashed line in the subsection of Figure 10). It should be noted that all tests, with the exception of VT1, used CFT piles with wall thicknesses significantly larger than what would typically be used in design. An oversized pile was used to ensure that the ultimate capacity of the cap could be observed prior to the plastic hinge forming in the CFT. Although a failure of the cap is not the desired behavior of this connection, it was purposefully implemented to observe the actual ultimate cap capacity and failure mechanisms. The oversized pile essentially became part of the testing apparatus, and the test focus was on the performance of the

cap. It should also be noted that the increased stiffness of the oversized piles could have an effect on the performance of these connections and the extent of observed failure mechanisms. This effect is believed to be minor, generally considering the relative stiffnesses between the steel piles and softer concrete caps. Further, the results obtained in this study may be considered conservative, considering the stiffer piles may be more damaging to the pile cap than a less stiff pile that typically would be used in design.

Table 5 provides the experimental parameters and material properties for the specimens in this phase of testing. These caps all had the same general dimensions and reinforcing cages, and the primary variable between tests was U-bar size and configuration, concrete strength, embedment depth, and loading scheme. An isometric view of a typical cap-reinforcing configuration is shown in Figure 13, and the details and dimensions of a standard cap are shown in Figure 14. The concrete caps had 457 by 457-mm cross sections and were 1,720 mm long. All CFTs had outside diameters of 219 mm (with varying thicknesses) and were 1,752 mm long. The longitudinal reinforcement in each specimen consisted of two imperial #4 deformed reinforcing bars (12.7-mm-diameter) and two imperial #5 (15.9-mm-diameter) bars on each face of the cap, as shown in Figure 14. The transverse reinforcement in each cap consisted of imperial #3 bars (9.5-mm diameter) spaced at 44.5 mm, over a region extending 338 mm on either side of the centerline of the pile. Note that the reinforcing schemes used in this phase of research did not include spiral reinforcement around the end of the embedded piles, as is required by some state DOTs for such connections. This was done purposefully, because

the U-bars are believed to more adequately/efficiently confine this region and transfer the loads away from the connection.

Table 5. Phase II experimental parameters and material properties

Table 1. Phase II Experimental Parameters and Material Properties

Test designation	Loading	Pile wall thickness (mm)	Embedment depth (mm)	f_c (MPa)	U-bar configuration	Failure mechanism
VT1	Pushover	6.35	228.6	43.1	#7 U-bar, exterior	Plastic hinge
VT2	Pushover	12.7	298.5	26.2	#4 and #5 U-bar, exterior	Cap fracture
VT2.5	Pushover	12.7	228.6	43.1	#7 U-bar, exterior	Cap fracture
VT3	Pushover	12.7	263.5	28.3	#7 U-bar, exterior	Cap fracture
CT1	Cyclic	18.5	298.5	27.6	#4 and #5 U-bar, exterior	Cap fracture
CT2	Cyclic	18.5	298.5	27.6	#4 and #5 U-bar, exterior and interior	Cap fracture

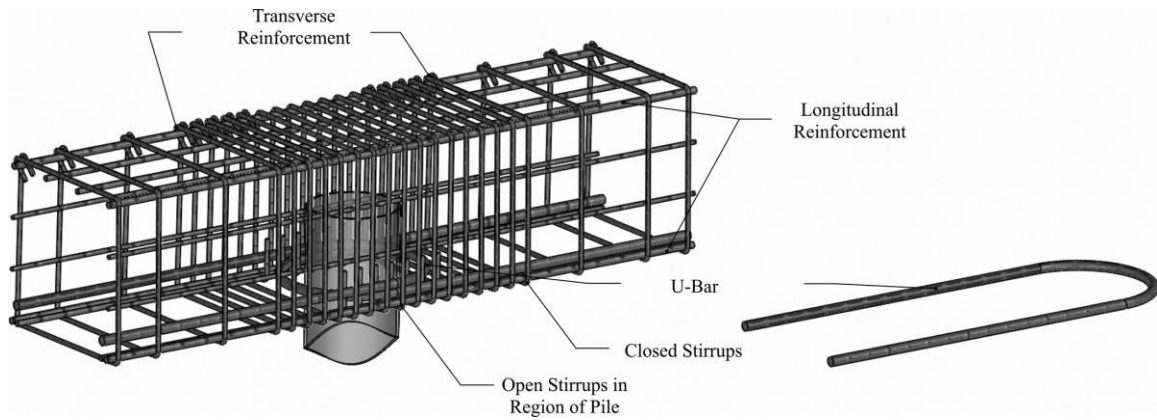


Figure 13. Typical reinforcing cage

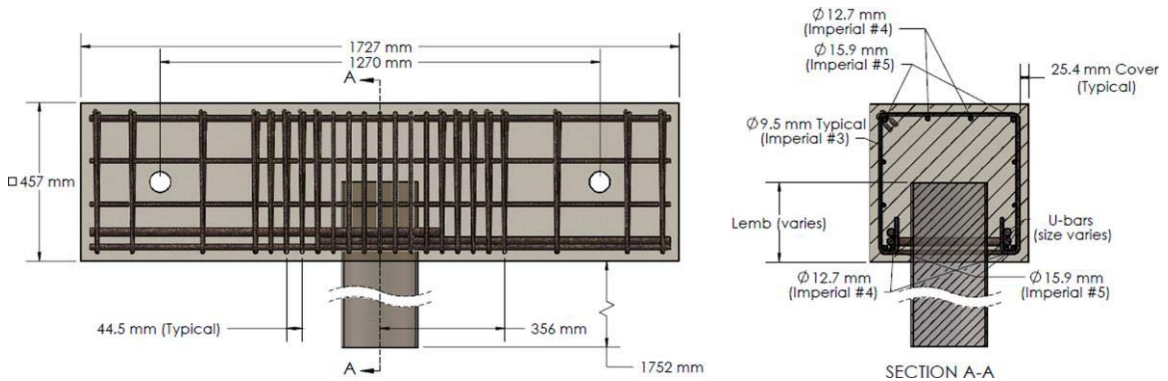


Figure 14. Typical connection detail

In Table 5 the first four models (VT1, VT2, VT2.5, and VT3) were monotonically loaded to failure, capturing the ultimate strength of each configuration and providing general information on failure mechanisms and post-failure ductility. Two more tests were completed using a cyclic load scheme (CT1 and CT2) to capture performance characteristics of the connections under multiple cycles of fully reversed, increasing load. Regarding variables between tests, VT1 used a smaller sized CFT (same diameter but with a thinner wall thickness, 6.35 mm) with an embedment depth of 228.6 mm. The U-bars in this specimen consisted of imperial #7 U-bars (22.2-mm diameter) around the CFT at the exterior face of the cap, as shown in Figure 15(a). VT2 had a reduced concrete strength (26.2 MPa) and an increased embedment depth (298.5 mm) relative to VT1. The U-bar configuration in this specimen had approximately the same cross-sectional area as that used in VT1, but consisted of one imperial #4 (12.7-mm) bar and one imperial #5 (15.9-mm) bar in each direction at the exterior of the cap. VT2.5 had the same configuration as VT1, because this specimen was constructed by simply inserting an undamaged CFT into the generally undamaged concrete cap from VT1. As is discussed in a later section, VT1 formed a plastic hinge in the CFT before any significant distress occurred in the pile cap; thus, to a large extent, this test only provided a conservative lower bound on the capacity of this cap configuration. Therefore, the VT1 cap was retested (as VT2.5) using a stronger, undamaged CFT. The stronger CFT used to replace the original CFT had a wall thickness of 12.7 mm. VT3 had the same U-bar configuration as VT1 with an embedment depth (263.5 mm) between that used in VT1/VT2.5 and VT2. The two cyclic load tests (CT1 and CT2) had the same configuration as VT2; however,

CT2 included a second set of U-bars near the tip of the embedded pile, as seen in Figure 15(b).

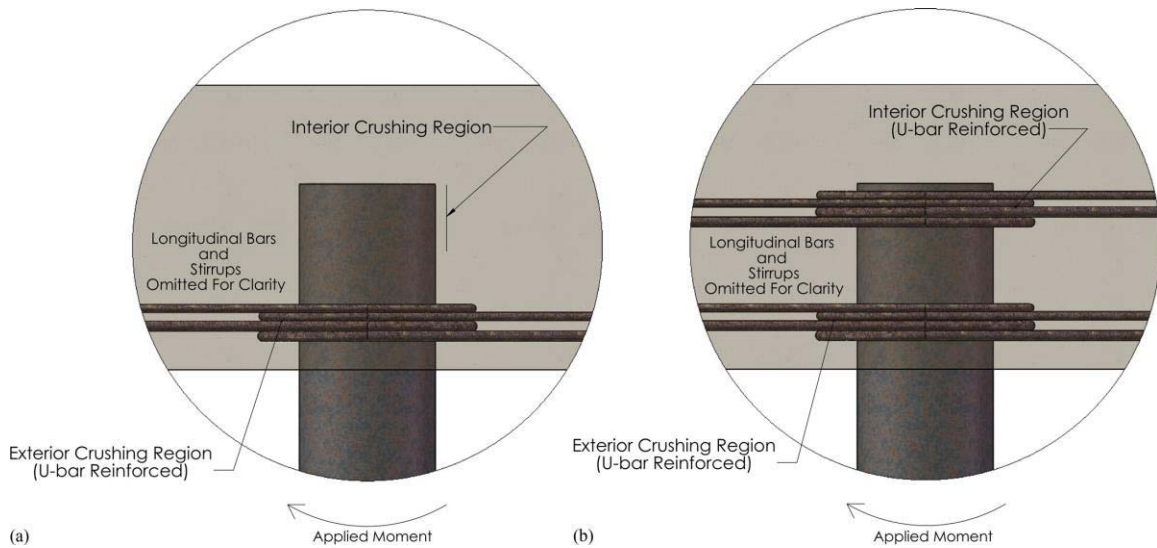


Figure 15. U-bar configuration: (a) CT1 U-bar configuration; (b) CT2 U-bar configuration

Test Setup and Instrumentation

The manner in which the test specimens were supported and loaded is shown in Figure 16. As shown in the figure, the concrete cap was pin supported at a span of 1.3 m, approximately representing a pile spacing of 2.6 m in a complete bent. These pin joints consisted of steel sleeves cast in the concrete cap providing through holes for threaded rod. A constant axial load of 66.7 kN was applied to the tip of the CFT pile using a 111-kN actuator to approximately represent gravity load effects. This axial load was applied through a steel frame on rollers to accommodate the lateral deflection of the pile during testing.

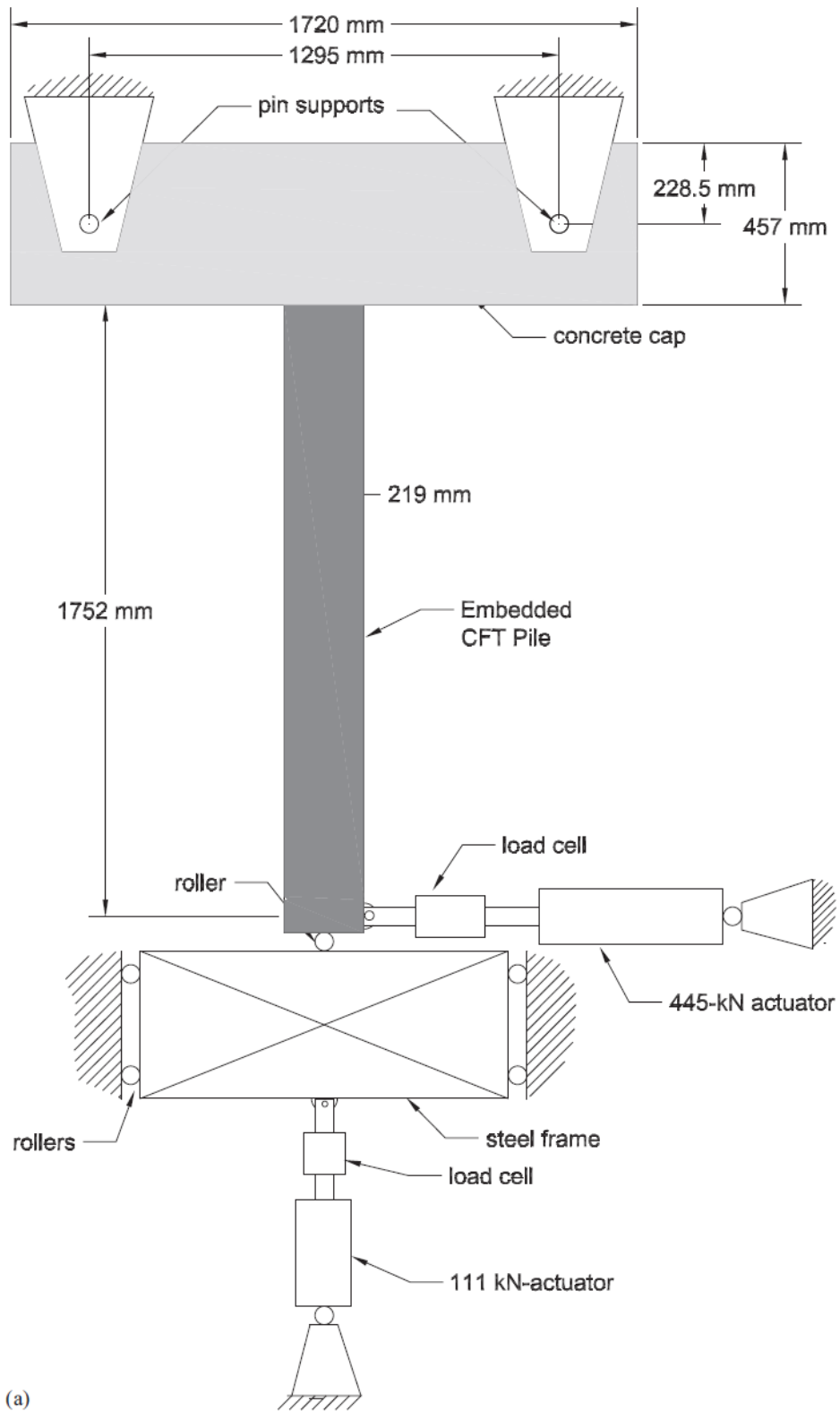


Figure 16. Test setup



(b)
Figure 16. *Continued*

The lateral load was applied at the tip of the pile using a 445-kN hydraulic actuator. Load, deflection, and strain were measured and recorded for each test. The lateral and axial loads were recorded via load cells attached to the ends of the actuators, whereas the deflections were recorded with linear string potentiometers at various locations along the height of the CFT. In each test, strains were measured at select locations on the steel pile and the reinforcement in the pile cap. Strain gauge locations changed between tests, based on the test objectives and experience gained from each successive test. Generally, the strain response was measured on the U-bars, the straight longitudinal bars on the bottom cap, and on selected transverse ties (Kappes et al. 2013).

Loading Schemes

In each of the monotonic tests (VT1 through VT3), the specimens were initially loaded until extensive failure was observed (i.e., a distinct loss in load-carrying capacity). The specimens were then typically loaded in the opposite direction until the tip of the pile reached the same maximum deflection that was observed on the initial push. The test was generally considered complete after the pile was returned to its starting position, although VT1 and VT2 were cycled through a second push cycle before concluding.

The CFT tip displacement history for the cyclic tests (CT1 and CT2) is shown in Figure 17. The tip was cycled at 0.5% drift intervals (with three cycles of fully reversed displacement at each interval) until a drift of 4% was reached. At this point, the increase in drift was at 1% intervals until 7% drift was reached (again with three cycles of fully reversed displacement at each interval). The tests concluded with drift cycles conducted at 9 and 11% drift.

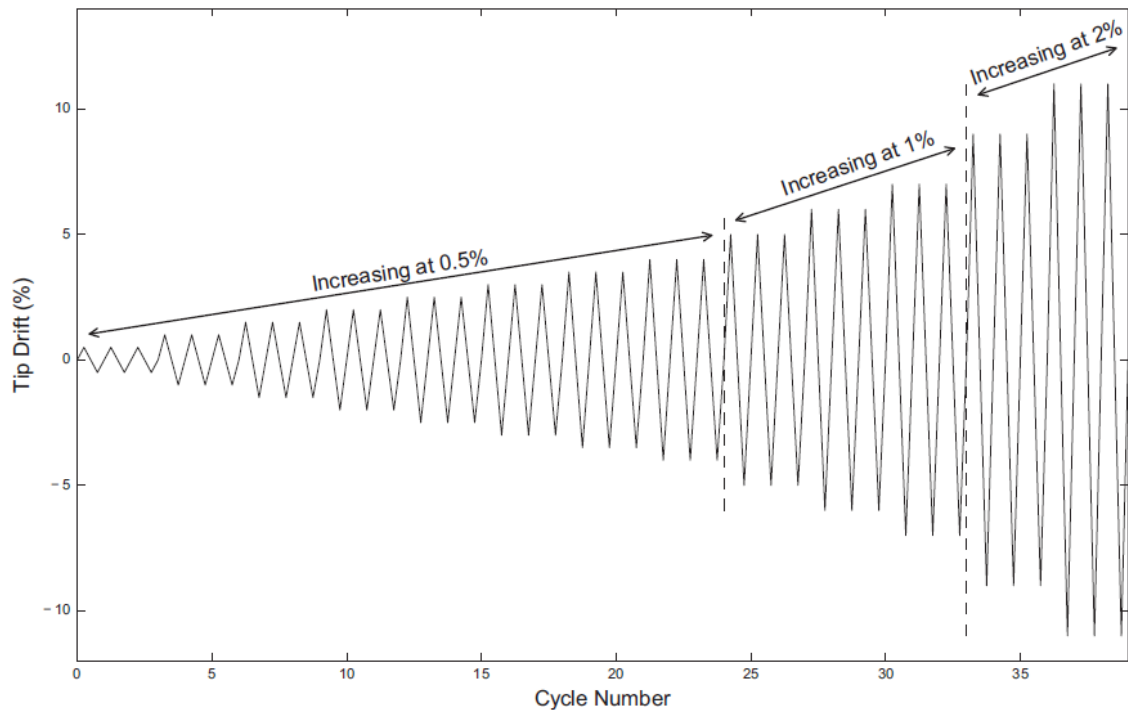


Figure 17. Cyclic-loading history for CT1 and CT2

Results

A summary of the test results including observed damage states is provided in Table 6, and the moment-drift response of each specimen is provided in Figure 18. The moments reported in this table and these figures are those in the CFT at the interface between the CFT and the pile cap. These moments are calculated from the applied lateral load, and are adjusted to include P-D effects from the axial load. Relative to overall performance, VT1 failed through the formation of a plastic hinge in the CFT pile, whereas the remaining models all failed from fracturing of the concrete pile cap (by intention, using an oversized pile).

Table 6. Summary of test results

Test designation	Failure mechanism	Cracking		Initial degree/crush		Exterior crushing		Longitudinal yielding		Splitting		Initial degradation		Max moment (kN m)
		Drift (%)	Moment (kN m)	Drift (%)	Moment (kN m)	Drift (%)	Moment (kN m)	Drift (%)	Moment (kN m)	Drift (%)	Moment (kN m)	Drift (%)	Moment (kN m)	
VT1	Plastic hinge	0.5	39.5	1.2	70.6	—	—	—	—	—	—	—	—	161.6
VT2	Cap fracture	0.6	62.3	1.1	83.5	5.7	218.3	12.0	233.2	7.1	231.3	—	—	235.6
VT2.5	Cap fracture	—	—	—	—	5.0	168.4	6.2	187.8	6.2	187.8	—	—	187.8
VT3	Cap fracture	0.4	48.2	1.3	92.7	5.8	205.7	4.8	188.7	5.8	205.7	—	—	205.7
CT1	Cap fracture	—	—	—	—	—	—	—	—	—	—	1.2	106.6	233.7
CT2	Cap fracture	—	—	—	—	—	—	—	—	—	—	2.0	178.7	246.5

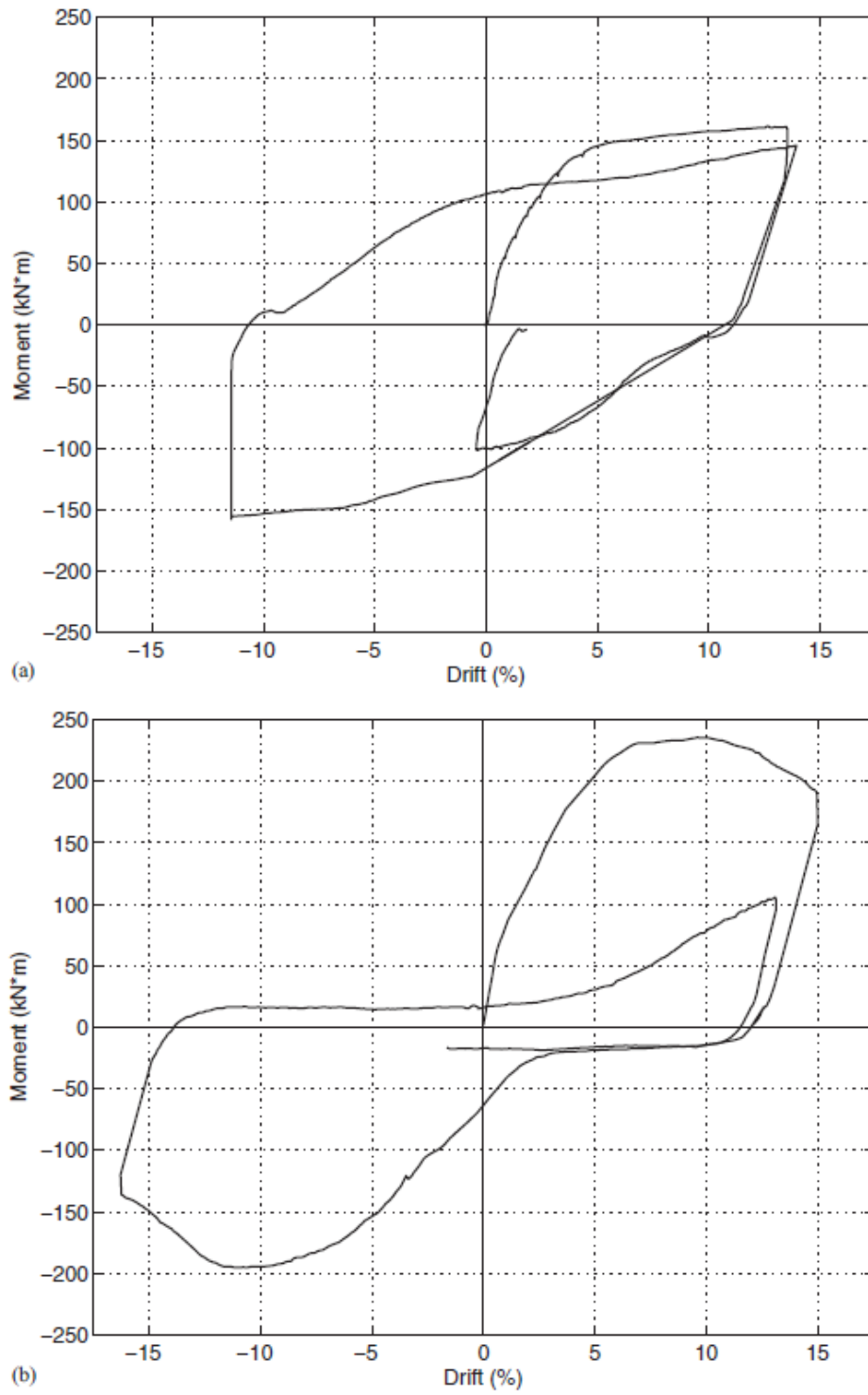
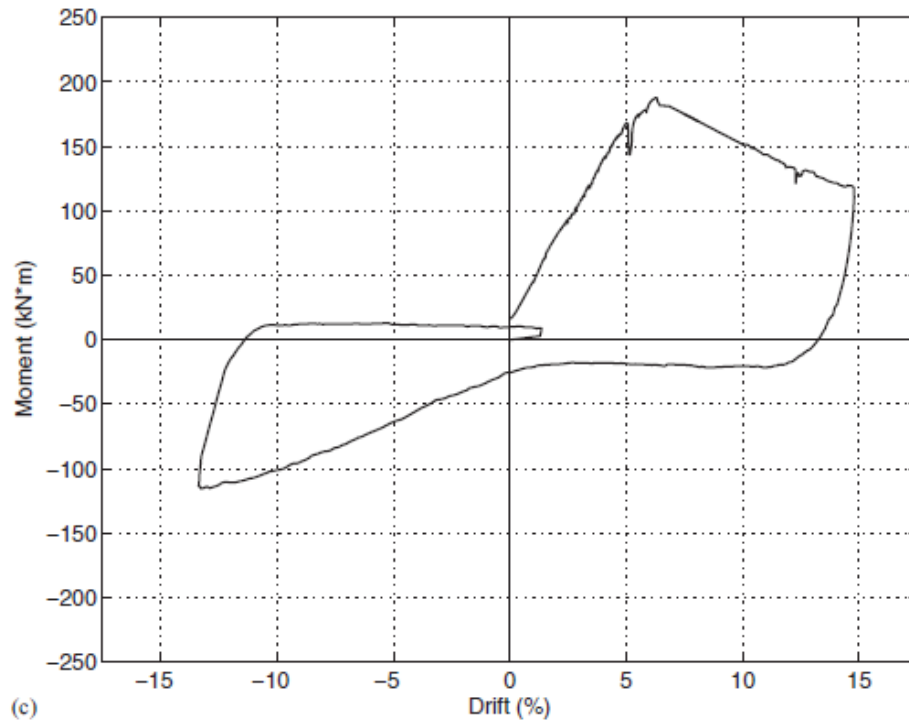
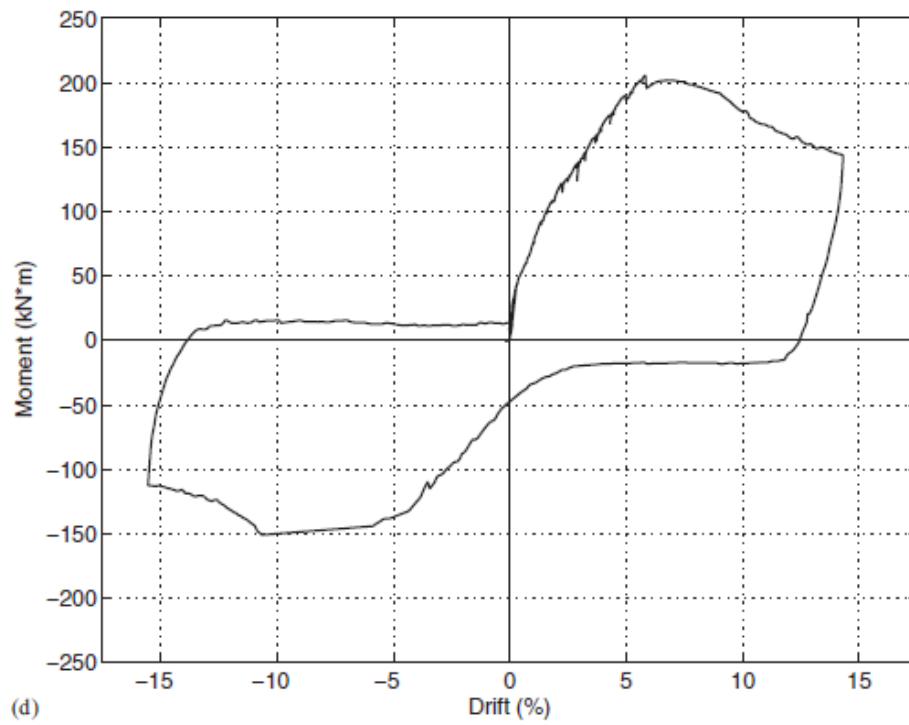


Figure 18. Force-deflection responses of test specimens: (a) VT1; (b) VT2; (c) VT2.5; (d) VT3; (e) CT1; (f) CT2

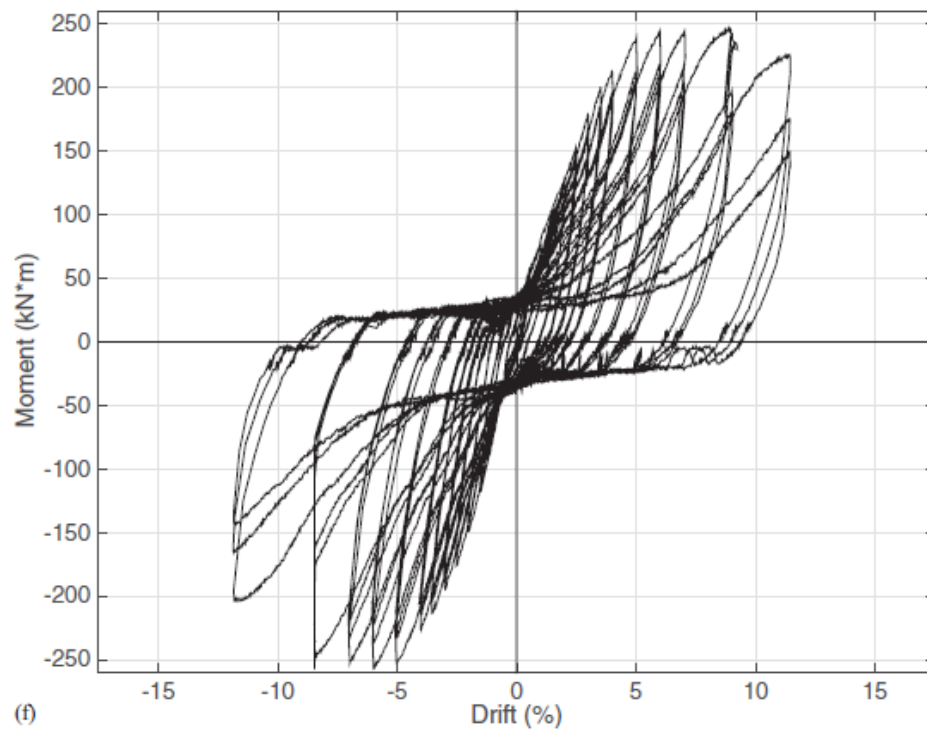
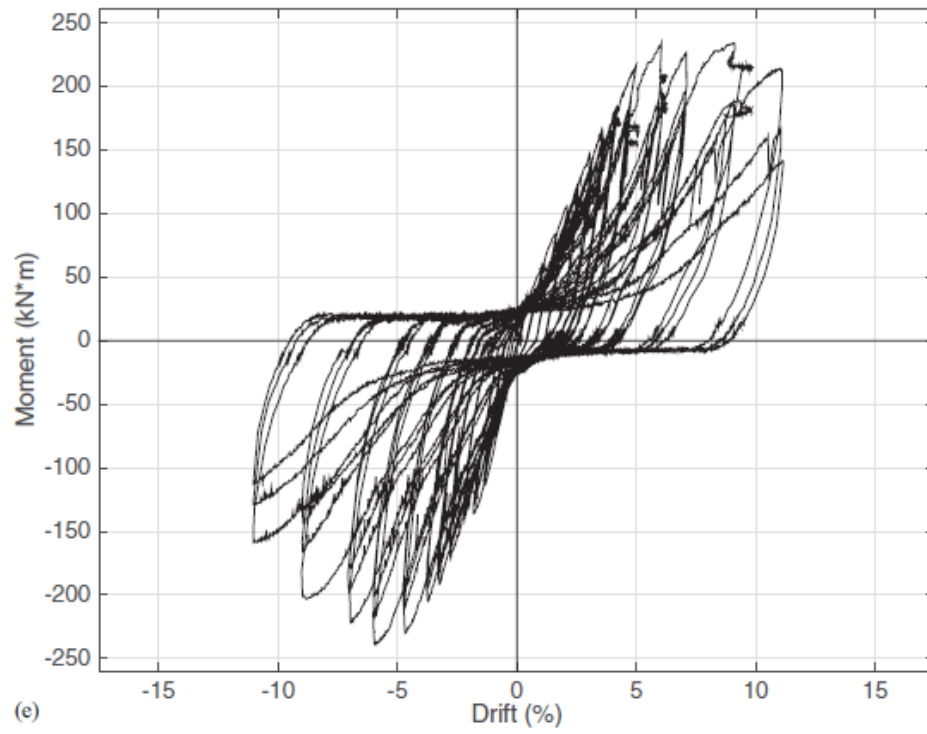


(c)

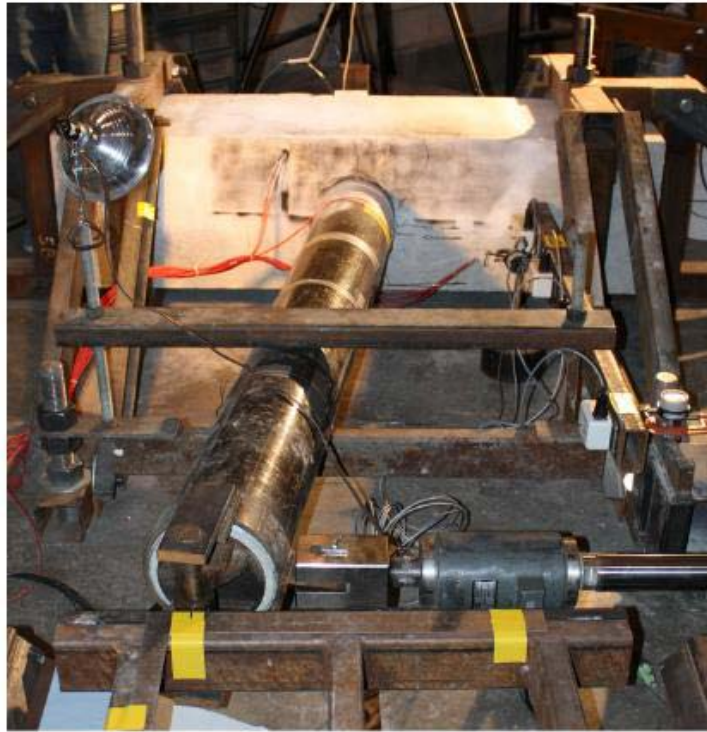


(d)

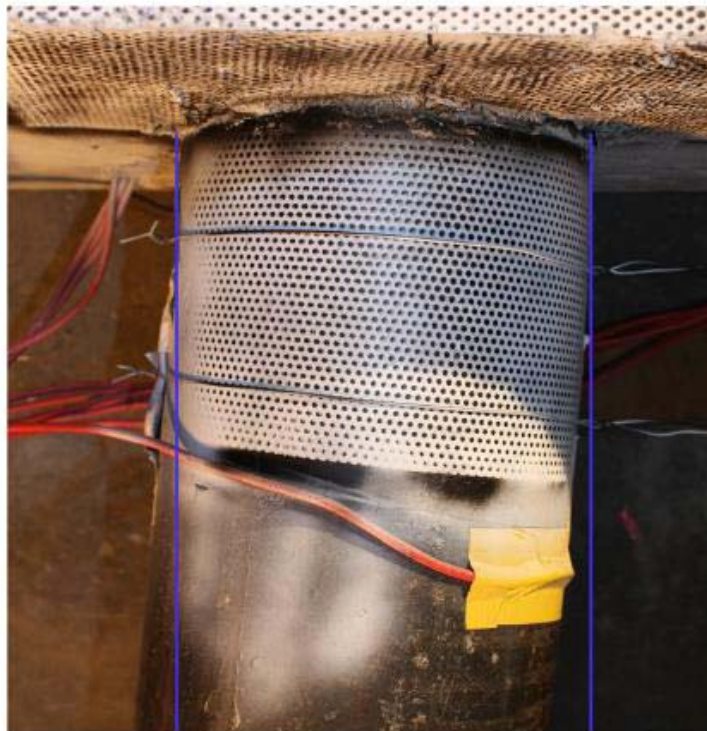
Figure 18. *Continued*

Figure 18. *Continued*

In VT1, the ultimate strength of the CFT pile, with a wall thickness of 6.4 mm and a diameter-to-thickness ratio of 34.5, was 161.6 kN m. As expected, the ductile nature of the plastic hinge in the CFT pile provided a very robust hysteresis response, shown in Figure 18(a), identified by a minimal loss in energy dissipation and load capacity for each completed load cycle. Figure 19 shows VT1 at maximum deflection, demonstrating the large drift possible using this system, while the concrete cap remains intact. Although this specimen was able to achieve the desired behavior, the actual ultimate capacity of this cap and the attendant absolute effect of the reinforcing scheme on cap capacity could not be determined, because the CFT failed before the cap capacity was reached.



(a)



(b)

Figure 19. VT1 test: (a) at maximum drift; (b) plastic-hinge region

As intended, the remaining pushover specimens failed in the cap, which was marked by a loss of lateral-load-carrying capacity, and was initiated by crushing in the compression region adjacent to the CFT pile and the formation of large compression struts extending from the steel pile to the outer edges of the concrete cap (Figure 20). The less desirable and less ductile behavior of this type of failure is shown in Figure 18(b–d), in which the hysteresis is pinched compared with VT1. The monotonic tests VT2, VT2.5, and VT3 had ultimate base-moment capacities of 235., 187.8, and 205.7 kN m, respectively. The two cyclic tests, CT1 and CT2, which were similar in design to VT2, had ultimate base moments of 233.7 and 246.5 kN m, respectively.



Figure 20. Typical cap at failure

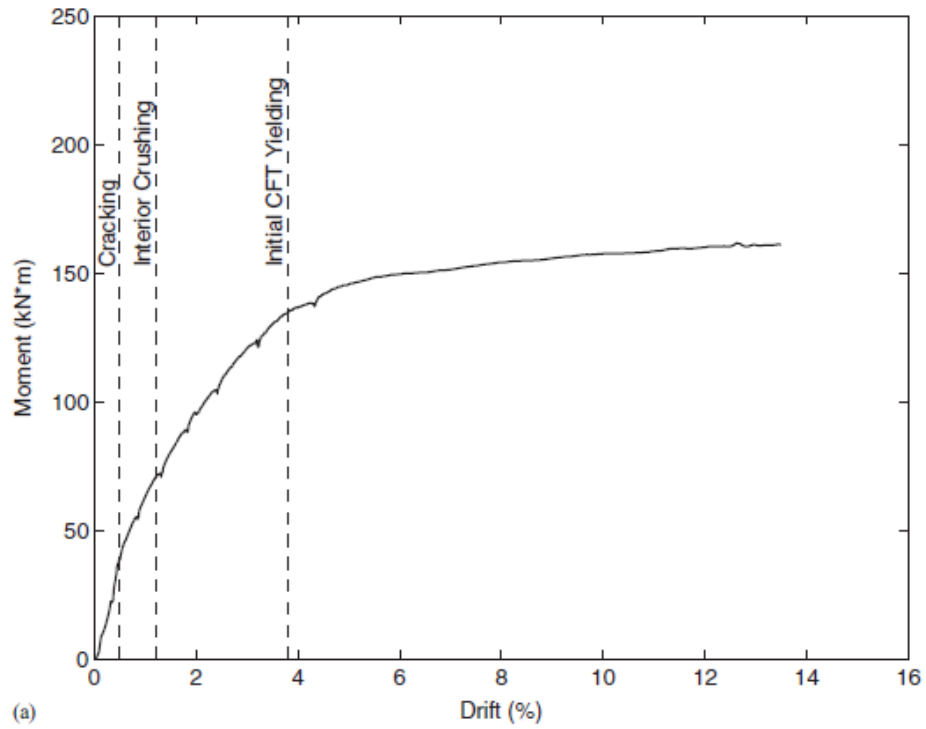
Discussion of Results

Monotonic Test Series: Observed Damage States

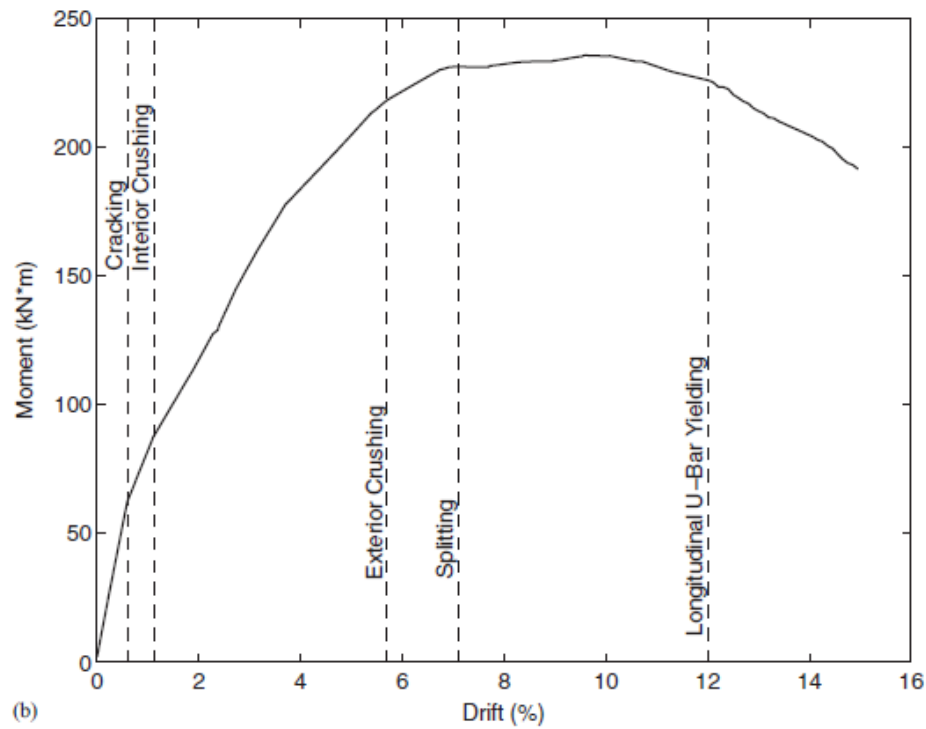
Table 6 provides a summary of test results for the monotonic specimens (VT1, VT2, VT2.5, and VT3), and the moment-drift responses for the first push to failure for

each specimen is grouped in Figure 21(a–d). In these figures and in Table 6, the various damage states that were observed in each test specimen are identified. These observed failures correlate with changes in the cap stiffness, as represented by associated changes in the slope of each moment-drift response.

Referring to Figure 21(a–d), some commonalities in basic behavior and associated failure mechanisms are apparent across all tests. Generally, the first distress in each specimen consisted of thin cracks forming in the cap concrete, followed by the concrete in the interior of the cap on the back side of the pile near the embedded tip being damaged/crushed (in the region identified in Figure 15). The initial cracking occurred across a range of drifts of 0.40–0.60% and moments ranging from 39.5 to 62.3 kN m. Interior damage/crushing was characterized by a change in stiffness and rigid body rotation that occurred prior to evident damage on the exterior of the concrete cap. This internal crushing occurred across a range of drifts of 1.1–1.3% and total moments of 70.6–92.1 kN m. Although these behaviors (initial cracking and interior crushing) are evident in the response from VT1, VT2, and VT3, they are absent in VT2.5. Test VT2.5 reused the cap from test VT1, which had already experienced these permanent distresses in the earlier test. Once again, although VT1 was apparently undamaged on the exterior, the distress it experienced in the first test was obvious when it was retested in VT2.5. The load displacement response for VT2.5 began with a stiffness consistent with a cracked cap with some permanent interior damage, as can be observed in Figure 21(a–c).

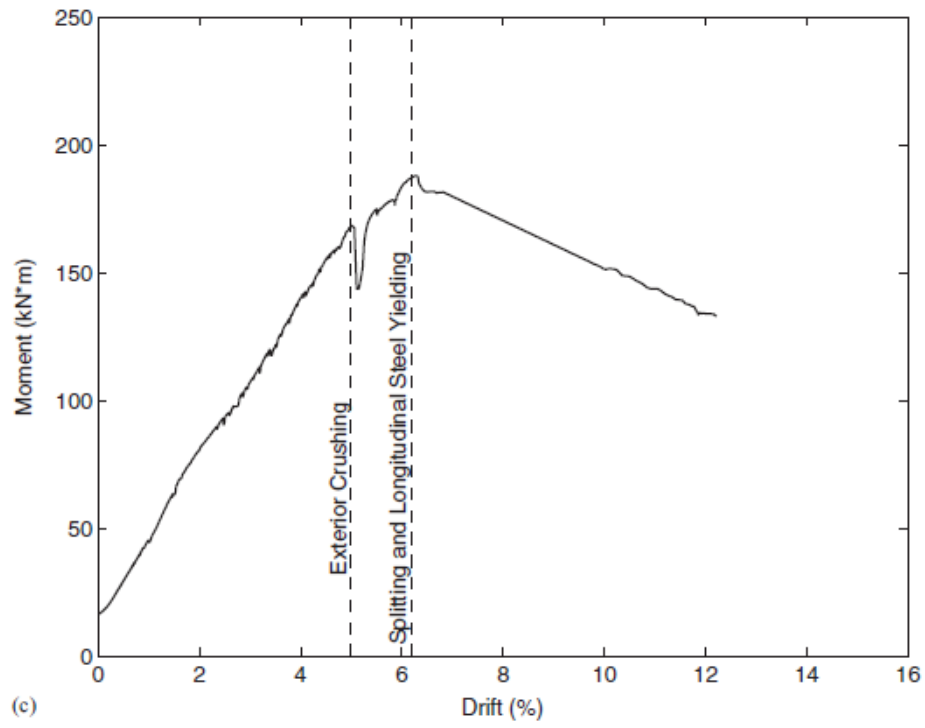


(a)

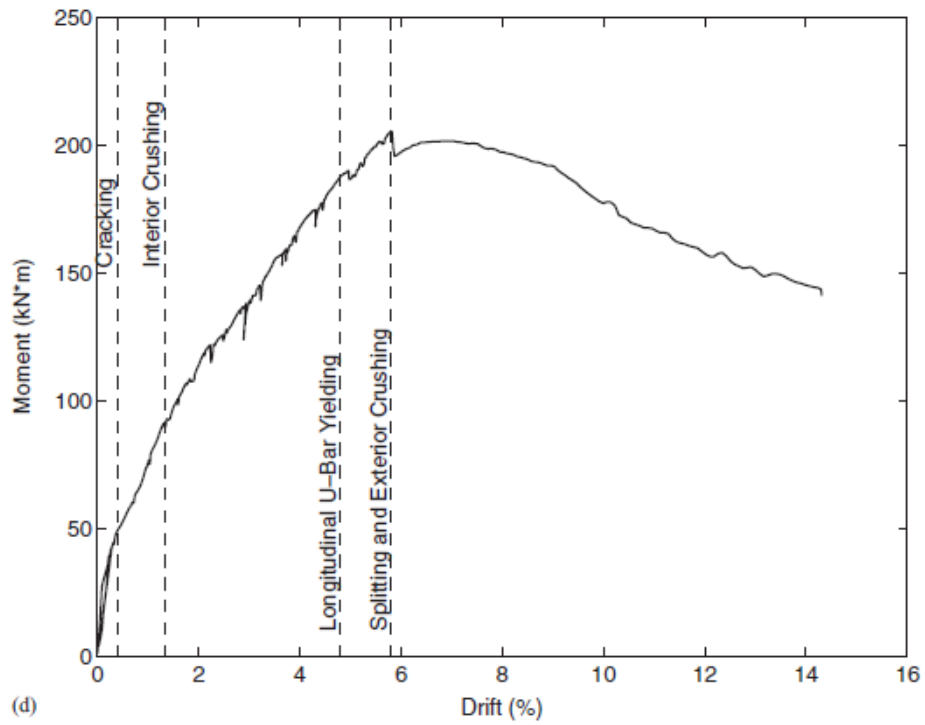


(b)

Figure 21. Pushover moment-drift responses: (a) VT1; (b) VT2; (c) VT2.5; (d) VT3



(c)



(d)

Figure 21. *Continued*

Following the occurrence of initial cracking and interior crushing/damage, the behaviors of VT1, VT2, VT2.5, and VT3 diverged as they were exercised through increasing levels of drifts. The moment-drift response of VT1, shown in Figure 21(a), subsequently exhibits a long yield plateau, as a plastic hinge formed in the CFT at a moment demand of 161.6 kN m. VT2, with an oversize pile, experienced crushing of the exterior concrete between the CFT and the U-bars on the front face of the pile at 5.7% drift and 218.3 kN m of total applied moment. Similarly, exterior concrete crushing was observed in VT2.5 and VT3 at closely comparable drift levels (5.0 and 5.8%, respectively). Such crushing was readily identified by visual observation, but there were also other more precise indicators of its occurrence. Typically, the strain gauge on the inside of the U-bar was disrupted as the concrete began to crush, and the transverse ties immediately next to the compression region transitioned from tension to bending. In VT3, longitudinal yielding of the U-bar reinforcement occurred prior to crushing of the exterior concrete. This yielding occurred at a drift of 4.8% and a moment of 188.7 kN m.

As the drift further increased from 6 to 7%, VT2, VT2.5, and VT3 all experienced splitting failures. The splitting failure mechanism consisted of a pair of cracks that originated at the face of the CFT and propagated out at approximately 30–45° (these cracks can be observed in Figure 20). This failure mechanism was assessed as yielding of the U-bar in the transverse direction (at the apex of the U) and yielding of the transverse reinforcement adjacent to the face of the CFT. For VT2.5, splitting occurred simultaneously with yielding of the longitudinal reinforcing steel. Because of the multiple failure mechanisms, the moment capacity of VT2.5 then steadily decreased for the

remainder of the test [Figure 21(c)]. For VT3, yielding of the longitudinal reinforcement occurred slightly before splitting, which occurred coincident with crushing of the exterior concrete (at a drift of 5.8%). Once again, because of the multiple failure mechanisms, the moment capacity then steadily decreased in a very similar fashion to VT2.5. Returning to VT2, following exterior crushing of the cap at a drift of 5.7% as mentioned previously, the splitting failure occurred at 7.1% drift and moment demand of 231.3 kN m. As the drift further increased, reinforcement in the longitudinal direction eventually yielded at a drift of 12% and moment of 235.6 kN m, and the moment capacity began to gradually decrease as significant damage to the cap was incurred.

The primary difference between tests in this series was the embedment depth. These findings indicate the importance of this parameter on cap performance, as has been observed in previous research. Generally, an increase in embedment depth resulted in an increase in ultimate moment carrying capacity and an increase in drift and moment at the onset of the various damage states. This effect was significant, despite concrete strength varying between tests. Compared with the Phase I research, the caps from this phase of research performed significantly better than those from the original effort, providing increased strength while having significantly less longitudinal reinforcing steel. These increased capacities are most likely attributed to the combination of two features of the specimens in this test series: an increased embedment depth and a more effective reinforcement configuration. All of the specimens from this test series used U-shaped reinforcing bars to confine the concrete immediately around the embedded pile and to transfer loads away from the connection area.

Cyclic Test Series

Although the discussion of the monotonic test series in a previous section focused on the moments and drifts at which various damage states occurred, CT1 and CT2 provided an opportunity to (1) isolate the effects of cycling, because CT1 is identical to VT2 with the exception of loading scheme; (2) identify the initiation of permanent degradation in cap performance; and (3) isolate the effects of including an additional U-bar near the tip of the embedded pile, because this was the only parameter that varied between CT1 and CT2 (Figure 15).

The effects of cycling can be observed by comparing VT2 and CT1, because the only difference between these two tests was loading scheme. The moment-drift response from VT2 is overlaid on the cyclic moment-drift envelope from CT1 in Figure 22. This moment-drift envelope consists of the peak moment and corresponding drift for each cycle in one direction for this test. As can be seen in this figure, the responses are very similar, with similar initial stiffnesses and ultimate capacities (both with ultimate capacities of around 235 kN m). Although the monotonic test did not provide any indication of the degradation that occurred under repeated displacement cycles, it did envelope the general behavior during the cyclic test, up through and beyond the point at which the ultimate capacity was reached. Thus, these similarities indicate that the behaviors identified in a monotonic test provide a reasonable assessment of pile-cap performance under a more complicated cyclic history. Beyond 8.5% drift, the moment carrying capacity of the cap in cyclic test CT1 noticeably decreased compared with that

of the cap in the monotonic test, VT2. This loss in capacity was attributed to the accumulated degradation from the cyclic displacement history.

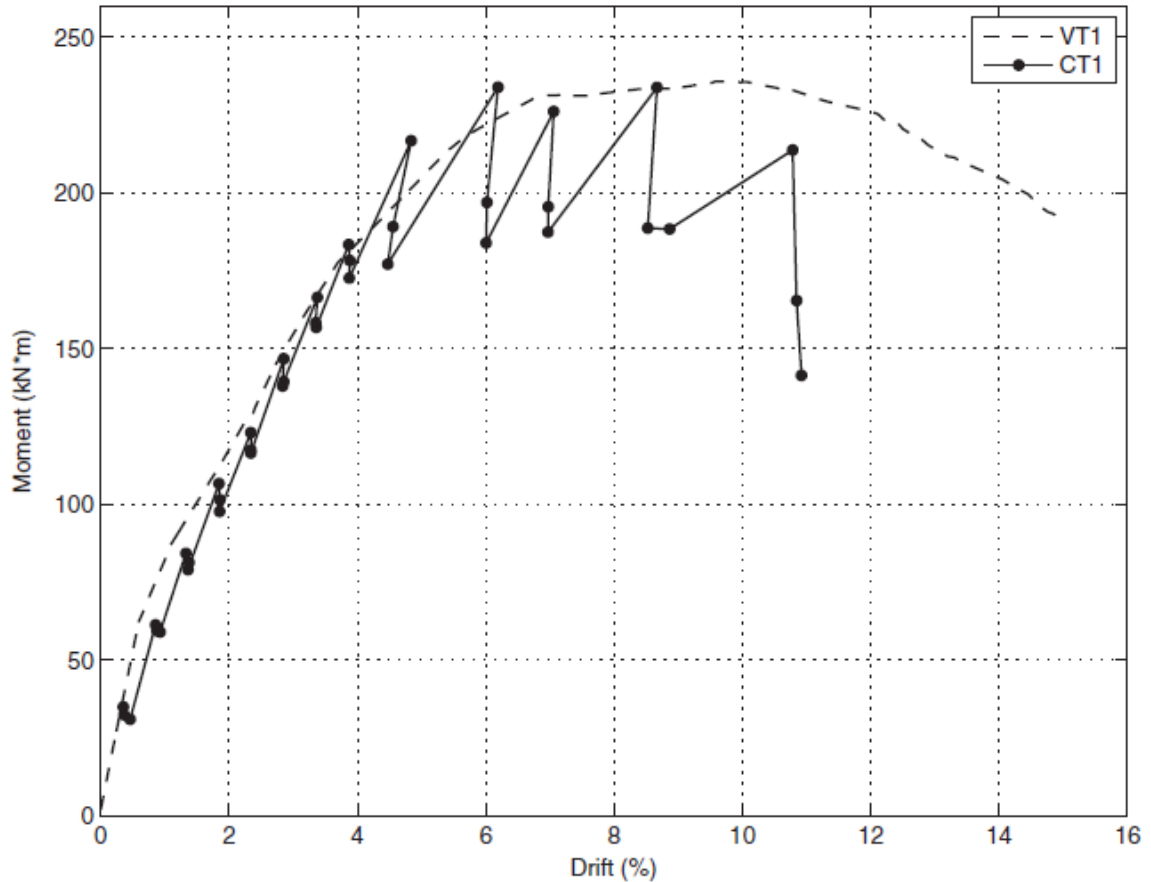


Figure 22. Response comparison between VT2 and CT1

The onset of degradation in the connection is important because it indicated a decrease in elastic behavior and the initiation of a loss of fixity in the connection (i.e., onset of pinching in the hysteresis response). For this work, the onset of degradation was quantified as the drift step at which the moment generated in the connection obviously decreased on each repeated displacement cycle at that same drift level. To evaluate the onset of this damage state, the moment-drift envelopes for both specimens in each direction are plotted in Figure 23, and the first occurrence of permanent degradation in

the cyclic moment carrying ability of the caps is identified at the delineated drift levels. Initial degradation began at drift levels of about 1.2 and 2.0%, for CT1 and CT2, respectively. This drift level for CT1 is the same drift level at which interior crushing occurred in VT2, indicating that loss of fixity may be associated with interior crushing of the concrete near the tip of the embedded pile. Further, the delayed onset of this degradation in CT2 may be caused by the presence of the additional U-bar in CT2 and the subsequent effect this U-bar has on crushing in this region. Also, as can be observed in Figure 23, the effects of including an interior U-bar near the tip of the embedded pile goes beyond just delaying the onset of degradation: CT2 was stiffer and had a higher ultimate capacity than CT1 (247 kN m versus 235 kN m).

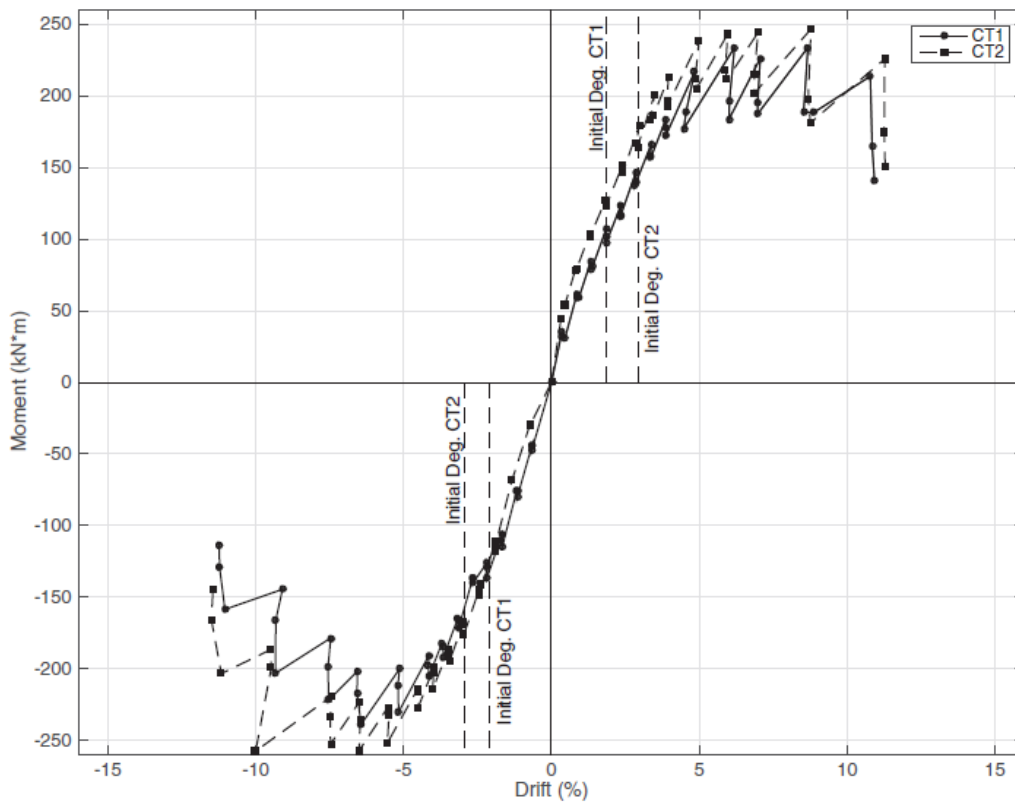


Figure 23. Cyclic envelopes

Proposed Design Methodology

A design methodology for CFT to concrete pile-cap connections was developed based on the results of both phases of this research. The design methodology presented in this paper is for the connection only, and it presumes that the initial design of the CFT and bridge bent to support global gravity and lateral loads have been completed. Thus, the size of the CFT and the general dimensions and global reinforcing scheme of the pile cap will be known prior to designing the connection details. The intent of this guide is to provide adequate embedment of the CFT in the concrete cap to eliminate crushing of the cap concrete immediately adjacent to the CFT, as well as to provide the additional longitudinal and transverse reinforcement needed to confine this region of the connection. The connection design consists of (1) determining the moment demand to be transmitted through the connection, often corresponding to the plastic-moment capacity of the CFT; (2) setting the required embedment depth of the CFT based on this moment demand; (3) sizing the U-bars and designating required locations; and (4) determining the required transverse reinforcement. Each of these steps is discussed in further detail in the following sections.

Determining Plastic-Moment Capacity of CFT

Using the plastic-moment capacity of the CFT as the design demand for the connection, its capacity, M_p , is calculated using the AISC plastic-stress distribution method (AISC 2011), because this method was shown by Bruneau and Marson (2004) and Lehman and Roeder (2012) to provide an efficient and accurate means of predicting this capacity. Using this method, the capacity is obtained by first assuming that the steel

has fully yielded in compression and tension, that the concrete carries no tension, and that the compressive stress in the concrete is uniform and equal to 95% of the unconfined compressive strength of the concrete, f'_c . Capacity is then solved by enforcing equilibrium across the CFT cross section. It is important to accurately predict this capacity, because it will be used as the maximum moment demand on the connection, M_u , and will thus be used to set the embedment depth and size the U-bar reinforcement.

Embedment Length

The embedment length of the CFT (L_{emb}) is set such that the stress in the concrete adjacent to the CFT does not exceed the factored bearing capacity of the confined concrete in this region, which in terms of stress can be expressed as the product $\phi_b f_u$, where ϕ_b is the bearing strength reduction factor and f_u is the ultimate bearing stress. The ultimate bearing stress of the confined concrete can be expressed as the unconfined compression strength, f'_c , times a confinement factor, α .

A relationship between the factored bearing capacity of the confined concrete and embedment length can be developed by enforcing moment equilibrium in the connection using the simplified mechanics model shown in Figure 24.

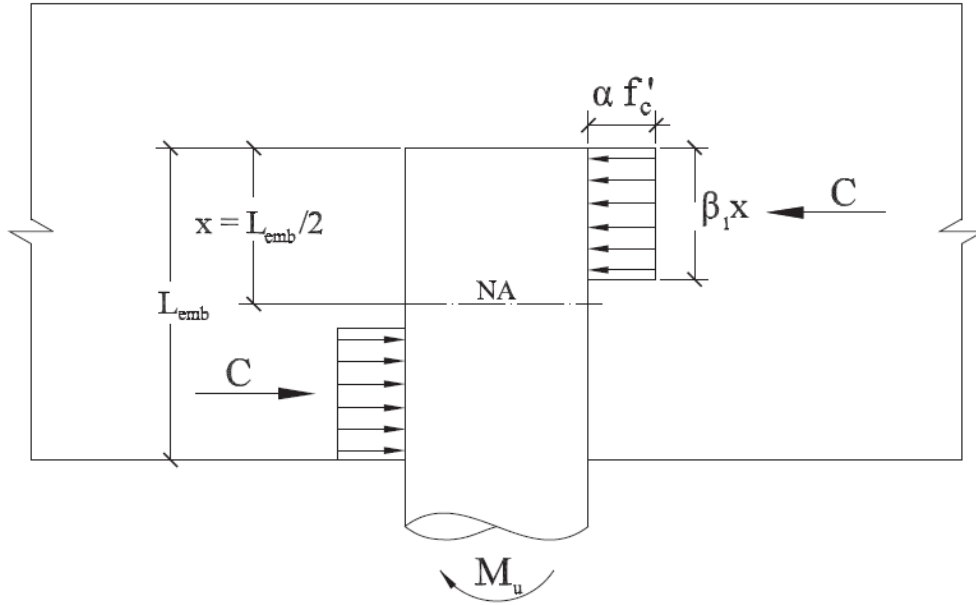


Figure 24. Simplified mechanics in pile cap

Equation 1.
$$M_u = \phi_b \alpha f'_c \beta_1 D \frac{L_{emb}^2}{2} \left(1 - \frac{\beta_1}{2}\right)$$

Equation 2.
$$\phi_b f_u = \phi_b \alpha f'_c = \frac{2 \cdot M_u}{D \beta_1 \left(1 - \frac{\beta_1}{2}\right) L_{emb}^2}$$

The required embedment depth can be obtained from this equation.

Equation 3.
$$L_{emb} \geq \sqrt{\frac{2 \cdot M_u}{D \beta_1 \left(1 - \frac{\beta_1}{2}\right) \phi_b \alpha f'_c}}$$

where D is the diameter of the CFT; and $\phi_b = 0.7$, which is the strength reduction factor for bearing on concrete prescribed by AASHTO 5.5.4.2 (AASHTO 2010); and β_1 is a

parameter for determining the depth of a rectangular stress block that reasonably approximates the actual parabolic stress distribution of concrete in compression. This parameter was empirically derived for the analysis/design of reinforced concrete beams to account for variations in the stress–strain response of different concretes, and in the current American Concrete Institute (ACI) methodology decreases with increasing compressive strength, because concrete typically becomes stiffer and more brittle with increasing compressive strength. In current ACI 318 (ACI 2011) provisions, β_1 is prescribed to be 0.85 for concretes up to 30 MPa, decreasing at a rate of 0.08 for each increase of 10 MPa, with a lower limit of 0.65. Although this parameter was originally developed for compression zones in reinforced concrete beams, it proved to be an adequate means of approximating the stress distribution in this case.

The α factor in this equation is equal to 1.8 and is included to amplify the unconfined compressive strength in this region to account for the effects of confinement. This parameter was empirically derived with damage data from the Phase I and Phase II efforts discussed in this paper, and in particular it was calibrated such that a bearing failure would be expected to occur at the moments associated with the external crushing damage state observed in the test specimens. Specifically, α was calibrated so that moment calculated using Equation 1 (assuming $\phi_b = 1.0$) closely matched the observed moment in which external crushing was observed to occur. Once the embedment depth is set, the connection should be evaluated to ensure that punching shear will not be an issue.

U-Bar Size and Configuration

U-shaped reinforcing bars are included in the connection design to assist in carrying the loads exerted on the cap in this region and to confine the concrete adjacent to the CFT. These U-bars are to be included near the tip of the embedded pile and at the bottom of the cap near the CFT embedment location [as seen in Figure 15(b)]. They are to be sized to carry 30% of the compressive forces developed in the concrete cap due to the moment demand exerted by the CFT, which are calculated using the simple mechanics model presented in Figure 24. The assumption that the U-bars are designed to carry 30% of this load rather than the full amount is empirically derived and is justified because the simplified model (1) ignores the longitudinal steel already included in the cap for the global response, (2) ignores other load-carrying mechanisms conservatively not considered in this model (e.g., longitudinal reinforcing steel present in the cap for global bending), and (3) neglects the effects of the increased moment arms that these U-bars have relative to the resultant compressive forces. Thus, the required cross-sectional area of steel, A_s , for the U-bars can be calculated with the following equation:

$$\text{Equation 4.} \quad A_s = 0.3 \frac{\varphi_b \alpha f'_c \beta_1 (L_{emb}/2) D}{f_y} = 0.3 \frac{M_u}{L_{emb} \left(1 - \frac{\beta_1}{2}\right) f_y}$$

where f_y is the yield stress of the U-bar steel.

Transverse Reinforcement

The transverse reinforcement for this connection is to be sized/detailed according to Section 5.10.11.4.1d of AASHTO LRFD Bridge Specifications (AASHTO 2010),

which specifies the transverse reinforcement for core confinement at plastic-hinge zones in pile bents, because the demands exerted on these connections are similar to the demands exerted in the connections discussed in this paper. For rectangular sections, this section of code provides two limits for the required area of transverse steel, A_{sh} , as follows:

$$\text{Equation 5.} \quad A_{sh} \geq 0.3 \cdot s \cdot h_c \cdot \frac{f'_c}{f_y} \cdot \left(\frac{A_g}{A_c} - 1 \right)$$

$$\text{Equation 6.} \quad A_{sh} \geq 12 \cdot s \cdot h_c \cdot \frac{f'_c}{f_y}$$

where s is the spacing of the transverse reinforcement and should not exceed 100 mm; and h_c is the height of the confined core, which in this connection should be taken as height of the cap less the specified clear cover. This area of confinement is to extend one-half the cap height beyond the pile in each direction.

Discussion

Although not all parameters of this design methodology were specifically exercised in the experimental research discussed in this paper (e.g., transverse reinforcement detailing requirements), it is important to note that the test specimens that met the minimum requirements of this methodology did not fail prematurely due to cap damage (e.g., external crushing, cap splitting). The proposed design methodology provides a good starting point for the design of CFT to concrete pile-cap connections;

however, additional research is required to further develop this methodology and verify its efficacy for all possible cap configurations and demands.

Summary and Conclusions

Concrete-filled steel tube piles connected at the top by a concrete pile cap in bridges have been found to be a very efficient bridge support system that offers low initial cost, short construction time, a robust force-deflection behavior, and a long service life. Although the response of this system under gravity loads is well understood, the response of this system under extreme lateral loads is difficult to reliably predict. In particular, the behavior of the connection between the CFT pile and the concrete pile cap is especially complex and difficult to analyze. This connection was the focus of the research presented in this paper.

In this research, a total of 11 CFT pile-to-pile cap connections were tested, five during Phase I and six during Phase II. All of the connections were tested until failure under combined axial and lateral loads. Nine of the specimens were tested under monotonic loading, providing general information on limit states, ultimate loads, and post-failure ductility. Two additional tests were completed using a cyclic-loading scheme to capture the performance of the connections under multiple cycles of fully reversed, increasing load. A preliminary design guide was developed based on the results of the tests. The following conclusions can be drawn from this investigation:

1. Four key limit states were observed in this type of connection: (1) formation of a plastic hinge in the CFT, (2) interior and exterior crushing of the concrete in the cap, (3) yielding of the longitudinal

reinforcement in the cap, and (4) splitting of the concrete cap. The latter three limit states would result in loss of fixity of the connection, resulting in reduced energy dissipation.

2. The cap limit states, and the subsequent cyclic degradation and loss of fixity in the connection, may be avoided with an appropriate embedment length and a simple reinforcing scheme consisting of U-bars encircling the CFT and tightly spaced transverse reinforcement in the connection region.
3. The initial degradation in the cyclic response of the connections was most likely caused by crushing of the concrete near the tip of the embedded pile. The inclusion of U-bars near the tip of the pile delayed the onset of this damage state.
4. A preliminary design guide for the connection was developed that determines the required embedment length, as well as the necessary U-bar size and configuration, and transverse reinforcement details. The specimens tested in this research that met the requirements of this design methodology did not fail due to premature damage of the concrete caps.

Although this research provides useful information regarding the behavior and design of CFT to concrete pile-cap connections, further research is required to more fully characterize this behavior and further develop the proposed design methodology. For example, several aspects of the design methodology rely on empirical assumptions that

may not be valid for all possible cap configurations, thus further testing and/or further analytical modeling should be conducted to validate/modify these assumptions. The authors are currently conducting such research. It should also be noted that while the focus of this research was on the seismic performance of this system, this system/methodology may be used to design elements to resist other lateral loads, such as wind or ice loading, which may control in areas of low seismicity.

Acknowledgements

The authors acknowledge the financial support for this project provided by the Montana Department of Transportation (MDT) and the Research and Innovative Technology Administration (RITA) of the U.S. DOT through the Western Transportation Institute at Montana State University (MSU). We also recognize and thank the MDT Research Section and the technical panel for their participation in this project. Several students at MSU have participated in this research, and their contributions have been very beneficial. Specifically, the work of Tim White, Josh Norquist, and Bethany Kappes was greatly appreciated.

References

- AASHTO. (2010). *AASHTO LRFD bridge design specifications, customary U.S. units*, 5th Ed. with 2010 Interim Revisions, Washington, DC.
- ACI (American Concrete Institute) (2011). "Building code requirements for structural concrete." *ACI 318*, American Concrete Institute, Farmington Hills, MI.
- AISC. (2011). *Steel construction manual*, American Institute of Steel Construction, Chicago.
- Bruneau, M., and Marson, J. (2004). "Seismic design of concrete-filled circular steel bridge piers." *J. Bridge Eng.*, 10.1061/(ASCE)1084-0702(2004)9:1(24), 24–34.
- Hsu, H. L., and Lin, H.W. (2006). "Improving seismic performance of concrete-filled tube to base connections." *J. Constr. Steel Res.*, 62(12), 1333–1340.
- Kappes, L., Berry, M., and Stephens, J. (2013). "Performance of steel pipe pile-to-concrete cap connections subject to seismic or high transverse loading: Phase III confirmation of connection performance." *FHWA/MT-13-001/8203*, Montana Dept. of Transportation, Montana State Univ., Bozeman, MT.
- Kingsley, A. (2005). "Experimental and analytical investigation of embedded column base connections for concrete filled high strength steel tubes." M.S. thesis, Civil and Environmental Engineering, Univ. of Washington, Seattle.
- Kingsley, A., Williams, T., Lehman, D., and Roeder, C. (2005). "Experimental investigation of column-to-footing connections for high strength vanadium steel concrete filled tube construction." *Int. J. Steel Struct.*, 5(4), 377–387.
- Lee, J. (2011). "Experimental investigation of embedded connections for concrete filled tube column connections to combined axial–flexural loading." M.S. thesis, Univ. of Washington, Seattle.
- Lehman, D. E., and Roeder, C. W. (2012). "Foundation connections for circular concrete-filled tubes." *J. Constr. Steel Res.*, 78, 212–225.
- Marson, J., and Bruneau, M. (2004). "Cyclic testing of concrete-filled circular steel bridge piers having encased fixed-based detail." *J. Bridge Eng.*, 10.1061/(ASCE)1084-0702(2004)9:1(14), 14–23.
- McFarlane, I. S. (2006). "Non-linear finite element analysis of concrete filled high strength steel tubes: Structural performance and sensitivity to design parameters." M.S. thesis, Univ. of Washington, Seattle.

- Moon, J., Lehman, D. E., Roeder, C. W., and Lee, H.-E. (2013). "Strength of circular concrete-filled tubes with and without internal reinforcement under combined loading." *J. Struct. Eng.*, 10.1061/(ASCE)ST.1943-541X.0000788, 139(12), 04013012.
- Moon, J., Roeder, C. W., Lehman, D. E., and Lee, H. E. (2012). "Analytical modeling of bending of circular concrete-filled steel tubes." *Eng. Struct.*, 42, 349–361.
- O'Neill, K. (2011). "Experimental investigation of circular concrete filled steel tube geometry on seismic performance." M.S. thesis, Univ. of Washington, Seattle.
- Roeder, C. W., Lehman, D. E., and Bishop, E. (2010). "Strength and stiffness of circular concrete-filled tubes." *J. Struct. Eng.*, 10.1061/(ASCE)ST.1943-541X.0000263, 1545–1553.
- Rollins, K., and Stenlund, T. (2010). "Final report: Laterally loaded pile cap connections." *UT-10.16*, Utah Dept. of Transportation, Salt Lake City, UT.
- Silva, P. F., and Seible, F. (2001). "Seismic performance evaluation of cast-in-steel-shell (CISS) piles." *ACI Struct. J.*, 98(1), 36–49.
- Silva, P., Sritharan, S., Seible, F., and Priestly, M. (1999). *Full-scale test of the Alaska cast-in-place steel shell three column bridge bent*, Univ. of California, San Diego, La Jolla, CA.
- Stephens, J., and McKittrick, L. (2005). "Final report: Performance of steel pipe pile-to-concrete bent cap connections subject to seismic or high transverse loading." *FHWA/MT-05-001-8144*, Montana Dept. of Transportation, Bozeman, MT.
- Stephens, M. T., Berg, L., Lehman, D. E., and Roeder, C. W. (2014). "Seismic design of circular concrete filled tube bridge pier connections for accelerated bridge construction." *ASCE/SEI Structures Congress*, Boston, MA.
- Williams, T. (2007). "Experimental investigation of high strength concrete filled steel tubes in embedded column base foundation connections." M.S. thesis, Civil and Environmental Engineering, Univ. of Washington, Seattle.

CHAPTER FOUR - ANALYSIS METHODOLOGY FOR CONCRETE-FILLED
STEEL PIPE PILES TO CONCRETE CAP CONNECTIONS

Contribution of Authors and Co-Authors

Manuscript in Chapter 4

Author: Lenci Kappes

Contributions: Designed and built laboratory test specimens. Conducted load testing of model pile-to-pile cap connections, including the collection and analysis of test data. Introduced, derived, and developed moment-rotation algorithm. Wrote the first draft of the manuscript.

Co-Author: Dr. Michael Berry

Contributions: Assisted in concept development for the laboratory test series. Provided technical expertise on data analysis and development of proposed algorithm. Provided feedback on early drafts of the manuscript.

Co-Author: Dr. Jerry Stephens

Contributions: Assisted in concept development for the laboratory test series. Provided technical expertise on data analysis and development of proposed algorithm. Provided feedback on early drafts of the manuscript.

Manuscript Information Page

Lenci Kappes, Michael Berry, Jerry Stephens

Status of Manuscript:

- Prepared for submission to a peer-reviewed journal
- Officially submitted to a peer-review journal
- Accepted by a peer-reviewed journal
- Published in a peer-reviewed journal

Abstract

This study focused on the development of an analysis methodology for predicting the ultimate seismic capacity of concrete-filled steel pipe pile (CFT) to reinforced concrete pile cap connections. This methodology is similar in form to a moment-curvature analysis. It begins by discretizing the connection elements into individual fibers and then imposing a rotation on the connection. The strains in the individual fibers are then obtained from this rotation based on strain-displacement compatibility, and attendant stresses are determined using nonlinear material responses. Finally, the location of the neutral axis is iteratively found by imposing equilibrium on the connection. Once developed, this methodology was calibrated/evaluated with a series of experimental tests. This methodology proved to be an efficient and effective means for predicting the ultimate capacity of CFT to concrete pile cap connections. The average ratio of measured to predicted capacities was 0.99 with a coefficient of variation of 5.4 percent for the nine test specimens in the test series.

Introduction

An accelerated bridge construction (ABC) technique commonly used by several state departments of transportation for short and medium span bridges uses concrete-filled steel tube (CFTs) piles as the primary support system. This system consists of a series of circular CFT piles connected at the top by a concrete pile cap (Figure 25). Following this technique, the steel pipe piles are driven to their required depth and are terminated above grade just below the deck level. The formwork for the concrete pile cap is then placed around the ends of the piles, and the reinforcing cage for the cap is tied

within this formwork. Subsequently, concrete is placed in the hollow steel tubes and the cap formwork. Following this approach, the steel piles extend into the cap; they are not terminated at the interface, as is often done. This method simplifies construction and helps facilitate a positive connection between the CFT and concrete cap.

Using CFTs in this manner helps to reduce construction times, as the steel pipe pile serves as the formwork for the columns, and can provide structural capacity while the concrete cures and gains strength. The advantages of using CFTs in this application go beyond efficiency, in that CFTs have been shown to have enhanced capacity and ductility (Marson and Bruneau, 2004). This enhanced performance is due to a symbiotic relationship between the concrete and steel. That is, the concrete inside the steel tube not only adds stiffness and strength to the cross section, it also delays the onset of buckling in the steel tube. In turn, the steel tube acts to confine the concrete, enhancing its compressive strength and ultimate strain.

In order to take full advantage of the enhanced performance characteristics of the CFTs, the reinforced concrete cap must be strong enough to support formation of a plastic hinge in the CFT under extreme lateral loads. This failure mechanism is preferable to failure of the concrete cap, due to the enhanced energy-dissipating characteristics of the CFT (i.e. more robust hysteresis response under lateral loads).

The structural performance of CFTs under seismic excitations has been well-established through a significant amount of research conducted in the past decade (Moon et al., 2012, 2013; Roeder et al., 2010; Bruneau and Marson, 2004; McFarlane, 2006). However, the performance of the connections between CFTs and various reinforced

concrete elements has not been as thoroughly investigated, and thus has been the focus of several recent research endeavors (Hsu and Lin, 2006; Marson and Bruneau, 2004; Silva et al. 1999; Silva and Seible, 2001; Rollins and Stenlund 2010; Kingsley, 2005; Kingsley et al. 2005; Williams 2007; Lee 2011; O'Neill, 2011; Lehman and Roeder, 2012, Stephens et al., 2014). This research has resulted in a better understanding of the interactions between concrete and CFT elements, but a majority has not specifically addressed connections between CFTs and concrete pile caps.

Furthermore, many of the CFT-to-pile cap connection details currently used in practice are extremely congested and difficult to construct, and their performance, notably during seismic events, are somewhat uncertain. In order to advance the state of practice, research on such connections was recently conducted at Montana State University (MSU) (Stephens and McKittrick, 2005; Kappes et al., 2013; Kappes et al., 2016). This research involved testing a series of 11 connection specimens, and concluded with a preliminary design methodology that included the use of U-shaped reinforcing bars encircling the end of the embedded CFT (Figure 25). This reinforcing scheme was shown to be a very effective and efficient method for reinforcing this connection and forcing the desired failure mechanism. That being said, this preliminary research stopped short of developing a reliable analysis methodology capable of accurately modeling/quantifying the complex interactions between the CFT, the concrete, and the reinforcing steel within this connection. Appropriately quantifying these complex interactions is a necessary step for the development of a robust/efficient design

methodology capable of predicting the behavior/capacity of CFT to pile cap connections under varying design parameters/constraints.

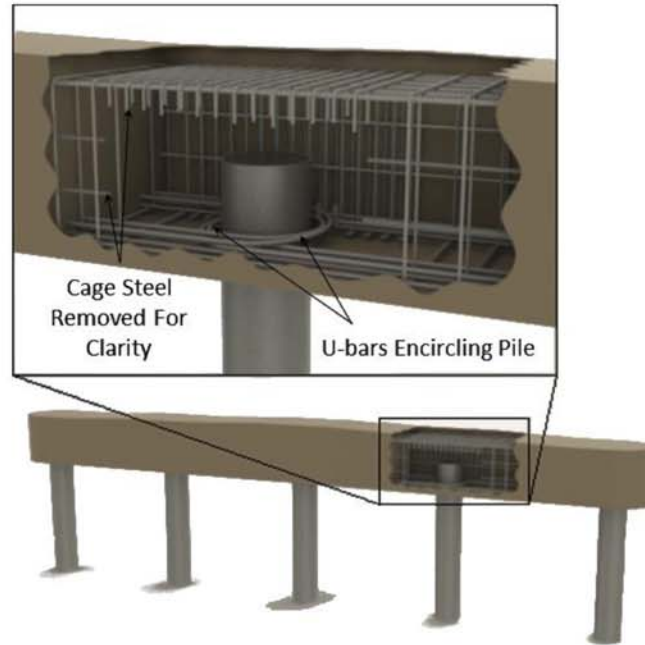


Figure 25. Typical bridge bent with U-bar reinforcing steel

The research discussed herein focused on the establishment and verification of a simple analysis methodology capable of predicting the ultimate strength of CFT to concrete pile cap connections. The relative simplicity of the proposed analysis method, in contrast to a full 3D finite element model, is beneficial considering the method can be readily applied or duplicated with standard computer software, and has minimal processing time.

In this paper, the proposed analysis methodology is presented first, followed by an evaluation of this modeling strategy with experimental data. The paper concludes with a summary of the work performed and a discussion of future work that can be drawn from this research.

Proposed Analysis Methodology

In the proposed analysis methodology, the external moment and shear from the pile (M_{conn} and V_{conn}) are resisted by the concrete and U-bars immediately surrounding the pile, as shown in Figure 26. The reactive forces in the concrete consist of components acting normal to the surface of the pile, friction forces acting parallel to the surface between the steel and concrete, and interface shear at the tip of the pile. The analysis methodology is implemented similar to a conventional moment-curvature analysis typically used for beams and columns. The proposed methodology begins by discretizing the surface of the concrete surrounding the pile into individual fibers, and then imposing a rigid-body rotation to the connection region. Based on this rotation, a compatibility relationship is used to determine the strains in the concrete fibers and U-bar reinforcing steel. Constitutive relationships are then used to determine the subsequent stresses in the materials, and ultimately to determine the resultant concrete and steel forces. Equilibrium is then enforced between the internal forces and external moments and shears. The following subsections discuss each of these steps (i.e., enforcement of compatibility, constitutive relationships, and equilibrium) in greater detail.

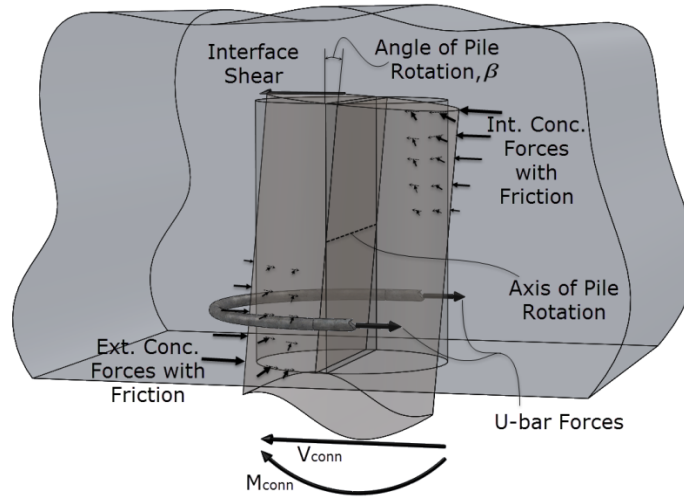


Figure 26. Imposed rotation and resultant internal stresses

Compatibility

A compatibility relationship relating a pile rotation to radial concrete strain and steel strain is necessary for the proposed moment-rotation methodology. In this methodology, the surface of the cap surrounding the pile is first discretized vertically into n_{vert} subdivisions (indexed with i), and radially into n_{rad} subdivisions (indexed with j), as seen in Figure 27. The embedded pile is assumed to be rigid, and a rotation of the pile is assumed to impose a linear distribution of displacements along the length of the embedment, with an assumed axis of rotation in which there is no displacement. For an imposed rotation of angle β and assumed location of the axis of rotation ($d_{rot.axis}$), the lateral displacement at a given layer (Δ_i) a distance c_i from the axis of rotation can be calculated as follows.

$$\Delta_i = c_i \cdot \tan \beta \quad (\text{Eq 1})$$

The lateral strain, ε_i , in the surrounding concrete at this layer can then be estimated from this displacement by dividing it by an assumed effective length factor, L_{eff} .

$$\varepsilon_i = \frac{\Delta_i}{L_{eff}} \quad (\text{Eq 2})$$

The radial strain distribution in the concrete along the surface of the pile at this layer can then be approximated by transforming the lateral strains with the following equation:

$$\varepsilon_{ij} = \varepsilon_i \cdot \sin^2(\theta_j) = \frac{\Delta_i \cdot \sin^2(\theta_j)}{L_{eff}} = \frac{c_i \cdot \tan \beta \cdot \sin^2(\theta_j)}{L_{eff}} \quad (\text{Eq 3})$$

where, the j index refers to a radial subsection along the surface of the pile, and θ_j is the angle indicated in the figure.

The longitudinal strains in the U-bar reinforcing steel are estimated from the same imposed rotation as used for the concrete by first calculating the displacement at the location of the U-bar, Δ_{ubar} , and then dividing this displacement by an assumed effective length factor, $L_{eff,ubar}$, with the following equation. This relationship is shown in the following equation for which the k index refers to each U-bar in the connection region and $c_{ubar,k}$ is the distance from the axis of rotation to each indexed U-bar.

$$\varepsilon_{ubar,k} = \frac{\Delta_{ubar}}{L_{eff,ubar}} = \frac{c_{ubar,k} \cdot \tan \beta}{L_{eff,ubar}} \quad (\text{Eq 4})$$

These radial strains in the concrete and the longitudinal strains in the U-bars are used to estimate the stresses, and ultimately the forces exerted on the surface of the

embedded pile, as will be discussed in the following sections. The effective length factors are empirically derived in a later section.

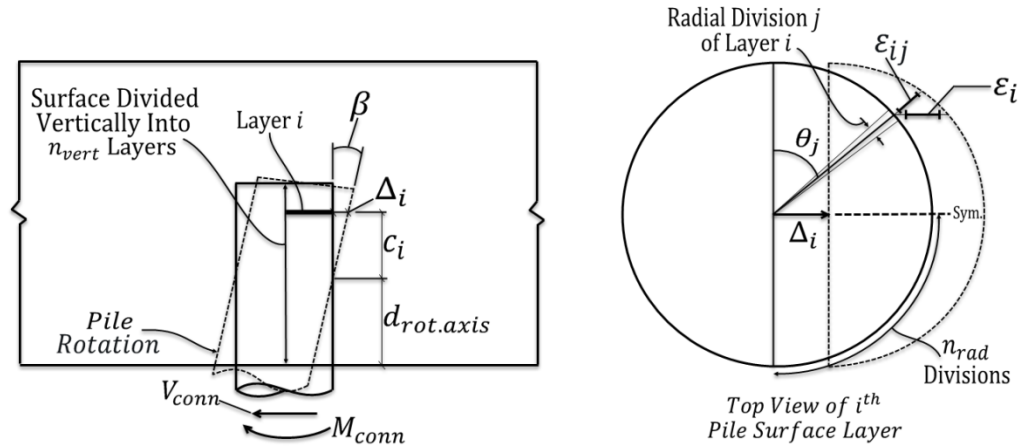


Figure 27. Pile rotation, displacements, and radial strain distribution

Constitutive Relationships

The concrete model proposed by Mander et al. (1988) is used in the proposed methodology to model the stress-strain response of the concrete immediately surrounding the embedded pile (Figure 28). The Mander model provides a general stress-strain model useful for a variety of applications, such as providing a concrete confinement relationship for both circular and rectangular cross-sections. The formulation of the model relates the confinement of the concrete to the strain energy capacity of the surrounding steel. More specifically, the Mander concrete model is based on the premise that the energy stored in the surrounding steel, as the concrete attempts to strain outward against the steel due to a compressive axial load, is available to balance the energy stored in the compressed concrete (Marsh et al., 2014). The Mander concrete model is very general in its formulation, providing methods to adjust the lateral confining stress effects based on the

shape of the section, as well as the size and configuration of the confining steel reinforcement.

For the proposed methodology, the various parameters in this model were selected based on recommendations by Marsh et al. (2014) and Mander et al. (1988). The concrete within the transverse stirrup reinforcement is assumed to be confined, and thus has an increased ultimate stress (f'_{cc}) and ultimate strain (ϵ_{cu}); whereas, the cover concrete outside of the stirrups is assumed to be unconfined. Guidance for the remaining terms (f'_{ce} , ϵ_{co} , ϵ_{sp} , and ϵ_{cc}) defining the concrete material models shown in Figure 28, are based on commonly accepted values and functions identified in Marsh et al. (2014), Mander et al. (1988), and *AASHTO Seismic Guide, 2nd ed.* (2011).

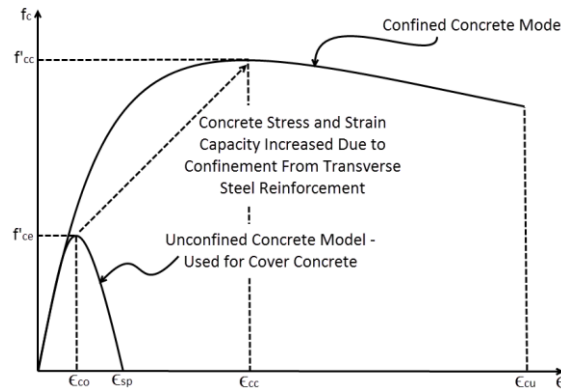


Figure 28. Assumed concrete material model (Mander et al., 1988)

The stress-strain response of the steel is represented using the nonlinear model shown in Figure 29, which has components to account for the yield plateau and the onset of strain hardening (Chen and Duan, 2014; Barker and Puckett, 2013). The yield stress (f_y), the ultimate stress (f_u), and strain limits for the steel (ϵ_y , ϵ_{sh} , ϵ_{su}^R , and ϵ_{su}) are

selected in accordance to the *AASHTO Seismic Guide, 2nd ed.* (2011). Similar to the concrete model, this steel material model is commonly used for bridge design, and these important modeling assumptions are consistent with the current state of practice.

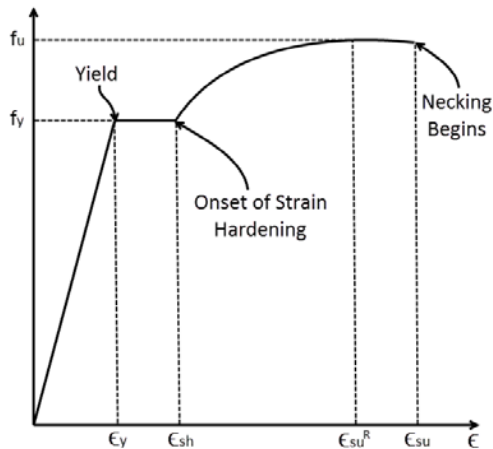


Figure 29. Assumed stress-strain response of U-bar

Forces and Equilibrium

In the proposed methodology, the external moment and shear are assumed to be resisted by several internal forces, as was shown in Figure 26. These forces consist of radial concrete forces acting normal to the surface of the embedded pile, friction forces acting parallel to the surface of the pile, interface shear at the tip of the pile, and the forces from the U-bars encircling the pile. This section provides an overview of how these forces are calculated, and how equilibrium is enforced in the proposed methodology. To facilitate this, the effective surfaces in the cap that resist the rotation of the pile are shown in Figure 30, along with the differential areas and key dimensions that are used for calculating the above mentioned forces. The U-bar forces are also shown in

this figure, along with the interface shear force between the top of the embedded pile and the concrete cap.

Radial Concrete and Friction Forces. As discussed previously, the radial concrete stresses are calculated for a given rotation using the strains obtained from the assumed compatibility relationship (Eq 3) and concrete material model (Figure 28). The forces resulting from these radial concrete stresses are then calculated by multiplying these stresses (σ_{ij}) by the area (A_{ij}) over which they act, as is shown in differential form (Eq 5) and discrete (Eq 6) form below. Recall that subscripts i and j refer to the discretized vertical layers and discretized radial subsections, respectively, of the connection region. Additionally, these forces act on two separate surfaces labeled the exterior and interior compression surfaces as shown in Figure 30.

$$dF = \sigma_{rad} \cdot dA \quad (\text{Eq 5})$$

$$F_{ij} = \sigma_{ij} \cdot A_{ij} \quad (\text{Eq 6})$$

The resultant radial concrete force can then be obtained by accumulating these forces over the surface of the embedded pile. The magnitudes of the surface-friction forces ($F_{surf-frict,ij}$ and $F_{surf-frict,ij}$ in Figure 30) are obtained as the product of the radial forces and the effective coefficient of friction between the pile steel and the cap concrete, μ , assuming impending slip of the surfaces when the ultimate strength of the connection is approached. The radial concrete forces and the surface friction forces can be decomposed into components acting in the longitudinal (x-direction) and transverse directions (y-direction) for a given layer, as shown in Figure 31. The forces in the longitudinal direction are of particular interest in the proposed methodology as they resist

the external moment (M_{conn}) and shear (V_{conn}), while the forces in the transverse direction may be useful in the design of the transverse reinforcement, although this is beyond the scope of this paper and will be investigated in a later study.

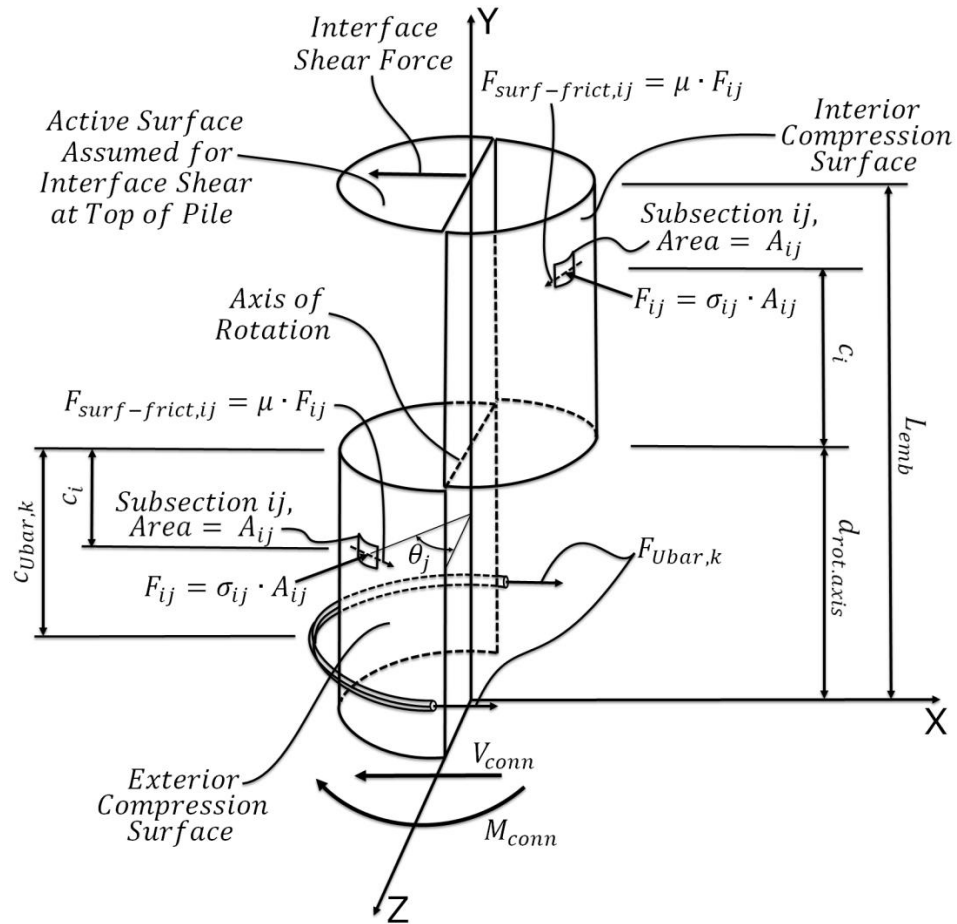


Figure 30. Effective areas and dimensions

The resultant forces in the x-direction from the radial concrete stresses (F_{conc_x-dir}) and friction forces (F_{frict_x-dir}) are obtained by accumulating the x-component of the differential forces over the surface of the embedded pile, as follows.

$$F_{conc_x-dir} = \int_A \sin \theta \cdot dF = \sum_{i=1}^{n_{vert}} \sum_{j=1}^{n_{rad}} \sin \theta_j \cdot F_{ij} \quad (\text{Eq 7})$$

$$F_{frict_x-dir} = \int_A \mu \cdot \cos \theta \cdot dF = \sum_{i=1}^{n_{vert}} \sum_{j=1}^{n_{rad}} \cos \theta_j \cdot \mu \cdot F_{ij} \quad (\text{Eq 8})$$

The moments around the point of rotation resulting from the radial forces (M_{z_conc}) and friction forces (M_{z_frict}) can be calculated with the following equations.

$$M_{z_conc} = \int_A c \cdot \sin \theta \cdot dF = \sum_{i=1}^{n_{vert}} \sum_{j=1}^{n_{rad}} c_i \cdot \sin \theta_j \cdot F_{ij} \quad (\text{Eq 9})$$

$$M_{z_frict} = \int_A c \cdot \mu \cdot \cos \theta \cdot dF = \sum_{i=1}^{n_{vert}} \sum_{j=1}^{n_{rad}} c_i \cdot \cos \theta_j \cdot \mu \cdot F_{ij} \quad (\text{Eq 10})$$

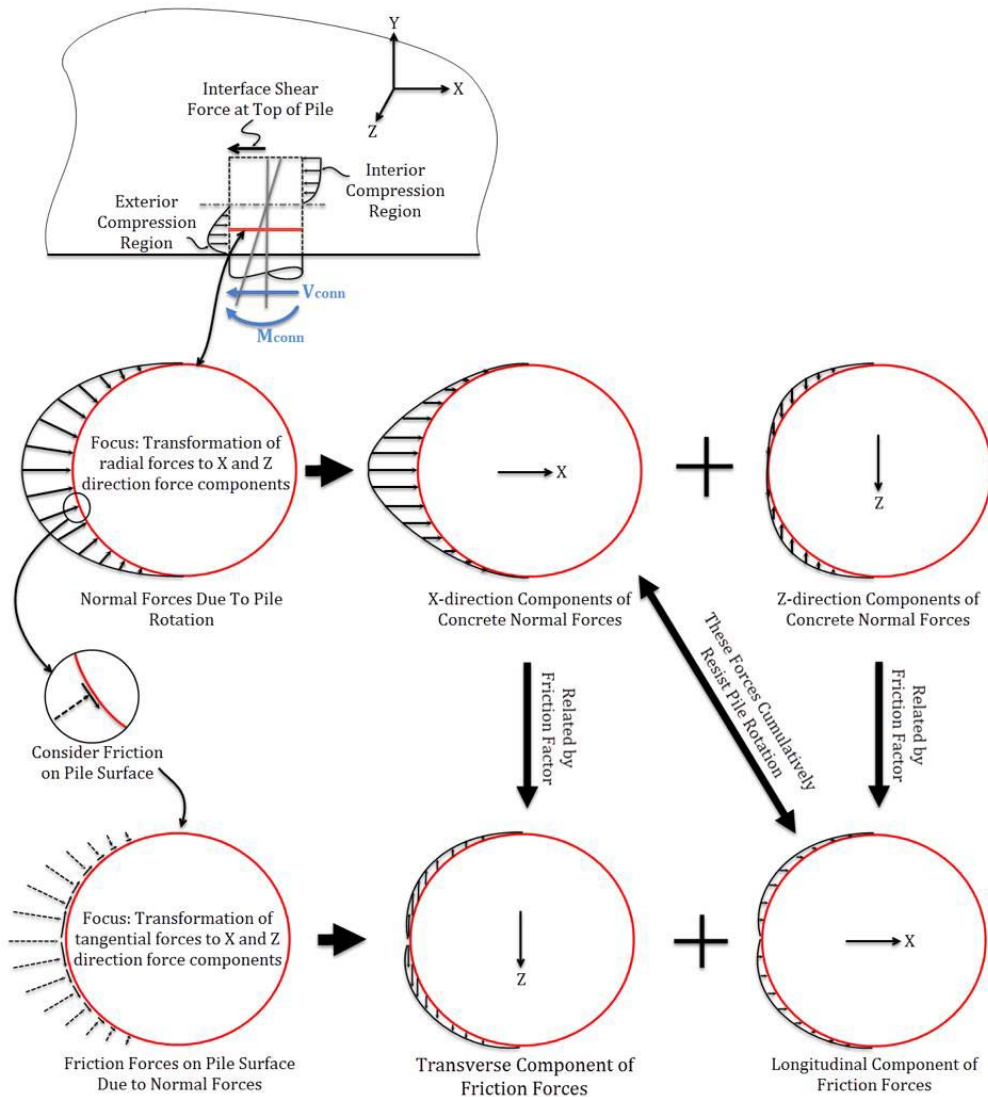


Figure 31. Internal force components

U-Bar Reinforcement Forces. The stresses in the U-bars for a given rotation are calculated using the strains obtained from the compatibility relationship (Eq 4) and steel material model (Figure 29). The forces from the U-bars ($F_{Ubar,k}$) are then calculated from these stresses by multiplying by their respective areas, as is done in the following equation.

$$F_{Ubar,k} = 2 \cdot A_{Ubar,k} \cdot \sigma_{Ubar,k} \quad (\text{Eq 11})$$

The resultant force from the U-bars (F_{Ubars}) is then obtained as follows.

$$F_{Ubars} = \sum_{k=1}^{n_{ubar}} 2 \cdot A_{Ubar,k} \cdot \sigma_{Ubar,k} \quad (\text{Eq 12})$$

Similarly, the moments are calculated with the following equation.

$$M_{z_Ubar} = \sum_{k=1}^{n_{ubar}} c_{Ubar,k} F_{Ubar,k} \quad (\text{Eq 13})$$

The area of the U-bar must be doubled to account for both ends of a single U-bar undergoing strain, introducing the factor of two in Eq 11 and Eq 12.

Interface Shear Force. In this methodology, the interface shear component at the top of the pile ($F_{Interface\ Shear}$) is calculated according to *AASHTO LRFD, 7th ed.*, Article 5.8.4, assuming a concrete area equal to half the area of the cross-section of the pile (Figure 30). Only half of the cross-sectional area is used due to an assumption that under large lateral loads, half of the tip of the pile will be in compression, while the other half will lift away from the tip concrete (thus shear cannot be transferred across this part of the interface). The interface shear force is assumed to be fully engaged as the ultimate strength of the connection is approached. The moment due to the interface shear force can be determined by subtracting the distance to the rotation axis ($d_{rot.axis}$) from the embedment length of the pile in the cap (L_{emb}) as shown in the following equation.

$$M_{z_shear} = F_{Interface\ Shear} (L_{emb} - d_{rot.axis}) \quad (\text{Eq 14})$$

Equilibrium. As stated previously, the internal forces and moments are calculated for an assumed angle of rotation, β , and an assumed rotation axis location $d_{rot.axis}$. These forces, and the resultant moments, must be in equilibrium with the external shear and moment, as shown in the following equations.

$$F_{conc_x-dir} + F_{frict_x-dir} + F_{Ubarx} + F_{Interface\ Shear} = V_{conn} \quad (\text{Eq 15})$$

$$M_{z_conc} + M_{z_friction} + M_{z_Ubar} + M_{z_shear} + V_{conn}d_{rot.\ axis} = M_{conn} \quad (\text{Eq 16})$$

If these forces and moments are not in equilibrium, the assumed rotation angle or axis location must be adjusted accordingly until the system is in equilibrium. A further constraint in this situation is that the external shear and moment are related through an assumed inflection point location, as shown in Eq 17 and Figure 32. This relationship requires a double iterative procedure in which both rotation angle and rotation location are varied accordingly, until equilibrium is met.

$$V_{conn} = \frac{M_{conn}}{d_{pile_infl.}} \quad (\text{Eq 17})$$

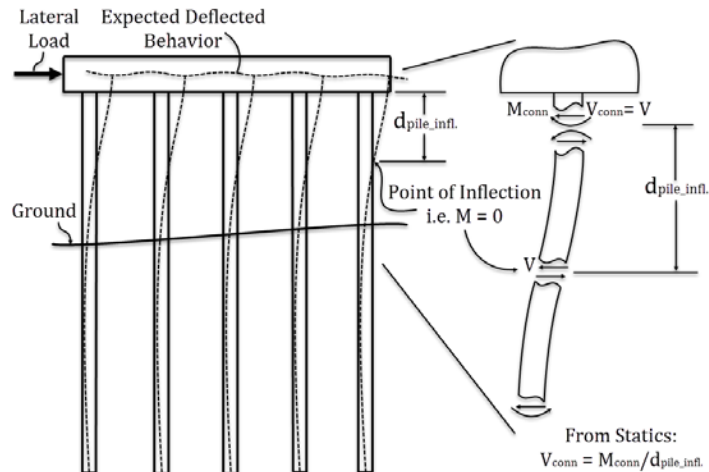


Figure 32. External loads and assumed inflection point

This entire process is carried out for increasing angles of rotation, β , until the ultimate capacity is reached, while recording the moment, rotation, and location of the rotation axis.

Calibration and Evaluation of Proposed Methodology

The experimental tests conducted on CFT pile to pile cap connections at MSU provide a valuable array of data to exercise/calibrate the proposed analysis methodology. In this section, a brief overview of this dataset is provided, followed by a discussion of modeling assumptions and parameter calibration. This modeling strategy is then applied first to a single specimen, and then to the full dataset. The results of this analysis are then discussed.

Experimental Dataset

The research completed at MSU on a series of CFT pile-to-pile cap connections consisted of two main phases. The first phase (Stephens and McKittrick, 2005) consisted

of a total of five tests, and the second phase (Kappes, et al., 2013; Kappes, et al., 2016) tested six additional connection specimens. Two of these test specimens failed through a plastic hinge mechanism in the CFT; thus, nine of these eleven tests are useful for the evaluation of the proposed methodology.

These specimens were approximately half-size models of a typical bridge bent subsection, constructed with CFT piles, joined by a reinforced concrete pile cap. The models were designed to represent an interior section of such a bent, centerline-to-centerline between pile supports; thus, each model consisted of a single pile and an attendant length of pile cap (Figure 33). The CFT-to-pile cap connections were tested so as to generate the deflected shape expected in this subsection of the bent subjected to a lateral load, as shown in Figure 33. A typical test specimen is illustrated in Figure 34.

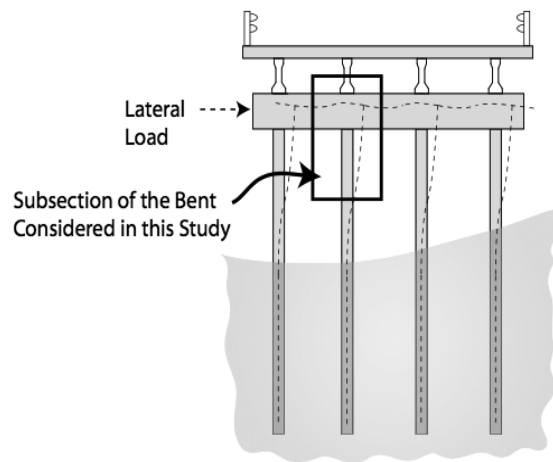


Figure 33. CFT piles and concrete pile cap

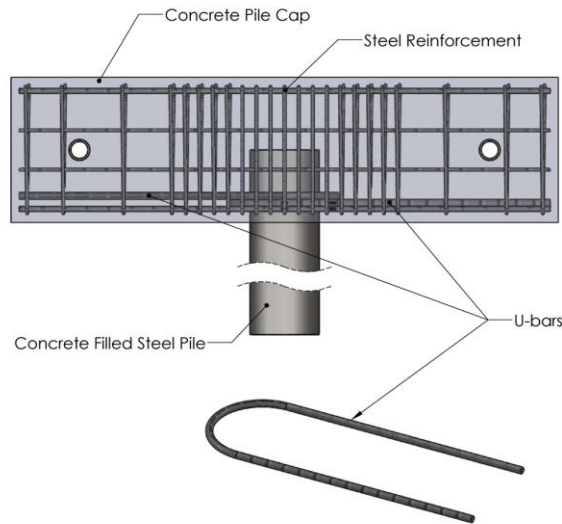


Figure 34. Typical test specimen

Each model was subjected to gradually increasing lateral load applied to the tip of the pile, while the pile cap was held stationary. Coincident with the lateral load, a constant axial force was applied to represent gravity load effects. The majority of the tests consisted of a primary load event for each model, in which the lateral load was monotonically increased until the lateral capacity of the connection was achieved. In some cases, the model was additionally subjected to reversed load cycles, to assess the residual strength and energy dissipation characteristics of the connection. The final two tests incorporated a cyclic loading scheme to compare the effect of the two different load regimes (sequential cycles of increasing full reversed loads, versus single monotonic test to failure). During each test, the load and displacement response of the connection was measured and recorded. Measurements were also made of the strains in the CFT pile and in the cap concrete. In select tests, strains in various bars of the reinforcing cage were also measured.

Connection strength is influenced by a variety of factors related to its configuration, including the embedment length of the pile into the cap, the strength of the concrete, the size and location of any U-bar reinforcement encircling the pile, and the spacing and size of the transverse reinforcement. Table 7 provides a summary of the test specimens and key test parameters for both phases of the research (Phase I – PC test series; Phase II – VT/CT test series).

Application of Modeling Strategy to Dataset and Parameter Calibration

The proposed methodology was implemented in *Python* (Python Software Foundation), and applied to the dataset discussed above to evaluate its effectiveness and to calibrate the key modeling parameters (e.g., μ , L_{eff}). Based on this analysis, it was determined that $\mu=0.55$ was an appropriate value for the coefficient of friction between the concrete cap and the surface of the steel pile, which is consistent with what other researchers have found for this coefficient (Rabbat and Russell, 1985). It was determined that the assumed effective length factors L_{eff} and $L_{eff,ubar}$, did not have a significant effect on the predicted ultimate capacities of the connections; however, and as was expected, they did have a significant effect on the predicted rotations associated with these ultimate capacities. Note that comparing estimated rotations to observed rotations was difficult for this dataset, since rotations of the embedded ends of the piles were not directly measured during testing. For this research, $L_{eff} = 20 \text{ in}$ and $L_{eff,ubar} = 30 \text{ in}$ were used because they provided reasonable estimates of ultimate capacity and estimated pile rotations.

The capacity of each test specimen was estimated using the proposed moment-rotation methodology with the parameters discussed above. Table 8 provides a comparison of the measured and calculated capacities of these specimens. As can be seen in this table, the proposed methodology closely predicts the actual capacity across the wide range of reinforcing schemes (including configurations without U-bars, with U-bars, and with a double set of U-bars), concrete strengths and embedment depths considered in the tests, with an average measured to predicted ratio of 0.99 with a coefficient of variation of 5.4%.

Application to VT2

To further evaluate the proposed methodology and assist in visualizing the resultant forces at play, its application to the VT2 test are reviewed here in greater detail. The VT2 specimen had an embedment length of 11.75 in, a concrete strength of 3.8 ksi, and had two sets of U-bars encircling the pile in the exterior compression region of the connection. The respective size and spacing of the transverse reinforcement was #3 stirrups at 1.75 in.

To illustrate the forces in the connection region, the predicted resultant 3D forces in the connection are shown in Figure 35 for VT2 at 145 ft-kips of applied moment. Additionally, the distribution of forces along the embedment length is shown in Figure 36 at various load stages. In this figure, the total resultant load is shown along with the contributions from the various load carrying mechanisms (i.e. concrete normal force, interface shear, friction, and U-bar force). Also shown in the upper left corner of each

figure is the overall predicted moment-rotation relationship for the specimen, along with an indication of where the respective load falls in this relationship.

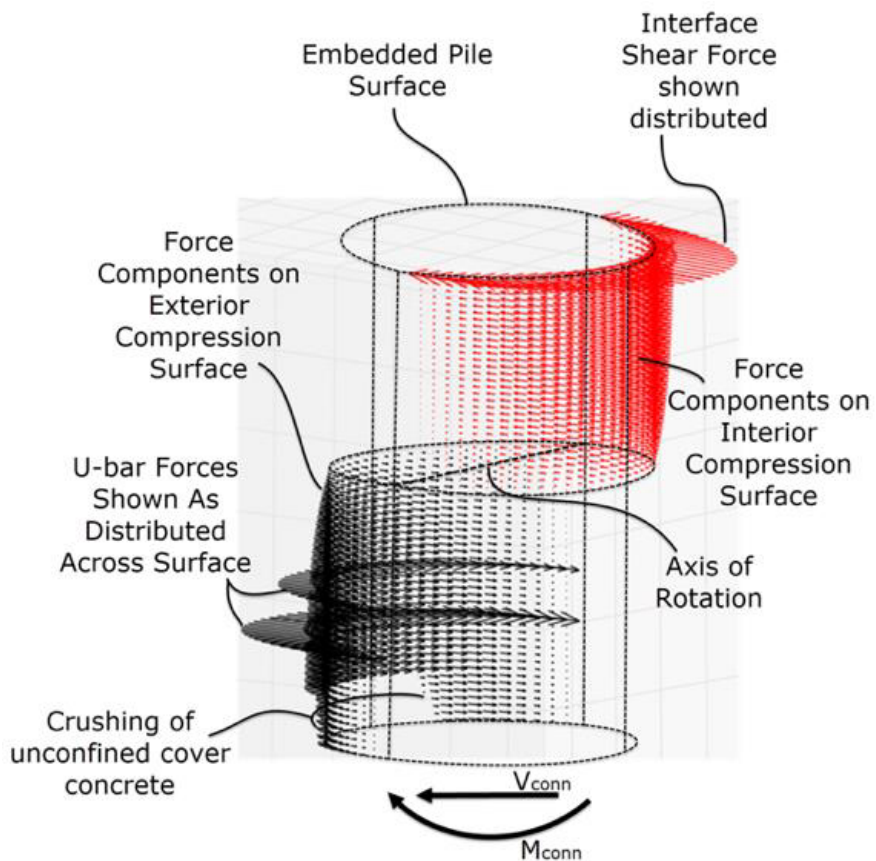
Table 7. MSU testing summary of pile-to-pile cap connections

Test	Embedment Length	Concrete Strength	Transverse Rein. *		Longitudinal Rein. **		Ubar Rein. ***			Quarter Section
			Size	Spacing	Size	Quantity	Size	Ext	Int	
PC1	L1 = 9 in	4.8 ksi	#2	S1 = 3 in S4 = 6 in	#3	4	NA	-	-	
PC2	L1 = 9 in	5.3 ksi	#2	S1 = 3 in S4 = 6 in	#3	4	NA	-	-	
PC3	L1 = 9 in	3.2 ksi	#3	S1 = 3 in S4 = 6 in	#4	4	NA	-	-	
PC3a	L1 = 9 in	3.9 ksi	#3	S2 = 2 in S4 = 6 in	#6	4	NA	-	-	
VT1/ VT2.5	L1 = 9 in	6.3 ksi	#3	S3 = 1.75 in S4 = 6 in	#4	2	#7	Y	N	
					#5	2				
VT2	L2 = 11.75 in	3.8 ksi	#3	S3 = 1.75 in S4 = 6 in	#4	2	#4	Y	N	
					#5	2				
VT3	L3 = 10.375 in	4.1 ksi	#3	S3 = 1.75 in S4 = 6 in	#4	2	#7	Y	N	
					#5	2				
CT1	L2 = 11.75 in	4.2 ksi	#3	S3 = 1.75 in S4 = 6 in	#4	2	#4	Y	N	
					#5	2				
CT2	L2 = 11.75 in	4.2 ksi	#3	S3 = 1.75 in S4 = 6 in	#4	2	#4	Y	Y	
					#5	2				

* Spacing of stirrups closest to embedded CFT
 ** Longitudinal Steel included in both top and bottom reinforcing layers
 *** U-bars placed in both directions

Table 8. Measured and predicted ultimate capacities

Specimen	Predicted (ft-kips)	Measured (ft-kips)	Measured/Predicted	Comments
PC1	80	82	1.03	Single Hoop Ignored
PC2	86	74	0.86	Single Hoop Ignored
PC3	80	76	0.95	Full Length Spiral Approx. By Averaging Dia.
PC3a	102.7	102	0.99	Full Length Spiral Approx. By Averaging Dia.
VT1/VT2.5	134.2	138.5	1.03	
VT2	171.1	173.8	1.02	
VT3	148.6	151.7	1.02	
CT1	175.2	174.2	0.99	Cyclic Test: Actual Avg. of 172.4 and 176.0
CT2	190.2	185.8	0.98	Cyclic Test: Actual Avg. of 181.8 and 189.5
Average			0.99	
Coefficient of Variation			5.4%	



3D Representation of Forces For VT2 @ 145 kip-

Figure 35. 3D representation of internal forces in VT2 at Moment = 145ft-kip

Referring to Figure 36, as would be expected, the concrete forces begin elastic, and become nonlinear with increasing lateral load. At 100 ft-kips of applied moment (Figure 36b), note the dip in the concrete forces near the bottom face of the cap. This dip occurs because the concrete at this location (near a free surface) is considered unconfined, and thus loses capacity (crushes) at a relatively lower compression stress (Figure 28). At 145 ft-kips, the cover concrete near the exterior of the cap further loses strength and the U-bars yield, which in turn results in the initiation of softening of the overall moment-rotation relationship. This also corresponds to a potential decrease of fixity of the connection, which would result in a loss of energy dissipation capacity. In Figure 36d, at an applied moment of 160 ft-k, the pile has rotated beyond the ultimate capacity of the connection, corresponding to significant damage in the cap, with almost complete crushing of the unconfined concrete near the surface of the cap and initiation of crushing damage in the adjacent confined concrete toward the interior of the cap.

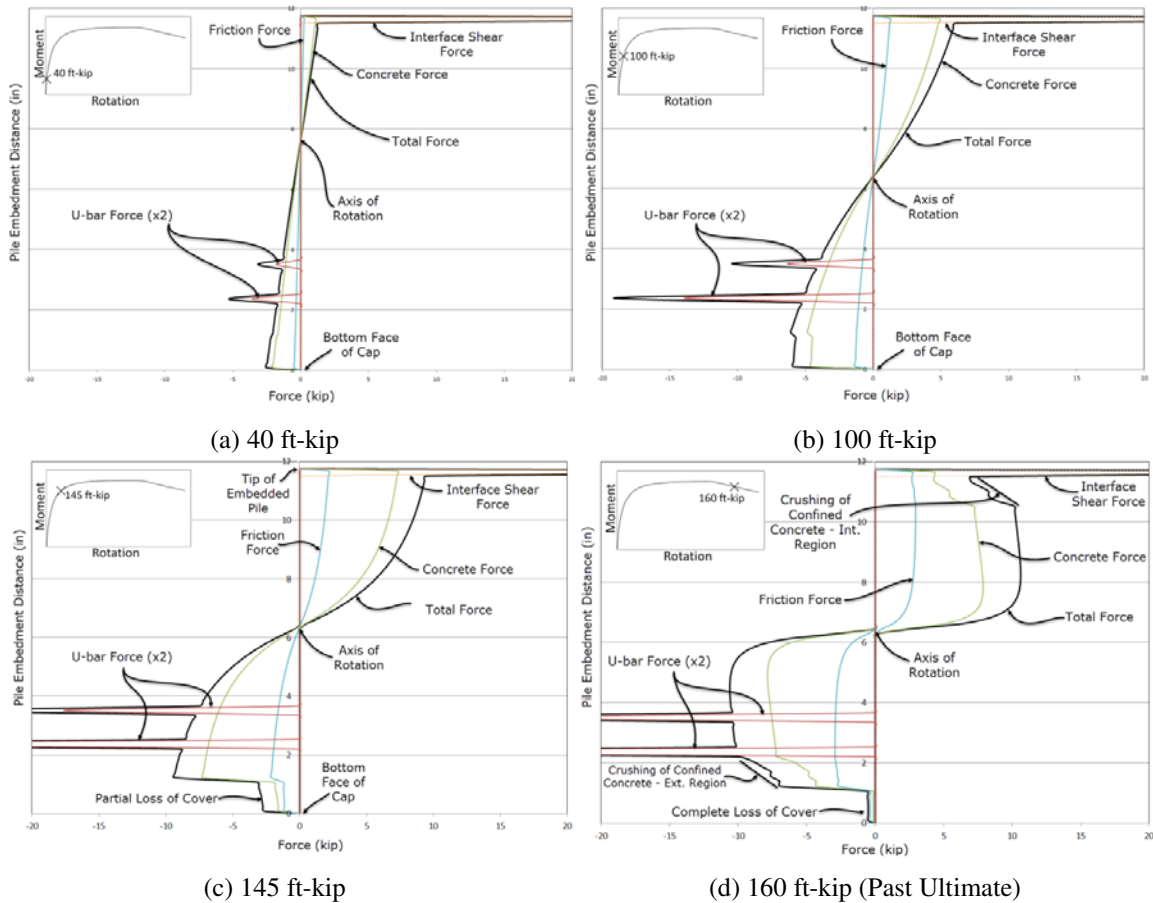


Figure 36. Summary of forces at each layer along the embedment depth at various applied moments – VT2

Summary and Conclusions

The behavior and performance of CFT pile-to-pile cap connections is often uncertain, leaving a designer to include large margins of safety when implementing these types of connections. In some cases, due to these uncertainties, this type of connection may even be avoided despite the system's economic and construction benefits. In this study, a simple moment-rotation methodology to determine the behavior and ultimate strength of such connections was developed. For an assumed rotation of the embedded pile in the pile cap, corresponding internal strains in the concrete are calculated based on

strain-displacement compatibility, attendant stresses are determined using nonlinear constitutive stress-strain relationships, and equilibrium is enforced between the associated internal force resultants and external applied demands. An iterative process is used until a solution is reached that is consistent with all constraints.

This methodology proved to be an effective and efficient means of predicting the ultimate capacity of such connections, an important component in their design to ensure the desired failure response of the overall system. The proposed methodology was applied to a dataset of 9 CFT to concrete pile cap connection specimens to predict their ultimate capacity. The average ratio of measured/predicted capacity was 0.99 with a coefficient of variation of 5.4%. In addition to accurately predicting the ultimate capacity of the connection, output from this methodology lends itself to predicting intermediate damage states in the connection that may lead to loss of energy dissipation capacity, such as extent of concrete spalling/crushing and loss of fixity.

While in the absence of proven design approaches for this connection, the proposed methodology may be found useful in its current form, and it will continue to be developed in future research. Specifically, the proposed methodology will be further developed by applying it to a larger dataset of connection test specimens to determine its effectiveness over a wider array of connection details and geometry. Future connection specimens may be tested as part of this work. Further, the ability of this methodology to predict the onset of intermediate damage will be investigated by comparing progressive model behavior to damage states observed in the test data. In particular, the onset of spalling/crushing will be investigated along with splitting of the concrete cap. Once the

accuracy of this methodology is confirmed, a parametric study will be carried out to investigate the importance/effectiveness of various design parameters (e.g., embedment depth, transverse reinforcement details, U-bar size and placement). Further, use of the forces in the transverse direction will be studied relative to reinforcing requirements in this direction. This research is expected to lead to the development of a more formal design methodology for such connections, and, accordingly to more widespread usage of the connection.

References

- AASHTO. (2010). *AASHTO LRFD bridge design specifications, customary U.S. units*, 5th Ed. with 2010 Interim Revisions, Washington, DC.
- AASHTO. 2011. *AASHTO Guide Specifications for LRFD Seismic Design*, 2nd Edition, with 2015 Interim Revisions.
- Barker, R.M., and Puckett, J.A. *Design of Highway Bridges – An LRFD Approach*. John Wiley and Sons, Inc., New Jersey, 3rd Edition, 2013.
- Chen, W., and Duan, L. *Bridge Engineering Handbook – Seismic Design*. CRC Title, 2nd Edition, 2014.
- Hsu, H.L., and Lin, H.W. “Improving Seismic Performance of Concrete-Filled Tube to Base Connections.” 2006. *J. Constr. Steel Res.*, 1333-1340.
- Kappes, L., M. Berry, and J. Stephens. 2013. *Performance of Steel Pipe Pile-to-Concrete Cap Connections Subject to Seismic or High Transverse Loading: Phase III Confirmation of Connection Performance*. Montana Department of Transportation.
- Kappes, L., M. Berry, F. Murray, J. Stephens, K. Barnes. 2016. *Seismic Performance of Concrete-Filled Steel Tube to Concrete Pile-Cap Connections*. ASCE, *J. Bridge Eng.*
- Kingsley, A. “Experimental and Analytical Investigation of Embedded Column Base Connections for Concrete Filled High Strength Steel Tubes.” M.S. Thesis, Civil and Environmental Engineering, Univ. of Washington Seattle.
- Kingsley, A., Williams, T., Lehman, D., and Roeder, C. “Experimental Investigation of Column-to-Footing Connections for High-Strength Vanadium Steel Concrete Filled Tube Construction.” 2005. *Int. J. Steel Struct.*, 5(4), 377-387.
- Lee, J. “Experimental Investigation of Embedded Connections for Concrete Filled Tube Column Connections to Combined Axial-Flexural Loading.” 2011. M.S. Thesis, Univ. of Washington, Seattle.
- Lehman, D.E., and Roeder, C.W. “Foundation Connections for Circular Concrete-Filled Tubes” 2012. *J. Constr. Steel Res.*, 78, 212-225.
- Mander, J., Priestley, M., and Park, R. (1988). "Theoretical Stress-Strain Model for Confined Concrete." *J. Struct. Eng.*, 10.1061/(ASCE)0733-9445(1988)114:8(1804), 1804-1826.

- Marsh, M.L., Buckle, I.G., and Kavazanjian, E. Jr. LRFD Seismic Analysis and Design of Bridges Reference Manual, NHI Course No. 130093 and 130093A. Publication FHWA-NHI-15-004. FHWA, U.S. Department of Transportation, 2014.
- Marson, J., and Bruneau, M. "Cyclic Testing of Concrete-Filled Circular Steel Bridge Piers Having Encased Fixed-Based Detail." 2004. J. Bridge Eng., 14-23.
- McFarlane, I. S. "Non-linear Finite Element Analysis of Concrete Filled High Strength Steel Tubes: Structural Performance and Sensitivity to Design Parameters." 2006. M.S. thesis, Univ. of Washington, Seattle.
- Moon, J., Lehman, D.E., Roeder, C.W., and Lee, H.E. "Strength of Circular Concrete-Filled Tubes With and Without Internal Reinforcement Under Combined Loading." 2013. J. Struct. Eng.
- Moon, J., Roeder, C.W., Lehman, D.E., and Lee, H.E. "Analytical Modeling of Bending of Circular Concrete-Filled Steel Tubes." 2012. Eng. Struct., 42, 349-261.
- O'Neill, K. "Experimental Investigation of Circular Concrete Filled Steel Tube Geometry on Seismic Performance." 2011. M.S. Thesis, Univ. of Washington, Seattle.
- Python Software Foundation. Python Language Reference, version 2.7. Available at <http://www.python.org>.
- Rabbat, B. G., and Russell, H. G. "Friction Coefficient of Steel on Concrete or Grout." 1985. J. Struct. Eng. 505-515.
- Roeder, C. W., Lehman, D. E. and Bishop, E. "Strength and Stiffness of Circular Concrete-Filled Tubes." 2010. J. Struct. Eng. 1545-1553.
- Rollins, K., and Stenlund, T. "Final Report: Laterally Loaded Pile Cap Connections." 2010. UT-10.16, Utah Dept. of Transportation, Salt Lake City, UT.
- Silva, P.F. and Seible, F. "Seismic Performance Evaluation of Cast-In-Steel-Shell (CISS) Piles." 2001. ACI Struct. J., 98(1), 36-49.
- Silva, P., Sritharan, S., Seible, F., and Pristly, M. Full-Scale Test of the Alaska Cast-In-Place Steel Shell Three Column Bridge Bent. 1999. Univ. of California, San Diego, La Jolla, CA.
- Stephens, Jerry, and Ladean McKittrick. 2005. Final Report: Performance Of Steel Pipe Pile-To-Concrete Bent Cap Connections Subject To Seismic Or High Transverse Loading. Montana Department of Transportation.

Stephens, M.T., Berg, L., Lehaman, D.E., and Roder, C.W. "Seismic Design of Circular Concrete Filled Tube Bridge Pier Connections For Accelerated Bridge Construction." 2014. ASCE/SEI Structures Congress, Boston, MA.

Williams, T. "Experimental Investigation of High Strength Concrete Filled Steel Tubes in Embedded Column Base Foundation Connections." 2007. M.S. Thesis, Civil and Environmental Engineering, Univ. of Washington, Seattle.

REFERENCES CITED

REFERENCES CITED

- AASHTO. (2010). *AASHTO LRFD bridge design specifications, customary U.S. units*, 5th Ed. with 2010 Interim Revisions, Washington, DC.
- ACI (American Concrete Institute) (2011). “Building code requirements for structural concrete.” *ACI 318*, American Concrete Institute, Farmington Hills, MI.
- AISC. (2011). *Steel construction manual*, American Institute of Steel Construction, Chicago.
- AASHTO. 2011. *AASHTO Guide Specifications for LRFD Seismic Design*, 2nd Edition, with 2015 Interim Revisions.
- Barker, R.M., and Puckett, J.A. *Design of Highway Bridges – An LRFD Approach*. John Wiley and Sons, Inc., New Jersey, 3rd Edition, 2013.
- Bruneau, M., and Marson, J. (2004). “Seismic design of concrete-filled circular steel bridge piers.” *J. Bridge Eng.*, 10.1061/(ASCE)1084-0702(2004)9:1(24), 24–34.
- Chen, W., and Duan, L. *Bridge Engineering Handbook – Seismic Design*. CRC Title, 2nd Edition, 2014.
- Hsu, H.L., and Lin, H.W. “Improving Seismic Performance of Concrete-Filled Tube to Base Connections.” 2006. *J. Constr. Steel Res.*, 1333-1340.
- Kappes, B. *Photo of Pryor Creek Intermediate Bent*. Montana Department of Transportation, Huntley, MT.
- Kappes, L. (2012). *Validation of Pile-to-Pile Cap Bridge Connection Design*. Montana State University, Civil Engineering, Bozeman.
- Kappes, L., M. Berry, and J. Stephens. 2013. *Performance of Steel Pipe Pile-to-Concrete Cap Connections Subject to Seismic or High Transverse Loading: Phase III Confirmation of Connection Performance*. Montana Department of Transportation.
- Kappes, L., M. Berry, F. Murray, J. Stephens, K. Barnes. 2016. *Seismic Performance of Concrete-Filled Steel Tube to Concrete Pile-Cap Connections*. ASCE, *J. Bridge Eng.*
- Kingsley, A. “Experimental and Analytical Investigation of Embedded Column Base Connections for Concrete Filled High Strength Steel Tubes.” M.S. Thesis, Civil and Environmental Engineering, Univ. of Washington Seattle.

- Kingsley, A., Williams, T., Lehman, D., and Roeder, C. "Experimental Investigation of Column-to-Footing Connections for High-Strength Vanadium Steel Concrete Filled Tube Construction." 2005. *Int. J. Steel Struct.*, 5(4), 377-387.
- Lee, J. "Experimental Investigation of Embedded Connections for Concrete Filled Tube Column Connections to Combined Axial-Flexural Loading." 2011. M.S. Thesis, Univ. of Washington, Seattle.
- Lehman, D.E., and Roeder, C.W. "Foundation Connections for Circular Concrete-Filled Tubes" 2012. *J. Constr. Steel Res.*, 78, 212-225.
- Mander, J., Priestley, M., and Park, R. (1988). "Theoretical Stress-Strain Model for Confined Concrete." *J. Struct. Eng.*, 10.1061/(ASCE)0733-9445(1988)114:8(1804), 1804-1826.
- Marsh, M.L., Buckle, I.G., and Kavazanjian, E. Jr. LRFD Seismic Analysis and Design of Bridges Reference Manual, NHI Course No. 130093 and 130093A. Publication FHWA-NHI-15-004. FHWA, U.S. Department of Transportation, 2014.
- Marson, J., and Bruneau, M. "Cyclic Testing of Concrete-Filled Circular Steel Bridge Piers Having Encased Fixed-Based Detail." 2004. *J. Bridge Eng.*, 14-23.
- McFarlane, I. S. "Non-linear Finite Element Analysis of Concrete Filled High Strength Steel Tubes: Structural Performance and Sensitivity to Design Parameters." 2006. M.S. thesis, Univ. of Washington, Seattle.
- Moon, J., Lehman, D. E., Roeder, C. W., and Lee, H.-E. (2013). "Strength of circular concrete-filled tubes with and without internal reinforcement under combined loading." *J. Struct. Eng.*, 10.1061/(ASCE)ST.1943-541X.0000788, 139(12), 04013012.
- Moon, J., Roeder, C.W., Lehman, D.E., and Lee, H.E. "Analytical Modeling of Bending of Circular Concrete-Filled Steel Tubes." 2012. *Eng. Struct.*, 42, 349-261.
- O'Neill, K. "Experimental Investigation of Circular Concrete Filled Steel Tube Geometry on Seismic Performance." 2011. M.S. Thesis, Univ. of Washington, Seattle.
- Python Software Foundation. Python Language Reference, version 2.7. Available at <http://www.python.org>.
- Rabbat, B. G., and Russell, H. G. "Friction Coefficient of Steel on Concrete or Grout." 1985. *J. Struct. Eng.* 505-515.

- Roeder, C., & Lehman, D. (2008). An Economical and Efficient Foundation Connection for Concrete Filled Steel Tube Piers and Columns . *COMPOSITE Construction in Steel and Concrete VI; Engineering Conferences International* . Devil's Thumb Ranch, Colorado.
- Roeder, C. W., Lehman, D. E. and Bishop, E. “Strength and Stiffness of Circular Concrete-Filled Tubes.” 2010. J. Struct. Eng. 1545-1553.
- Rollins, K., and Stenlund, T. “Final Report: Laterally Loaded Pile Cap Connections.” 2010. UT-10.16, Utah Dept. of Transportation, Salt Lake City, UT.
- Silva, P.F. and Seible, F. “Seismic Performance Evaluation of Cast-In-Steel-Shell (CISS) Piles.” 2001. ACI Struct. J., 98(1), 36-49.
- Silva, P., Sritharan, S., Seible, F., and Pristly, M. Full-Scale Test of the Alaska Cast-In-Place Steel Shell Three Column Bridge Bent. 1999. Univ. of California, San Diego, La Jolla, CA.
- Stephens, Jerry, and Ladean McKittrick. 2005. Final Report: Performance Of Steel Pipe Pile-To-Concrete Bent Cap Connections Subject To Seismic Or High Transverse Loading. Montana Department of Transportation.
- Stephens, M.T., Berg, L., Lehman, D.E., and Roder, C.W. “Seismic Design of Circular Concrete Filled Tube Bridge Pier Connections For Accelerated Bridge Construction.” 2014. ASCE/SEI Structures Congress, Boston, MA.
- Williams, T. “Experimental Investigation of High Strength Concrete Filled Steel Tubes in Embedded Column Base Foundation Connections.” 2007. M.S. Thesis, Civil and Environmental Engineering, Univ. of Washington, Seattle.

APPENDIX A

PERFORMANCE OF STEEL PIPE PILE-TO-CONCRETE BENT CAP
CONNECTIONS SUBJECT TO SEISMIC OR HIGH
TRANSVERSE LOADING: PHASE II

Steel Pipe Pile/Concrete Pile Cap Bridge Support
Systems:
Phase III
Confirmation of Connection Performance

Final Report

Prepared by:

Lenci Kappes, Mike Berry, and Jerry Stephens

of the

Western Transportation Institute/Civil Engineering Department
College of Engineering
Montana State University – Bozeman



Prepared for:

Montana Department of Transportation
Research Programs
2701 Prospect Avenue
Helena, Montana 59620

November 2012

TECHNICAL REPORT DOCUMENTATION PAGE

1. Report No. FHWA/MT-12-004/8203	2. Government Access No.	3. Recipient's Catalog No.	
4. Title and Subtitle Steel Pipe Pile/Concrete Pile Cap Bridge Support Systems: Phase III, Confirmation of Connection Performance		5. Report Date November 2012	
		6. Performing Organization Code	
7. Author(s) Lenci Kappes, Michael Berry, Jerry Stephens		8. Performing Organization Report Code	
9. Performing Organization Name and Address Western Transportation Institute PO Box 174250 Montana State University – Bozeman Bozeman, Montana 59717-4250		10. Work Unit No. (TRAIS)	
		11. Contract or Grant No. MSU G&C #4W2780 MDT Project #8203	
12. Sponsoring Agency Names and Addresses Research Programs Montana Department of Transportation 2701 Prospect Avenue Helena, Montana 59620-1001		13. Type of Report and Period Covered Final Report August 2009 – July 2012	
		14. Sponsoring Agency Code 5401	
15. Supplementary Notes: Research performed in cooperation with the Montana Department of Transportation and the US Department of Transportation, Federal Highway Administration. his report and related information can be found at http://www.mdt.mt.gov/research/projects/structures/seismic.shtml			
16. Abstract <p>The efficacy of a new procedure developed by the Montana Department of Transportation (MDT) to design concrete filled steel tube (CFT) pile to concrete pile cap connections was investigated in this project. A series of CFT piles embedded in a concrete pile cap is a desirable system to support small to mid-span bridges. Traditional methods for designing the connection between the CFT piles and pile cap often lead to congested and complex reinforcing schemes, and this complexity can limit the use of this support system. MDT has developed a simple design method for this connection utilizing a new reinforcing scheme that greatly simplifies the design and construction of this connection. The new reinforcing scheme includes U-shaped reinforcing bars that encircle the embedded CFT piles within the cap that counteract the moment related demands introduced by the embedded pile under lateral load events. The efficacy of the MDT design method implementing the new reinforcing scheme, which was developed from previous research and testing completed by Montana State University, is evaluated in this research.</p> <p>In particular, this report presents the details and results of tests on six half-size connections designed to exercise various design parameters in the MDT design guide. In these tests four primary limit states were observed: (1) formation of a plastic hinge in the concrete-filled steel tube, (2) crushing of the concrete surrounding the embedded pile, (3) yielding of the longitudinal reinforcement, and (4) splitting failure of the concrete cap. The MDT design methodology addresses all of these limit states fairly accurately. Some possible improvements to MDT's methodology suggested by the test results are presented and discussed.</p>			
17. Key Words Bridge substructure, pipe piles, concrete pile caps, bridge testing		18. Distribution Statement No restrictions. This document is available through NTIS, Springfield, Virginia 22161.	
19. Security Classif. (of this report) Unclassified	20. Security Classif. (of this page) Unclassified	21. No. of Pages 145	22. Price

Table of Contents

1	INTRODUCTION	121
1.1	BACKGROUND INFORMATION.....	121
1.2	RESEARCH OBJECTIVES AND SCOPE	123
2	PREVIOUS RESEARCH	125
2.1	METHODS FOR CALCULATING CFT STRENGTH.....	125
2.2	CFT CONNECTIONS	127
2.2.1	<i>Kingsley (2005) Review and Observations</i>	<i>128</i>
2.2.2	<i>Silva et al. (1999) Research</i>	<i>131</i>
2.2.3	<i>Rollins and Stenlund (2010) Research</i>	<i>132</i>
2.3	PREVIOUS PILE CAP TESTING AT MONTANA STATE UNIVERSITY.....	133
3	SUMMARY OF MDT DESIGN GUIDE.....	138
3.1	OVERVIEW	138
3.2	MDT DESIGN GUIDE METHODOLOGY	138
3.2.1	<i>Embedment Length</i>	<i>138</i>
3.2.2	<i>Plastic Moment Capacity of the Pile.....</i>	<i>141</i>
3.2.3	<i>Comparison of Demand and Pile Capacity</i>	<i>141</i>
3.2.4	<i>Normal Flexural Design</i>	<i>142</i>
3.2.5	<i>Additional Longitudinal Steel</i>	<i>143</i>
3.2.6	<i>Transverse Steel</i>	<i>144</i>
3.3	DISCUSSION	145
4	EXPERIMENTAL PROGRAM.....	148
4.1	FUNDAMENTAL TEST SPECIMEN DESIGN	150
4.2	SPECIMEN VT1 DESIGN.....	154
4.2.1	<i>Plastic Moment Capacity of the Pile.....</i>	<i>154</i>
4.2.2	<i>Embedment Length</i>	<i>155</i>
4.2.3	<i>Pile Cap Reinforcement</i>	<i>155</i>
4.3	SPECIMEN VT2 DESIGN.....	160
4.4	SPECIMEN VT2.5 DESIGN.....	161
4.5	SPECIMEN VT3 DESIGN.....	161
4.6	SPECIMEN CT1 DESIGN.....	162
4.7	SPECIMEN CT2 DESIGN.....	162
4.8	SPECIMEN CONSTRUCTION	163
5	TEST SETUP.....	166
5.1	INSTRUMENTATION	167
5.2	TEST CONDUCT	170
5.2.1	<i>Monotonic Test Conduct</i>	<i>170</i>
5.2.2	<i>Cyclic Test Conduct.....</i>	<i>171</i>
6	TEST RESULTS	172
6.1	VERIFICATION TEST 1 – VT1	173
6.2	VERIFICATION TEST 2 – VT2	176

6.3	VERIFICATION TEST 2.5 - VT2.5	180
6.4	VERIFICATION TEST 3 – VT3	184
6.5	CYCLIC TEST 1 – CT1	188
6.6	CYCLIC TEST 2 – CT2	190
7	DISCUSSION OF RESULTS	193
7.1	OVERVIEW	193
7.1.1	<i>Monotonic Test Series</i>	193
7.1.2	<i>Cyclic Test Series</i>	198
7.2	CYCLIC BEHAVIORS	200
7.2.1	<i>Cyclic vs. Monotonic Behavior</i>	200
7.2.2	<i>Effect of Additional Interior U-bar</i>	201
7.3	MDT DESIGN GUIDE	203
7.3.1	<i>Plastic-Moment Capacity of CFT</i>	204
7.3.2	<i>Concrete Crushing Limit State</i>	204
7.3.3	<i>Yielding of Longitudinal Reinforcement</i>	207
7.3.4	<i>Splitting</i>	209
7.3.5	<i>Other Observations</i>	209
8	SUMMARY AND CONCLUSIONS	212
9	WORKS CITED	216
	APPENDIX A – MDT DESIGN GUIDE	217
	APPENDIX B – TEST SPECIMEN DESIGN CALCULATIONS	224
	APPENDIX C – STRAIN GAGE DATA	239

LIST OF FIGURES

FIGURE 1: TYPICAL MDT CONCRETE-FILLED STEEL PILE AND CONCRETE PILE CAP BRIDGE SUBSTRUCTURE SUPPORT SYSTEM (PRYOR CREEK BRIDGE NEAR HUNTLEY, MT - COURTESY OF MDT (2012))	121
FIGURE 2: TYPICAL BRIDGE BENT WITH U-BAR REINFORCING STEEL (OPTION 1).....	123
FIGURE 3: RATIO OF PREDICTED TO EXPERIMENTAL FLEXURAL STRENGTHS (KINGSLEY, 2005)	126
FIGURE 4: CFT-TO-CONCRETE CONNECTIONS (KINGSLEY, 2005)	128
FIGURE 5: REINFORCING SCHEME FOR (SILVA, SRITHARAN, SEIBLE, & PRIESTLY, 1999)	132
FIGURE 6: BASIC CAP CONFIGURATION	134
FIGURE 7: TEST SETUP (STEPHENS & MCKITTRICK, 2005)	134
FIGURE 8: TYPICAL FAILURE MECHANISM SEEN IN PC-1 THROUGH PC-3A (STEPHENS & MCKITTRICK, 2005) ..	136
FIGURE 9: REINFORCING STEEL FOR PC-4	137
FIGURE 10: ASSUMED WHITNEY STRESS DISTRIBUTION FOR DETERMINING EMBEDMENT LENGTH	139
FIGURE 11: MINIMUM LONGITUDINAL STEEL IMPLEMENTATION	142
FIGURE 12: MDT DESIGN GUIDE SCHEMES FOR ADDITIONAL REINFORCEMENT LONGITUDINAL STEEL.....	143
FIGURE 13: TRANSVERSE STEEL REPRESENTATION	145
FIGURE 14: COMPARISON OF REINFORCEMENT SCHEMES	147
FIGURE 15: TYPICAL BRIDGE BENT WITH ASSUMED DEFLECTED SHAPE.....	148
FIGURE 16: TYPICAL TEST SPECIMEN.....	149
FIGURE 17: CAPACITIES FROM CRUSHING LIMIT STATE PER THE MDT DESIGN GUIDE	151
FIGURE 18: GENERAL DESIGN PARAMETERS ESTABLISHED FROM PREVIOUS TESTING.....	154
FIGURE 19: LONGITUDINAL STEEL DESIGN AND PLACEMENT.....	157
FIGURE 20: ADDITIONAL LONGITUDINAL STEEL DESIGN AND PLACEMENT.....	158
FIGURE 21: STEEL REINFORCEMENT SCHEME FOR VT1	159
FIGURE 22: STACKED U-BAR CONFIGURATION USED IN VT2	160
FIGURE 23: EXTERIOR AND INTERIOR U-BARS FOR CT2	162
FIGURE 24: STRUCTURAL ELEMENTS READY FOR CONCRETE PLACEMENT	164
FIGURE 25: TYPICAL STEEL REINFORCEMENT CAGE CONSTRUCTION (VT1 SHOWN).....	165
FIGURE 26: GENERAL TEST SETUP LAYOUT (ALL LENGTHS IN UNITS OF INCHES).....	166
FIGURE 27: AN OVERVIEW OF THE TEST SPECIMEN, FRAME, AND HYDRAULIC ELEMENTS	167
FIGURE 28: LOAD AND DISPLACEMENT LOCATIONS (ALL LENGTHS IN UNITS OF INCHES).....	169
FIGURE 29: TYPICAL STRAIN GAGE PLACEMENT ON U-BAR.....	170
FIGURE 30: CYCLIC LOADING HISTORY FOR CT1 AND CT2	171
FIGURE 31: VT1 APPLIED MOMENT (W/P-DELTA) VS. LATERAL DRIFT.....	174
FIGURE 32: VT1 APPLIED MOMENT (W/ P-DELTA) VS. LATERAL DRIFT - FIRST PUSH ONLY	174
FIGURE 33: VT1 FAILURE: PLASTIC HINGE IN THE STEEL PILE IN THE POSITIVE DIRECTION.....	175
FIGURE 34: VT1 FAILURE: PLASTIC HINGE IN THE STEEL PILE IN THE NEGATIVE DIRECTION	176
FIGURE 35: VT2 APPLIED MOMENT (W/ P-DELTA) VS. LATERAL DRIFT.....	178
FIGURE 36: VT2 APPLIED MOMENT (W/ P-DELTA) VS. LATERAL DRIFT - FIRST PUSH	179
FIGURE 37: VT2 FAILURE AT MAXIMUM DEFLECTION ON INITIAL PUSH	179
FIGURE 38: VT2 FAILURE AT MAXIMUM DEFLECTION ON RETURN PULL	180
FIGURE 39: VT2.5 APPLIED MOMENT (W/P-DELTA) VS. LATERAL DRIFT.....	181
FIGURE 40: VT2.5 APPLIED MOMENT (W/ P-DELTA) VS. LATERAL DRIFT - FIRST PUSH ONLY	182
FIGURE 41: VT2.5 FAILURE AT MAXIMUM POSITIVE DEFLECTION.....	183
FIGURE 42: VT2.5 FAILURE AT MAXIMUM NEGATIVE DEFLECTION	184
FIGURE 43: VT3 APPLIED MOMENT (W/ P-DELTA) VS. LATERAL DRIFT.....	185
FIGURE 44: VT3 APPLIED MOMENT (W/ P-DELTA) VS. LATERAL DRIFT - FIRST PUSH	186
FIGURE 45: VT3 FAILURE AT MAXIMUM DEFLECTION ON INITIAL PUSH	187
FIGURE 46: VT3 FAILURE AT MAXIMUM DEFLECTION ON INITIAL PULL	187
FIGURE 47: CT1 CYCLIC RESPONSE	189

FIGURE 48: CT1 CYCLIC LOAD PEAKS VS. PERCENT DRIFT	189
FIGURE 49: CT1 NEAR THE COMPLETION OF TESTING	190
FIGURE 50: CT2 COMPLETE CYCLIC RESPONSE.....	191
FIGURE 51: CT2 CYCLIC LOAD PEAKS VS. DRIFT.....	191
FIGURE 52: CT2 NEAR THE COMPLETION OF TESTING	192
FIGURE 53: OVERVIEW OF RESULTS FOR MONOTONIC TESTS (VT1, VT2, VT2.5, VT3)	196
FIGURE 54: EXTERIOR AND INTERIOR CRUSHING REGIONS IN THE CONCRETE CAP.....	197
FIGURE 55: OVERVIEW OF RESULTS, MAXIMUM MOMENT IN EACH DISPLACEMENT CYCLE FOR CT1 AND CT2	199
FIGURE 56: RESPONSE COMPARISON BETWEEN VT2 AND CT1	201
FIGURE 57: CT1 AND CT2 CYCLIC DEGRADATION COMPARISON – POSITIVE CYCLES	202
FIGURE 58: CT1 AND CT2 CYCLIC DEGRADATION COMPARISON – NEGATIVE CYCLES	203
FIGURE 59: COMPARISON OF U-BAR REINFORCING SCHEMES, CT1 AND CT2.....	203
FIGURE 60: CRUSHING LIMIT STATE - PREDICTED VS. EXTERIOR CRUSHING OBSERVED VALUES.....	206
FIGURE 61: CRUSHING LIMIT STATE - PREDICTED VS. INTERIOR CRUSHING OBSERVED VALUES	207
FIGURE 62: ADDITIONAL LONGITUDINAL STEEL LIMIT STATE	209

LIST OF TABLES

TABLE 1: EXPERIMENTAL PARAMETERS AND MATERIAL PROPERTIES (STEPHENS & MCKITTRICK, 2005).....	135
TABLE 2: TEST RESULTS (STEPHENS & MCKITTRICK, 2005)	136
TABLE 3: SUMMARY OF DESIGN PARAMETERS, MONOTONIC TESTS	152
TABLE 4: SUMMARY OF DESIGN PARAMETERS, CYCLIC TESTS.....	153
TABLE 5: SUMMARY OF TEST RESULTS.....	173
TABLE 6: SUMMARY OF CYCLIC RESPONSE	198
TABLE 7: SUMMARY OF DESIGN PARAMETERS - MONOTONIC TESTS	225
TABLE 8: SUMMARY OF DESIGN PARAMETERS – CYCLIC TESTS	226

DISCLAIMER STATEMENT

This document is disseminated under the sponsorship of the Montana Department of Transportation and the United States Department of Transportation in the interest of information exchange. The State of Montana and the United States Government assume no liability of its contents or use thereof.

The contents of this report reflect the views of the authors, who are responsible for the facts and accuracy of the data presented herein. The contents do not necessarily reflect the official policies of the Montana Department of Transportation or the United States Department of Transportation.

The State of Montana and the United States Government do not endorse products of manufacturers. Trademarks or manufacturers' names appear herein only because they are considered essential to the object of this document.

This report does not constitute a standard, specification, or regulation.

ALTERNATIVE FORMAT STATEMENT

MDT attempts to provide accommodations for any known disability that may interfere with a person participating in any service, program, or activity of the Department. Alternative accessible formats of this information will be provided upon request. For further information, call (406) 444-7693, TTY (800) 335-7592, or Montana Relay at 711.

ACKNOWLEDGMENTS

The authors would like to acknowledge the financial support for this project provided by the Montana Department of Transportation (MDT) and the Research and Innovative Technology Administration (RITA) at the United States Department of Transportation through the Western Transportation Institute at Montana State University. We also wanted to recognize and thank the MDT Research Section and the technical panel for their participation in this project.

UNIT CONVERSIONS

Measurement	Metric	English
Length	1 cm	0.394 in
	1 m	3.281 ft
	1 km	0.621 mile
Area	1 cm ²	0.155 in ²
	1 m ²	1.196 yd ²
Volume	1 m ³	1.308 yd ³
	1 ml	0.034 oz
Force	1 N	0.225 lbf
	1 kN	0.225 kip
Stress	1 MPa	145 psi
	1 GPa	145 ksi
Unit Weight	1 kg/m ³	1.685 lbs/yd ³
Velocity	1 kph	0.621 mph

EXECUTIVE SUMMARY

The Montana Department of Transportation (MDT) has found concrete-filled steel tube (CFT) piles connected at the top by a concrete pile cap to be a very cost effective support system for short and medium span bridges. This type of system offers low initial cost, short construction time, low maintenance requirements, and a long service life. From a structural engineering perspective, these systems must provide acceptable performance under gravity (i.e., self weight and vehicle loads) and lateral loads (i.e., extreme ice, wind, and seismic events). While the gravity load performance of these systems is well understood, their strength and ductility under extreme lateral loads is more difficult to reliably predict using conventional design procedures. Therefore, MDT sponsored a research project at Montana State University (MSU), completed in 2005, to investigate the performance of these systems under extreme lateral loads. As part of this investigation, MSU conducted five physical tests on half-size models of the CFT to concrete pile cap connection. The models were designed to replicate the behavior of full-size connections under reversed seismic loads. Four different reinforcing schemes within the connection zone were evaluated.

Based on the results of the tests conducted at MSU in 2005, in conjunction with established structural engineering principles, MDT developed a new design procedure to determine the reinforcing steel required in the pile cap to produce the desired system performance under lateral loads. While the layout of the reinforcing steel generated by this design procedure is generally similar to the successful layout that was evaluated in the final pile cap test, there are several differences between the reinforcing configuration that was tested and what the design procedure generates. Notably, the design procedure provides for a simpler arrangement of the reinforcement (single set of U-shaped bars) that offers some advantages relative to the constructability of the pile cap, and this specific arrangement had not been tested.

Therefore, the objective of this project was to further validate MDT's new CFT to concrete pile cap connection design methodology by physically testing connections designed according to this new procedure. A total of six half-size connection specimens were tested under axial and lateral load until failure. Specifically, four different configurations were tested under monotonic and cyclic loads. Three of these configurations were designed in accordance with the design guide; the fourth configuration incorporated a second set of U-bars encircling the pile in the interior of the cap (close to the tip of the embedded pile).

In the first four tests (VT1, VT2, VT2.5, and VT3), the connection configurations were subjected to monotonic loading, capturing the ultimate strength of each configuration and providing general information on limit states of concern and post-failure ductility. Two more tests were completed using a cyclic load scheme (CT1 and CT2) to capture performance characteristics of the connections under multiple cycles of fully reversed, increasing load. The second of these two cyclic-load tests was conducted on the cap configuration consisting of two sets of U-bars.

Each specimen consisted of a single CFT pile and an attendant length of pile cap. The pile cap was held in position on each end (at the theoretical points of inflection in the cap of a full bent when subjected to a lateral load), while a lateral load was applied to the tip of the pile. In addition to subjecting the connections to a lateral load, a constant axial force was applied during the tests to generate the gravity load effects that were expected to be present in the real structures during a lateral load event. Measurements were subsequently made during each test of the loads applied to the connection, and of the global displacements and internal strains that resulted from these loads.

Four key limit states were observed in these tests: (1) formation of a plastic hinge in the CFT, (2) internal and exterior concrete crushing, (3) yielding of the longitudinal reinforcement, and (4) splitting of the concrete cap. Based on the results of this investigation, the following conclusions were made regarding the efficacy of the MDT design methodology at addressing these limit states.

1. The MDT design methodology predicts the capacity of the CFT solely based on properties of the steel pipe, and ignores the effects of concrete and axial load. In many design scenarios, this simplification would be conservative; however, this simplification would be unconservative if the design of the connection assumes that plastic hinging limits the maximum moment transferred to the cap. One possible improvement might be to adopt AISC's methodology for calculating the plastic-moment capacity of CFTs, as this methodology has been shown to be accurate at axial load ratios (i.e., ratio of applied axial load to ultimate axial capacity) common in bridge applications.
2. While the design guide accurately predicts/delays the limit state of exterior crushing of the cap concrete in the connection zone (which signifies/initiates ultimate failure), it is not effective at predicting the onset of crushing of the concrete in the interior of the cap, which was shown to reduce connection fixity (resulting in a pinched hysteresis response) and increase degradation under cyclic loads. This concern could be addressed by reducing allowed concrete

compressive strengths and/or including interior U-bars near the tip of the embedded pile, which were shown to delay the onset of this limit state.

3. Yielding of the longitudinal reinforcement was predicted well by the design guide; however, this provision may still merit further review and revision. The design methodology primarily addresses this limit state by including additional steel beyond that which is required from a normal design of the cap for global bending. This process is dependent upon a calibration factor (75 percent reduction in required steel from a mechanics model) based on empirical data from the test series completed for MDT at MSU in 2005 (Stephens and McKittrick, 2005). Although this methodology was shown to be effective in this test series, the efficacy of this calibration factor has not been verified across all possible cap configurations. To address the possibility that this factor could vary with various connection characteristics, it may be desirable to develop a mechanics model to better describe the effect of U-bars on this limit state, and reduce reliance upon empirical factors.
4. The splitting limit state (marked by yielding of the transverse reinforcement, and formation of splitting cracks) was observed in all test specimens, but not until after other limit states had been reached. While this limit state was not directly a focus of this investigation, this positive performance indicates that the MDT design methodology of using AASHTO's specifications for minimum reinforcement in plastic-hinge zones, and including U-bars, is effective at delaying it. That being said, however, the amount of transverse reinforcement specified following this approach is not directly based on the moment demand the connection must carry. Development of a more robust analytical model may be merited to reduce reliability on empirical factors and improve design efficiency.
5. In executing this project, a thorough review of the design guide beyond just those parameters directly exercised in this test series was completed. This review revealed a specific aspect of the design guide that apparently could yield unconservative results, and thus should be addressed. The provision of concern determines whether the connection will be specifically designed to carry the moment demand on it, or if the reinforcing provided in a normal flexural design for global bending is sufficient. This branching is based on the moment demand's relation to the plastic-moment capacity of the CFT, and is reliant on an assumption that the dimensions and reinforcing of the cap cross-section proportionally increase with increased pile capacity. However, this assumption may not be valid, as some bent configurations may fall outside of those typically

encountered in developing this provision. To address this situation, this “branch” in the design guide could be removed. If it were removed, the connection would always be designed to include additional reinforcement based on the moment demand in the form of U-bars.

Developing a robust design methodology for any structural system is a serious undertaking that often involves several iterations of review and revision. The current MDT guide has started well down this path for designing CFT pile to concrete pile cap connections. As time and resources permit, consideration should be given to further testing and analysis to address the various issues identified in this project, as they have been summarized above.

1 INTRODUCTION

1.1 Background Information

As implemented by the Montana Department of Transportation (MDT), a series of concrete-filled steel pipe piles embedded in a concrete pile cap can be a desirable solution for supporting small to mid-span bridges. This system is fast and efficient to construct and, with proper design, improves the ductile response and overall strength of the structure. A typical bent constructed using this system is shown in Figure 1, which in this case specifically consists of seven concrete-filled steel piles embedded in a concrete pile cap.



Figure 1: Typical MDT concrete-filled steel pile and concrete pile cap bridge substructure support system (Pryor Creek Bridge near Huntley, MT - courtesy of MDT (2012))

The structural benefits of a concrete-filled steel tube (CFT) are well known. In the case of the concrete-filled steel pile, the flexural capacity and ductility of the steel tube when subjected to lateral loads (e.g., during a seismic event) is enhanced by the concrete. The concrete inside the tube not only adds stiffness and strength to the cross section, it also delays the onset of buckling of the steel tube. Further, the compression strength of the concrete is also enhanced by the confinement provided by the steel tube. The basic ductility provided by the steel tube may be very beneficial to the overall response of the structure if sufficient strength is provided by the concrete pile cap to ensure the formation of a plastic hinge in the CFT. This failure mechanism is preferable to failure of the concrete cap due to its enhanced energy-dissipating characteristics (i.e. more robust hysteresis response under lateral loads). Thus, proper design of the cap and notably the connection to the CFT is essential to ensure the design loads can be carried by these elements without failure.

While a significant amount of research has been focused on the structural performance of CFTs, fewer projects have focused on the details of their connection to reinforced concrete elements, i.e. pile caps; thus, the need for more research in this area. Furthermore, many of the CFT-to-pile cap connection details currently used in practice are extremely congested and difficult to construct, and their performance, notably during seismic events, may be somewhat uncertain. In light of this situation, research was conducted on this connection at Montana State University (MSU) in 2005 under the sponsorship of MDT. Data collected during this effort was subsequently used by MDT to formulate a design guide for a concrete-filled steel pipe-to-pile cap connection (Stephens and McKittrick 2005).

The MDT design guide essentially provides a method to design CFT-to-concrete pile cap connections such that the concrete pile cap can withstand the design moment delivered by the CFT pile without experiencing significant damage. The basic connection configuration used by MDT is shown in Figure 2. Based on the design moment the cap must withstand, the guide can be used to determine the minimum embedment depth of the CFT in the cap, as well as to provide guidance on placing additional reinforcing steel around the embedded CFT. This additional reinforcing steel is further specified to be in the form of U-bars, which encircle each embedded CFT (Figure 2), or a combination of U-bars and longitudinal bars inserted through the pile.

While based on engineering principles and the results of various physical tests completed in the 2005 research conducted at MSU (Stephens and McKittrick, 2005), the reinforcing configurations used in the MDT design guide were not specifically tested, making it

imperative to test typical connections produced following this design guide to verify their performance.

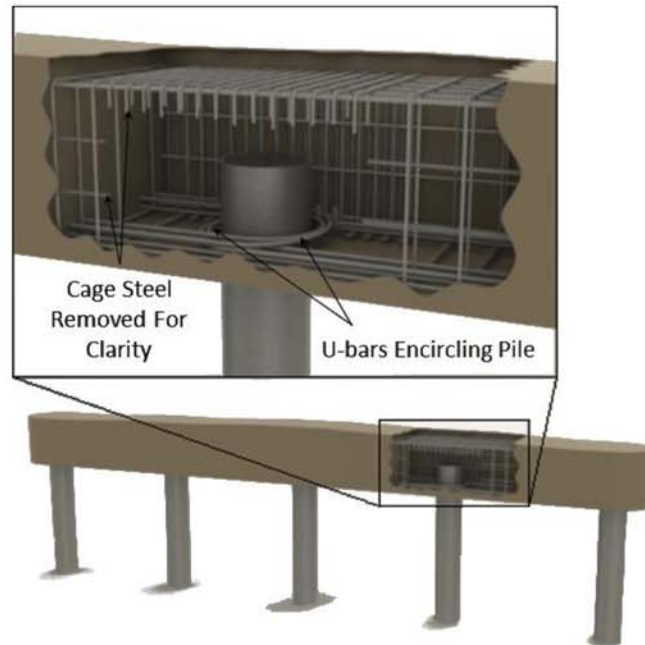


Figure 2: Typical bridge bent with U-bar reinforcing steel (Option 1)

1.2 Research Objectives and Scope

The primary objectives of this research were to:

- a) verify that the MDT design guide for CFT-to-concrete pile cap connections produces designs that provide the required structural strength and ductility,
- b) gain further insights on basic connection behavior under monotonic and cyclic loads, and
- c) determine possible improvements in the design methodology.

In particular, this report presents the results and subsequent conclusions from tests on four (three unique) CFT-to-pile cap connections designed using the MDT guide. The three unique designs were chosen to exercise the design guide and determine its capability to provide sufficient pile cap strength. These designs all used the U-bar rather than the through bar connection configuration, as the U-bar configuration was judged to be simpler to construct and was expected to offer better performance. Testing was done on $\frac{1}{2}$ -size models of the connection. In the first four tests, the connections were subjected to monotonic loading, capturing the ultimate strength of each configuration.

Two more tests were completed using a cyclic load scheme to capture performance characteristics of the connections under multiple cycles of fully reversed, increasing load.

2 PREVIOUS RESEARCH

As mentioned previously, there are numerous benefits realized in using CFTs in structural applications. To realize many of these benefits, however, the connections between CFTs and other structural elements, such as pile caps and foundations, need to be designed and detailed such that the full moment of the CFT can be achieved. Therefore, it is essential to be able to reasonably predict the strength of the CFT and the behavior and capacity of the connection. This chapter presents a summary of recent research in this area. This chapter first discusses methods for calculating CFT strength, followed by a discussion on previous research on various CFT connections. This chapter concludes with a discussion of previous MDT funded research at MSU in this area.

2.1 Methods for Calculating CFT Strength

One of the more prominent studies focused on determining the plastic-moment capacities of CFTs was completed by Bruneau & Marson (2004). The objective of this research was to determine the adequacy of current design practices for predicting the plastic-moment capacity of CFTs (i.e. CAN/CSA-S16.1-M94, AISC LRFD 1994, and Eurocode 4 1994 standards), as compared to experimental data gathered from test specimens that were evaluated in a laboratory setting. The research team found that all methods evaluated were conservative to varying degrees. Although providing extra strength in a structural element (beyond that explicitly considered in design) is often viewed as a positive and conservative practice, this is not always the case. For seismic design of bridge substructures, a capacity protected design method is used for sizing elements adjoining to bridge piers where plastic hinges may form. Thus, an underestimation of the moment capacity of the bridge pier could lead to unwanted damage in the less-ductile concrete cap (Bruneau and Marson 2004). Therefore, the researchers developed new design equations to better represent the observed test results. Since completion of their study these design equations have been implemented in the 2001 edition of the Canadian CSA-S16-01 “Limit State Design of Steel Structures” standards.

The American Institute of Steel Construction identifies two methods for determining the strength of CFTs, assuming certain conditions are met (AISC 2011). The first method is the plastic stress distribution method. The second method identified by AISC (2011) is the strain compatibility method, which assumes a linear strain distribution across the cross section. The concrete strain for this method is limited to $0.003 \text{ in}/\text{in}$. AISC (2011) states that for both of these methods, the tensile capacity of the concrete is assumed to be zero.

Kingsley (2005) compared both the plastic stress distribution method and the strain compatibility method to published results of 22 CFT tests with a multitude of CFT diameter to tube thickness (D/t) ratios, axial-load ratios (P/P_0), and concrete and steel strengths. A summary plot from this research is provided in Figure 3, which plots the ratio of calculated flexural strength to experimental flexural strength (M_n/M_{exp}) versus the axial-load ratio, P/P_0 .

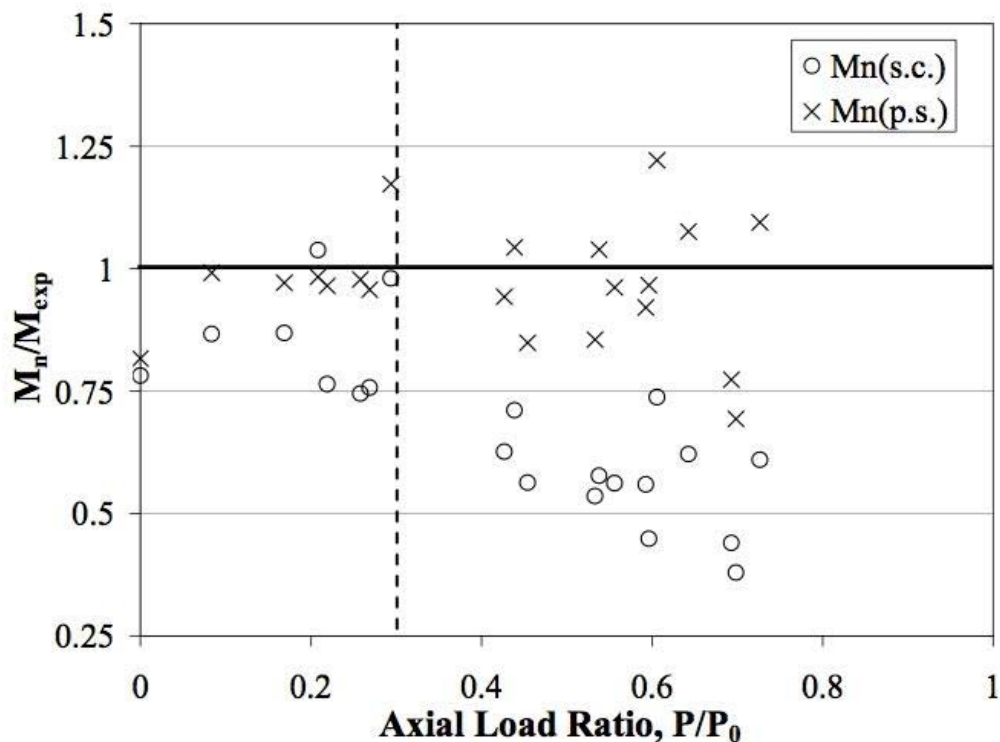


Figure 3: Ratio of predicted to experimental flexural strengths (Kingsley, 2005)

As can be seen in this figure, the plastic stress distribution method predicted the flexural strength fairly well with the average M_n/M_{exp} very near 1.0. The strain compatibility method was much more conservative than the plastic distribution method, with the majority of M_n/M_{exp} values much less than 1.0. Kingsley (2005) further points out that the strain compatibility method becomes increasingly conservative as P/P_0 increases. The researcher attributes the conservativeness of the strain compatibility method to the code prescribed 0.003 in/in strain limit on the concrete, which is typically associated with limiting spalling on conventional reinforced concrete sections. This limit is not applicable to CFTs due to the effect of confinement provided by the steel tube. Furthermore, the effectiveness of the confinement may increase and the 0.003 strain limit

may be more conservative at higher axial loads due to the tri-axial stress state of the concrete.

Kingsley also points out that due to other design considerations (e.g., slenderness), CFT columns are rarely subjected to axial loads with P/P_o ratios greater than 0.3. This limit is represented in Figure 3 with the vertical dashed line. As can be seen in this figure, the accuracy of both methods is improved in this region.

2.2 CFT Connections

One issue that has hindered the usage of CFTs in structural applications is the lack of connection design methods. Several research projects have been conducted on this topic, many of which are discussed in an extensive literature review done by Kingsley (2005) as part of a study focused on CFT to foundation connections. Kingsley categorized the connections using four general types: exposed base plate, embedded, structural steel embedded in concrete, and semi-embedded, as seen in Figure 4. This section reviews some of the key observations from Kingsley's literature review, and some key findings from Kingsley's research. Additionally, this section reviews several studies not discussed in Kingsley's review. Finally, this section concludes with a discussion of previous MDT funded research conducted at MSU (Stephens and McKittrick, 2005) on these connections.

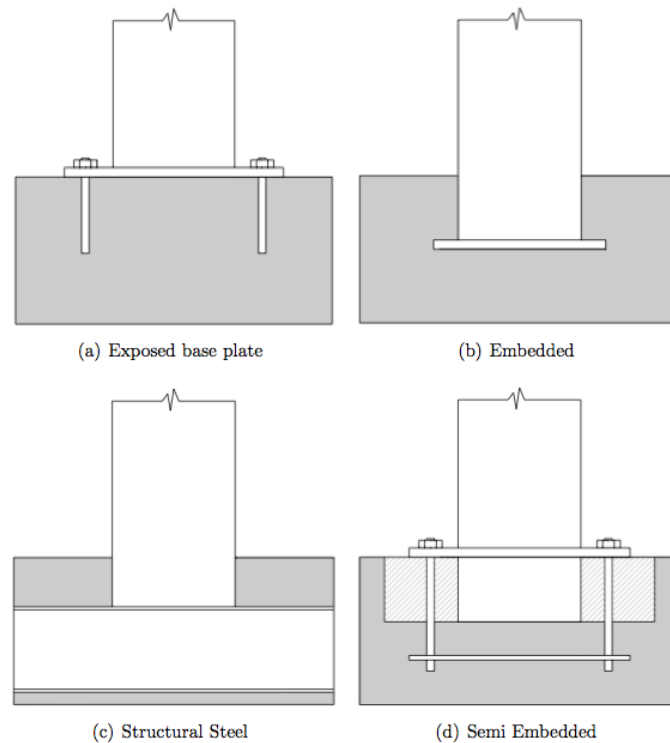


Figure 4: CFT-to-concrete connections (Kingsley 2005)

2.2.1 Kingsley (2005) Review and Observations

Kingsley completed an extensive literature review and conducted her own research as well on CFT connections, as is summarized below. The exposed base-plate connection shown in Figure 4a consists of a steel plate welded to a CFT column. The base plate is then bolted to the concrete; therefore, the bolts, or anchor rods, provide the resistance needed to withstand a moment demand in the connection from a lateral load placed on the CFT column. Kingsley (2005) relates the rotational stiffness of the connection to the dimensions and thickness of the base plate as well as the tensile resistance provided by the anchor rods. Typically, this type of connection only provides a partially-fixed end condition, and unsatisfactory performance of base plate connections during recent earthquake events have necessitated improvements with regard to the seismic performance of CFT-to-concrete connections (Kingsley 2005). Additionally, the exposed base plate connection may require special consideration with regard to shear transfer across the connection. Gomez et al., (2009) detail tests in which the shear is transferred through friction between the base plate and the grouted footing through anchor rod

bearing and shear key bearing. Each of these mechanisms typically adds complexity to the design and constructability of the connection compared to other connections that embed the CFT.

An embedded (as opposed to exposed) base plate connection is shown in Figure 4b. This connection is typically more rigid than the exposed base plate configuration and approaches a fully fixed end condition (Kingsley 2005). The rotation of the column is resisted by both the length it is embedded in the concrete and bearing on the base plate. In addition, the anchor rods (similar to the ones shown for the exposed base plate) could also be included, but for a sufficiently embedded CFT the moment, axial forces, and shear at the connection are mostly resisted by the bearing of the column and the base plate against the concrete, while the anchor rods are typically designed for construction loads (Grauvaridell, et al. 2005). Kingsley (2005) states that an embedment length equal to twice the diameter of the column cross-section is recommended to ensure a fixed end condition. Due to the deep embedment, bearing on the column is the predominant mechanism resisting the moment demand on the connection; therefore, the researcher points out that additional consideration of the steel reinforcement is necessary to prevent excessive damage and strength deterioration in the concrete. Furthermore, Kingsley (2005) notes that when the CFT has a shallow embedment depth in the concrete, bearing on the column is not adequate for developing the full moment strength of the column and plastification is achieved only when large, thick base plates and numerous anchor rods are used. Therefore, while this connection type can be designed so that a plastic hinge forms in the CFT prior to degradation of the concrete base, it has limitations including the requirement of deep embedment depths and potentially including additional anchor bolts. The detail necessitates a welded connection between the end plate and the CFT, and the inclusion of the embedded anchor bolts will often require the concrete to be placed in two lifts, further complicating construction.

While the embedded base plate connection provides adequate connection response as previously discussed, if maximum fixity of the connection and high seismic forces are of concern, structural steel can be fixed to the end of the tube, as shown in Figure 4c. Typically, a plate is first welded to the CFT, which is then connected to the structural elements (i.e. two channels). Another plate may be attached to the underside of the structural elements. All of the steel is then embedded in the concrete. Kingsley (2005) noted that the steel is only subjected to insignificant stresses, while the concrete foundation likely provides most of the resistance to the moment demand of the column. While this method's performance is good, constructability and cost are obvious disadvantages to this connection method.

The final method discussed by Kingsley is the semi-embedded connection shown in Figure 4d. While this connection is more complex than the embedded base plate configuration discussed previously, it has increased moment resistance. Kingsley (2005) describes three force resisting mechanisms for the semi-embedded connection which are: the bearing capacity provided by the couple from the CFT embedded in the concrete; anchor rod tensile capacity between the exterior base plate and the interior base plate; and an increased capacity inhibiting column pullout due to vertical reinforcement in the connection region. Even with the increased number of load paths resisting the column rotation, embedment length was still a controlling factor for the performance of the connection. For short embedments (i.e. 0.1 to 0.5 times the diameter of the pile), the steel tube remained elastic and yielding in the anchor bolts controlled the ultimate strength (Kingsley 2005). Kingsley (2005) noted that for intermediate embedments (i.e. 0.5 to 1.0 times the diameter of the pile), there was significant strength deterioration during cyclic loading due to heavy cracking of the concrete cap, and severe damage in the concrete cap controlled the maximum strength of the specimens. For an embedment of 2.0 times the diameter of the pile, it was also reported that no concrete cracking was observed, and the maximum strength of the specimen was limited by column yielding and local buckling.

Very similar to the embedded base plate connection previously discussed, Kingsley (2005) researched CFT-to-concrete connections using an annular ring welded to the end of the steel tube of the CFT. The CFT and annular ring were then embedded in the concrete at varying embedment depths. Embedment depths were either 0.6 or 0.9 of the diameter of the CFT. Pertinent results from this study include:

1. Connections with less embedment sustained more damage in the concrete, leading to significant deteriorations in strength;
2. The presence of vertical reinforcement did not increase the strength or stiffness of the connection, but concrete damage was reduced;
3. For the shallower embedment, the drift due to damage of the footing was approximately 90 percent of the total drift, while for the deeper embedment, the drift due to damage of the footing did not exceed 50 percent;
4. The longer embedment was necessary to provide the desired energy dissipation and deformation capacity required for high seismic demands (Kingsley 2005).

While the annular ring provides additional resistance to the moment demand, the results above suggest that the moment arm of compression regions on the CFT due to the embedment of the CFT in the concrete cap play an integral role in the overall response. Therefore, confinement of the concrete in these compression regions is an important parameter for improving the performance of the connection, as this confinement will

increase strength of the cap, helping to delay the damage to the concrete in the compression regions.

For all of these connections, the embedment length of the CFT in the concrete cap was found to be a very important parameter controlling the connection response. Kingsley (2005) reported that embedment lengths exceeding one and two times the diameter of the pile are necessary to ensure that the column strength can be developed.

Other connection methods outside of those described by Kingsley (2005) have been recently researched, and are covered in the following sections.

2.2.2 Silva et al. (1999) Research

Silva, et al. (1999) investigated the design and performance of three full-size bridge bents for the State of Alaska Department of Transportation and Public Facilities. These full-size bridge bents were designed using CFT-to-concrete pile cap connections in which the steel casing of the CFT column was not embedded into the concrete pile cap. Instead, internal reinforcing steel was used inside the steel casing of the CFT and extended into the concrete pile cap providing the tensile capacity for the connection. A typical reinforcing scheme for this type of connection is shown in Figure 5. The figure also shows a plan view of the CFT, detailing the amount of longitudinal steel that extends into the concrete pile cap.

The researchers found that the connection performed well under cyclic loading without any significant degradation to its lateral load resisting ability. Furthermore, the researchers stated that the development of plastic hinges in the columns (each full-size bent had three columns) confirmed that the anchorage details of the column bars were adequate as the concrete pile cap remained elastic with only evenly distributed cracking evident.

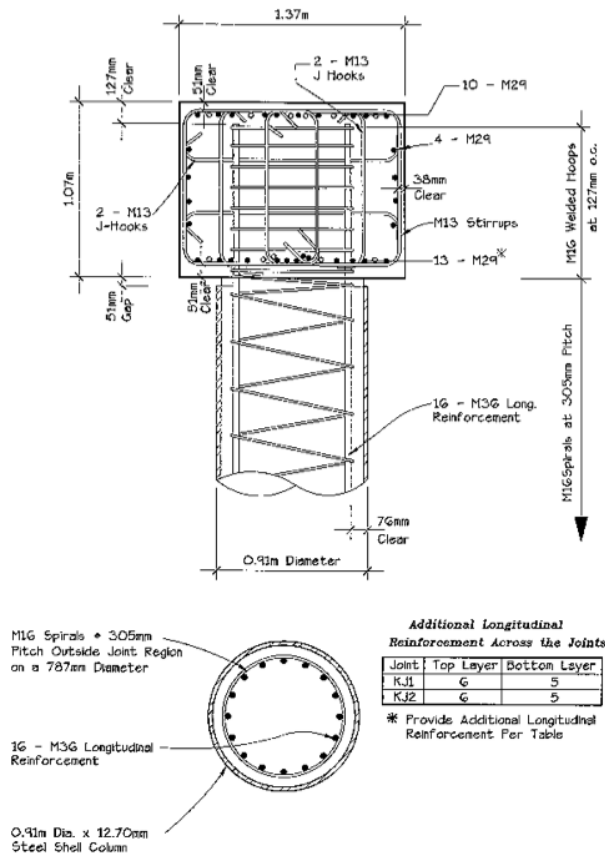


Figure 5: Reinforcing scheme for (Silva, et al. 1999)

Silva, et al. (1999) provided several design recommendations for this type of connection, including design equations for specifying the amount of steel needed for the connection area in the form of additional vertical stirrups, steel hoops, and additional top and bottom longitudinal steel. Separate design methods were developed for the tee-joints formed by interior columns and the knee-joints formed by exterior columns for the bent.

While the researchers were successful in obtaining the desired seismic design objective of maximizing energy dissipation in the bent during a seismic event for the aforementioned connection, the design methodology and connection resulting from this research is fairly complex and results in a significant amount of reinforcing steel spanning between the CFT and into the column connection. This additional steel is typically not specified in connections in which the CFT is embedded into the pile cap.

2.2.3 Rollins and Stenlund (2010)

Researchers at Brigham Young University teamed with the Utah Department of Transportation to complete a study in 2010 focused on characterizing the response of on-

grade concrete pile cap-to-steel pile connections. Lateral-load tests were performed on four pile caps, each with two 40-foot fully embedded piles for support. The reinforcement details were varied for two of the tests with embedment lengths of 6 and 12-inches, while the remaining two test specimens relied solely on deeper embedment lengths (12 and 24-inches) and no reinforcement to resist the lateral loads applied to the connection. The caps were loaded laterally until failure, and the force and deflection were monitored throughout the test. Similar to other research results, testing indicated that the connection can obtain the full moment capacity of the pile solely through embedment length, with no reinforcement required. The reinforced connections with reduced embedment lengths achieved between 40 and 60 percent of their pile moment capacity, which was still significantly higher than the moment capacity predicted by PCI equations. The reinforcement used for some of the connections included spirally-tied cages extending down into the concrete-filled pile and up into the concrete cap. On a separate note, load-displacement curves indicated that a “fixed-head” assumption is appropriate when modeling the pile (Rollins and Stenlund 2010).

2.3 Previous Pile Cap Testing at Montana State University

Stephens and McKittrick (2005) tested five embedded CFT to pile cap connections. All specimens used the same basic reinforcing scheme (Figure 6) in the pile cap. The intended variable between the tests was the specific amount and placement of this reinforcement in the pile cap, although the strength of the steel pipe pile and of the concrete also incidentally varied in some tests. Figure 7 shows the basic test setup, and Table 1 provides the experimental parameters and material properties used in this research. As the project advanced, the configuration of each successive model was adjusted based on the results of the preceding test. In general, the amount of reinforcement in the cap was increased in each test, starting with a model depicting current practice, up to a model with seven times the original amount of longitudinal and transverse reinforcing steel. In addition to the amount of reinforcement increasing with each test, the configuration of the reinforcing steel also varied, with the final test using a combination of spirals and U-shaped bars to confine the embedded pile.

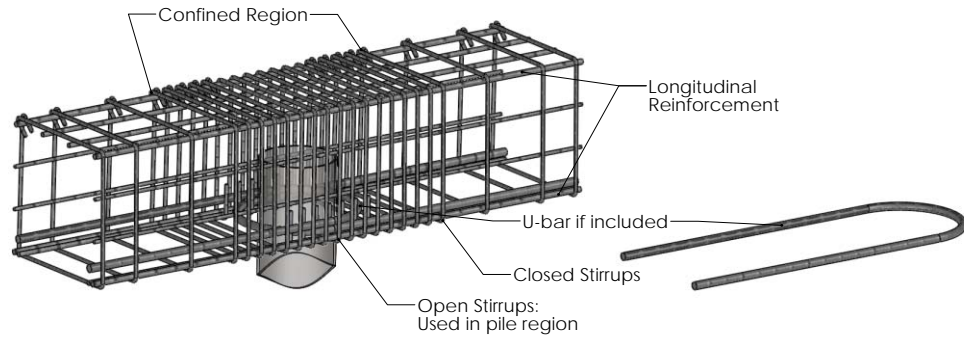


Figure 6: Basic Cap Configuration

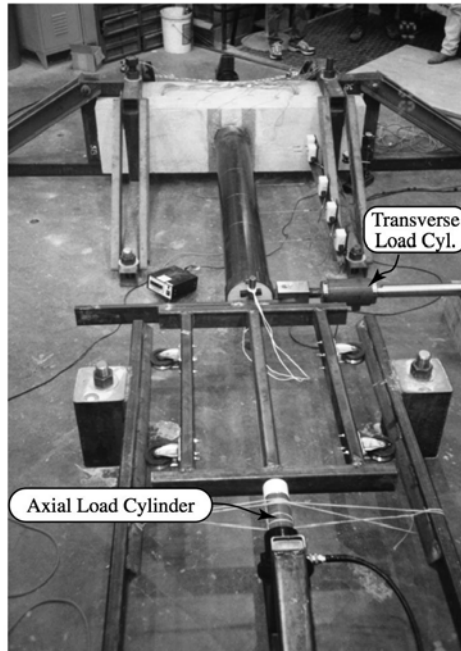
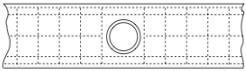
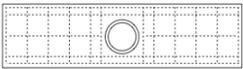
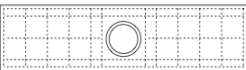
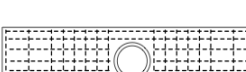
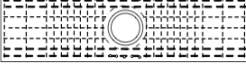


Figure 7: Test Setup (Stephens and McKittrick 2005)

Table 1: Experimental Parameters and Material Properties (Stephens and McKittrick 2005)

Item	Pipe Pile Wall Thickness, in	Longitudinal Steel Ratio, %	Transverse Steel Ratio, %	Yield Strength of Pile Steel ^a , psi	Concrete Strength ^a , psi	Comments	Reinforcing Layout
Full Size	0.5	0.40	0.09	35,000	4,000 ^a	Timber Creek Bridge, Powder River County, MT	
PC-1	0.32	0.41	0.09	53,000	4,832	Relative amount of reinforcement similar to that in full size structure	
PC-2	0.25	0.41	0.09	56,000	5,326	Same reinforcement as in PC-1, reduced wall thickness for pipe pile	
PC-3	0.25	1.09	0.24	53,000	3,150	Reinforcement increased by a factor of 3 compared to PC-1, concrete strength noticeably low compared to other models	
PC-3a	0.25	2.11	0.65	53,000	3,945	Reinforcement increased by a factor of 5 compared to PC-1	
PC-4	0.25	2.83	0.70	60,000	4,682	Longitudinal reinforcement increased by a factor of 7 compared to PC-1	

^a actual strengths at time of test reported for models, minimum design values reported for full size bridge

These CFT to pile cap connections were all loaded with a monotonically increasing lateral load until failure, and then in some cases cycled to evaluate the post-peak energy dissipation characteristics of the specimen. Table 2 summarizes the results from this series, including the observed failure mechanism and maximum moment observed in each test. Referring to Table 2, all of the specimens, with the exception of PC-4, failed due to crushing of the pile cap directly behind the pile and the formation of large cracks apparently along two compression struts (Figure 8) extending outward from the pile (in the direction of the applied load) to the faces of the cap. As can be seen in Table 2, the capacity of the caps generally increased with increasing amounts of longitudinal and transverse reinforcing steel. Of these specimens, PC-4 was the only specimen to achieve the desired failure mechanism (the formation of a plastic hinge in the CFT pile). This was achieved using a large amount of longitudinal and transverse reinforcement (seven times that of the original specimen) in a significantly congested reinforcing scheme (Figure 9) that included spirals and U-shaped bars around the embedded pile. Although this specimen was able to achieve the desired capacity, the actual ultimate capacity of this heavily reinforced cap and the attendant absolute effect of the reinforcing scheme on cap capacity could not be determined, as the pile failed before the cap capacity was reached.

Table 2: Test Results (Stephens and McKittrick 2005)

Test	Distinguishing Feature of the Test	Long Steel (%)	Trans Steel (%)	Pile Configuration	Failure Mechanism	Maximum Moment at Failure(ft-k)	Displacement Ductility	Condition at Failure
Full Size	generic full size cap and pile	0.40	0.09	0.50 inch wall, D/t = 32	unknown	unknown	unknown	unknown
1	believed to be scale model of full size structure, pipe pile judged to be relatively stiffer than it should have been	0.41	0.09	0.32 inch wall, D/t = 27	cracking of concrete cap	82	3.3	
2	same cap configuration as in PC-2, decreased wall thickness of pipe	0.41	0.09	0.25 inch wall, D/t = 34.5	cracking of concrete cap	74	3.3	
3	same pipe configuration, increased reinforcing steel in the cap	1.09	0.24	0.25 inch wall, D/t = 34.5	cracking of concrete cap	76	3.5	
3a	same pipe configuration, further increased reinforcing steel in the cap	2.11	0.65	0.25 inch wall, D/t = 34.5	cracking of concrete cap	102	2.6	
4	same pipe pile configuration, further increased reinforcing steel in the cap	2.83	0.70	0.25 inch wall, D/t = 34.5	plastic hinge in steel pipe pile	121	>3.9*	

* minimum value, connection was still carrying full failure load at point at which test was terminated



Figure 8: Typical Failure Mechanism seen in PC-1 through PC-3a (Stephens and McKittrick 2005)

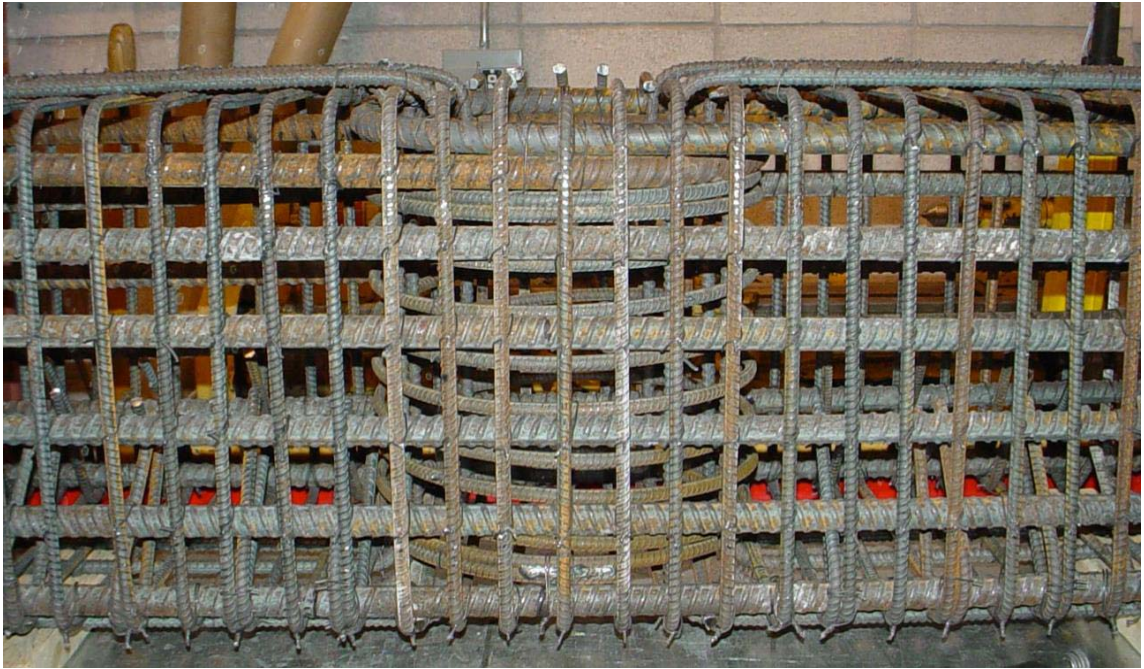


Figure 9: Reinforcing Steel for PC-4

3 SUMMARY OF MDT DESIGN GUIDE

3.1 Overview

Based in part on the results of the tests conducted by Stephens and McKittrick (2005), MDT developed a method for designing pile-to-pile cap connections, which is summarized in a MDT design guide. The MDT design process steps through the CFT pile-to-pile cap connection starting with determination of the embedment length required to carry the design moment demand between the CFT pile and the cap. The intent of the guide essentially is to provide adequate embedment of the CFT in the concrete cap to eliminate crushing of the cap concrete immediately adjacent to the CFT. Then, the moment required to generate a plastic hinge in the CFT is determined. If the design moment demand is equal to or approaches the plastic moment capacity of the CFT, reinforcing beyond the minimum amount required based on normal flexural design is added to ensure the cap can carry the design moment delivered from the CFT without experiencing excessive distress. The additional steel is specified to be either all U-shaped reinforcing steel (i.e., longitudinal bars that are bent 180 degrees to encircle the embedded pile) or a combination of U-shaped reinforcing steel and reinforcing steel placed through the pile. Finally, the guide specifies transverse reinforcement in the cap based on concrete confinement considerations.

These steps are reviewed in this chapter, followed by a discussion of critical areas of the design guide that require empirical verification. Note that a summary of the MDT design guide is included in Appendix A.

3.2 MDT Design Guide Methodology

3.2.1 Embedment Length

The MDT design guide assumes that the size of the pile (i.e., its diameter, D) as well as the required moment demand, M_u , are known prior to designing the pile-to-pile cap connection details. The required embedment length and reinforcing steel for the cap are then determined by modeling stress conditions in the concrete adjacent to the pile using a simple Whitney stress block approach (Figure 10). Such an approach is often used in modeling flexural behavior in reinforced concrete members. The connection model is solely focused on the moment demand to be transferred through the connection zone; effects of the axial load and shear force carried by the CFT on stress conditions are neglected relative to the magnitude and importance of the moment induced effects.

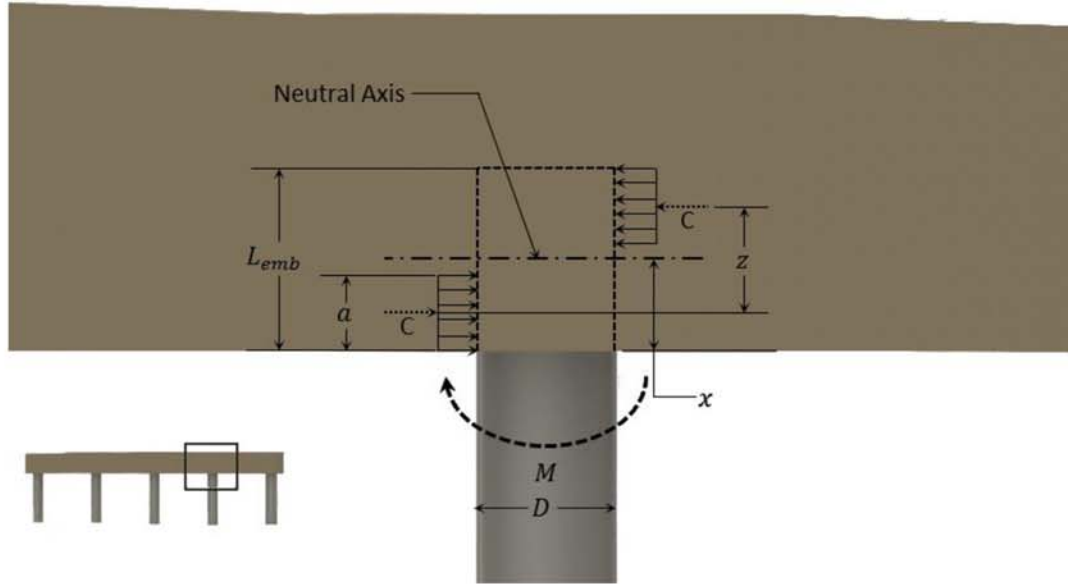


Figure 10: Assumed Whitney Stress distribution for determining embedment length

Referring to Figure 10, and in accordance with simple equilibrium considerations, the resultant of the upper compression block is taken to be equal to that of the lower compression block. Therefore, the location of the neutral axis, x , is one-half the embedment length, L_{emb} ,

$$x = \frac{L_{emb}}{2} \quad \text{Equation 3.1}$$

Additionally, the depth of the stress block, a , can be calculated following typical reinforced concrete design practice as a fraction of the neutral axis depth,

$$a = \beta_1 \cdot x \quad \text{Equation 3.2}$$

The β_1 parameter is a factor for determining the depth of a rectangular stress block that reasonably approximates the actual parabolic stress distribution that more realistically forms in this situation; β_1 is a function of the concrete compression strength (Wang, Salmon and Pincheira 2007).

Thus, as an embedment length has been assumed, the depth of the stress block, a , can be calculated from Equations 3.1 and 3.2, the moment arm, z , between the compression stress resultants (see Figure 10) can be determined,

$$z = L_{emb} - a \quad \text{Equation 3.3}$$

Also, by enforcing moment equilibrium of the forces shown in Figure 10, the moment demand, M_u , can be related to the compression force resultant, C ,

$$M_u = C \cdot z \quad \text{Equation 3.4}$$

Further, the concrete compression resultant, C , can be calculated as the magnitude of the stress in the concrete, f_u , multiplied by the projected area it acts over, which is equal to the pile diameter, D , multiplied by the depth of the stress block, a ,

$$C = f_u \cdot a \cdot D \quad \text{Equation 3.5}$$

Thus, for a given moment demand, M_u , the associated stress demand in the concrete, f_u , can be solved by substituting Equation 3.5 into Equation 3.4, and rearranging terms,

$$f_u = \frac{M_u}{a \cdot D \cdot z} \quad \text{Equation 3.6}$$

Equation 3.6 can be re-expressed in terms of the “input” parameters of the problem, namely, the embedment length, L_{emb} , the pile diameter, D , and the design moment demand, M_u ,

$$f_u = \frac{2 \cdot M_u}{D \cdot \beta_1 \cdot \left(1 - \frac{\beta_1}{2}\right) \cdot L_{emb}^2} \quad \text{Equation 3.7}$$

Finally, the concrete compression stress demand, f_u , can be compared to the design concrete compression strength, f_n , to determine the adequacy of the assumed embedment length, L_{emb} . The factored compression strength, f_n , is taken as the unconfined compression strength, f'_c , multiplied by a confinement factor, α , and a strength reduction factor, φ_b ,

$$f_u \leq \{f_n = \varphi_b \cdot \alpha \cdot f'_c\} \quad \text{Equation 3.8}$$

The φ_b factor is defined as 0.7 in AASHTO 5.5.4.2 for bearing on concrete. The α parameter is a factor used to increase the strength of the concrete based on confinement considerations. The MDT design guide defines the α parameter to be 1.8, based on the previous work completed by Stephens and McKittrick (2005).

Referring to Equation 3.7, increasing the embedment length of the pile will decrease the crushing demand on the concrete, within a practical limit as other load and cover concerns may limit the embedment. Therefore, an appropriate embedment length, L_{emb} , can be determined, with the intent to eliminate concrete crushing as the controlling failure mechanism.

3.2.2 Plastic Moment Capacity of the Pile

After determining the necessary embedment length of the pile in the pile cap, the plastic moment capacity of the concrete-filled steel pile is calculated.

The MDT design guide simplifies this calculation by basing the plastic moment capacity of the CFT solely on the plastic section modulus of the steel pile, Z , and ignoring any increase in capacity due to the concrete fill. The plastic section modulus of the steel pile can be determined simply from the pile diameter, D , and the pile wall thickness, t_p ,

$$Z = \frac{D^3}{6} - \frac{(D - 2 \cdot t_p)^3}{6} \quad \text{Equation 3.9}$$

The plastic moment capacity of the steel pile is then simply calculated as,

$$M_{n_{pile}} = F_y \cdot Z \quad \text{Equation 3.10}$$

where F_y is the yield strength of the steel pile. The yield strength, F_y , is specified with over-strength considerations taken into account and should not be the specified minimum yield strength of the steel pile.

As previously mentioned, the increased plastic moment capacity of the CFT due to the concrete-fill is not considered in Equation 3.10; the design guide uses an additional over-strength factor of 1.25 to account for this and other uncertainties in the design approach. The final plastic-moment capacity, M_p , of the concrete-filled steel pile is thus defined by the design guide as:

$$M_p = 1.25 \cdot M_{n_{pile}} \quad \text{Equation 3.11}$$

The calculated plastic moment capacity of the pile, M_p , is then used as part of a limit state check for additional steel.

3.2.3 Comparison of Demand and Pile Capacity

The MDT design guide provides a check to determine whether additional reinforcement is necessary in the cap (beyond the minimum required reinforcement described in Section 3.2.4 below) to ensure the cap can carry the design moment demand. It accomplishes this

by comparing the required moment demand specified for the connection, M_u , with a percentage of the plastic-moment capacity of the pile, M_p , which was calculated in the previous section. The guide specifies that additional reinforcement is necessary in the cap when $M_u > 0.60 \cdot M_p$; otherwise, the minimum required reinforcement is expected to be adequate to transfer the design moment M_u . A damage threshold at an applied moment of $0.75 M_p$ was seen in the tests conducted by Stephens and McKittrick (2005). To conservatively address this situation a threshold value of 0.60 is used.

3.2.4 Normal Flexural Design

The normal flexural design procedure for the concrete cap includes designing the longitudinal reinforcing steel in a member to ensure: adequate flexural strength (AASHTO LRFD 5.7.2.2.), that the cracking moment does not exceed the ultimate post-crack capacity (AASHTO LRFD 5.7.3.3.2), that longitudinal cracking due to splitting isn't an issue (AASHTO LRFD 5.7.3.5), and that the minimum amount of steel to prevent shrinkage and temperature cracks is included (AASHTO LRFD 5.10.8). Typical flexural reinforcement is shown in Figure 11.

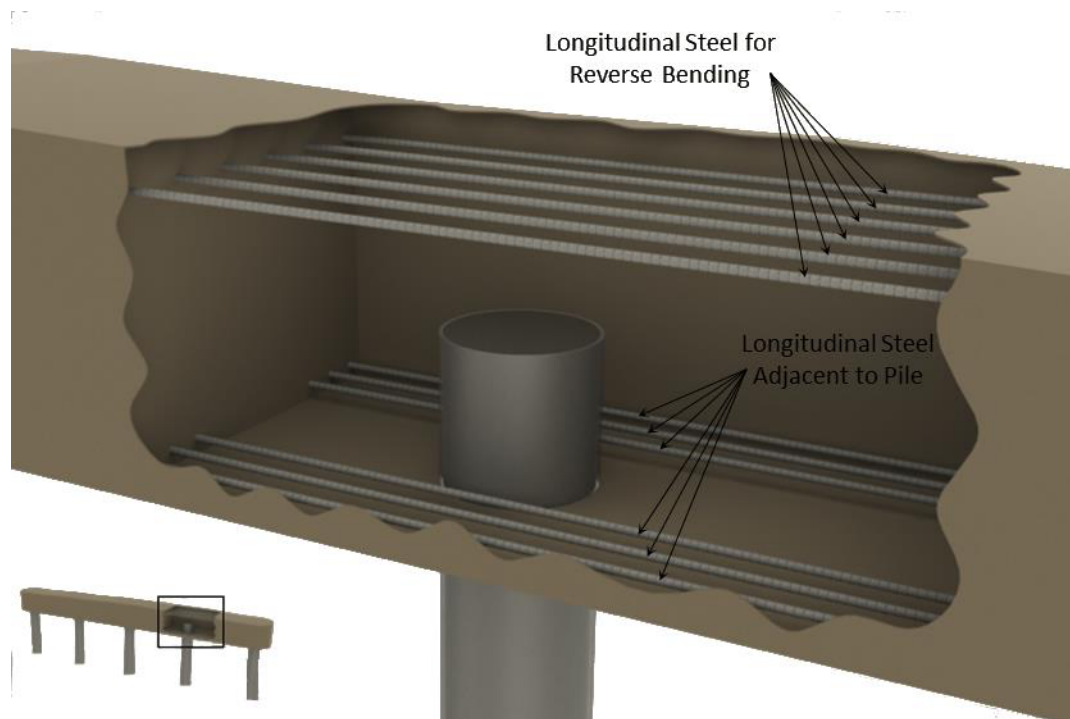


Figure 11: Minimum longitudinal steel implementation

3.2.5 Additional Longitudinal Steel

If necessary, i.e., if $M_u > 0.6 \cdot M_p$, the design guide provides a method to calculate the amount of additional longitudinal reinforcement steel necessary to ensure the cap will be able to develop the full design moment without significant degradation in the connection zone. This additional steel, to be placed in the bottom of the cap, is calculated based on the resultant force, C , which develops in the cap concrete adjacent to the embedded CFT under the design moment, as previously shown in the analysis model presented in Figure 10. Setting the resultant compression force, C , equal to a balancing tension force calculated as an area of steel, A_s , multiplied by the yield strength of the steel, f_y , and using Equations 3.5 and 3.6, it can be shown that,

$$A_s = \frac{M_u}{\phi_f \cdot z \cdot f_y} \quad \text{Equation 3.12}$$

where a capacity reduction factor, ϕ_f , of 0.9 has been introduced, consistent with a LRFD approach for ductile steel tensile failure mechanisms.

The design guide then reduces the amount of reinforcing steel to be added to the cap to 25-percent of the amount calculated in Equation 3.12. This reduction is done in light of the minimum steel already specified in the cap (as described in Section 3.2.4), as well as other load carrying mechanisms conservatively not considered in the simple analysis model being used. The guide further specifies that the additional reinforcing steel should be added in a U-shape configuration (U-bar), or as steel reinforcement placed continuously through the embedded CFT (through-bar). These configurations are shown in Figure 12a and Figure 12b, respectively. Further, the design guide indicates that a U-bar must be used in combination with the through-bar when the through-bar option is chosen.

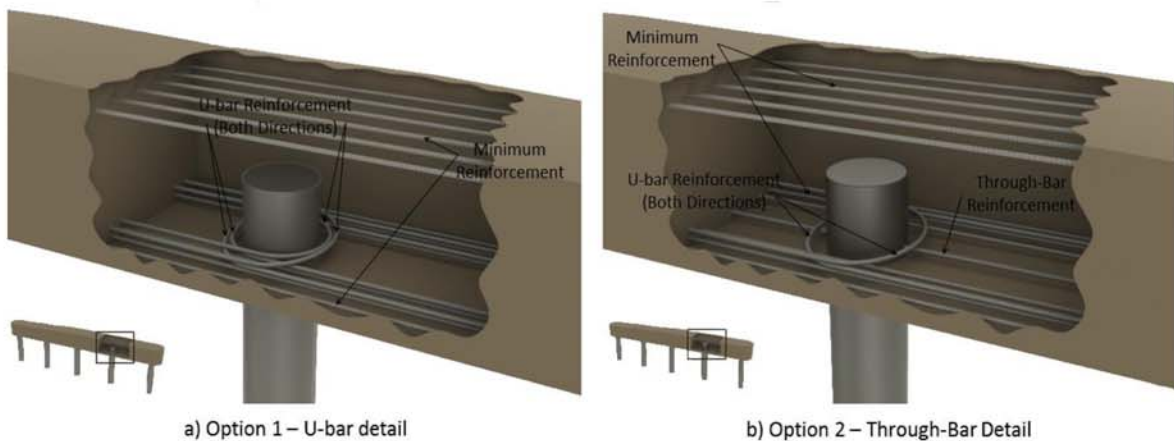


Figure 12: MDT design guide schemes for additional reinforcement longitudinal steel

3.2.6 Transverse Steel

The MDT design guide prescribes the amount of transverse steel necessary in the cap basically using the requirements of section 5.10.11.4.1d of AASHTO LRFD Bridge Specifications. This code section specifies the transverse reinforcement for core confinement at plastic-hinge zones in pile bents (AASHTO 2011). For a rectangular cross section, it identifies two limit states for defining the area of the transverse steel, A_{sh} . Both of these limit states are functions of the spacing of the transverse steel. Therefore, by assuming a stirrup (hoop) spacing, the necessary steel area can be determined.

The first limit state, shown in Equation 3.13, is a function of the gross area of the section, A_g , and the core area of the section, A_c , as well as the ratio of the compression strength of the concrete and the yield stress of the steel, f'_c and f_y , respectively.

$$A_{sh} \geq 0.30 \cdot s \cdot h_c \cdot \frac{f'_c}{f_y} \cdot \left[\frac{A_g}{A_c} - 1 \right] \quad \text{Equation 3.13}$$

Note that s is the spacing of the hoops and shall not exceed 4.0 in as specified in AASHTO LRFD 5.10.11.4.1d. The h_c parameter is the core dimension in the direction under consideration and the design guide further specifies this to be the width of the core, w_{core} . Therefore, in the design guide, Equation 3.13 is shown as Equation 3.14 (MDT 2005).

$$A_{sh} \geq 0.30 \cdot s \cdot w_{core} \cdot \frac{f'_c}{f_y} \cdot \left[\frac{A_g}{A_c} - 1 \right] \quad \text{Equation 3.14}$$

The second limit essentially provides a lower bound on the ratio of A_g/A_c in Equation 3.20; therefore, the second limit state will specify a minimum amount of confinement steel for situations when the core area is close to the gross area of the section. The design guide form of this equation is,

$$A_{sh} \geq 0.12 \cdot s \cdot w_{core} \cdot \frac{f'_c}{f_y} \quad \text{Equation 3.15}$$

and as previously mentioned in the description of the first limit state, the h_c parameter in the AASHTO equation is equal to the width of the core, w_{core} , shown here. A typical transverse reinforcement scheme is shown in Figure 13. Several intricacies that are important and may not be immediately apparent relative to this transverse steel arrangement shown in Figure 13 are:

1. Open stirrups are only used in the pile region; closed stirrups are used in all other regions;
2. The region in which confining steel is required extends one-half the cap height beyond the pile in each direction;
3. The stirrup spacing in the confined region is defined by Equations 3.14 and 3.15;
4. The maximum stirrup spacing is not to exceed one-quarter of the minimum member dimension or 4.0 in center-to-center.
5. The details of the closed stirrup configurations are governed by AASHTO LRFD 5.10.11.4.1d recommendations.

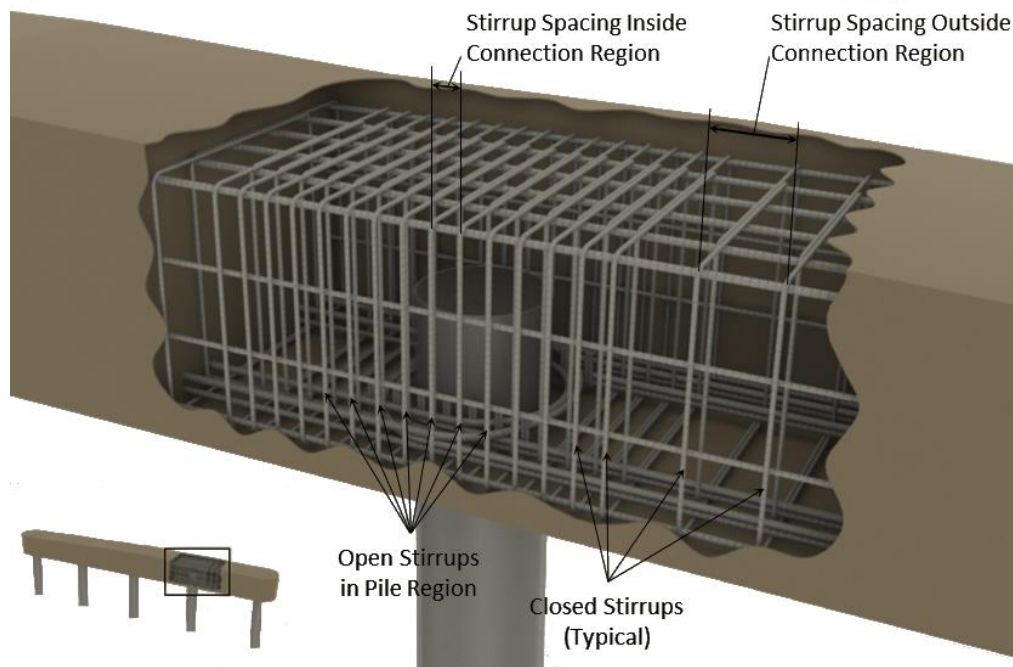


Figure 13: Transverse steel representation

3.3 Discussion

As described above, the MDT design guide outlines a methodology for the design of CFT-to-concrete pile cap connections that generates the pile embedment depth and minimum cap reinforcement required to ensure the cap can carry the bending moment imparted to it by the pile without experiencing extensive degradation. This methodology is unique in its simplicity and results when compared to other designs for pile-to-pile cap connections. To emphasize this point, Figure 14a shows the amount of steel used to obtain a plastic hinge in the concrete-filled steel pipe pile following a more conventional

reinforcing design methodology as was done by Stephens and McKittrick (2005). In contrast, Figure 14b shows the reinforcing cage, which results from using the MDT design guide for the same moment demand. The MDT approach reduces the amount of longitudinal and confining steel required to maintain the integrity of the connection region in the cap by using U-shaped bars encircling the pile to obtain the desired capacity and performance.

While the MDT methodology is based on the testing completed by Stephens and McKittrick (2005), in the interest of providing the best possible and most complete guidance on connection design, it includes innovations and elements that were not specifically evaluated in that test program. Some of these features of the methodology are discussed in more detail below.

First and foremost, configuring the primary longitudinal reinforcing steel in the connection zone in a U-shape encircling the embedded pile as a singular means of increasing the capacity of the cap was not specifically tested in that program. The closest configuration tested by Stephens and McKittrick (2005) did include U-shaped reinforcement encircling the pile, but it also included a spiral around the pile through which the longitudinal bars were hooked (see Figure 14a). While the U-bar configuration used by itself was expected to perform well, this expectation can only be confirmed through testing. On a related matter, the guide uses a concrete confinement factor in establishing the useable compression strength of the concrete in the cap of 1.8, as directly suggested by the test results (Stephens and McKittrick, 2005). Due to the expected efficiency of the U-bar reinforcement configuration that was adopted in the design guide, however, the amount of confining steel in the cap is generally reduced relative to that used in the test program. This change could affect the physical level of confinement provided by the reinforcing steel and the attendant concrete confinement factor that should be used in the design process.

The MDT design guide also uses a simplified approach to determine the amount of additional longitudinal steel that may be required (above minimum standard thresholds) to develop the design capacity of the cap in the connection zone. While this approach is based on observations made in the test program, it appears to be more empirical than mechanistic in nature, and its robustness in addressing various design situations (i.e., a variety of cap and pile geometries and applied loads) needs to be further evaluated. In developing the design guide, MDT also needed to determine a formal methodology to systematically design the transverse steel required in the pile cap. The guide uses the AASHTO requirements for confinement of the core concrete in columns at plastic-hinge

zones in pile bents (AASHTO, 2011) for this purpose, which once again is expected to be adequate, but can only be verified through testing.

From an analytical perspective, the MDT methodology uses a relatively simple model to represent conditions in the pile cap adjacent to the steel pipe pile. This model is based on the well-accepted Whitney stress block approach to representing flexural compression behavior in concrete. In applying this approach, however, many assumptions must be made, and only a few tests are available on a few connection configurations to judge the accuracy of these assumptions.

In light of these various observations, MDT made the decision to conduct the additional series of CFT pile-to-pile cap connection tests described in the next Chapter of this report. The connections tested were directly designed following the guide with the intent of further evaluating its performance.



(a) Stephens and McKittrick (2005) Test 5



(b) MDT Design Guide Test 1

Figure 14: Comparison of reinforcement schemes

4 EXPERIMENTAL PROGRAM

An experimental program was executed to verify that the MDT design guide for detailing CFT-to-concrete pile cap connections generated configurations with the expected behavior and strength. Ideally, this program would have been conducted using full-size connections subjected to realistic lateral loads, i.e., a full bridge bent consisting of several piles and the pile cap, subjected to a programmed dynamic base excitation. In light of available resources and facilities, and consistent with earlier pile cap testing done at MSU for MDT (Stephens and McKittrick, 2005), it was determined that the program objectives could be realized using half-size models of a subsection of a typical bridge bent, centerline-to-centerline between pile supports (see Figure 15), subjected to quasi-static monotonic and cyclic loads to failure. Thus, each connection model consisted of a single pile and an attendant length of pile cap. The models were statically tested so as to generate the deflected shape expected in this subsection of a full-size bent subjected to a lateral load, as shown in Figure 15.

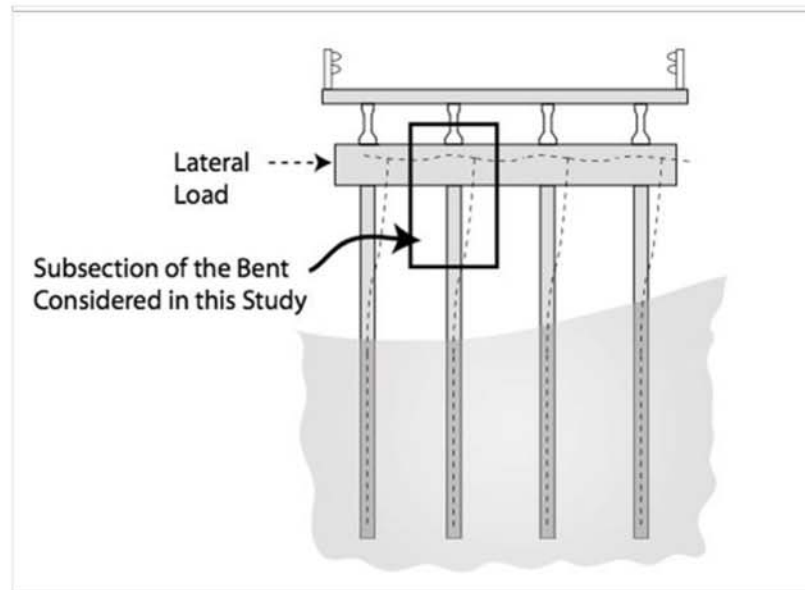


Figure 15: Typical bridge bent with assumed deflected shape

A typical test specimen is shown in Figure 16. The U-bar, rather than the through bar, connection configuration was used for all the models, as the U-bar configuration was judged to be simpler to construct and was expected to offer better performance than the through bar concept. Four different configurations were tested. Three of these configurations were designed in accordance with the design guide; the fourth

configuration incorporated a second set of U-bars encircling the pile in the interior of the cap (close to the tip of the embedded pile). With the exception of the first test, all tests were purposefully designed so that failure would occur in the pile cap rather than the CFT pile. This outcome was forced by deliberately using oversized pipe piles in the tests. As previously mentioned, the connection element of primary concern in this investigation was the pile cap rather than the CFT pile. Considerable work has been done studying the capacity and behavior of CFTs, while only limited research has been done on cap configurations pertinent to this study.

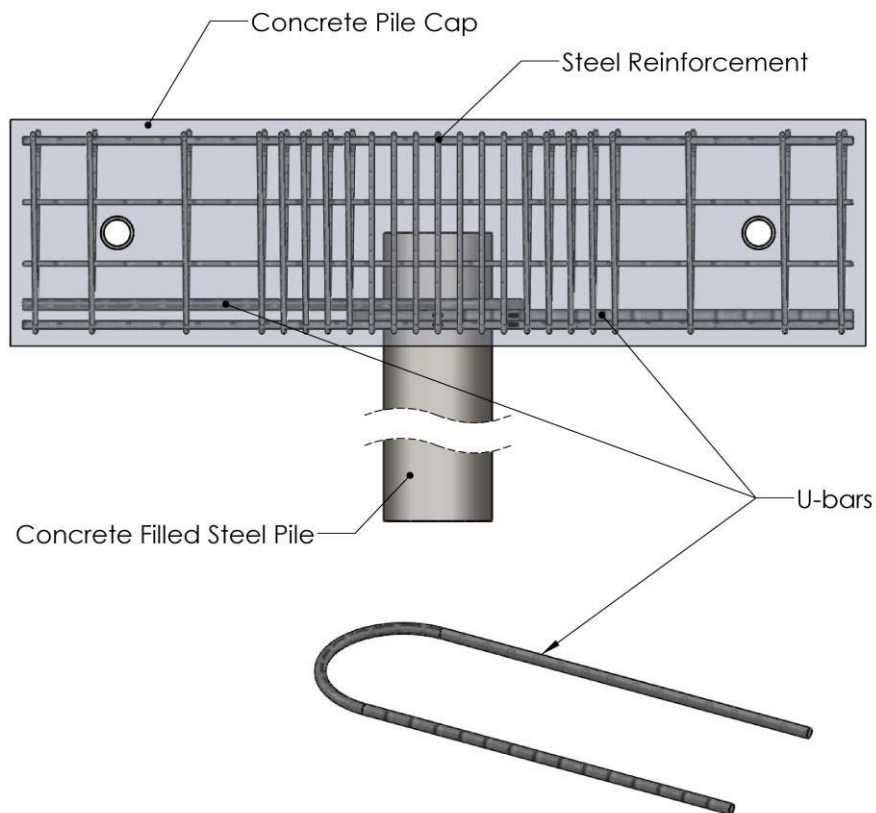


Figure 16: Typical test specimen

In the first four tests (VT1, VT2, VT2.5, and VT3), the connection configurations were subjected to monotonic loading, capturing the ultimate strength of each configuration and providing general information on post-failure ductility. Two more tests were completed using a cyclic load scheme (CT1 and CT2) to capture performance characteristics of the connections under multiple cycles of fully reversed, increasing load. The second of these two cyclic load tests was conducted on the cap configuration consisting of two sets of U-bars.

4.1 Fundamental Test Specimen Design

The primary variables from the MDT design guide equations evaluated in this investigation were CFT embedment length and pile cap concrete strength. Following the design guide, the moment capacity of the cap in the connection zone is controlled by one of three limit states: 1) crushing of the concrete adjacent to the embedded pile (addressed by Equation 3.8), 2) yielding of the “bottom” longitudinal reinforcing steel (addressed by Equation 3.12), and yielding of the transverse confining steel (addressed by Equations 3.14 and 3.15). For a given CFT and pile cap geometry, the first limit state is dependent on CFT embedment length and cap concrete strength; the second, embedment length, concrete strength, and steel yield strength; and the third, concrete strength and steel yield strength. Thus, in this investigation, the pile cap and CFT geometry were held constant, while the concrete strength and embedment length were varied.

The concrete pile cap used in all tests was 18-by-18-by-68 inches, with an 8.625 inch (outside diameter) CFT embedded in the center of the “bottom” face. These dimensions are approximately one-half the dimensions of the pile and pile cap used in the Timber Creek Bridge, which MDT indicated was representative of this type of substructure construction. The first limit state equation referred to above (for crushing of the cap concrete) was used with these dimensions to calculate the expected moment capacity of the pile cap as a function of embedment length for various concrete strengths. The results of these calculations are presented in Figure 17. Also shown on Figure 17 are the specific combinations of embedment length and design concrete strength for the models tested in this investigation. Additional features of the models tested in this investigation are summarized in Tables 3 and 4 for the monotonic and cyclic tests to failure, respectively. The information in these tables is grouped and ordered by row to successively follow the major steps in the design guide. In the sections that follow, a detailed review of the design of the first test specimen is presented followed by more cursory descriptions of the design of the remaining test specimens focusing on their differences from the first specimen. All of the original design calculations are included in Appendix B.

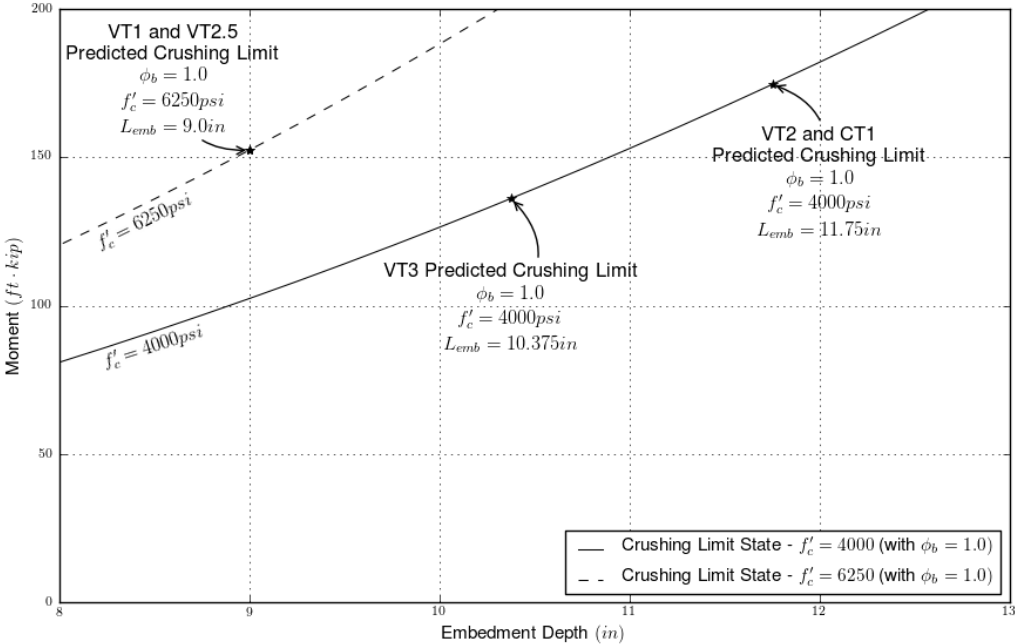


Figure 17: Capacities from crushing limit state per the MDT design guide

Table 3: Summary of design parameters, monotonic tests

Verification Test:		VT1	VT2	VT2.5	VT3
Concrete Crushing and Pile Embedment Requirements	Concrete Compression Strength	$f'c = 6.25$ ksi	$f'c = 4$ ksi	$f'c = 6.25$ ksi	$f'c = 4$ ksi
	β_1 (Based on Compression Strength)	$\beta_1 = 0.737$	$\beta_1 = 0.85$	$\beta_1 = 0.737$	$\beta_1 = 0.85$
	Embedment	$L_{emb} = 9.0$ in	$L_{emb} = 11.75$ in	$L_{emb} = 9.0$ in	$L_{emb} = 10.375$ in
	Concrete Confinement Factor	$\alpha = 1.8$			
	Moment Arm	$z = 5.175$ in	$z = 6.756$ in	$z = 5.681$ in	$z = 5.966$ in
	Predicted Crushing Capacity	$M_n = 138.8$ ft-kip $\phi_b \cdot M_n = 97.1$ ft-kip	$M_n = 175.6$ ft-kip $\phi_b \cdot M_n = 122.2$ ft-kip	$M_n = 138.8$ ft-kip $\phi_b \cdot M_n = 97.1$ ft-kip	$M_n = 136.1$ ft-kip $\phi_b \cdot M_n = 95.3$ ft-kip
	Pile Wall Thickness	$t_p = 0.25$ in	$t_p = 0.50$ in (over-sized to ensure failure in cap)		
	Calculated M_p of Pile (MDT Design Guide Method)	$M_p = 96.8$ ft-kip	$M_p = 182.5$ ft-kip (oversized to ensure failure in cap)		
Minimum Steel Requirements	Cracking Moment	$M_{cr} = 58.9$ ft-kip ($1.2 \times M_{cr} = 70.7$ ft-kip)			
	Minimum Required Steel based on $1.2 \times M_{cr}$	$A_{s_min} = 0.887$ in ²			
	Reinforcement Implemented for Cracking	2 #4s and 2 #5s $\rightarrow A_{s_min} = 1.0$ in ²			
Additional Steel Requirements	Additional Steel Description	1 #7 U-bar in each direction	1 #4 and 1 #5 in each direction	1 #7 U-bar in each direction	1 #7 U-bar in each direction
	Area of Additional Steel Implemented (U-bars)	$A_{s_Add} = 1.203$ in ²	$A_{s_Add} = 1.006$ in ²	$A_{s_Add} = 1.203$ in ²	$A_{s_Add} = 1.203$ in ²
	Predicted Capacity With Additional Steel	$M_n = 136.7$ ft-kip $\phi_f \cdot M_n = 123.1$ ft-kip	$M_n = 135.9$ ft-kip $\phi_f \cdot M_n = 122.3$ ft-kip	$M_n = 136.7$ ft-kip $\phi_f \cdot M_n = 123.1$ ft-kip	$M_n = 143.5$ ft-kip $\phi_f \cdot M_n = 129.2$ ft-kip
Transverse Steel Requirements	Transverse Steel Required	$A_{s_trans} = 0.22$ in ²			
	Spacing of Transverse Steel	$s = 1.75$ in			
	Reinforcement Implemented for Transverse	#3 stirrups @ 1.75 in $\rightarrow A_{s_trans} = 0.22$ in ²			
Verification Test:		VT1	VT2	VT2.5	VT3

Table 4: Summary of design parameters, cyclic tests

Cycle Test:		CT1	CT2
Concrete Crushing and Pile Embedment Requirements	Concrete Compression Strength	$f'_c = 4$ ksi	
	β_1 (Based on Compression Strength)	$\beta_1 = 0.85$	
	Embedment	$L_{emb} = 11.75$ in	
	Concrete Confinement Factor	$\alpha = 1.8$	
	Moment Arm	$z = 6.76$ in	$z = 6.75$ in
	Predicted Crushing Capacity ($\phi_b = 0.7$)	$M_n = 175.6$ ft·kip $\phi_b \cdot M_n = 122.2$ ft·kip	$M_n = 175.6$ ft·kip $\phi_b \cdot M_n = 122.2$ ft·kip
	Pile Wall Thickness	$t_p = 0.73$ in (over-sized to ensure failure in cap)	
	Calculated M_p of Pile (MDT Design Guide Method)	$M_p = 248.5$ ft·kip (oversized to ensure failure in cap)	
Minimum Steel Requirements	Cracking Moment	$M_{cr} = 58.9$ ft·kip ($1.2 \times M_{cr} = 70.7$ ft·kip)	
	Minimum Required Steel based on $1.2 \times M_{cr}$	$A_{s_min} = 0.887$ in ²	
	Reinforcement Implemented for Cracking	2 #4s and 2 #5s $\rightarrow A_{s_min} = 1.0$ in ²	
Additional Steel Requirements	Additional Steel Description	1 #4 and 1 #5 in each direction (double stacked)	
	Area of Additional Steel Implemented (U-bars)	$A_{s_Add} = 1.006$ in ²	$A_{s_Add} = 2.012$ in ²
	U-bar Locations	Exterior Only	Interior and Exterior
	Predicted Capacity With Additional Steel	$M_n = 135.9$ ft·kip $\phi_r \cdot M_n = 122.3$ ft·kip	$M_n = 135.9$ ft·kip $\phi_r \cdot M_n = 122.3$ ft·kip
Transverse Steel Requ.	Transverse Steel Required	Same Confiruation as VT2	
	Spacing of Transverse Steel	$s = 1.75$ in	
	Reinforcement Implemented for Transverse	#3 stirrups @ 1.75 in $\rightarrow A_{s_trans} = 0.22$ in ²	
Cycle Test:		CT1	CT2

4.2 Specimen VT1 Design

The following section steps through the MDT design methodology described in Chapter 3 as applied to specimen VT1. As previously mentioned, the moment demand a connection needs to carry typically is known (i.e., M_u , with M_u often set equal to M_p of the CFT to ensure a ductile failure mechanism for the connection). Indeed, for the first test, VT1, the moment demand was assumed to be the plastic-moment capacity of the CFT. The basic cross section was predetermined as 18 in by 18 in to fit in the existing testing frame and to be consistent with the earlier tests conducted at MSU (Stephens and McKittrick, 2005).

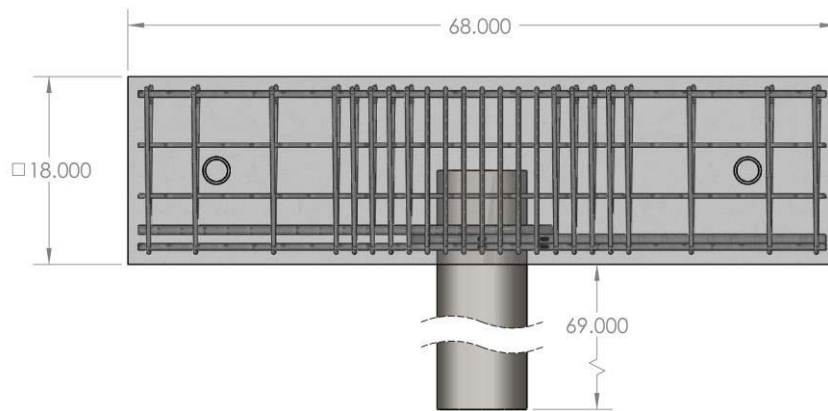


Figure 18: General design parameters established from previous testing

4.2.1 Plastic Moment Capacity of the Pile

The specific size of the steel pile used in VT1 was based on the previous research by Stephens and McKittrick (2005). In the earlier tests, the outer diameters of the steel pipe piles were all 8.625 in, and it was determined that a wall thickness of 0.25 in provided a similar diameter-to-thickness ratio (34.5) as a full-size pile used by MDT. Therefore, the first step in designing test specimen VT1 was to calculate the plastic-moment capacity of a concrete-filled steel pile with these dimensions. The steel pipe was specified to be ASTM A53 Grade B steel, which has a minimum yield stress of 35,000 psi. Prior testing by Stephens and McKittrick (2005) indicated that the actual pile yield stress averaged about 53,000 psi. Therefore, the higher yield strength value of 53,000 psi was used in calculating the pile's plastic-moment capacity.

The three equations used in the MDT design guide to calculate the plastic-moment capacity of the concrete-filled steel pile were presented in Chapter 3, and are repeated here for convenience as Equations 4.1 through 4.3.

$$Z = \frac{D^3}{6} - \frac{(D - 2 * t_p)^3}{6} \quad \text{Equation 4.1}$$

$$M_{n_{pile}} = F_y \cdot Z \quad \text{Equation 4.2}$$

$$M_u = M_p = 1.25 \cdot M_{n_{pile}} \quad \text{Equation 4.3}$$

Recall from Chapter 3 that D and t_p are the outside diameter and wall thickness of the steel pile, respectively, and that the 1.25 factor in Equation 4.3 accounts for the contribution of increased capacity due to the concrete-fill in the steel pipe, as well as other factors. Thus, for the first test specimen the demand placed on the pile-to-pile cap connection from the concrete-filled steel pile was calculated to be $M_u = 96.8$ ft·kip.

4.2.2 Embedment Length

The next step in the design process was to calculate the necessary embedment length of the CFT so that the cap could carry the design moment demand, M_u , without crushing of the concrete pile cap. As outlined in Chapter 3, this is calculated based on a model that uses a simple Whitney stress block approach to represent the stresses in the concrete. The crushing limit state was checked using the equations for stress demand and capacity previously described in Chapter 3 and repeated here as Equation 4.4.

$$f_u \leq \{f_n = \phi_b \cdot \alpha \cdot f'_c\} \quad \text{Equation 4.4}$$

The compressive stress demand, f_u , is a function of M_u and L_{emb} , as shown in Equation 3.7. To be consistent with prior testing completed by Stephens and McKittrick (2005), an embedment length of 9 in was used. For the compression strength, ϕ_b was set to 1.0 instead of 0.7 because the model was being built in laboratory conditions where construction was precise and the material parameters were well known. The concrete confinement factor, α , was set at 1.8. The final parameter in the equation, f'_c of the concrete, was set at a target value of 4,000 psi, although the actual concrete strength at the time of testing was 6,250 psi. Therefore, and as shown in more detail in Appendix B, the demand on the concrete, $f_u = 6.8$ ksi, was less than the capacity of the concrete, $f_n = 7.2$ ksi, which verified that the 9-in embedment length was adequate.

4.2.3 Pile Cap Reinforcement

As previously described in Chapter 3, the design guide evaluates the reinforcing steel required in the cap in two steps: the longitudinal steel required as part of MDT's normal flexural design, followed by calculation of any additional steel in the connection zone necessary to carry the full moment demand from the CFT. Additional steel is required if

the design demand exceeds 60 percent of the plastic-moment capacity of the pile, which is obviously the situation in this case (recall that M_u was assumed to be equal to M_p).

Beginning with the longitudinal steel requirements from a normal flexural design, the decision was made to use the reinforcing required to carry the cracking moment as a baseline for these designs. The cracking moment of the cap can be determined from Equation 4.5, where f_r is the modulus of rupture and is equal to 727 psi for the design compression strength, f'_c , of 4,000 psi concrete ($11.5\sqrt{f'_c}$, AASHTO 5.4.2.6).

$$M_{cr} = \frac{f_r \cdot w \cdot h^2}{6} \quad \text{Equation 4.5}$$

The calculated cracking moment for this specimen was 58.9 ft·kip. The design guide further specifies that the design capacity, M_n , should be taken as $1.2 \cdot M_{cr}$ (consistent with AASHTO requirements), from which the minimum area of steel can be calculated using Equation 4.6.

$$M_n = A_s \cdot f_y \cdot \left(d - 0.59 \cdot \frac{A_s \cdot f_y}{f'_c \cdot w} \right) \quad \text{Equation 4.6}$$

Recall that d is the distance from the compression surface to the center of the longitudinal steel, f_y is the yield strength of the longitudinal steel, and w is the width of the cap. These parameters were defined as shown in Figure 19. Therefore, for VT1 the required area of steel, A_s , was found to be 0.9 in^2 , for which two #4 and two #5 bars ($A_s \approx 1.0 \text{ in}^2$) were chosen. This configuration of steel was placed in both the top and bottom surfaces of the cap to cover fully reversed bending. Note that four #3 bars were also placed on the sides of the cap, which are also shown in Figure 19, as such bars were similarly placed in the full-size example detail provided with the MDT design guide (see Appendix A).

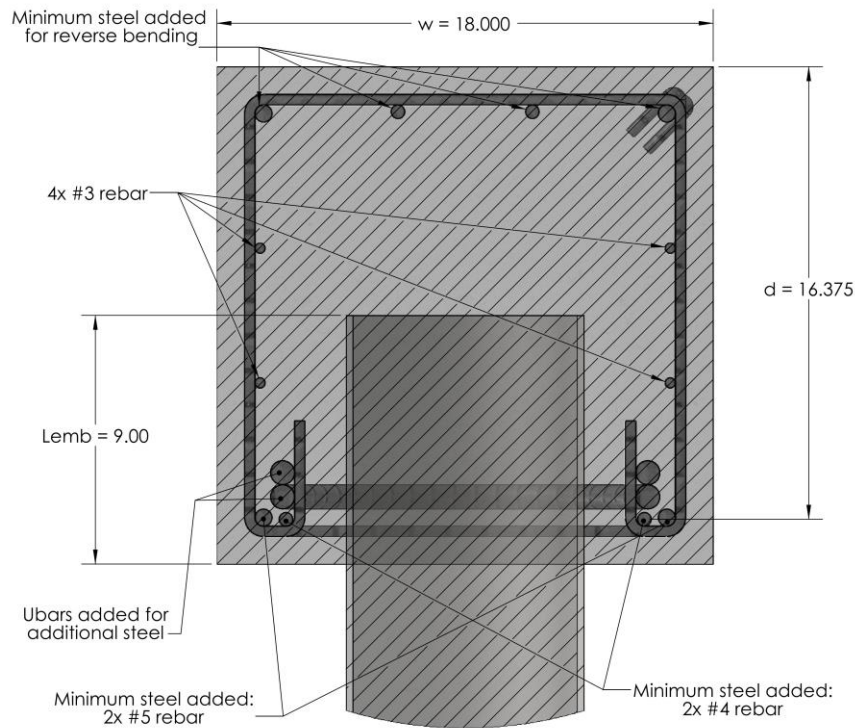


Figure 19: Longitudinal steel design and placement

Relative to additional steel, the MDT design guide specifies that 25 percent of the area of steel calculated by Equation 3.12, reproduced below as Equation 4.7 for convenience, should be used. Furthermore, the guide specifies the additional steel to be in a U-shaped configuration or a through-bar configuration. All of the tests in this study used only U-bars as additional reinforcement.

$$A_{s_{add}} = 0.25 \cdot \frac{M_u}{\phi_f \cdot z \cdot f_y} \quad \text{Equation 4.7}$$

In evaluating this equation, M_u was set at 96.8 ft·kip (the plastic-moment capacity of the CFT), ϕ_f was set at 0.9, and z was solved from Equations 3.1 through 3.3 using L_{emb} of 9.0 in. The additional steel to add, $A_{s_{add}}$, for VT1 was calculated to be 1.04 in². Therefore, a #7 U-bar was selected as additional reinforcement in each direction, as it provided 1.20 in² (1 #7 has a cross sectional area of 0.60 in², which is doubled when used as a U-bar) of steel in each direction. Note that a single #6 U-bar in each direction was too light (0.88 in²), and while a #4 U-bar in combination with a #5 U-bar in each direction was a very good fit (1.01 in²), it was judged undesirable to stack the U-bar reinforcement in the first test (although this was implemented in VT2).

The U-bar configuration for VT1 is shown in Figure 20. Note that the U-bars were located as close to the exterior of the cap as physically allowed, maximizing the moment arm resisting the pile moment.

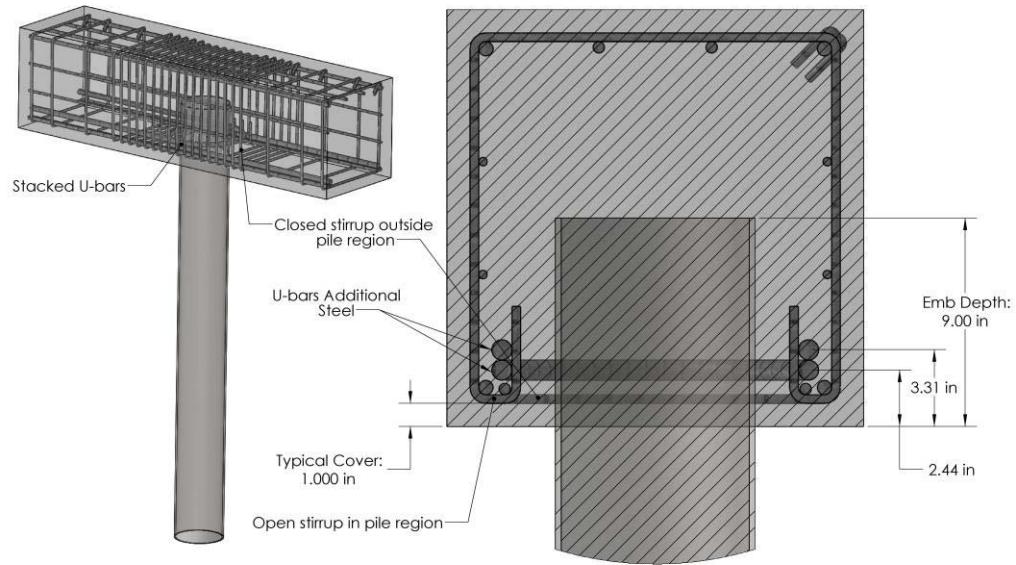


Figure 20: Additional longitudinal steel design and placement

The stirrup configuration for VT1 is also shown in Figure 20, which also represents the complete steel cage used for VT1. In the transverse direction, the design guide (again following AASHTO) specifies two equations which control the design of the reinforcement, as previously described in Chapter 3, which are repeated here as Equations 4.8 and 4.9.

$$A_{sh} \geq 0.30 \cdot s \cdot w_{core} \cdot \frac{f'_c}{f_y} \cdot \left[\frac{A_g}{A_c} - 1 \right] \quad \text{Equation 4.8}$$

$$A_{sh} \geq 0.12 \cdot s \cdot w_{core} \cdot \frac{f'_c}{f_y} \quad \text{Equation 4.9}$$

Recall, that s is the spacing of the transverse reinforcement, and w_{core} is the width of the concrete core. Also, A_g and A_c are the gross area and the core area of the concrete cap cross section, respectively. While there was some design choice in the spacing, s , 1.75 in was chosen to keep consistent with previous testing. For the design of VT1, a cover of 1 in was used, which was consistent with previous testing completed by Stephens and McKittrick (2005) and resulted in using 16 in for the width of the core, w_{core} , and in the calculation for the core area, A_c . Thus, for a design compression strength of concrete, f'_c ,

of 4,000 psi and a steel yield stress, f_y , of 60,000 psi, the amount of steel area needed, A_{sh} , was 0.22 in². This is approximately the area that two legs of a #3 stirrup provide. The stirrups that fall in the pile location are open and designed to leave 1.5 in of clearance around the embedded steel pile. In accordance with the design guide, the stirrup spacing of 1.75 in was maintained a distance equal to the half of the height of the cap beyond each face of the pipe pile in the longitudinal direction. Outside of this region, the stirrup spacing was set at 6.0 in.

A detail of the resulting reinforcing cage is shown in Figure 21.

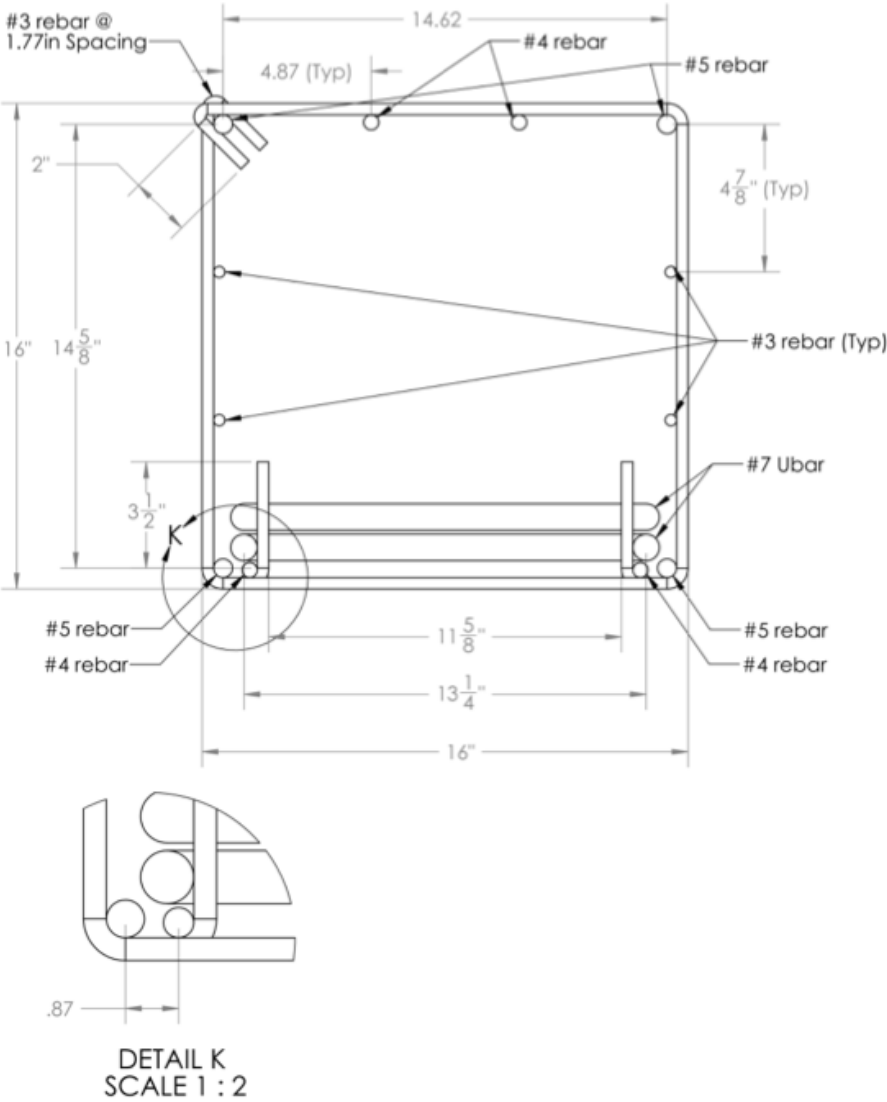


Figure 21: Steel reinforcement scheme for VT1

4.3 Specimen VT2 Design

Test specimen VT2 was configured to exercise the design guide at a higher level of moment demand than was used in VT1. The design moment was increased by 25 percent over VT1 to 122.0 ft·kip, with this increased demand being accommodated by increasing the pile embedment length. Based on this moment demand and with a $\phi_b = 0.7$ (ϕ_b was set to 1.0 for VT1), an embedment length of 11.75 in was determined for VT2 following the design guide (see Appendix B). Besides the embedment length change, the only other change in the design parameters for VT2 was the specific configuration of the U-bars. Following the design guide, the additional area of steel required for the VT2 design moment demand was calculated to be 1.002 in², nearly identical to what was required by VT1 (Table 3). A change in design strategy was implemented at this point with the goal of more closely matching the calculated U-bar steel area with the selected bars. Thus, a combination of a #4 and a #5 U-bar was used, rather than the single #7 U-bar used in test VT1. The “double” U-bars were placed staggered in opposing directions as shown in Figure 22.

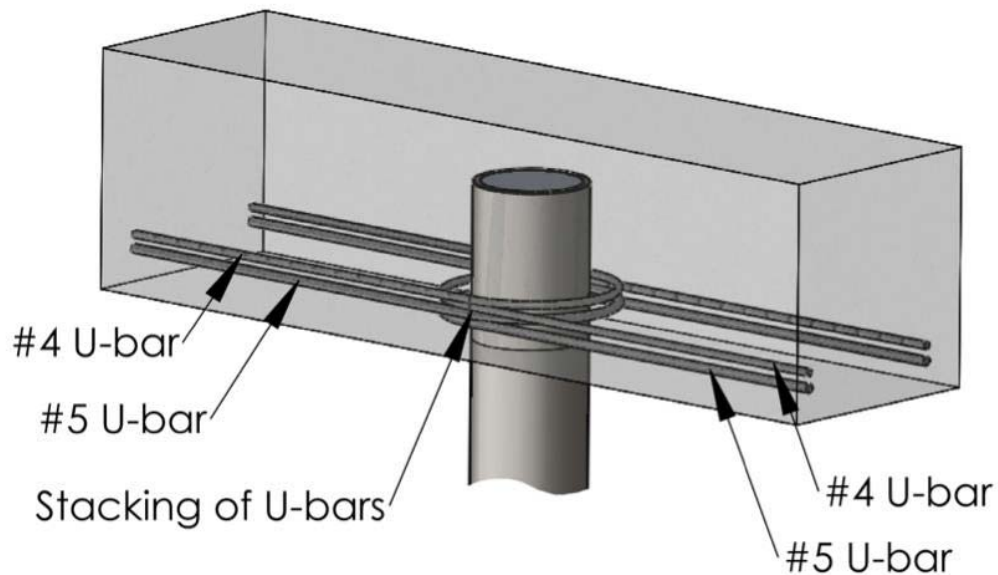


Figure 22: Stacked U-bar configuration used in VT2

Also beginning with VT2, a change in test strategy was introduced, which was to increase the wall thickness of the CFT to force connection failure to occur in the concrete pile cap. In the first test, VT1, failure consisted of the formation of a plastic hinge in the concrete-filled steel pile; to avoid limiting the results of all the tests to this failure mechanism, the wall thickness of the steel pipe pile was increased in all subsequent tests to purposely

increase the moment capacity of the CFT pile beyond the capacity of the concrete pile cap. This test strategy reflected that all the parameters varied in this series of tests affected the design and performance of the concrete pile cap, rather than the CFT pile. A pipe pile wall thickness of 0.5 in was used in VT2.

4.4 Specimen VT2.5 Design

VT2.5 was constructed by simply inserting the undamaged CFT from VT2 into the generally undamaged concrete cap from test VT1. In test VT1, a plastic hinge formed in the CFT before any significant distress occurred in the pile cap; thus, to a large extent, this test only provided a conservative lower bound on the capacity of this cap configuration. Therefore, the VT1 cap was retested (as VT2.5) using the stronger CFT from VT2. The first step in assembling VT2.5 using the cap from VT1 and the CFT from VT2 was to remove the original pipe pile from VT1. While the cap from VT1 was “undamaged” during that test, the pile did debond and separate from the cap, allowing it be readily withdrawn from the cap following the test. Similarly, the VT2 CFT easily slid into the resulting socket with a relatively “snug” fit between the pile and pile cap (no grout or other filler/bonding material was used).

Note that Table 3 shows slight differences in certain test parameters between VT1 and VT2.5, such as the moment arm length, z , and the crushing strength, f_u , even though it is the exact same pile cap. VT1 was designed with a concrete compression strength of 4,000 psi, while the physical test specimen had a concrete compression strength of 6,250 psi; therefore, in the design of test VT2.5, the known compression strength of the pile cap was used, resulting in certain design values deviating from VT1. Notably, in light of this difference in concrete compressive strength, the moment capacity predicted by the MDT design guide for cap specimen VT2.5 was 107 ft·kip (152.5 ft·kip with ϕ_b set to unity).

4.5 Specimen VT3 Design

Specimen VT3 was very similar in design to VT1 except that instead of specifying a design moment, the embedment length was chosen to be 10.375 in, midway between the embedment lengths of 9.0 in and 11.75 in used in VT1 (and VT2.5) and VT2, respectively. At this embedment length, the pile cap capacity was calculated to be 112 ft·kip (160 ft·kip with ϕ_b set to unity) using the MDT design guide. Note that in designing VT3, the decision was made to set ϕ_f to unity (compared to ϕ_f of 0.9 used in test VT1). This resulted in a required U-bar area of 1.141 in² for VT3, which is an increase of 10 percent when compared to VT1, but a single #7 U-bar in each direction still provided sufficient additional reinforcement. Similar to VT2 and VT2.5, this test also

used the oversized concrete-filled steel pile (wall thickness of 0.5 in) to assure that the ultimate capacity of the cap was realized.

4.6 Specimen CT1 Design

Specimen CT1 was largely identical in design to VT2; the only difference between the two models was that the thickness of the steel pile was increased in CT1 to 0.75 in to ensure a cap failure in both cyclic test specimens (it was believed CT2 might have an increased capacity over other the other connection models tested, as it contained additional U-bars as described below). From a testing perspective, CT1 was loaded cyclically, while VT2 was loaded monotonically to failure, as previously discussed.

4.7 Specimen CT2 Design

Specimen CT2 was very similar to CT1, with the addition of an interior set of U-bars located approximately 0.75 in below the embedded pile tip as shown in Figure 23. Previous testing indicated that localized crushing of the concrete was occurring in this interior region around the pile prior to reaching the design moment of the cap. To better control test parameters between CT1 and CT2, they were cast from a single batch of concrete.

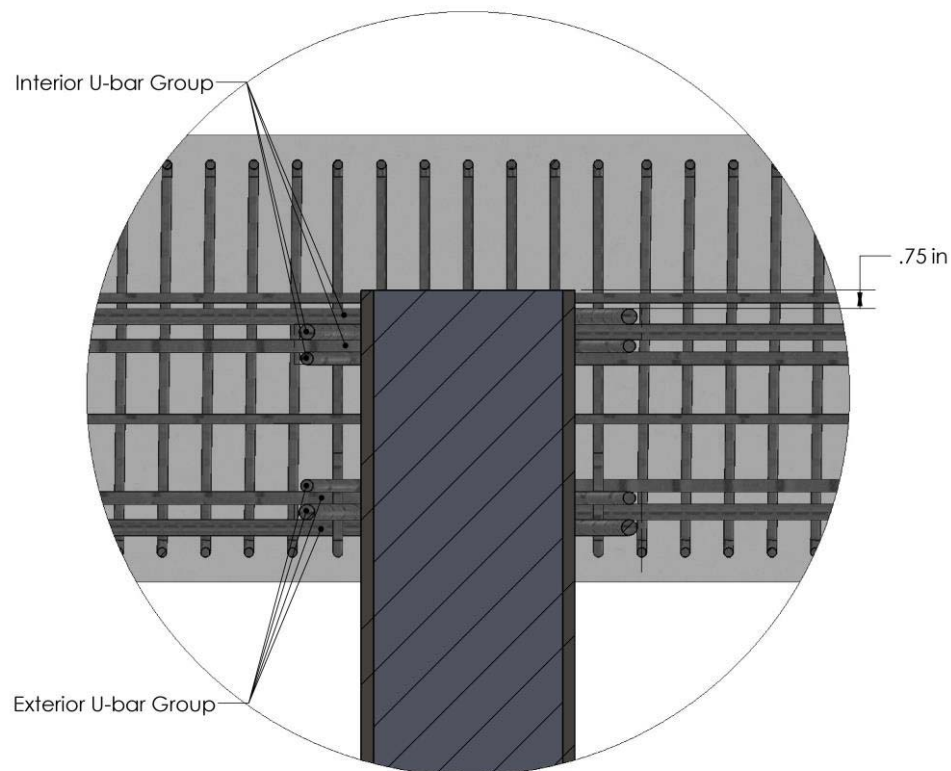


Figure 23: Exterior and interior U-bars for CT2

4.8 Specimen Construction

The test specimens were constructed in the Structures Laboratory at MSU. Out of convenience, the specimens were cast in an inverted position, as shown in Figure 24. For each specimen, the steel reinforcement cage was constructed per the specifications discussed in the previous section (Figure 25). Strain gages were placed in strategic locations on the reinforcing bars (as is discussed in more detail in Appendix C). The completed cage was placed in the pile cap form, after which the steel pipe pile was positioned in the cage in the cap. A local batch plant supplied concrete. Consolidation of the concrete was achieved using a vibratory stinger. The open side of the pile cap was finished using hand trowels to achieve a smooth finish. Fifty 4x8 cylinders were cast as well as three 6x12 cylinders for each concrete pile cap. Most of these cylinders were stored in a moist cure room and used to determine the progressing strength of the concrete over time. For all the tests, the concrete strength for the test specimen was based on the average of three or more moist cured 4x8 test cylinders.

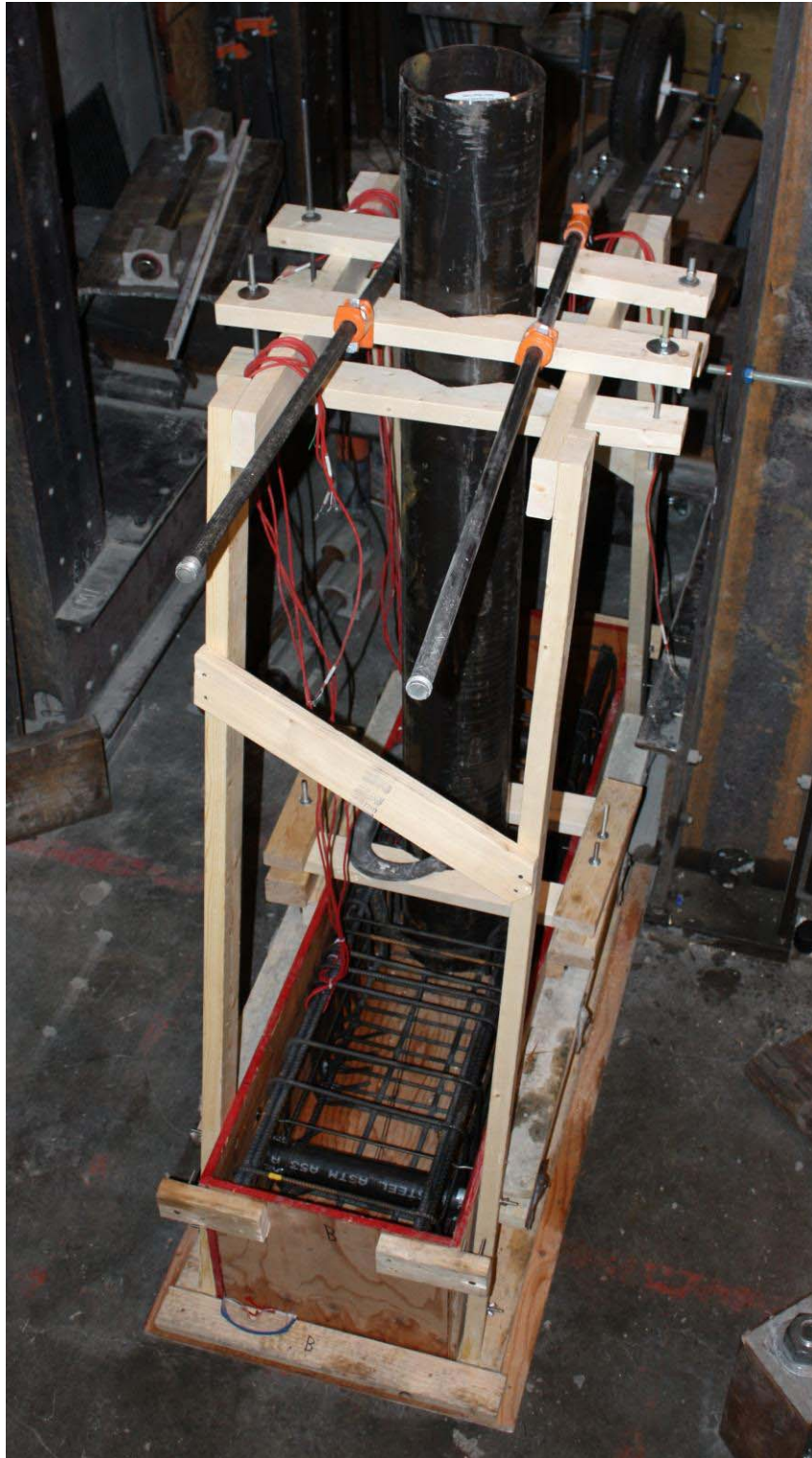


Figure 24: Structural elements ready for concrete placement

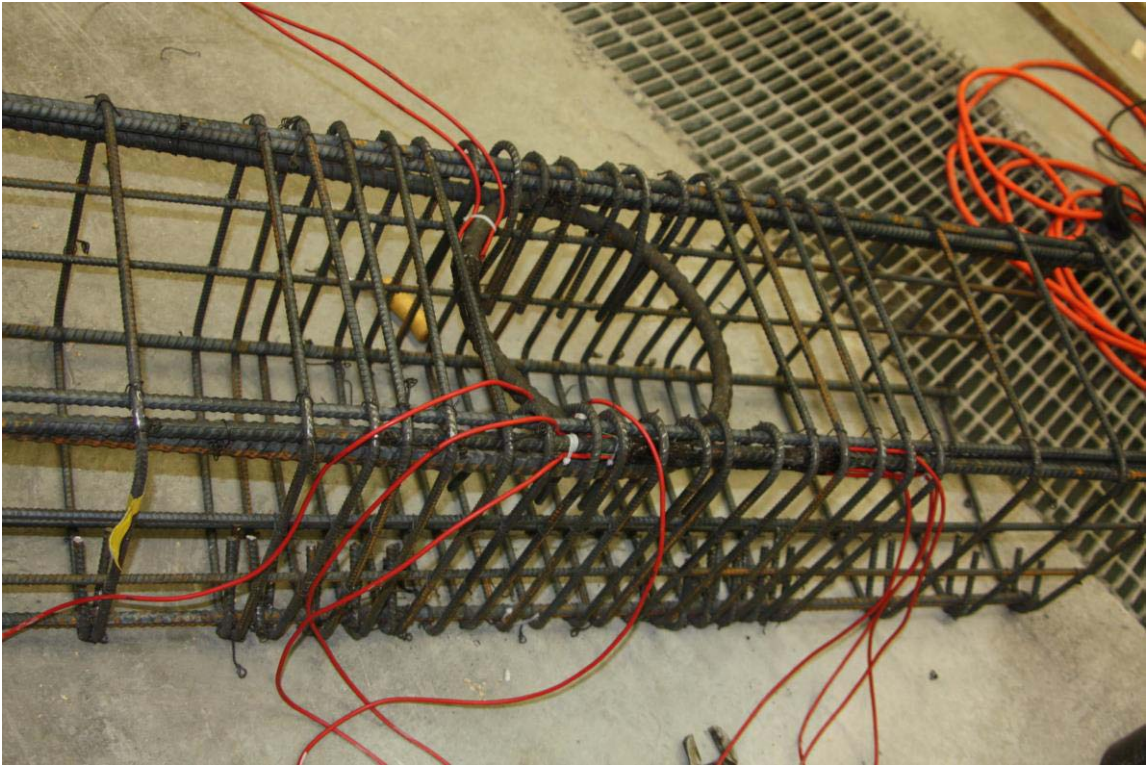


Figure 25: Typical steel reinforcement cage construction (VT1 shown)

5 TEST SETUP

The manner in which the test specimens were supported and loaded is shown schematically in Figure 26. For convenience, the specimens were tested in the horizontal plane using the strong floor in the MSU structures laboratory as shown in Figure 27. As shown in the figure, the concrete cap was pin supported at a span of 51 in (matching the diagonal spacing of holes in the MSU Structures Lab floor, and approximately representing a pile spacing of 102 in in a full size bent). These pin joints consisted of steel sleeves cast in the concrete cap providing through holes for threaded rod. During the test, lateral load was applied at the tip of the pile using a hydraulic jack. Note also that a constant axial load of 15 kips was applied to the system to approximately represent gravity load effects.

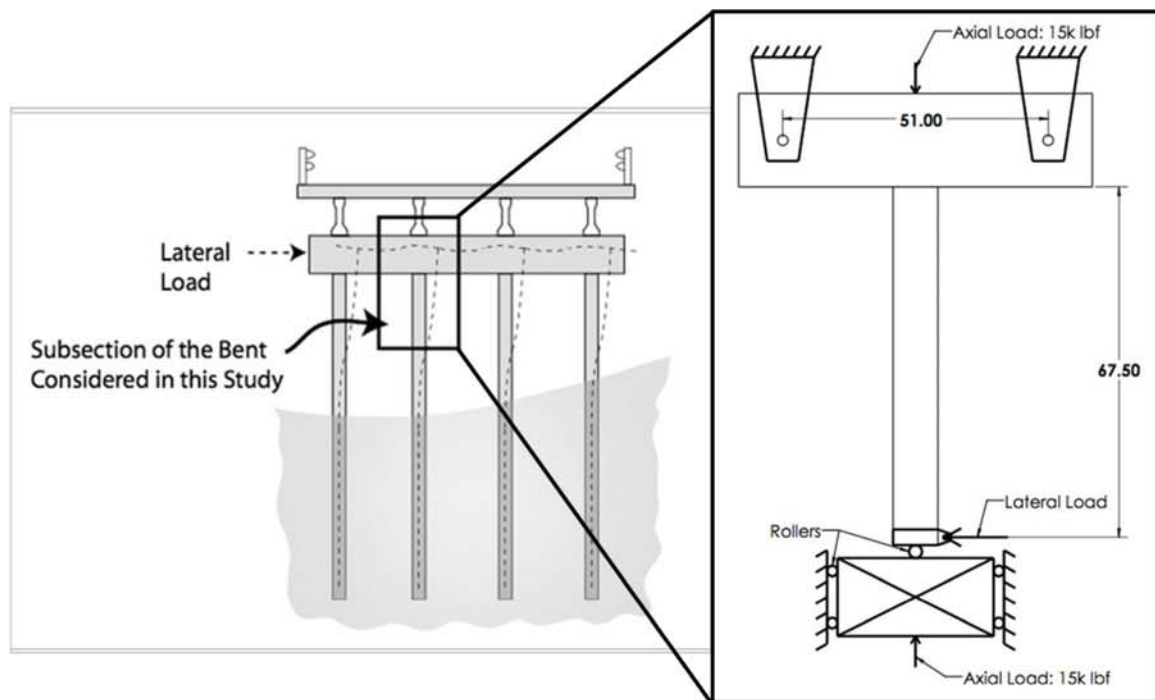


Figure 26: General test setup layout (all lengths in units of inches)

Referring to Figure 27, the lateral load was applied through the long hydraulic jack located in the upper part of the figure, oriented perpendicular to the steel pile. Two smaller jacks placed in line with the pile were used to apply the axial load; these jacks were pressurized from the same hydraulic source using a splitter; thus, the force applied by each jack was equal. At the tip of the pile, the axial load was applied through a steel frame on rollers to accommodate the lateral deflection of the pile during testing.

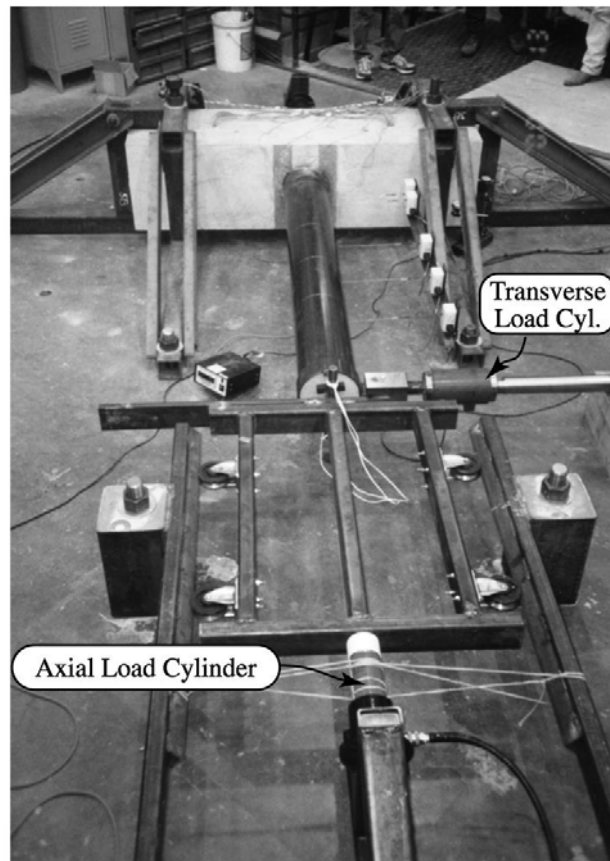


Figure 27: An overview of the test specimen, frame, and hydraulic elements

5.1 Instrumentation

Load, deflection, and strain were measured and recorded for each test. The locations of the load and deflection measurements are shown in Figure 28. Both the axial and lateral loads were monitored. Deflection was measured in six places along the length of the pile. Five of the six displacements were obtained through the Celesco displacement gages shown in the figure, while the remaining displacement measurement was via a transducer on the lateral hydraulic jack; therefore, the sixth displacement is located at the tip of the pile. Measuring along the CFT from the face of the concrete pile cap as shown in Figure 28, the gages were located at: (1) 2.875 in, (2) 6.0 in, (3) 18 in, (4) 29.75 in, (5) 47.8125 in, (6) 67.5 in (pile tip).

In each test, strains were measured at selected locations on the steel pile and/or the reinforcement in the pile cap. Strain gage locations changed between tests, based on the test objectives and experience gained from each successive test. For example, the strain

of the steel pile was measured in the first test, VT1, when the expected outcome was the formation of a plastic hinge in the pile. In later tests, when an oversized steel pile was used, more strain gages were placed on the steel reinforcement inside the concrete pile cap. Therefore, specific strain gage locations are identified in Chapter 6 and in Appendix C, where the strain results are presented. That being said, in general the strain response was measured on the U-bars, the straight longitudinal bars on the bottom cap, as well as on selected transverse ties.

The steel reinforcement to be strain gaged was held out of the reinforcement cage until after the gages were installed. For example, strains were measured at three locations on the exterior most U-bar in VT1 as shown in Figure 29. All gages were installed following standard strain gaging procedures.

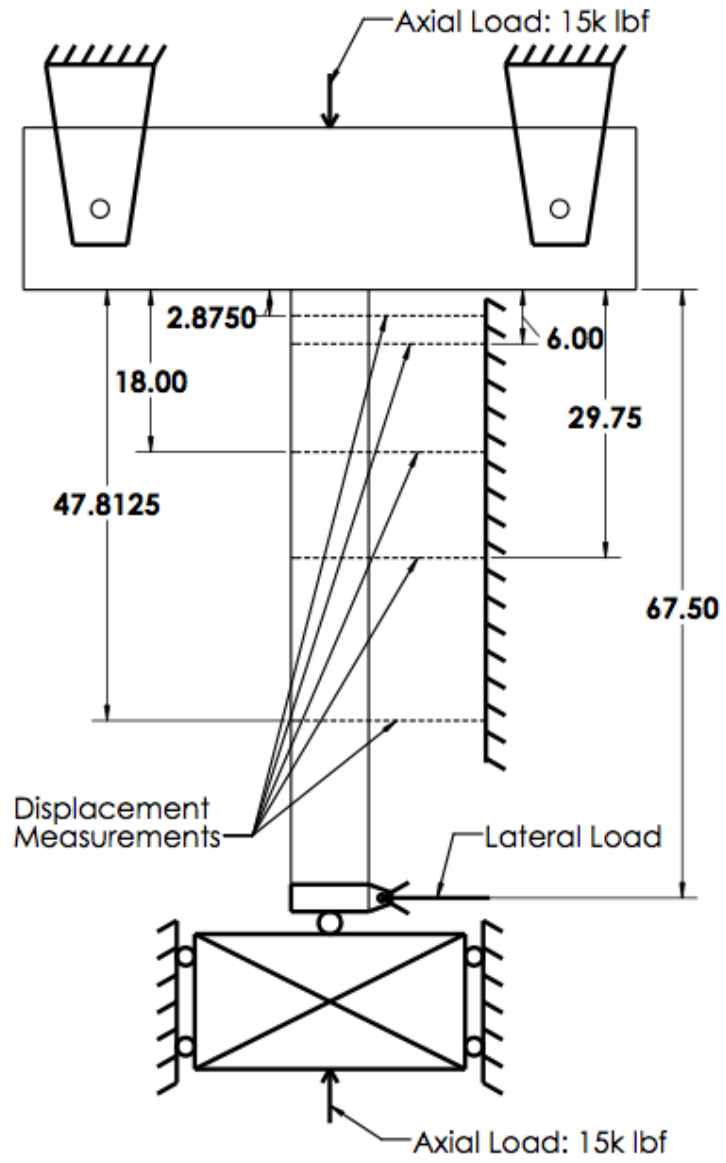


Figure 28: Load and displacement locations (all lengths in units of inches)



Figure 29: Typical strain gage placement on U-bar

5.2 Test Conduct

All tests were conducted in the MSU Structures Laboratory. Due to the different nature of the monotonic and cyclic tests, they are discussed separately below.

5.2.1 Monotonic Test Conduct

In each of the monotonic tests (VT1 to VT3), the specimens were initially loaded in the positive direction (defined as away from the hydraulic ram in Figure 27) until extensive failure was observed (i.e., a distinct loss in load carrying capacity). The specimens were then unloaded and the pile pulled back to its starting position. Then the specimen was loaded in the negative direction (defined as toward the hydraulic ram in Figure 27) until the tip of the pile reached the same deflection as the first positive cycle. The test was generally considered finished after the pile was returned to its starting position, although on the first and second test (VT1 and VT2), the test specimen was cycled through a second positive cycle before finishing the test.

The specimens were generally loaded in increments between 2,000 to 5,000 lbf of applied lateral tip load, at which point the load was held and any observed distress (e.g., cracking) was documented. After the relevant documentation was obtained, the load was increased until the next load increment was reached. Also, when significant structural damage and changes in behavior in the test specimen were noticed, loading was stopped so that notes, pictures and cracking in the concrete could be recorded. This

strategy helped ascertain behavioral changes as the test specimen began to fail, independent of the nature and type of failures encountered.

As previously mentioned, lateral and axial load, pile deflection, and strain information were recorded. The sampling rate at which this information was captured was between 0.5 and 1.0 samples per second for the monotonic tests.

5.2.2 Cyclic Test Conduct

The displacement history for CT1 and CT2 is shown in Figure 30. The pile tip drift was cycled at 0.5 percent intervals (with three cycles of fully reversed displacement at each interval) until a drift of 4.0 percent was reached. At this point, the increase in pile tip drift was at 1.0 percent intervals until 7.0 percent drift was reached (again with three cycles of fully reversed displacement at each interval). The tests concluded with drift cycles conducted at 9.0 percent drift and 11.0 percent drift.

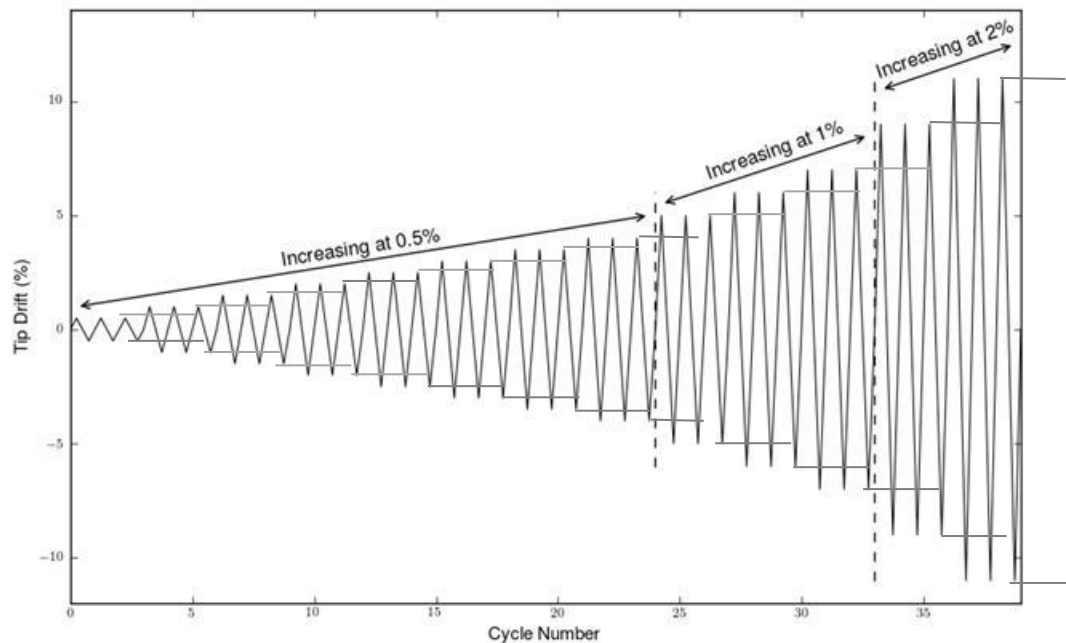


Figure 30: Cyclic loading history for CT1 and CT2

Similar to the monotonic tests, load, pile deflection, and strain were all recorded throughout each test. The sampling rate was changed to 0.25 samples per second (from 0.5 - 1.0 samples per second used in the monotonic test) to increase resolution.

6 TEST RESULTS

The results of the monotonic and cyclic tests conducted on the six CFT pile-to-concrete pile cap connections described in Chapter 4 are reported in this chapter. An overview of the important parameters characterizing each test along with the corresponding test results is presented in Table 5. Referring to this table, significant items that varied from test to test are the U-bar configuration, the pile embedment length and the concrete compression strength. Relative to general performance, VT1 failed through the formation of a plastic hinge in the CFT pile, while the remaining tests all failed by fracturing the concrete pile cap. The change in failure mechanisms was intentional and was achieved through a change in test methodology, in which a purposely over-sized steel pile was used to ensure the capacity of the cap was achieved. In VT1, the ultimate strength of the CFT pile, with a wall thickness of 0.25 in and a D/t of 34.5, was 119.2 ft·kip. In the remaining monotonic tests (VT2, VT2.5, and VT3), failure occurred by fracturing of the concrete pile caps. The ultimate strengths of the concrete pile caps in each of these tests were 173.8 ft·kip, 138.5 ft·kip, and 151.7 ft·kip, respectively. The two cyclic tests, CT1 and CT2, which were similar in design to VT2, had ultimate strengths of 172.4 ft·kip and 181.8 ft·kip, respectively.

The results of each of the tests are presented in more detail in the following sections.

Table 5: Summary of test results

	Test	U-bar Configuration	U-bar Location	Pile Embedment Length	Concrete Strength	Failure Mechanism	Maximum Moment at Failure
Monotonic	VT1	Single #7 U-bar in each direction	Exterior Only	9.0 in	6250 psi	Plastic hinge in steel pipe pile	119.2 ft-kip
	VT2	Single #4 and #5 U-bar in each direction	Exterior Only	11.75 in	3800 psi	Fracture of the concrete pile cap	173.8 ft-kip
	VT2.5	Single #7 U-bar in each direction	Exterior Only	9.0 in	6250 psi	Fracture of the concrete pile cap	138.5 ft-kip
	VT3	Single #7 U-bar in each direction	Exterior Only	10.375 in	4100 psi	Fracture of the concrete pile cap	151.7 ft-kip
Cyclic	CT1	Single #4 and #5 U-bar in each direction	Exterior Only	11.75 in	4200 psi	Fracture of the concrete pile cap	172.4 ft-kip
	CT2	Single #4 and #5 U-bar in each direction	Interior and Exterior	11.75 in	4200 psi	Fracture of the concrete pile cap	181.8 ft-kip

6.1 Verification Test 1 – VT1

The purpose of the first test, VT1, was to create a baseline for a CFT pile-to-pile cap design completed with the MDT design guide, while maintaining consistency with the previous testing completed by Stephens and McKittrick (2005); therefore, the two key design features of VT1 included a 9.0 in pile embedment length and a design moment capacity of 96.8 ft-kip based on a steel pile with a wall thickness of 0.25 in as detailed in Chapter 4. The outcome of this test, as shown in Table 5, was the formation of a plastic hinge in the CFT pile; therefore, the focus of this section is directed more towards the response of the plastic hinge in the CFT pile. The concrete pile cap is analyzed in more detail when its capacity is realized in VT2.5, which reused the undamaged pile cap from this test.

The entire moment-drift response for this specimen is shown in Figure 31, while the first push is shown in Figure 32. Referring to these figures, percent drift was calculated as a ratio of the tip deflection to the length of the non-embedded portion of the steel pile. The reported total moment applied to the pile during the test includes the moment associated with the application of the lateral load as well as the moment due to P-delta effects from the axial load. As shown in the figures, the CFT pile tip was pushed in one direction until failure was evident at a load of 119.2 ft-kip. The tip of the pile was then returned back to zero drift. Due to a problem with instrumentation, a portion of the load data for the return of the first push was not measured, which is identified in the figure. The steel pile tip was then pulled in the opposite direction until approximately the same amount of drift had been reached as the first push. The tip of the pile was returned to zero drift. Finally, a second push and return to zero drift was completed.

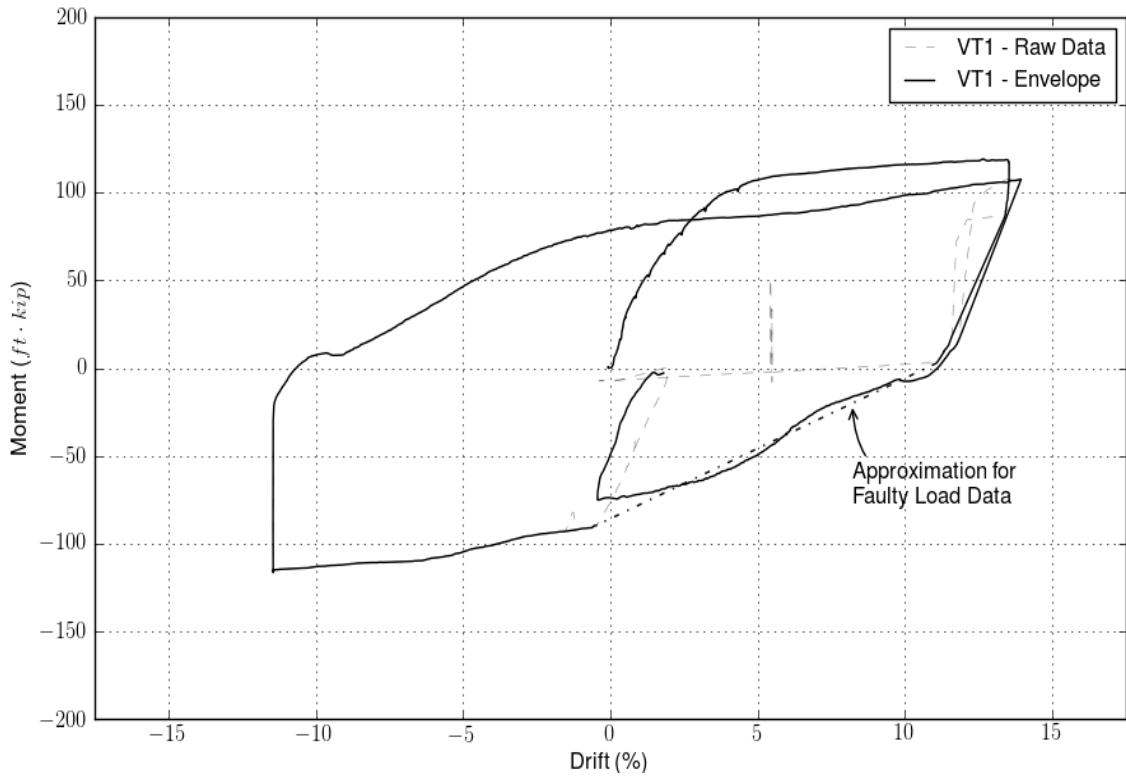


Figure 31: VT1 Applied Moment (w/P-Delta) vs. Lateral Drift

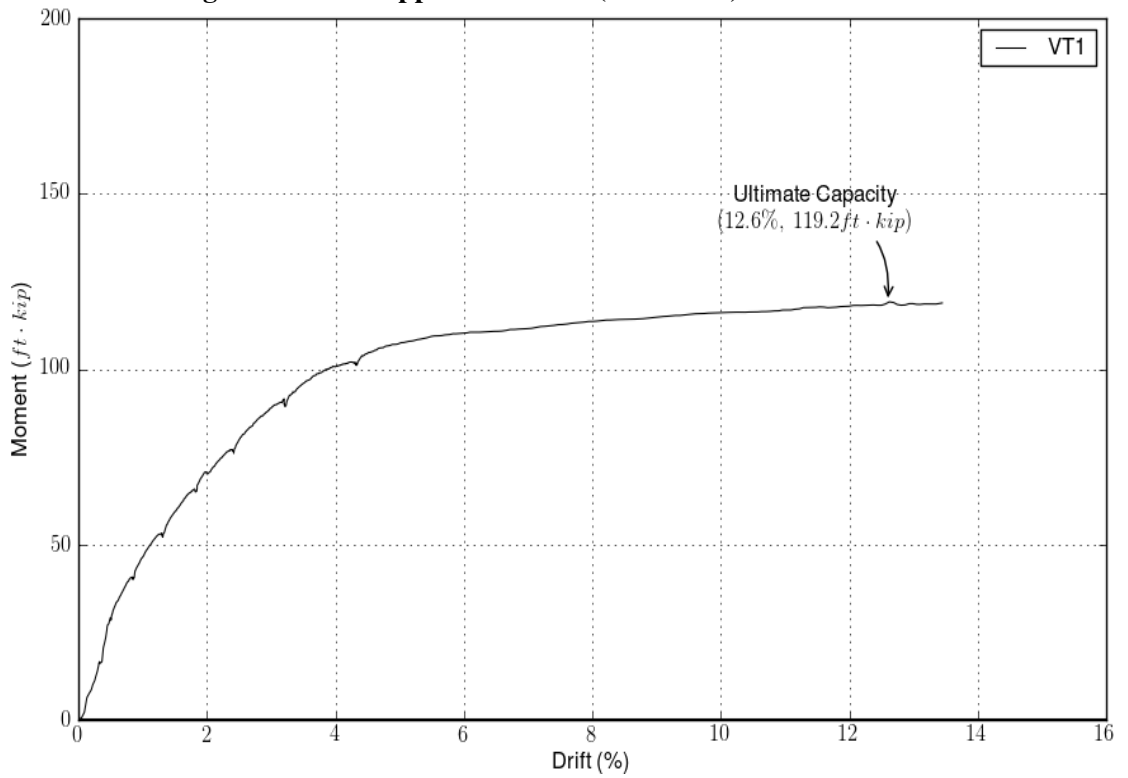


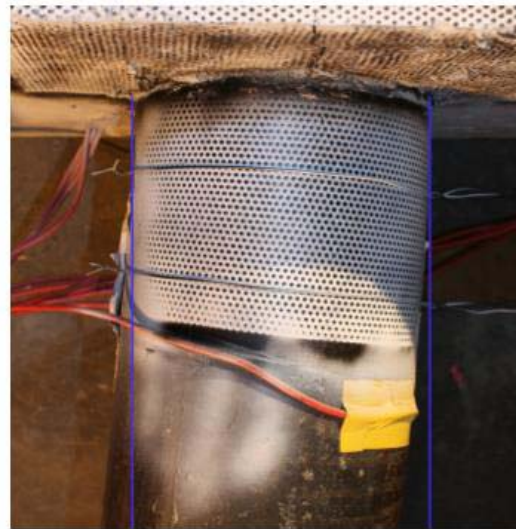
Figure 32: VT1 Applied Moment (w/ P-Delta) vs. Lateral Drift - First Push Only

As expected, the ductile nature of the plastic hinge in the CFT pile provided a very robust hysteresis response, identified by a minimal loss in energy dissipation and load capacity for each completed load cycle.

Figure 33a shows VT1 at the maximum positive deflection achieved during the test. For reference, in this figure the steel pile tip is deflected about 9.25 in from its original position in the positive (extension) direction of the hydraulic ram applying the lateral load. A top view of the plastic hinge in the pile at the maximum positive deflection is shown in Figure 33b. Two lines were added in the figure on either side of the pile to better show the rotation of the pile across the plastic hinge zone. Figure 34a shows the state of the pile cap at the maximum negative deflection. Note that the concrete pile cap appears undamaged except for some minor cracking in the concrete. A close-up of the plastic hinge zone for the negative cycle is shown in Figure 34b. Typical for a CFT failure, the steel tube is buckling outwards in this figure.



(a) VT1 at maximum deflection



(b) Top view of plastic hinge region

Figure 33: VT1 failure: plastic hinge in the steel pile in the positive direction

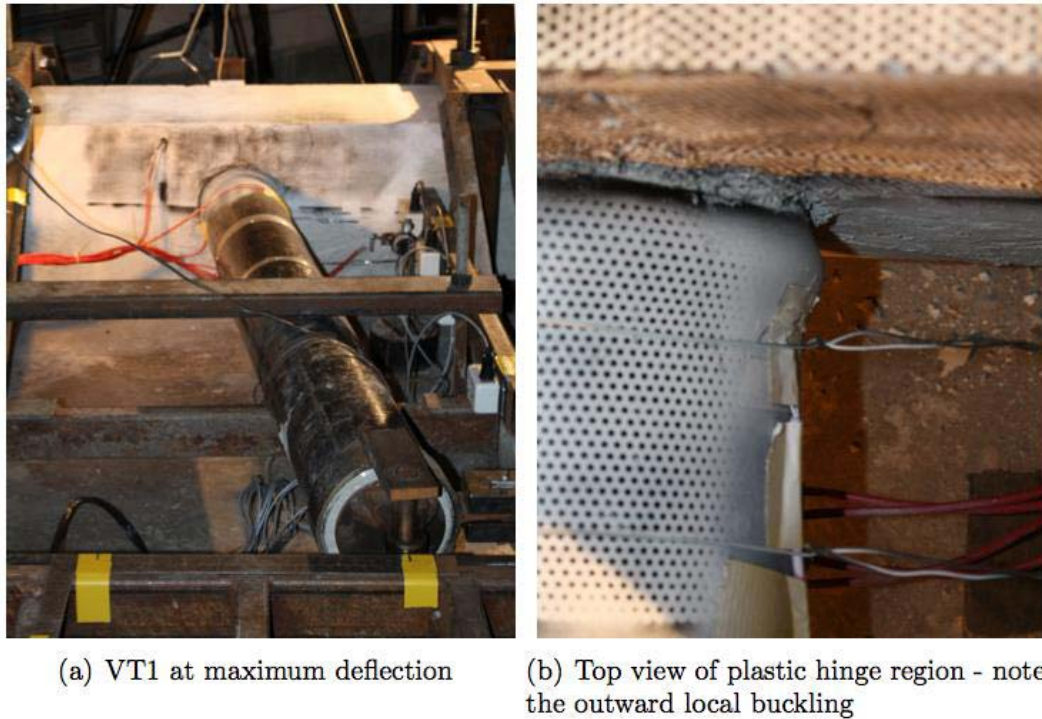


Figure 34: VT1 failure: plastic hinge in the steel pile in the negative direction

6.2 Verification Test 2 – VT2

The second test, VT2, was designed to further exercise the MDT design guide by increasing the moment demand on the concrete pile cap by approximately 25 percent, which resulted in an increased embedment length of 11.75 in. Additionally, an overly stiff and strong steel pile was used in this test, to force the failure into the concrete pile cap.

Similar to VT1, the load and deflection at the tip of the pile are presented in terms of moment and percent drift in Figure 35 and Figure 36. The steel pile tip was initially pushed monotonically until the concrete pile cap fractured at a moment of 173.8 ft-kip. The pile tip was then pulled to a similar negative displacement. The pile tip was then cycled through a positive displacement and returned to its original position to complete the test.

As expected, in VT2 the concrete pile cap fractured while the CFT pile remained relatively undamaged. Accordingly, several important behaviors are apparent in the moment-drift response of VT2. The first noticeable difference between VT2 and VT1 is the degradation of the response as each load cycle was completed in VT2. The ultimate strength of the first negative cycle relative to the first positive cycle for VT2 shows a decrease in capacity of 17 percent, while in VT1 this decrease was only 2 percent. The

ultimate strength of the second push relative to the first push for VT2 shows a decrease of 55 percent, which is due to the significant amount of permanent damage evident in the concrete pile cap in Figure 37 and Figure 38. Further examination of Figure 35 shows a “pinched” hysteresis response; that is, a significant amount of energy dissipation capacity is lost during each cycle because of the decreased capability of the concrete pile cap to resist the moment at lower drift levels after it has been fractured. Thus, the comparison of the moment-drift curves for VT1 and VT2 clearly indicates the desirable improvement in behavior offered by plastic hinging in the steel pile (VT1) compared to fracture of the pile cap (VT2).

Note that in these moment-drift figures (Figure 35 and Figure 36), the “dips” in the response are due to a faulty hydraulic line on the main ram that was applying the lateral load to the pile tip. During testing, it was advantageous to stop applying load to the steel pile tip as testing proceeded to allow for documentation of the condition of the cap as a function of load step. For VT2, each time the pump driving the hydraulic ram was stopped, pressure in the hydraulic system dropped (due to a leak in the hydraulic line), resulting in a drop in load. The deflection did not decrease accordingly, because the 15 kip axial load was always applied, which due to the deflection of the pile and friction in the system, effectively held it in place.

VT2 is shown in Figure 37 and Figure 38 when the CFT pile was at its maximum deflection of 10.5 in in the positive and negative direction, respectively. In both of these figures, crushing of the concrete in the cap immediately alongside the pile in the exterior compression region was evident as well as significant cracking from the pile to the edges of the pile cap at approximately 20-degree angles.

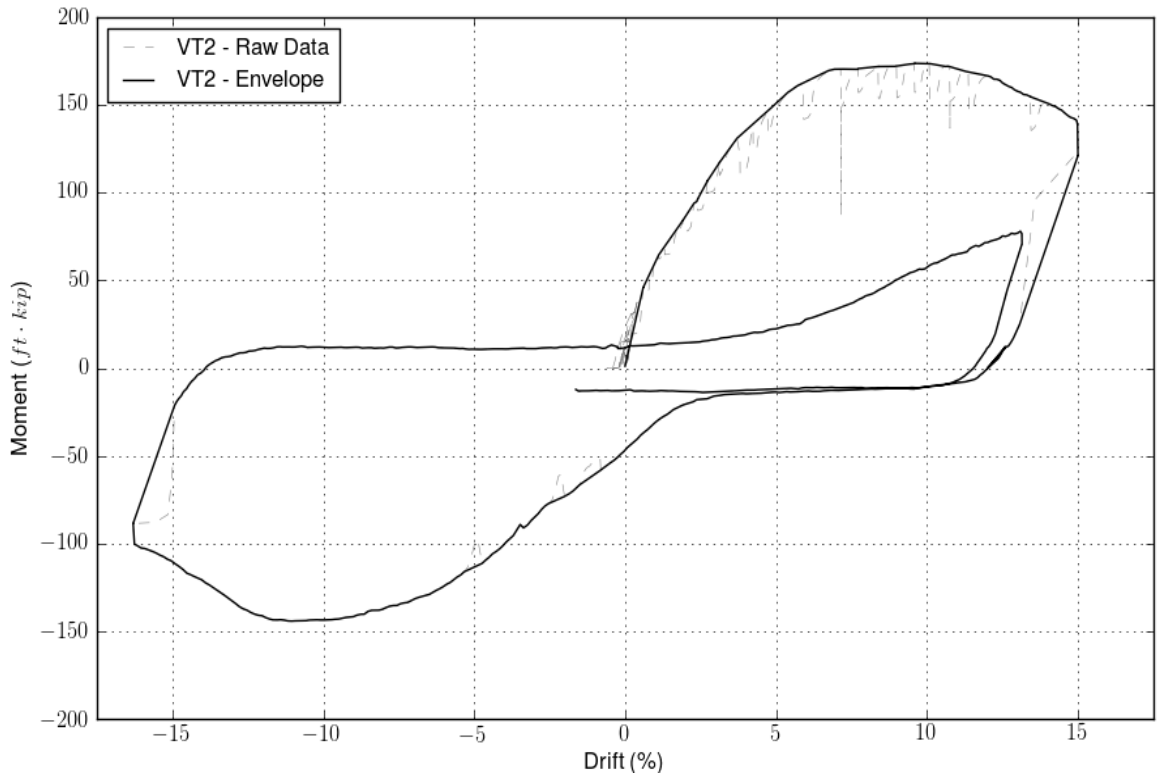


Figure 35: VT2 Applied Moment (w/ P-Delta) vs. Lateral Drift

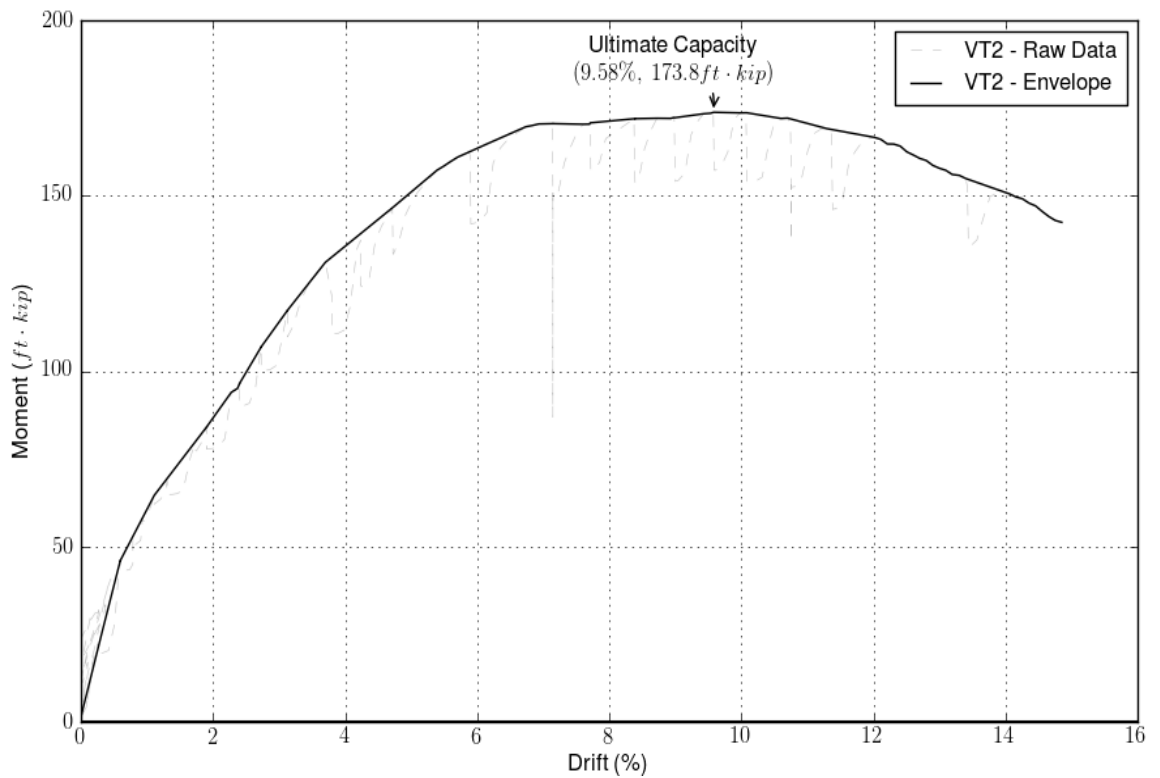


Figure 36: VT2 Applied Moment (w/ P-Delta) vs. Lateral Drift - First Push



Figure 37: VT2 Failure at maximum deflection on initial push



Figure 38: VT2 Failure at maximum deflection on return pull

6.3 Verification Test 2.5 - VT2.5

VT2.5 was a combination of structural components from VT1 and VT2, as previously introduced. It consisted of the concrete pile cap from VT1 and the over-sized steel pile used in VT2; thus, all of the concrete pile cap parameters identified for VT1 remain similar, including the concrete strength, embedment length and U-bar configuration. The goal of the test was to determine the ultimate capacity of the concrete cap used in VT1, as only the plastic-moment capacity of the CFT pile was determined in that test. This is of particular interest mainly to determine the effects of higher strength concrete (recall $f'_c = 6,250$ psi for VT1/VT2.5 versus $f'_c = 4,000$ psi for VT2 and VT3) on pile cap response.

The moment-drift response for VT2.5 is reported in Figure 39 and Figure 40. As with the previous tests, the pile was pushed until failure in the cap and then returned to its zero drift position. The ultimate capacity of this pile cap was 138.5 ft·kip. This is lower than VT2, which had an ultimate capacity of 173.8 ft·kip, and was likely due to a shorter embedment length of the steel pile of 9.0 in for VT2.5 compared to 11.75 in for VT2. The pile was then pulled in the opposite direction until approximately the same drift was achieved and then returned back to the zero drift position. Similar to the concrete pile cap failure in VT2, the overall response for VT2.5 is very “pinched”, meaning that the fracturing of the concrete cap resulted in a large reduction in energy dissipation capacity, especially at lower drift levels. Also, the second cycle shows a reduction in the concrete

cap capacity of 38 percent when compared to the initial push, which further suggests degradation of the concrete pile cap.

Recall that VT2.5 is made up of the pile cap from VT1 and the CFT pile from VT2; therefore, the pile was not cast into the concrete pile cap for this test. A small test load was placed on the pile at the start of the test in the opposite direction of the first push cycle as shown in Figure 39. The response in this initial test loading indicates a small amount of inelastic behavior is already evident, likely due to permanent damage sustained to the interior of the concrete cap during test VT1. Note that once the play was removed by moving the pile from one side to another, the rest of the moment-drift curve represents the response of the concrete cap when resisting the movement of the pile. A more detailed discussion of this behavior is included in Chapter 7.

Another irregularity in the moment-drift response for VT2.5 is the large load drop visible just after the ultimate capacity was achieved. During the test, the hydraulic pump supplying pressure to the lateral hydraulic ram was inadvertently turned off and, thus, this large dip is not of structural significance when analyzing the response for VT2.5.

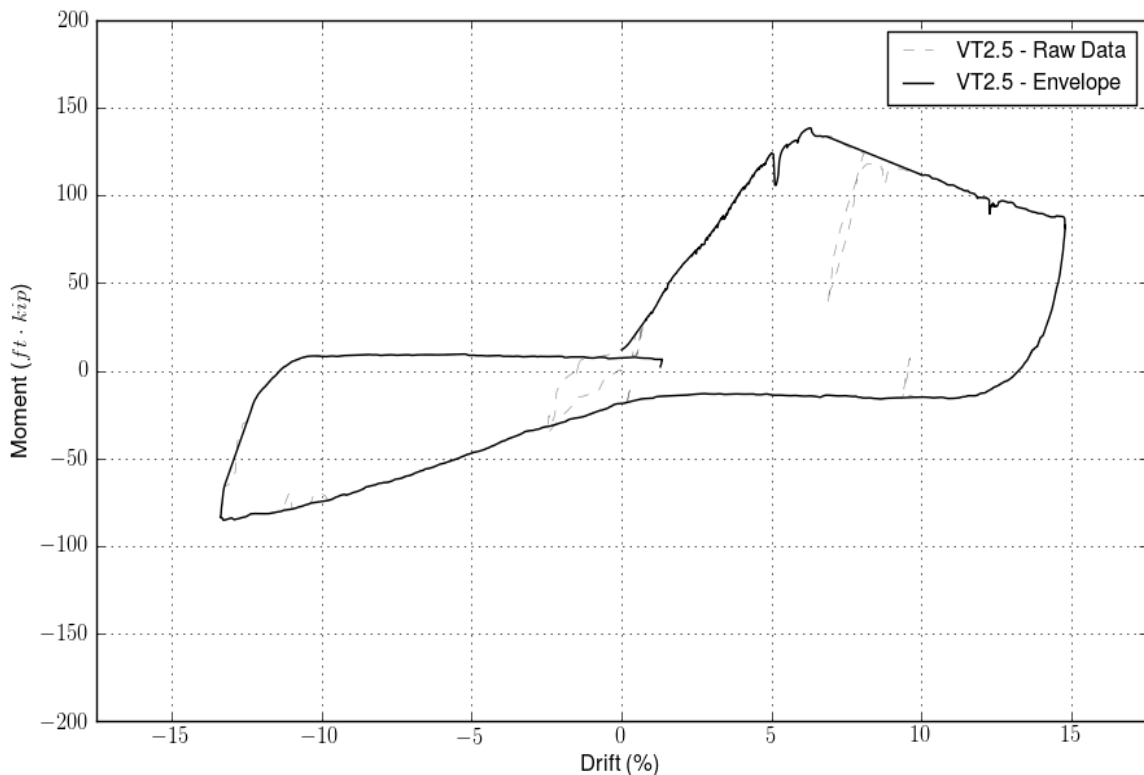


Figure 39: VT2.5 Applied Moment (w/P-Delta) vs. Lateral Drift

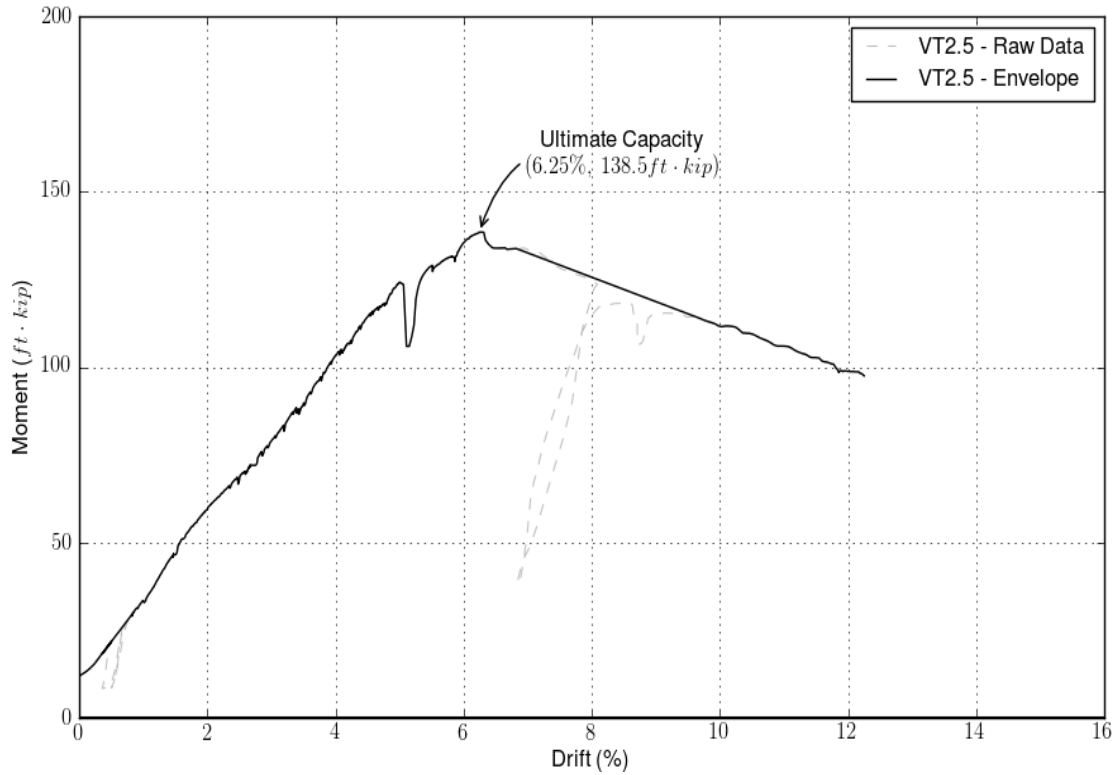


Figure 40: VT2.5 Applied Moment (w/ P-Delta) vs. Lateral Drift - First Push Only

The failed condition of the VT2.5 cap for the first monotonic push is shown in Figure 41, and was very similar in appearance to the cap failure of VT2. There are visual signs of concrete crushing in the compression region adjacent to the steel pile and large compression struts extending from the steel pile to the outer edges of the concrete cap. Additionally, the first push resulted in rupture of the concrete to the left of the pile.



Figure 41: VT2.5 Failure at maximum positive deflection

The return of the pile in the opposite (negative) direction to its maximum tip displacement is shown in Figure 42. This failure had signs of crushing of the concrete on the exterior face of the cap, as well as the formation of the compression struts from the pile to the edge of the cap, which is similar to the first push. One difference between the push and pull failures is the lack of the rupture type failure on the return negative cycle that was evident on the first positive cycle.



Figure 42: VT2.5 Failure at maximum negative deflection

6.4 Verification Test 3 – VT3

VT3 was developed to further investigate the design guide's treatment of embedment length by using a length midway between those used in the previous tests. VT1/VT2.5 had an embedment length of 9.0 in, while VT2 had an embedment length of 11.75 in; therefore, VT3 had an embedment length of 10.375 in. Similar to VT2 and VT2.5, this test also utilized an over-sized steel pile to force the connection failure to occur in the concrete cap. VT3 was tested when the concrete strength was approximately 4,000 psi.

Consistent with the previous tests, the moment-drift response for the pile-to-pile cap connection in VT3 is reported in Figure 43 and Figure 44. The ultimate capacity of this pile cap was 151.7 ft·kip, which occurred at approximately 6 percent drift. The pile was pushed until failure in the cap was evident and then returned to its zero drift position. The pile was then pulled in the opposite direction until approximately the same drift was achieved and then returned back to the zero drift position. Note that a portion of the response of the second cycle was lost due to problems during acquisition. Therefore, the ultimate strength of the second cycle is unknown, but based on the general shape and magnitude of the data that is available during this cycle, a significant loss in strength is expected to have occurred between the two cycles. Similar to the concrete pile cap failures in VT2 and VT2.5, the overall response for VT3 is very pinched, meaning that

the fracturing of the concrete cap resulted in a large reduction in energy absorption capacity, especially at lower drift levels.

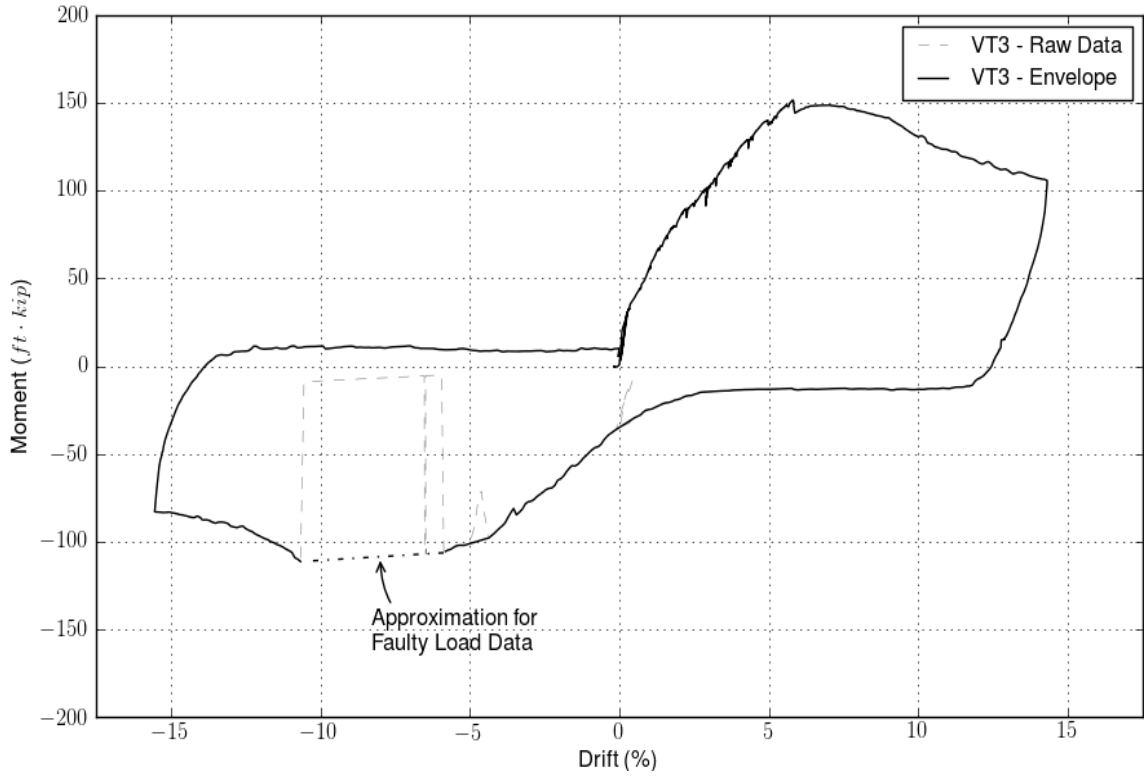


Figure 43: VT3 Applied Moment (w/ P-Delta) vs. Lateral Drift

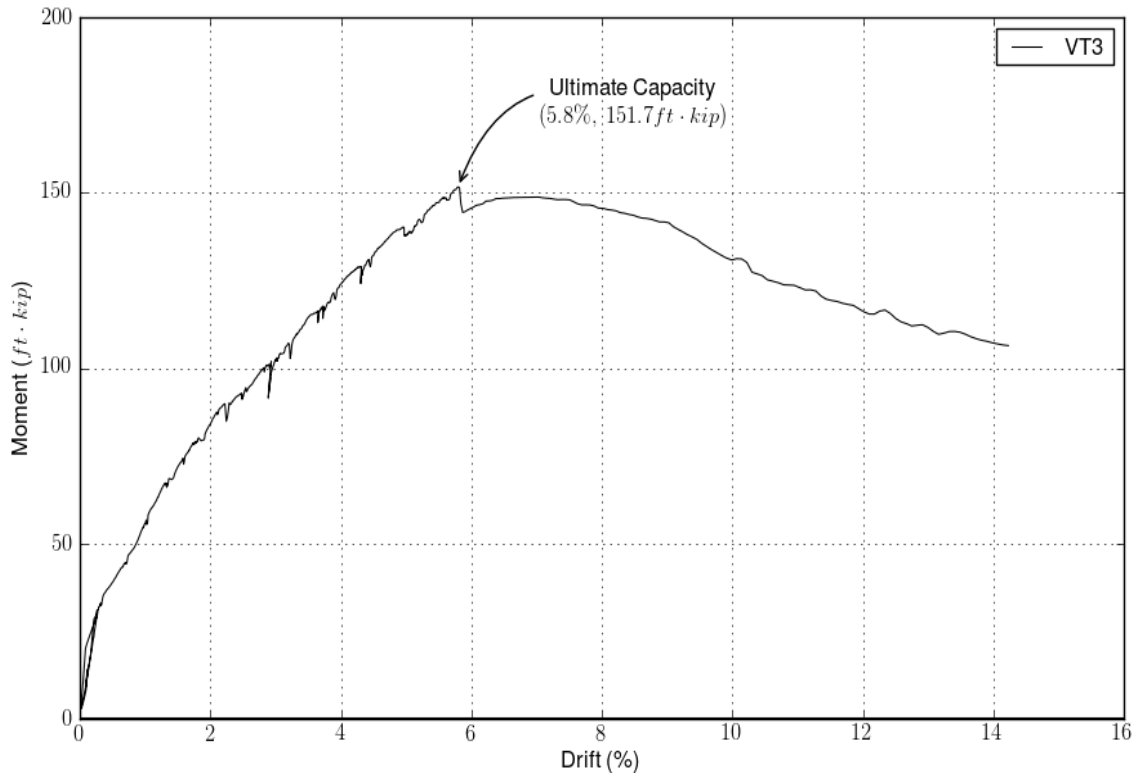


Figure 44: VT3 Applied Moment (w/ P-Delta) vs. Lateral Drift - First Push

The ultimate strength of VT3 (151.7 ft·kip) is between the ultimate strengths of VT2 (173.8 ft·kip) and VT2.5 (138.5 ft·kip), which was expected due to the embedment length of VT3 (10.35 in) being bounded by the embedment lengths of VT2 and VT2.5. The overall shape of the moment-drift response (Figure 43) is closer to that of VT2.5 (Figure 39), with a sudden small decrease in load capacity after the ultimate strength was achieved and a more immediate decrease in capacity. In contrast, VT2 had a much more subtle and gradual decrease in load capacity (Figure 35).

The condition of VT3 after the first monotonic push is shown in Figure 45. This is very similar to the failure of observed for VT2. There are visual signs of concrete crushing in the compression region adjacent to the CFT pile and large compression struts extending from the steel pile to the outer edges of the concrete cap.



Figure 45: VT3 Failure at maximum deflection on initial push

The return of the pile in the opposite (negative) direction to its maximum tip displacement is shown in Figure 46. This failure had signs of exterior concrete crushing as well as the formation of the compression struts from the pile to the edge of the cap, which is similar to the first push.



Figure 46: VT3 Failure at maximum deflection on initial pull

6.5 Cyclic Test 1 – CT1

CT1 was designed to determine if the behavior of the connection (more specifically the pile cap component of the connection) is different under monotonic versus cyclic loads. CT1 was constructed to replicate VT2. As previously introduced in the test conduct section of this report, it was subjected to a series of fully reversed displacement cycles of increasing magnitude, rather than being pushed to its ultimate capacity in a single event. While the loading scheme changed, almost all other test variables were kept the same between CT1 and VT2 (e.g., concrete strength, reinforcing scheme). The wall thickness of the CFT pile was slightly larger for CT1; however, the concept of using an oversized pile to purposely force the failure into the pile cap was the same.

Similar to the previous monotonic tests, the load-displacement response is represented in terms of the total applied moment at the connection (which includes P-delta effects) and the drift at the tip of the pile. The complete cyclic response for CT1 is shown in Figure 47. Additionally, the peak load and corresponding drift for each cycle are plotted separately in Figure 48. As previously noted, the cyclic response includes three cycles at each drift level before the drift was increased. As expected, the ultimate failure of this specimen was due to fracturing of the concrete pile cap. The maximum total moment carried by the cap was 176 ft·kip, and was experienced during a negative cycle at a drift of -4.9 percent. The maximum moment carried during the positive cycles was 172.4 ft·kip, and occurred at a drift of 4.2 percent. While the negative cycles demonstrated a higher maximum moment capacity than the positive cycles, this capacity tapered off more sharply upon subsequently cycling at higher drift levels than was seen for the positive cycles. For displacement cycles applied in both directions, the stiffest and strongest response was seen during the first displacement cycle of each displacement step, particularly as the displacement magnitudes increased. This degradation of strength with each successive cycle at the same displacement level is particularly evident in Figure 48. These behaviors are discussed in more detail in the following chapter.

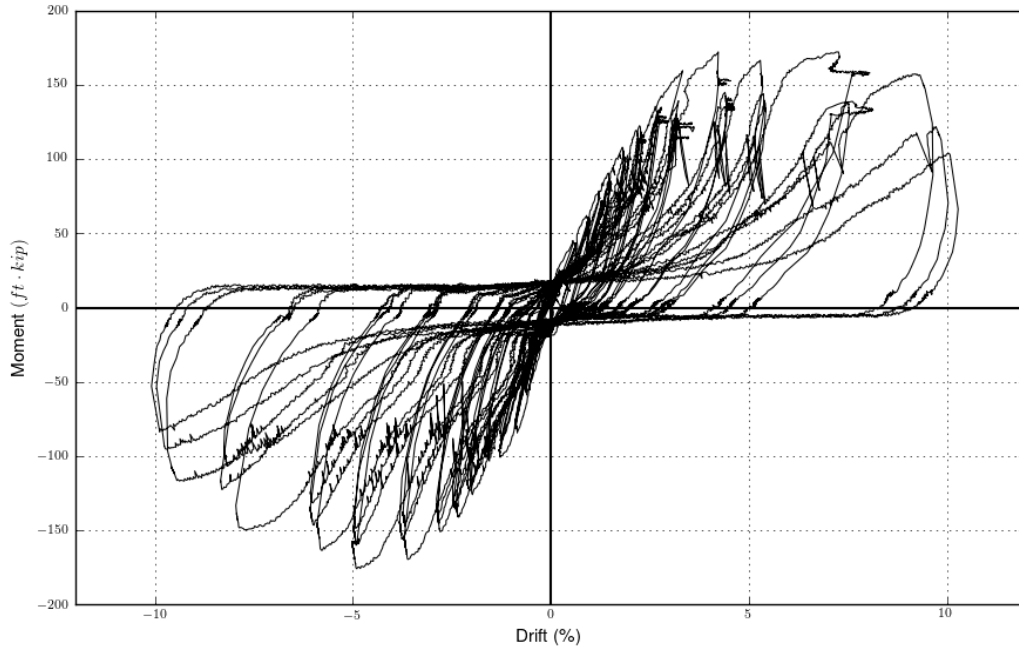


Figure 47: CT1 cyclic response

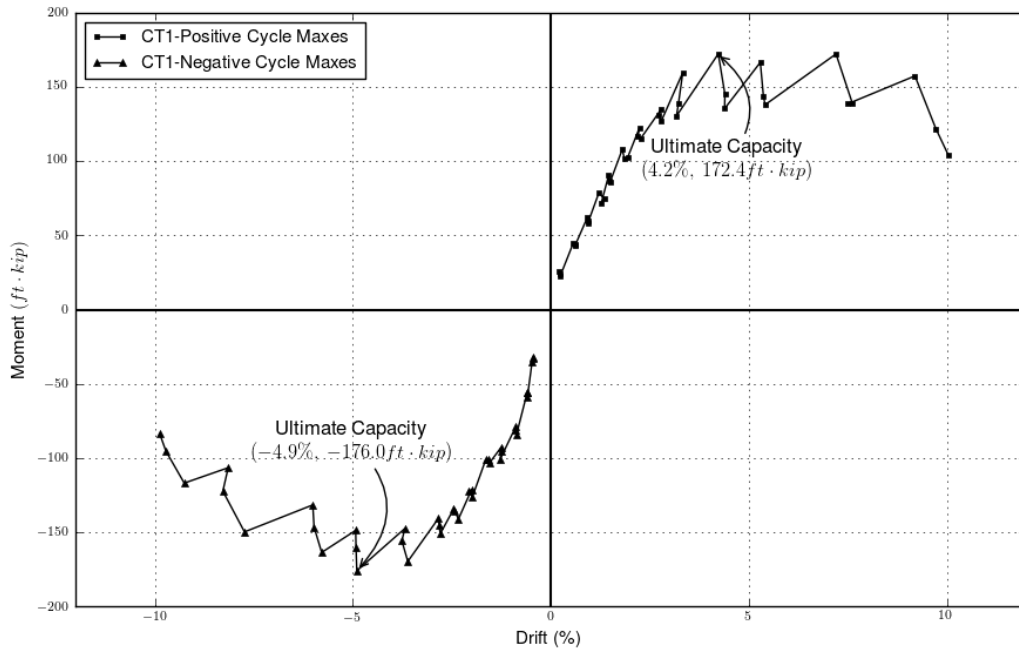


Figure 48: CT1 Cyclic Load Peaks vs. Percent Drift

As the displacement cycles increased in magnitude, CT1 eventually failed through crushing and fracture of the concrete pile cap, as was expected with the use of the oversized pile. Figure 49 shows CT1 near the completion of testing. While there is much interest in the response leading up to failure as cycling proceeded, CT1 ultimately failed

in a manner visually similar to the companion monotonic test VT2. Referring to Figure 49, the overall failure response of the cap included significant crushing on each side of the pile region, permanent elongation of the cap hole, as well as significant cracking in the concrete, including the compression struts as previously identified.



Figure 49: CT1 near the completion of testing

6.6 Cyclic Test 2 – CT2

CT2 was designed to evaluate the effect on cap performance of including internal U-bars located near the tip of the embedded pile. Aside from these additional interior U-bars, all other test parameters were kept as close as test conditions allowed to those of CT1 (and thus also VT2), including the applied displacement history.

Similar to the previous tests, the load vs. displacement is represented in terms of the total applied moment at the connection (which includes P-delta effects) and the drift at the tip of the pile. As previously noted, the cyclic response consists of three repeated displacement cycles at each increasing drift level. The complete hysteresis for CT2 is shown in Figure 50. Additionally, the peak resistance and corresponding drift for each displacement cycle are plotted in Figure 51. As expected, the specimen ultimately failed in the concrete cap in a manner similar to that observed in CT1 and VT2: crushing and splitting in the concrete pile cap.

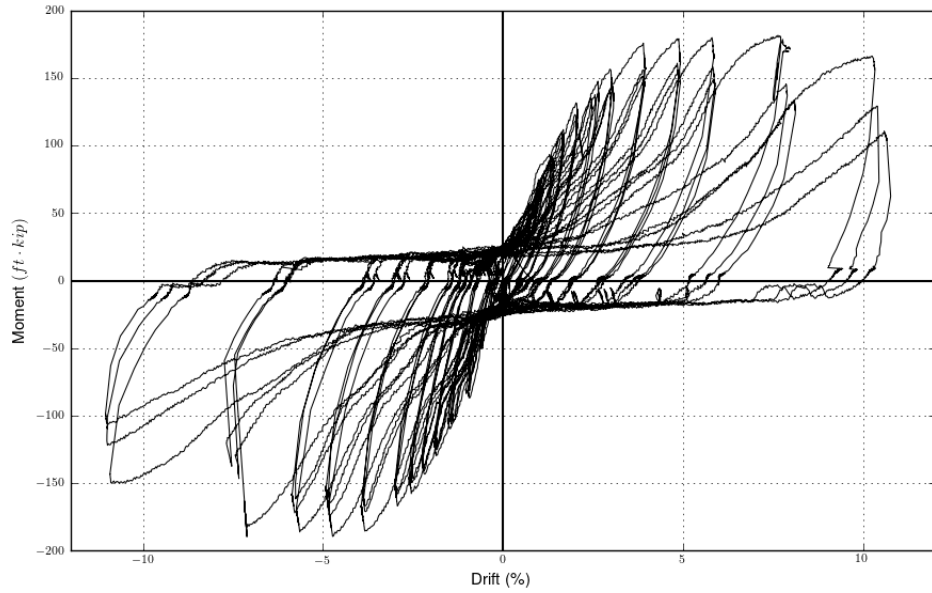


Figure 50: CT2 complete cyclic response

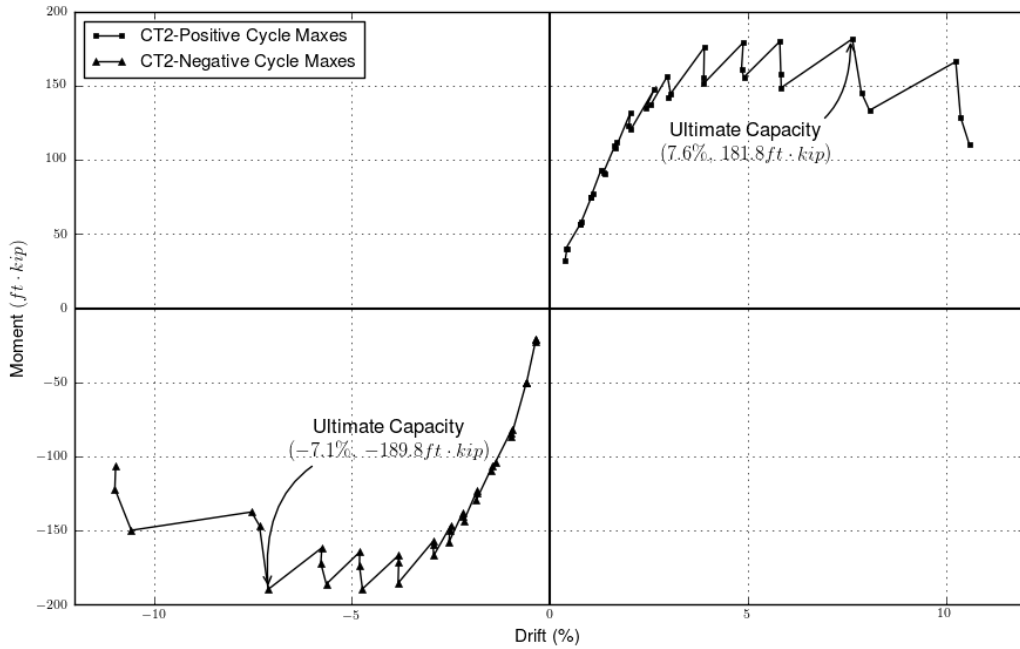


Figure 51: CT2 cyclic load peaks vs. drift

As expected for this type of failure, the response is very pinched, indicating reduced energy dissipation. Additionally, degradation in moment capacity between subsequent cycles at the same drift level is evident, but is delayed when compared to CT1. Finally, as the drift increases, the ultimate moment is reached at 181.8 ft-kip in the positive

direction, and 189.8 ft-kip in the negative direction. Note that this response is more balanced when compared to CT1. The condition of the specimen near the completion of testing is shown in Figure 52. While test CT2 was cyclic in nature and thus there is much interest in its response as cycling proceeded, the ultimate failure condition in most regards resembles that seen in the monotonic tests.



Figure 52: CT2 near the completion of testing

7 DISCUSSION OF RESULTS

Further insight on connection performance was realized by reviewing the tests results comparatively rather than individually as was done in the previous chapter of this report. Recall, four monotonic tests -- VT1, VT2, VT2.5 and VT3 -- and two cyclic tests -- CT1 and CT2 -- were conducted in this program. The monotonic tests were well suited for identifying different failure mechanisms as the connection was pushed in a single stroke to failure, while the two cyclic tests were useful in identifying early degradation in connection performance under repeated loadings. These comparative analyses revealed some trends in connection performance that the MDT design guide could more thoroughly address, as commented on below. The majority of these observations are related to the pile cap, as the test program was purposefully designed to focus on this element of the connection. That being said, in one test (VT1) a plastic hinge formed in the CFT, allowing for at least some comment on how the design guide treats this element of the connection.

7.1 Overview

7.1.1 Monotonic Test Series

The force-displacement responses (i.e., total moment as a function of drift) for the first push to failure in monotonic tests VT1, VT2, VT2.5, and VT3 are grouped in Figure 53 for comparison purposes. In this figure, the various failure mechanisms that were successively experienced by each test specimen are identified. These failures correlate with changes in the cap stiffness, as represented by associated changes in the slope of each moment-drift response. At each such major change in slope, vertical lines have been inserted on the figure marking the drift values and the corresponding moment values at which they occurred.

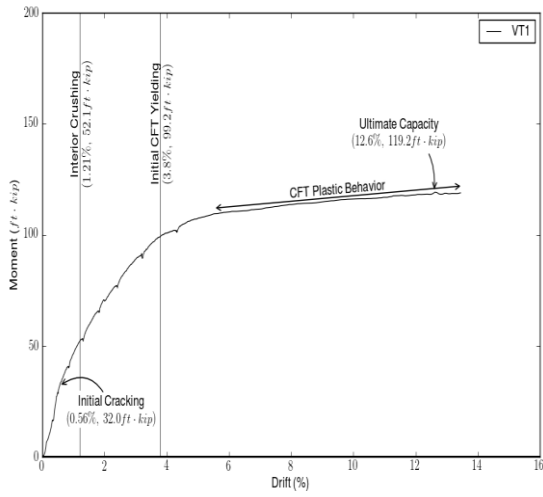
Referring to Figure 53, some commonalities in basic behavior and associated failure mechanisms are apparent across all tests. In general, the first distress in each specimen consisted of thin cracks forming in the cap concrete, followed by the concrete in the interior of the cap on the “back side” of the pile near the embedded tip being damaged (Figure 54). Initial cracking occurred across a range of drifts of 0.30 to 0.60 percent and moments ranging from 32 to 46 ft-kip. Interior damage/crushing was characterized by a change in stiffness that occurred prior to evident damage on the exterior of the concrete cap. This internal crushing occurred across a range of drifts of 1.11 to 1.32 percent and total moments of 52.1 to 67.2 ft-kip. While these behaviors (initial cracking and interior crushing) are evident in the response from VT1, VT2, and VT3, they are absent in VT2.5.

Test VT2.5 reused the cap from test VT1, which had already experienced these permanent distresses in that earlier test. Once again, while VT1 was apparently undamaged on the exterior, the distress it experienced in the first test was obvious when it was retested in VT2.5. The load displacement response for VT2.5 began with a stiffness consistent with a cracked cap with some permanent interior damage, as can be observed in Figure 53a and Figure 53c. The slope of the initial section of the load displacement response for VT2.5 closely matches the slope of the load displacement response in each of the other tests following the advent of initial interior concrete damage.

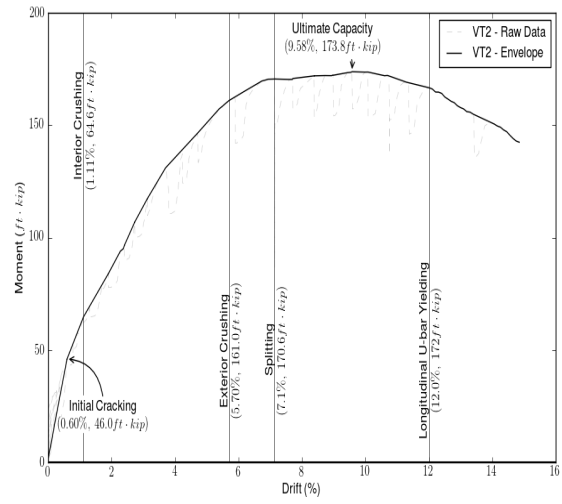
Following the occurrence of initial cracking and interior damage, the behaviors of VT1, VT2, VT2.5 and VT3 diverged as they were exercised through increasing levels of drifts. The load displacement response of VT1, shown in Figure 53a, subsequently exhibits a long yield plateau, as a plastic hinge formed in the CFT at a moment demand of 99.2 ft·kip. VT2, with an oversize pile, went on to next fail through crushing of the exterior concrete on the front face of the pile (Figure 54) at 5.7 percent drift and 161 ft·kip of total applied moment (Figure 53b). Similarly, crushing of the concrete between the CFT and the U-bar was also seen in VT2.5 and VT3 at closely comparable drift levels (5.0 and 5.8 percent, respectively). Such crushing was readily identified by visual observation, but there were also other more precise indicators of its occurrence. Typically, the signal from the strain gage on the inside of the U-bar was disrupted as the concrete began to crush, and the transverse ties immediately next to the compression region transitioned from tension to bending (see Appendix C). In the case of VT2 and VT2.5, crushing of the exterior concrete immediately followed crushing of the interior concrete adjacent to the pile, as the drift demand on the pile was increased. In VT3, longitudinal yielding of the U-bar reinforcement occurred prior to crushing of the exterior concrete. This yielding occurred at a drift of 4.8 percent and a moment of 139.2 ft·kip.

As the drift further increased from 6 to 7 percent, VT2, VT2.5 and VT3 all experienced “splitting” failures. “Splitting” was assessed as yielding of the U-bar in the transverse direction (at the apex of the “U”). In the case of VT2.5, splitting occurred simultaneously with yielding of the longitudinal reinforcing steel. Due to the multiple failure mechanisms, the moment capacity of VT2.5 then steadily decreased for the remainder of the test (Figure 53c). In the case of VT3, yielding of the longitudinal reinforcement occurred slightly before splitting, which occurred coincident with crushing of the exterior concrete (at a drift of 5.8 percent). Once again, due to the multiple failure mechanisms, the moment capacity then steadily decreased in a very similar fashion to VT2.5. Returning to VT2, following exterior crushing of the cap at a drift of 5.70 percent as mentioned above, the splitting failure occurred at 7.1 percent drift and moment demand

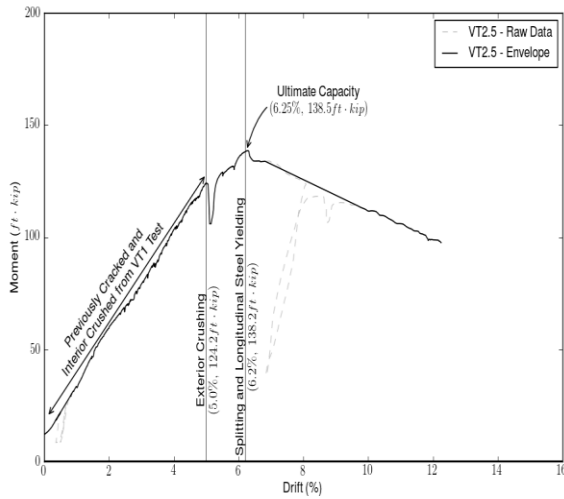
of 170.6 ft·kip. As the drift further increased, reinforcement in the longitudinal direction eventually yielded at a drift of 12.0 percent and moment of 167 ft·kip, and the moment capacity began to gradually decrease as significant damage to the cap was incurred.



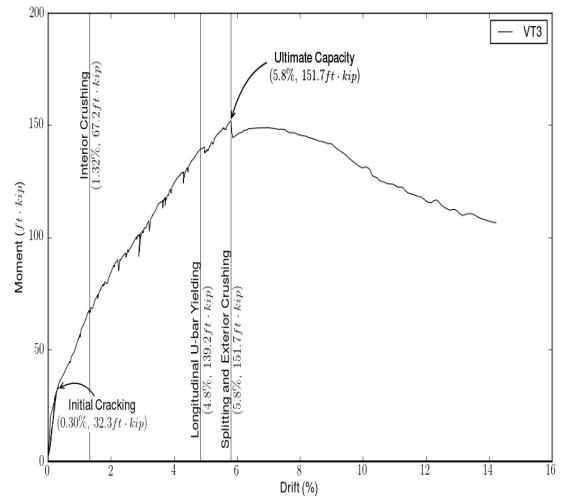
(a) VT1



(b) VT2



(c) VT2.5



(d) VT3

Figure 53: Overview of results for monotonic tests (VT1, VT2, VT2.5, VT3)

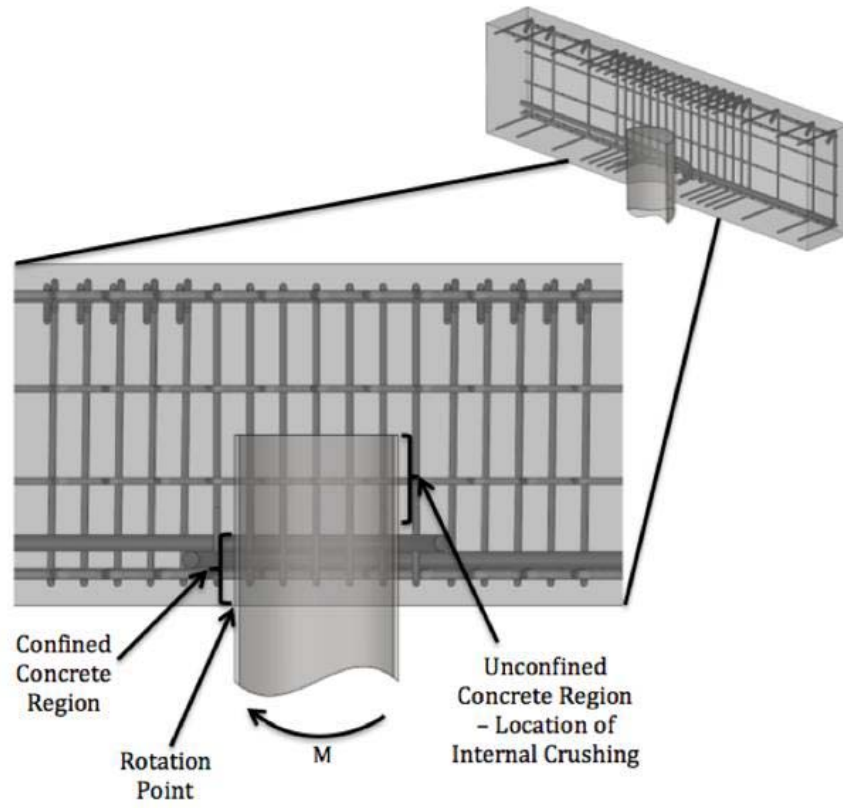


Figure 54: Exterior and interior crushing regions in the concrete cap

7.1.2 Cyclic Test Series

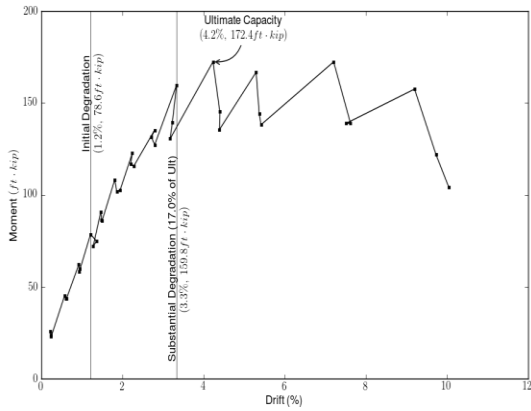
Envelopes of the maximum moments and drifts experienced in each displacement cycle in tests CT1 and CT2 are presented in Figure 55. While the discussion of the monotonic test series in the previous section focused on the moments and drifts at which various failure mechanisms occurred, the cyclic responses of CT1 and CT2 are better suited for identifying the initiation of permanent degradation in cap performance and then quantifying this degradation as cycling proceeded. Notably, the initial occurrence of permanent degradation under cyclic loading was determined to be that drift step at which the moment generated in the connection obviously decreased on each repeated displacement cycle at that same drift level (see Figure 55b). Further, this degradation in moment response had to then occur across the repeated displacement cycles at all remaining drift steps. Using these criteria, the first occurrence of permanent degradation in the cyclic moment carrying ability of the cap was identified at the drift levels delineated in Figure 55. These drift values and associated moments are also reported in Table 6. Thus, initial degradation began at drift levels from of 0.9 to 2.0 percent, and resulted in an average loss in moment demand at a these drift levels of approximately 3 percent, when expressed as a fraction of the maximum ultimate moment capacity of each specimen (these ultimate moment capacities are also shown in Figure 55 and reported in Table 6).

Substantial cyclic degradation of the cap performance was somewhat arbitrarily defined as a decrease of at least 10 percent or more in moment response across the three repeated displacement cycles at a given drift level. This level of degradation was reached at approximately the same drift level in all cases, nominally 3 percent. The corresponding maximum cap moments ranged from 159.8 to 185.7 ft·kip and are listed in Table 6.

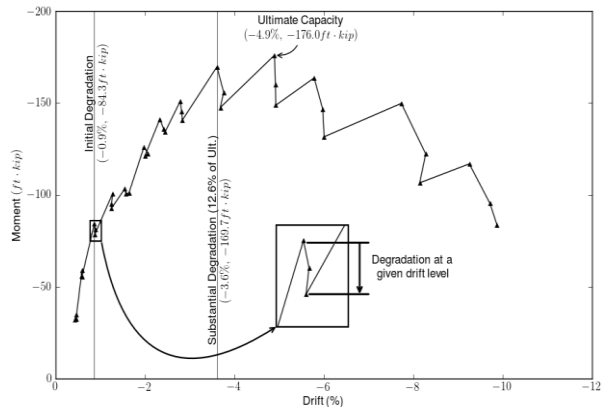
Finally, the ultimate capacity of each cap and corresponding drift levels at which they were achieved are also shown in Figure 55 and listed in Table 6. Moment capacities ranged from 172.4 to 189.8 ft·kip and were realized at drifts ranging from 172.4 to 189.8 ft·kip.

Table 6: Summary of cyclic response

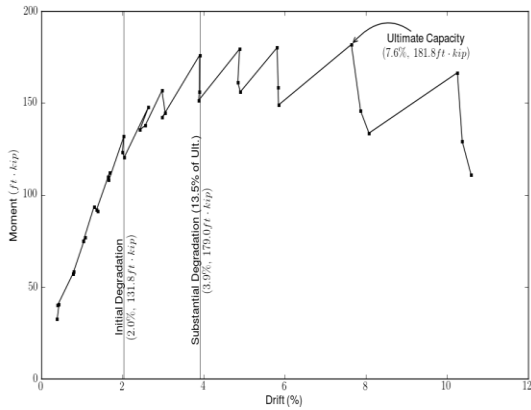
		Initial Degradation		Substantial Degradation		Ultimate Capacity	
		Drift	Moment	Drift	Moment	Drift	Moment
		(%)	(ft·kip)	(%)	(ft·kip)	(%)	(ft·kip)
CT1	Positive	1.2 %	78.6	3.3 %	159.8	4.2 %	172.4
	Negative	-0.9 %	-84.3	-3.6 %	-169.7	-4.9 %	-176.0
CT2	Positive	2.0 %	131.8	3.9 %	179	7.6 %	181.8
	Negative	-1.9 %	-129.7	-3.8 %	-185.7	-7.1 %	-189.8



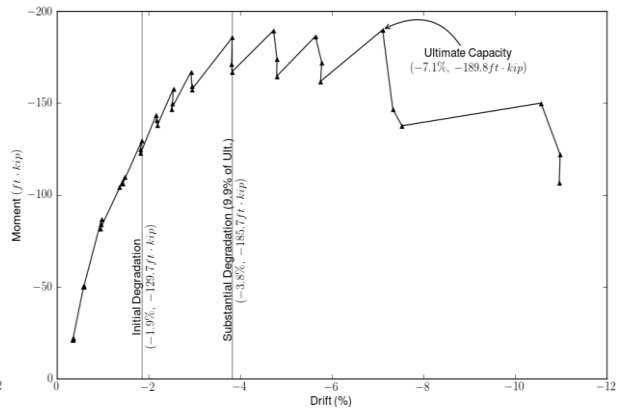
(a) CT1 – Positive Cycles



(b) CT1 – Negative Cycles



(c) CT2 – Positive Cycles



(d) CT2 – Negative Cycles

Figure 55: Overview of results, maximum moment in each displacement cycle for CT1 and CT2

7.2 Cyclic Behaviors

7.2.1 Cyclic vs. Monotonic Behavior

The cyclic test specimens were similar in design and construction to VT2, which was pushed monotonically to failure. Notably, CT1 closely replicated VT2 with respect to CFT embedment length, concrete strength, and reinforcing layout, providing an opportunity to compare monotonic versus cyclic behavior of the pile cap. The moment-drift response from VT2 is overlaid on the cyclic moment-drift envelope from CT1 (for the same “push” direction of loading) in Figure 56. The responses are very similar, especially until approximately 8.5 percent drift. While the monotonic test did not provide any indication of the degradation that occurred under repeated displacement cycles, it did envelope the general behavior during the cyclic test, up through and beyond the point at which the ultimate capacity was reached. Furthermore, the initiation of cyclic degradation identified in CT1 at a drift of 1.21 percent (see Figure 55a) is reasonably close to the drift of 1.21 percent at which interior crushing is thought to have occurred in VT2 (see Figure 53b). Thus, these similarities indicate that the behaviors identified in a monotonic test provide a reasonable assessment of pile cap performance under a more complicated cyclic history. Beyond 8.5 percent drift, the moment carrying capacity of the cap in cyclic test CT1 noticeably decreased compared to that of the cap in the monotonic test, VT2. This loss in capacity was attributed to the accumulated degradation from the cyclic displacement history.

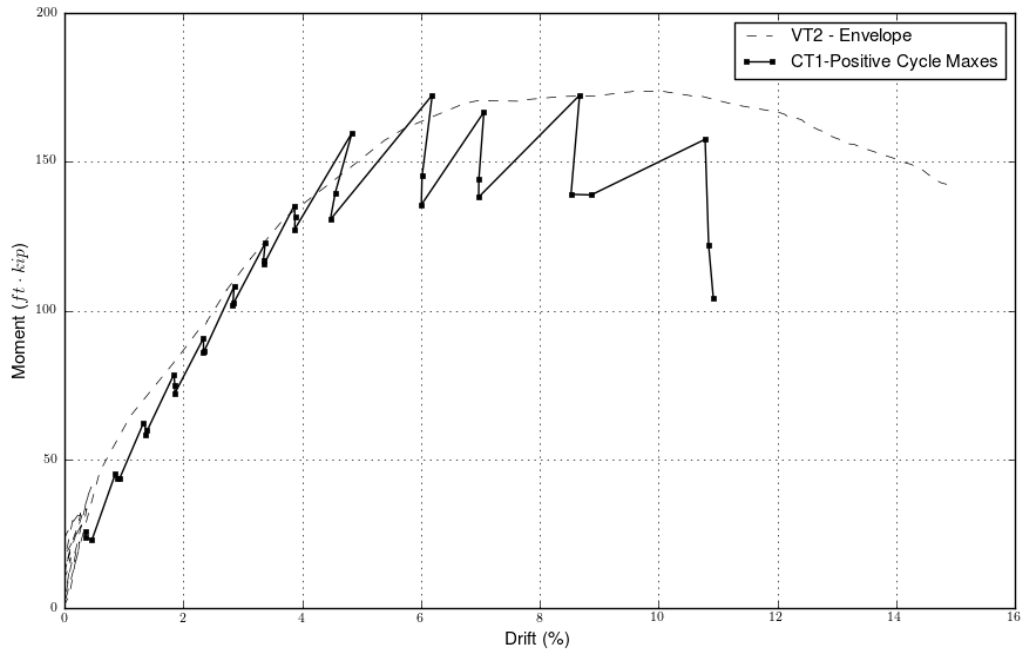


Figure 56: Response comparison between VT2 and CT1

7.2.2 Effect of Additional Interior U-bar

CT2 was constructed similar to CT1 but with the addition of interior U-bars encircling the tip of the embedded CFT; by comparing the responses for CT1 and CT2, the effect of these interior U-bars was characterized. To help visualize this comparison, the envelopes of the maximum moment and corresponding drifts during each cycle of response were modified as shown in Figure 57 and Figure 58. In these figures, the maximum moment at each drift step are connected by solid lines, and the degradation in moment response at each drift step is both delineated, as well as reflected by the size of the circle at each step. As before, the degradation across the three displacement cycles at each drift step is simply given as the change in moment across the three displacement cycles divided by the ultimate moment capacity of the cap.

Referring to Figure 57 and Figure 58, CT2, which had the additional interior U-bars, clearly performed better than CT1, which only had the exterior U-bars. At all drift levels, CT2 exhibited a stiffer response and greater moment resistance than CT1. The difference in stiffness and resistance was more pronounced between the two specimens for negative versus positive cycle events. This disparity is believed to be related to the specific arrangement of the U-bars in the models. When there is only one set of U-bars as shown in Figure 59a (as in CT1), the connection will have different responses associated with each direction due to the unbalanced moment arms provided by the “stacked” bar configuration. When both internal and external sets of U-bars are included (as in CT2), if

properly laid out, the moment arm of the connection will be the same in both directions as shown in Figure 59b.

Further, initial degradation due to cyclic loading occurred in CT1 at drifts of 1.21 and 0.87 percent (positive and negative cycle directions, respectively), while the corresponding drift levels at which this damage initiated in CT2 were substantially higher at 2.0 and 1.85 percent. Correspondingly, the increase in moment capacity between CT1 and CT2 relating to the initial degradation point was substantial; CT2, with the additional set of U-bars, had an increased moment capacity over CT1 of 40.4 and 35.0 percent in the positive and negative directions, respectively. This increase in capacity prior to initial degradation for CT2 is likely due to the elimination of the interior crushing failure associated with the initial degradation for CT1. Similarly, although somewhat closer in occurrence, while the onset of substantial cyclic degradation in CT1 was seen at drifts of 3.3 and 3.61 percent (positive and negative load directions, respectively), the corresponding drifts at which this damage was seen in CT2 were 3.9 and 3.8 percent. Generally as cyclic degradation initiated the degree of degradation was larger at each drift step in CT1 versus CT2; once substantial degradation occurred, the magnitude of this degradation was generally similar in both CT1 and CT2.

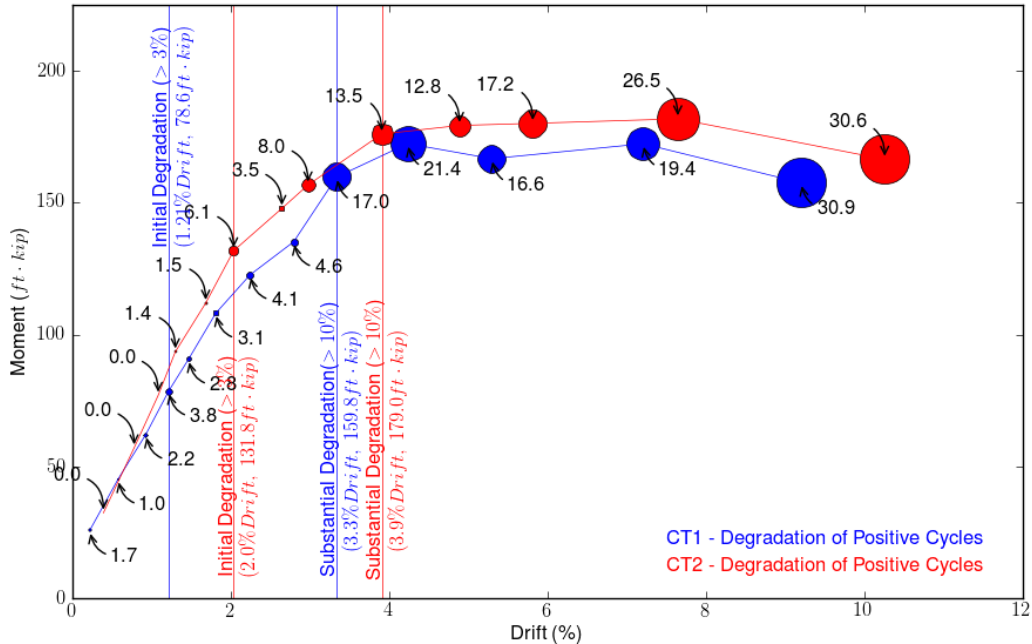


Figure 57: CT1 and CT2 cyclic degradation comparison – positive cycles

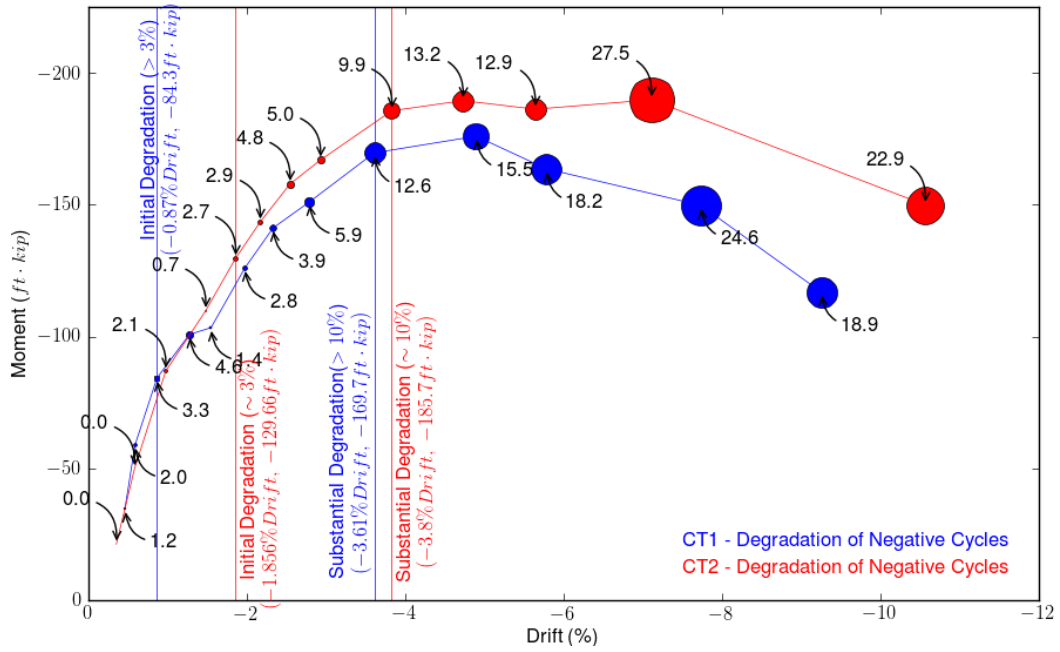
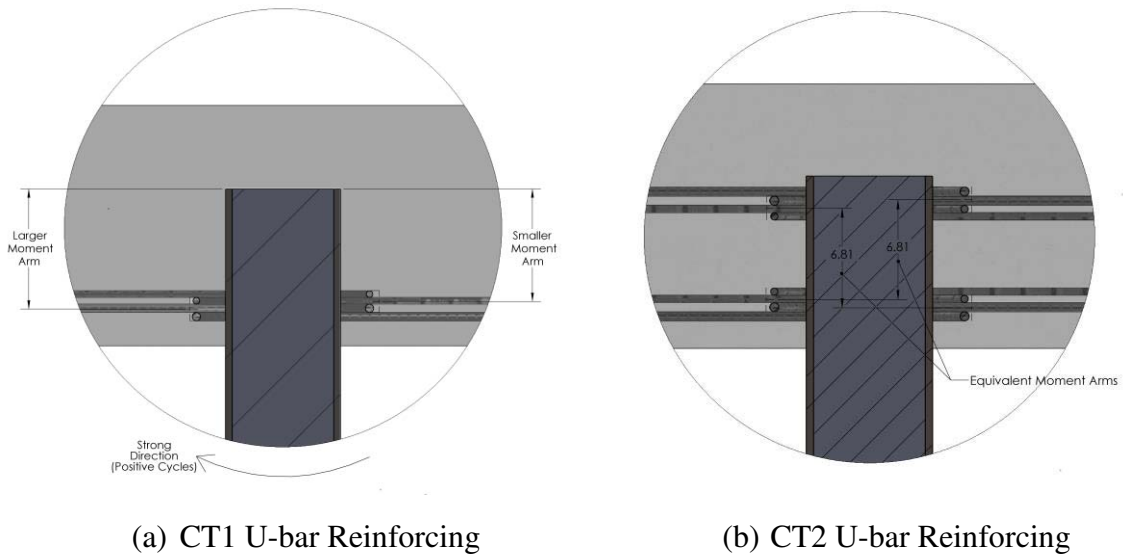


Figure 58: CT1 and CT2 cyclic degradation comparison – negative cycles



(a) CT1 U-bar Reinforcing

(b) CT2 U-bar Reinforcing

Figure 59: Comparison of U-bar reinforcing schemes, CT1 and CT2

7.3 MDT Design Guide

The MDT design guide directly or indirectly addresses all of the various failure mechanisms observed throughout this test series: (1) the formation of a plastic-hinge in the CFT, (2) interior and exterior concrete crushing, (3) yielding of the longitudinal reinforcement, and (4) splitting of the concrete due to transverse loads introduced from

the embedded CFT. This section discusses the efficacy of the design guide at predicting/preventing these mechanisms, as well as possible areas for improvement.

7.3.1 Plastic-Moment Capacity of CFT

While the focus of this test series was on the capacity of the concrete pile cap, a plastic hinge did form in the CFT in test VT1 (in all other tests, an oversized CFT was used to purposely force failure in to the pile cap). Plastic hinging in VT1 occurred at a moment of 119.2 ft·kip, which significantly exceeded the predicted capacity from the design guide of 96.8 ft·kip (with the 1.25 overstrength factor). As previously mentioned, the design guide equation ignores the presence of the concrete infill in the tube, which typically significantly increases the plastic moment capacity of the CFT. The method commended by AISC (introduced in Chapter 2) has been shown to closely predict the plastic moment capacity of CFTs. Therefore, it is suggested that the AISC method be considered by the design guide. Notably, there are two major concerns with underestimating the plastic moment capacity of the CFT:

1. if the design assumes plastic hinging of the CFT will limit the maximum moment demand that the pile cap needs to be designed for, it is unconservative to underestimate this parameter, and
2. while the current design guide methodology was calibrated to this approach for determining the plastic moment capacity of the CFT, if this value can be better established, it would seem reasonable to do so and modify the calibration process accordingly.

7.3.2 Concrete Crushing Limit State

The MDT design guide addresses the issue of concrete crushing by varying the embedment length of the embedded CFT to reduce the stresses on the concrete resulting from the applied moment. The relationship between embedment length, concrete strength, and moment capacity, previously defined in equation 4.1 is presented graphically in Figure 60 and repeated in Figure 61, for both compressive strengths used in this test series (4,000 psi and 6,250 psi). As expected, the moment capacity increases with increasing embedment length, and increasing concrete strength.

Overlaid on the predicted moment capacities in Figure 60 and Figure 61, respectively, are the actual applied moments at which exterior and interior crushing of the concrete adjacent to the CFT is estimated to have occurred in each test. Note that this behavior could only be readily evaluated in monotonic tests in which the cap failed, i.e., VT2, VT2.5 and VT3. In the mechanics model used by the design guide methodology (see Figure 10), concrete crushing is a possibility both in the compression stress block that

develops in the interior of the pile cap, as well as in the compression block near the exterior surface of the cap. In light of the basic unconfined nature of the concrete in the “exterior” compression block near the surface of the cap, attention in the earlier test series by Stephens and McKittrick was focused on preventing this failure mechanism by confining the concrete in this block using U-bars. Concrete crushing in the interior of the cap near the embedded tip of the pile was not seen as a concern, due to the mass of surrounding concrete in this area.

Referring to Figure 60, the MDT design guide reasonably predicted the occurrence of crushing of the concrete in the exterior compression block, although in two out of the three tests in which this behavior could be evaluated (VT2, VT2.5 and VT3), the predicted crushing moment was nominally greater than that predicted. More specifically, in VT2.5 and VT3, exterior concrete crushing occurred within approximately 10 percent of predicted values, while in VT2, exterior concrete crushing occurred approximately 20 percent below the predicted value. In two of the three tests, the crushing load was over predicted by the design guide. An important parameter in predicting the onset of exterior crushing is the concrete confinement factor, which was determined based on the model configurations tested by Stephens and McKittrick (2005). The U-bar configuration adopted by MDT in the design guide may not offer the same level of concrete confinement as was present in those earlier tests. This situation could possibly be addressed by re-evaluating this factor (i.e., decreasing it) based on a thorough analysis of all the data collected to date.

Relative to crushing/damage to the concrete in the interior compression block within the cap, the estimated moment at which this damage occurred in each test is overlaid on the predicted crushing moment from the design guide in Figure 61. Referring to this figure, crushing/damage to the interior concrete in the cap occurred at applied moments 36.7, 34.2 and 49.4 percent of the predicted capacities in VT2, VT2.5 and VT3. Additionally, the point identified as initial degradation for CT1 (78.6 ft·kip, see Figure 56b), which is believed to be internal crushing as well, was at 45.0 percent of the predicted capacity (same predicted capacity as VT2 of 174.6 ft·kip). Thus, while it would appear that the strategy of using U-bars to control crushing of the concrete in the exterior compression zone adjacent to the CFT has been successful, some degree of concrete degradation/crushing now is seen at relatively lower demand levels in the interior compression zone near the tip of the CFT. The effect of this interior crushing on connection performance was less obvious than that of external crushing. This internal crushing resulted in a reduction in cap stiffness (seen, for example, in Figure 53a), increased degradation with each repeated displacement cycle (highlighted in Figure 55b),

loss of energy dissipation capacity (see Figure 58), but little loss of ultimate load carrying capacity (see Figure 57). One method to control this behavior is to use a second set of U-bars circling the tip of the embedded pile in the interior of the cap, as was done in CT2; Figure 61 shows that initial degradation for CT2 was delayed when compared to VT2 and CT1, which did not have internal U-bars. Further note that the possibility has been raised and is under continued investigation that when initial distress was observed in CT2, it was related to longitudinal yielding of the U-bars rather than interior concrete crushing.

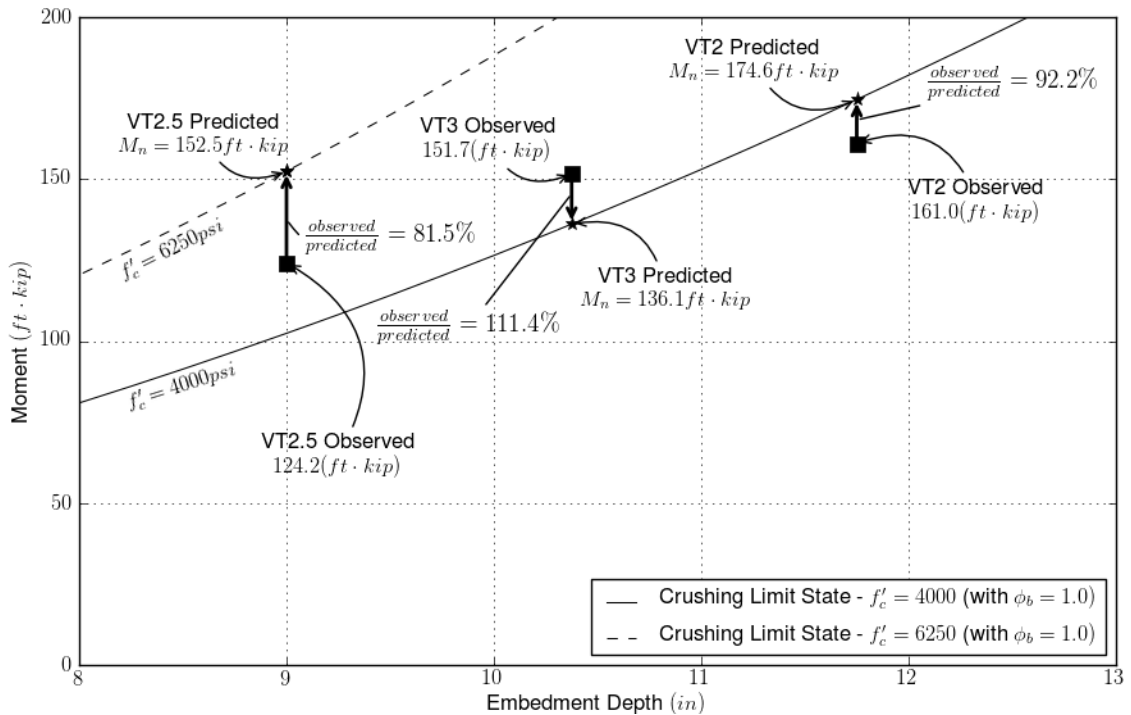


Figure 60: Crushing limit state - Predicted vs. Exterior Crushing Observed Values

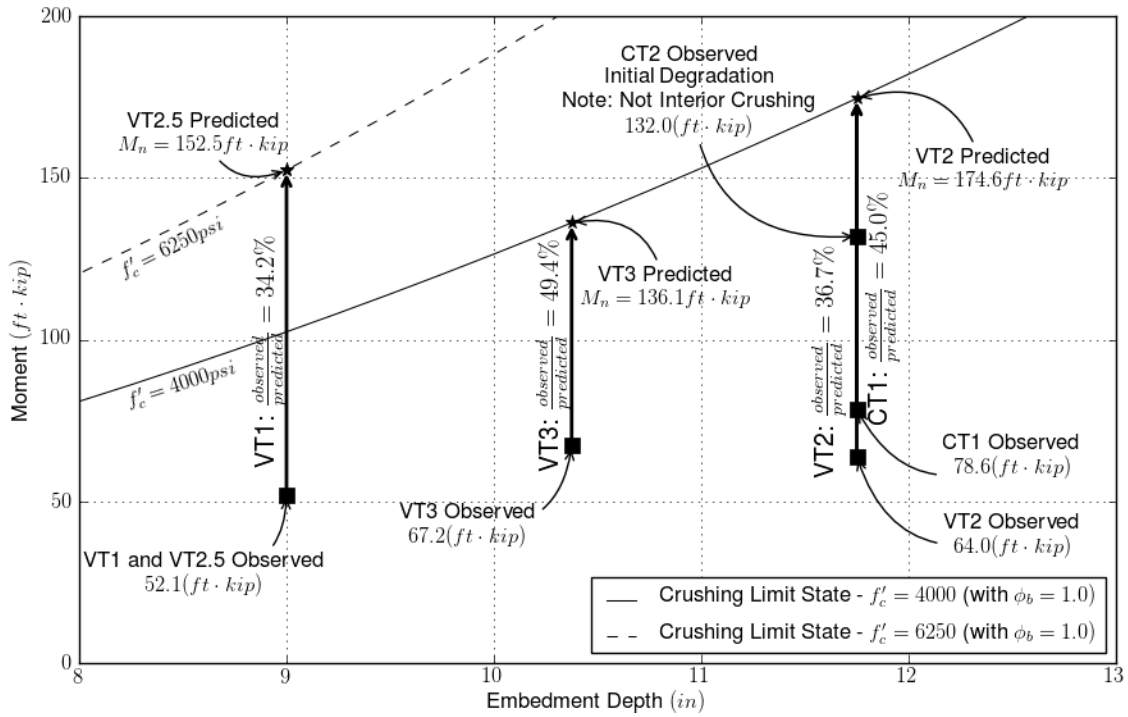


Figure 61: Crushing limit state - Predicted vs. Interior Crushing Observed Values

7.3.3 Yielding of Longitudinal Reinforcement

As was done for concrete crushing in the cap, the expected moment at which yielding of the longitudinal steel in the cap would be expected in each test based on the MDT design guide methodology is presented in Figure 62. The design guide addresses this demand on the cap by including additional longitudinal reinforcement in the form of U-bars if the design moment is sufficiently large to require such reinforcement. The amount of additional longitudinal reinforcing is dependent on several factors including the embedment length, L_{emb} , and the steel yield stress, f_y . Typically, the embedment length is known from the crushing limit state; therefore, the moment capacity for this limit state mainly depends on the amount of reinforcing added (in the form of U-bars). For the three embedment lengths tested, Equation 3.12 was used (including the suggested 25 percent calibration factor discussed in section 3.2.5), creating a relationship for the moment capacity and the additional longitudinal reinforcement required as shown in Figure 62.

In this test series, yielding of the longitudinal steel reinforcement was observed for VT2.5 and VT3 prior to the cap reaching its ultimate capacity, and the moments in which this limit state was reached for each of these specimens and the applied moments at which this yielding occurred are shown in Figure 62. While yielding of the longitudinal steel was also reported for VT2, this limit state was reached well after other limit states and

thus VT2 may not have behaved in a representative fashion. Both VT2.5 and VT3 had #7 U-bars, providing an equivalent area of reinforcing steel added of 1.2 in. Although the embedment length varied between the two tests (consisting of 9.0 and 10.375 in in tests VT2.5 and VT3, respectively), yield of the longitudinal U-bars happened at approximately 139 ft·kip in both tests. This value is reasonably close to the values predicted by the design guide, with VT2.5 10.1 percent above and VT3 3.1 percent below the expected results.

Despite the relatively close agreement in the actual and predicted moments at which the longitudinal steel yielded in these two tests, further review and revision of this part of the design guide may be merited. The present methodology is calibrated to the previous testing completed by Stephens and McKittrick (2005). Notably, the area of longitudinal steel required is calculated based on the design moment and then reduced by 75 percent; this reduction, empirically determined from test results, acknowledges the presence of minimum longitudinal steel already sized and placed in the cap, as well as the action of load carrying mechanisms not explicitly represented in the simple analytical model used in the design process. However, the basic connection configuration in VT2.5 and VT3 resembles in many regards (e.g., basic cap cross-section and pile diameter) that used in the calibration process, so these two tests may not offer a robust evaluation of the efficacy of the design methodology across all possible cap configurations. For example, the calibration factor of 75 percent may not be adequate as cap cross-section sizes are changed (which will also change the amount of normal reinforcement used) in relation to different design moments based on different controlling design criteria. It would be desirable to develop an analytical model that better describes the role of the U-bar reinforcement in the immediate area of the CFT pile to reduce reliance on empirical factors that may only be appropriate across a certain range of connection configurations.

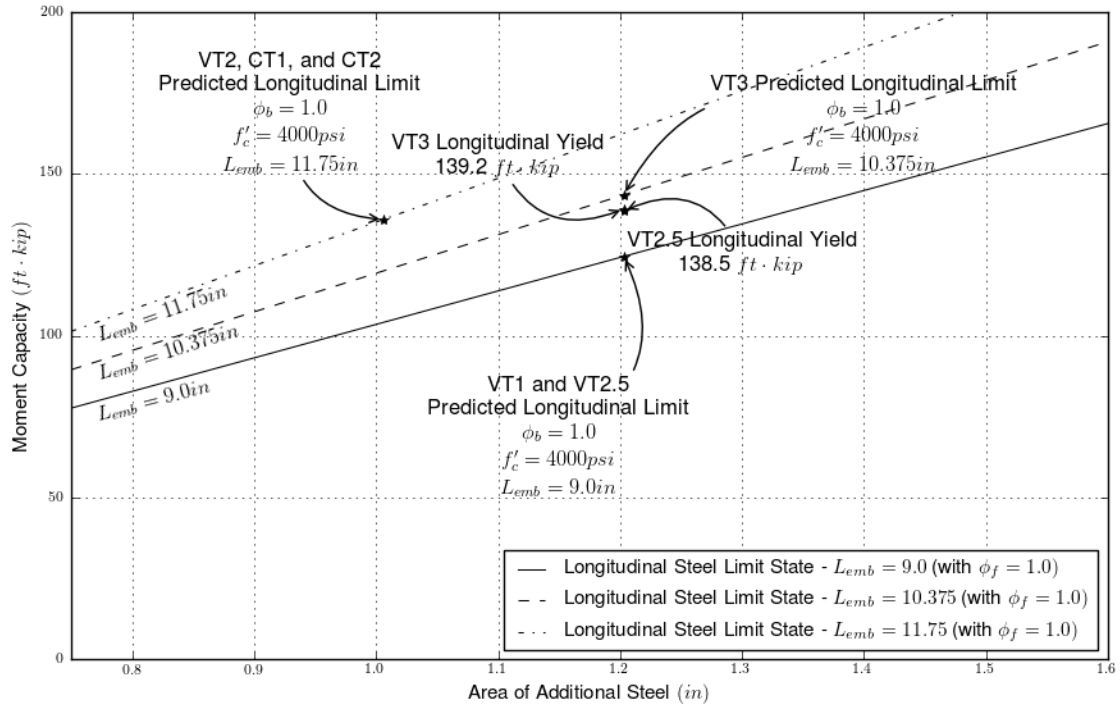


Figure 62: Additional longitudinal steel limit state

7.3.4 Splitting

Splitting of the cap is the final limit state that was observed in this test series, and this limit state was reached after or as other limit states were experienced. The design guide does not offer an analytical basis to determine a specific splitting capacity in terms of the configuration of the cap and reinforcing provided (i.e., the transverse ties and the U-bars). The design guide defines the amount of transverse steel in the cap using the AASHTO equations to calculate the transverse steel area and spacing required in plastic hinge zones of columns. These equations (reproduced as equations 3.13 and 3.14 in this report) are based simply on the geometry of the cap cross-section, the spacing of the stirrups, the compressive strength of the concrete, and the steel strength. This approach appears to be adequate, because as mentioned above, in all tests, other failure limits were experienced before splitting of the cap occurred. Nonetheless, sufficient test results may now be available to begin to develop and calibrate a simple analytical model to allow the transverse steel and U-bars to be sized for this limit state based on the design moment demand and cap configuration. The area of steel generated by this approach could then simply be compared with a minimum steel area determined by the current equations.

7.3.5 Other Observations

One outcome of this project has been a fairly thorough review of the MDT design guide methodology beyond just those provisions directly exercised in the test series. Notably in this regard, one step that may merit further review is the branching of the design process

based on the whether the design moment, M_u , exceeds 60 percent of the plastic moment capacity of the CFT pile, M_p (see Appendix A). In the earlier tests done by Stephens and McKittrick (2005), cap failure in the connection zone in lightly reinforced sections (i.e., no additional U-bar steel was used) only occurred when the applied moment exceeded 75 percent of the plastic-moment capacity of the CFT pile. Thus, with the intent of being conservative, a limit was implemented in the design guide requiring additional reinforcement adjacent to the pile in the form of U-bars when the design moment to be transferred through the connection exceeds 60 percent of the pile's plastic moment capacity. This approach would appear to rely on there being a consistent relationship between the plastic-moment capacity of the pipe pile and the moment capacity of the connection zone of the cap in which it is inserted. Such a relationship may exist for commonly used bent configurations. That is, in such configurations if pile strength is increased by increasing the pile diameter, the contact area between the pile and the cap will increase, thus keeping the compression stresses in the concrete adjacent to the pipe pile within acceptable limits. Further, as pile diameter increases, "standard/good practice" may dictate that the dimensions of the cap cross-section proportionally increase, thus generally providing increased resistance to other failure mechanisms in the cap in the connection zone (e.g., splitting).

The primary concern with the above described branching in the guide's design process is with possible bent configurations that fall outside those typically encountered and outside those used in developing this provision. If, for example, the pile wall thickness had been increased in the earlier test program, its moment capacity would have increased, and cap failure would have occurred at an applied moment less than 75 percent of the plastic moment capacity of the pile. In the current test series, this situation was purposefully generated by using "oversized" piles in most of the tests to force failure into the concrete caps.

Consider the pile used in VT2 of this test series, which had a plastic-moment capacity of 182 ft·kip (as calculated using the design guide approach). The current branch in the design guide would have indicated that significant distress in the connection region of the cap was unlikely to occur until the applied moment reached 109 ft·kip (60 percent of the plastic-moment capacity of the pile), and would actually not be expected until the applied moment reached 137 ft·kip (75 percent of plastic moment capacity of the pile). Thus, if VT2 was being designed, for example, for a moment of 105 ft·kip, the design guide would have indicated that no additional U-bar steel was necessary ($M_u = 105 \text{ ft}\cdot\text{kip} < 0.6 \cdot M_p = 109 \text{ ft}\cdot\text{kip}$). The resulting cap configuration would have been very similar to

that of the lightly reinforced sections tested by Stephens and McKittrick (2005) that did not have U-bars, which failed at moment demands of only 74 to 102 ft·kip (see Table 2).

Thus, the example above demonstrates that the design process needs to consider the strength of the concrete cap in the connection zone relative to the design moment it has to carry, regardless of the plastic moment capacity of the CFT pile (which possibly could be highly conservative in some cases for various reasons). One manner to ensure this happens in the context of the current design guide would be to simply remove that branch from the design process that allows additional reinforcing requirements to be bypassed if the design moment is less than 60 percent of the plastic moment capacity of the pile. This modification would result in some amount of additional reinforcement in the form of U-bars being part of all pile cap designs. Presuming U-bars are easily installed, the potential benefits of such a change in improved and more certain cap performance would outweigh the costs.

8 SUMMARY AND CONCLUSIONS

The Montana Department of Transportation commonly uses CFT piles connected at the top by a concrete pile cap in short/medium span bridges. They have found this system to be very efficient in that it offers low initial cost, short construction time, and a long service life with minimal maintenance. While the response of this system under gravity loads is well understood, its response of this system under extreme lateral loads is difficult to reliably predict. In particular, the behavior of the connection between the CFT pile and the concrete pile cap is especially complex and difficult to analyze. This connection has been the focus of many research projects over the past decade, and was the focus of an MDT funded study completed in 2005 (Stephens and McKittrick, 2005). Based on the results of that investigation, MDT developed a design methodology for this connection. While the connections generated with this methodology were similar to those tested in 2005, key differences were observed. Therefore, the objective of this study was to validate the MDT design guide by physically testing scaled CFT pile-to-pile cap connections designed following its provisions.

In this research, a total of six CFT pile-to-pile cap connections designed according to the MDT design methodology were tested until failure under lateral loads. Four specimens (three unique designs) were tested under monotonic loading, providing general information on limit states, ultimate loads, and post-failure ductility. Two additional tests were completed using a cyclic-loading scheme to capture the performance of the connections under multiple cycles of fully reversed, increasing load.

Four key limit states were observed in this test program: (1) formation of a plastic hinge in the CFT, (2) interior and exterior crushing of the concrete in the cap, (3) yielding of the longitudinal reinforcement in the cap, and (4) splitting of the concrete cap. Based on the results of this investigation, the following conclusions can be made regarding the efficacy of the MDT design methodology at addressing these limit states.

1. The MDT design methodology for predicting the plastic-moment capacity of the CFT only uses the properties of the steel pipe in this calculation, and simply ignores the effects that the concrete and axial load have on this capacity. In many applications, this simplification would be conservative; however, if the design assumes that plastic hinging will limit the maximum moment demand that the pile cap needs to be designed for, it is unconservative to underestimate this parameter. The methodology proposed by AISC (2011) to predict the plastic-moment capacity of CFTs has been

shown to accurately predict this capacity at axial-load ratios common in bridge applications, and may be suitable for use in the MDT design guide.

2. While the model used by the MDT design guide to predict/prevent concrete crushing is effective at predicting exterior crushing of the pile cap (which signifies the onset of ultimate failure), interior crushing occurs at a load significantly less than that predicted by the design guide. This interior crushing limit state results in a reduction in connection fixity and an increase in degradation under cyclic loading, both of which are undesirable in this application. This issue could be addressed by further reducing the allowed concrete compressive strengths (resulting in increased embedment depths) or by the inclusion of internal U-bars located near the tip of the embedded pile.
3. The longitudinal yielding limit state was well predicted by the MDT design guide; however, further review and revision of this provision may still be merited. This limit state is primarily addressed by the inclusion of additional longitudinal reinforcement in the pile cap, typically in the form of U-bars encircling the embedded pile. The design methodology sizes this additional steel based on the design moment, reduced by 75 percent. This reduction is empirically based on the limited set of test results from Stephens and McKittrick (2005), and was demonstrated to be sufficient in the specimens tested in the current study; however, this data set may not offer a robust evaluation of the efficacy of the design methodology across all possible cap configurations. To address this concern, it may be desirable to develop an analytical model that better describes the effect of the U-bar on this limit state, and reduce the reliance on empirical factors.
4. Splitting of the concrete cap was observed in all test specimens; however, it was not observed until after the other limit states were reached, indicating that the approach taken by the design guide (i.e., providing minimum transverse steel specified by AASHTO for plastic-hinge zones, and including U-bars) is sufficient at addressing this limit state. However, following this methodology, the amount of transverse reinforcement that is needed is not based on the specific design moment to be transferred through the connection, but rather simply on the connection geometry. While this limit state was not specifically studied in this or previous test series, sufficient data may now be available from these tests to begin developing an analytical model for splitting based on the moment demand and cap configuration. As with the longitudinal yielding limit state, this model would reduce reliance on empirical factors, and provide a more robust prediction for this limit state.

5. While the suggestions mentioned above are important for accurately predicting the limit states of this connection and ensuring efficient designs, the current design guide provisions appear to typically produce conservative designs across the limit states considered with respect to ultimate capacity. However, an incidental review of the design guide beyond just those provisions directly exercised in the test series revealed one aspect that appears to merit further review, in that it could yield unconservative results: the branching in the design process based on whether the design moment exceeds 60 percent of the plastic-moment capacity of the CFT. Following this provision, if the design moment is below this limit, no additional reinforcement is required immediately adjacent to the pile to ensure the integrity of the cap concrete in the connection zone. This branch is based on previous tests in which this limit was observed to be conservative. However, this provision is fundamentally based on the assumption that the dimensions and reinforcing of the cap proportionally increase with increased pile capacity, thus generally providing increased resistance to other limit states in the cap connection zone. However, possible bent configurations may fall outside of those typically encountered and outside those used in developing this provision. Thus, this fundamental assumption may not always be true, and this provision could yield an unconservative result in which the cap concrete in the connection zone is insufficient to carry the moment demand placed upon it. One manner to address this situation would be to remove this branch from the design methodology and to simply always calculate and provide some additional reinforcing in the form of U-bars.

Relative to the effect of cyclic loads on connection performance, the ultimate capacity of the cap was not significantly affected by whether the displacement at ultimate load was reached in a single monotonic stroke to failure, or if it was reached through a sequence of steps of increasing magnitude, with each step consisting of several cycles of fully reversed displacement at a constant amplitude. That being said, at relatively low loads in the cyclic tests, the response of the connection degraded across successive displacement cycles at each load step, as previously mentioned. This degradation consisted of softening of the force deformation response, and a loss of energy dissipation capacity in the connection. The onset of this degradation under cyclic loads was delayed considerably by adding a second set of U-bars encircling the tip of the embedded pile.

Developing a robust design methodology for any structural system is a serious undertaking that often involves several iterations of review and revision. The current MDT guide has started well down this path for designing CFT pile to concrete pile cap connections. As time and resources permit, further testing and analysis should be done

to further address the various issues identified in this project, as they have been summarized above.

9 WORKS CITED

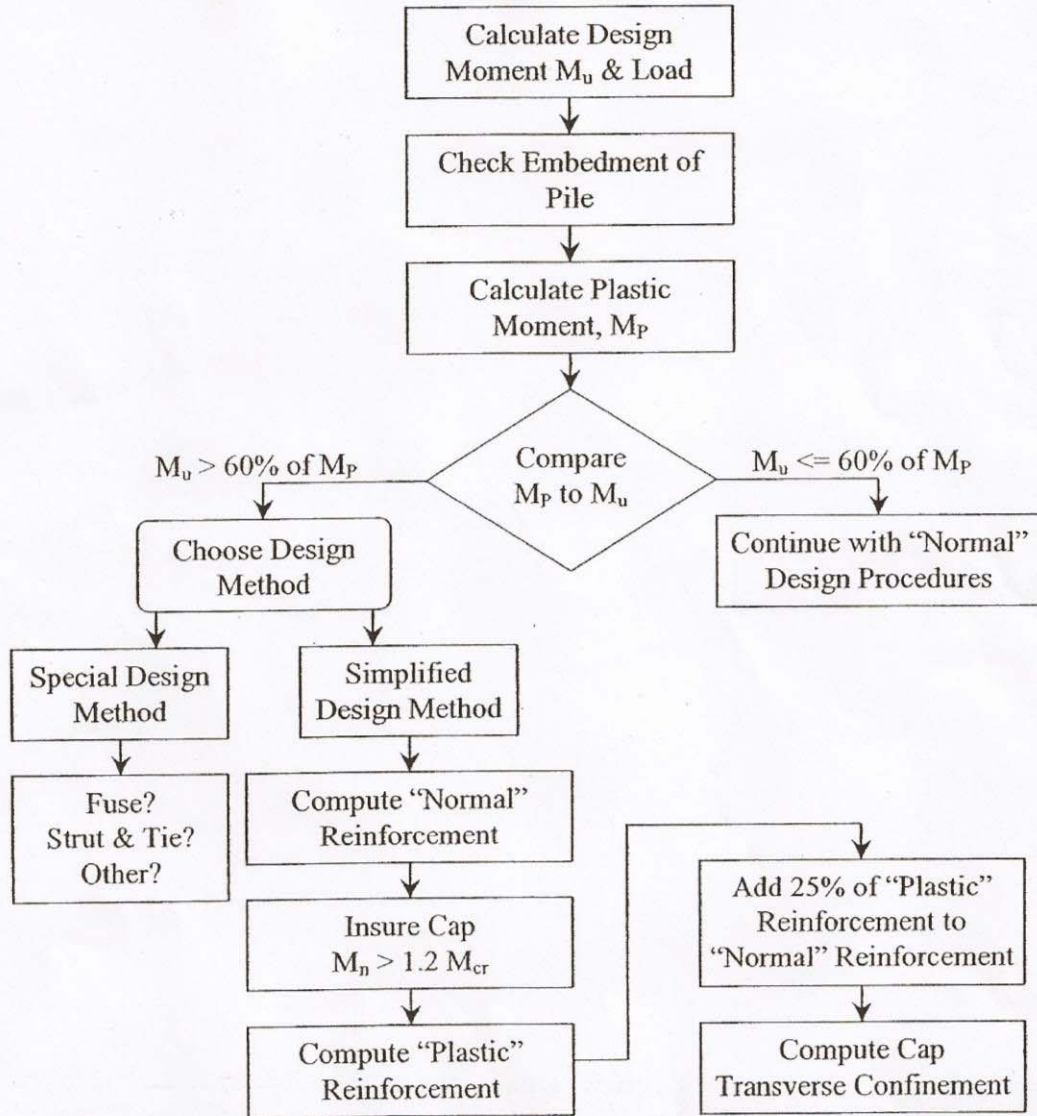
- AASHTO. *LRFD Bridge Design Specifications*. Washington, D.C.: American Association of State Highway and Transportation Officials, 2011.
- AISC. *Specifications For Structural Steel Buildings*. AISC, 2011.
- Bruneau, M., and J. Marson. "Seismic Design Of Concrete-Filled Circular Steel Bridge Piers." *Journal of Bridge Engineering*, 2004: 24-34.
- Gomez, Ivan, Amit Kanvinde, Chris Smith, and Gregory Deierlein. "Shear Transfer In Exposed Column Base Plates." 2009.
- Grauvilardell, Jorge E., Daeyong Lee, Jerome F. Hajjar, and Robert J. Dexter. "Synthesis Of Design, Testing And Analysis Research On Steel Column Base Plate Connections In High-Seismic Zones." Structural Engineering Report No. ST-04-02, Department of Civil Engineering, University of Minnesota, 2005.
- Kingsley, A. M. "Experimental And Analytical Investigation Of Embedded Column Base Connections For Concrete Filled High Strength Steel Tubes." Master's Thesis, University of Washington, 2005.
- MDT. *Pipe Pile To Concrete Cap Connection*. Design Guide, Helena: Montana Department of Transportation, 2005.
- Rollins, Kyle M, and Tony E Stenlund. *Laterally Loaded Pile Cap Connections (UT-10.16)*. Salt Lake City: Utah Department of Transportation, 2010.
- Silva, P. F., S. Sritharan, F. Seible, and M. N. Priestly. "Full-Scale Test Of The Alaska Cast-In-Place Steel Shell Three Column Bridge Bent." Technical Report, University of California, 1999.
- Stephens, J., and L. R. McKittrick. "Performance Of Steel Pipe Pile-To-Concrete Bent Cap Connections Subject To Seismic Or High Transverse Loading: Phase II." Civil Engineering, Montana State University, 2005.
- Wang, C. K., C. G. Salmon, and J. A. Pincheira. *Reinforced Concrete Design*. John Wiley & Sons, Inc, 2007.

APPENDIX B

MTD DESIGN GUIDE

APPENDIX A – MDT DESIGN GUIDE

Pipe Pile to Cap Connection Design



MSU Test PC4

Des. by: BLM Date: 2/25/2005

Page

Pipe Pile to Concrete Cap Connection

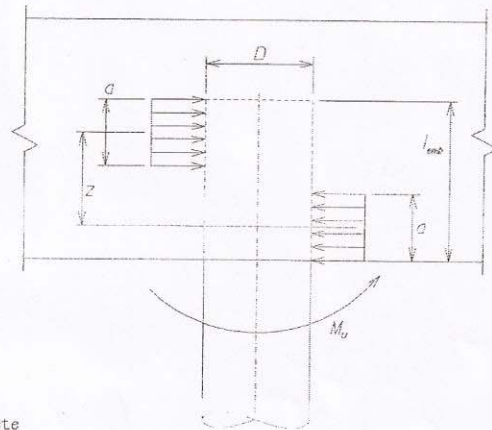
KN := 1000-newton

This design procedure is based on research results from Montana State University.

Reference: Performance of Steel Pipe Pile-to-Concrete Bent Cap Connections Subject to Seismic or High Transverse Loading: Phase II by J.E. Stephens and L.R. McKittrick of the Civil Engineering Dept. Montana State University - Bozeman. January 2005

STEP 1) Using Factored Pile Moment (M_u) determine minimum pile embedment.

Determin the minimum pile embedment to resist the pile moment with a force couple. The force couple is modeled using a Whitney Stress Block approximation.



Design Parameters

- $M_u := 121 \text{ft} \cdot \text{kip}$ Factored Moment at Pile Head
- $D := 8.625 \text{in}$ Outside Diameter of Pile
- $F_y := 53000 \text{psi}$ Pile Steel yield strength, ASTM A-252, Grade 2 (35 ksi)
- $l_{emb} := 9 \text{in}$ pile embedment
- $f_c := 4680 \text{psi}$ Concrete Cap Strength Class DD
- $\phi_b := 0.7$ LRFD 5.5.4.2 for bearing on concrete
- $t_p := 0.25 \text{in}$ Thickness of Pile wall

Calculate stress based on the Whitney Stress Block LRFD 5.7.2.2.

$$\beta_1 := \begin{cases} 0.85 & \text{if } f_c \leq 28 \text{ MPa} \\ 0.85 - \frac{f_c - 28 \text{ MPa}}{7 \text{ MPa}} \cdot 0.05 & \text{if } 28 \text{ MPa} < f_c \leq 56 \text{ MPa} \\ 0.65 & \text{otherwise} \end{cases} \quad \beta_1 = 0.82$$

$$a := \beta_1 \frac{l_{emb}}{2} \quad \text{Whitney stress block depth} \quad a = 94 \text{ mm}$$

$$z := l_{emb} - a \quad \text{Moment arm between stress blocks} \quad z = 135 \text{ mm}$$

$$f_u := \left(\frac{M_u}{a \cdot D \cdot z} \right) \quad M_u \text{ is divided by the plastic section} \quad f_u = 59.2 \text{ MPa}$$

Use a maximum concrete stress of $1.8f_c$ based on the Research by Montana State University; pp. 79, 82.

$$f_n := 1.8 \cdot f_c$$

$f_u \approx f_n$
OK for MSU test
Use ϕ_b for design

$\phi_b \cdot f_n = 40.7 \text{ MPa}$
 $f_n = 58 \text{ MPa}$
check $\phi_b \cdot f_n > f_u$?

Des. by: _____ Date: 2/25/2005

Page

Step 2) Compare Factored Pile Moment (M_u) to the Pile Plastic Moment Capacity (M_p).

These calculations assume that a concrete-filled pipe pile is a compact section.

$$Z := \frac{D^3}{6} - \frac{(D - 2 \cdot t_p)^3}{6} \quad \text{AISC 9th edition, pg 6-20}$$

$$Z = 287 \text{ cm}^3$$

$$M_n := F_y \cdot Z \quad (\text{eq for a compact section})$$

$$M_n = 105 \text{ m} \cdot \text{kN}$$

$$M_p := 1.25 \cdot M_n \quad \text{Steel overstrength factor Division 1A, 7.2.2(A)}$$

$$M_p = 96.8 \text{ ft} \cdot \text{kip}$$

$$M_u = 121 \text{ ft} \cdot \text{kip}$$

$$0.6 \cdot M_p = 58.1 \text{ ft} \cdot \text{kip}$$

check $M_u > 0.6 \cdot M_p$

Actual plastic moment measured from MSU Test

$M_p = 96 \text{ ft} \cdot \text{k}$
calculated by MSU

Step 3) For $M_u > 0.6M_p$, Include additional cap reinforcement

Research at MSU indicates pile embedment without additional reinforcement in the cap is sufficient for pile moments $M_u < 0.75 M_p$. For Pile moments $M_u > 0.6 M_p$, include additional confinement to insure adequate connection strength.

Provide Minimum Cap Flexural Reinforcement to insure $M_n > 1.2M_{cr}$. Where M_n is the nominal strength of the cap and M_{cr} is the cracking moment.

Additional longitudinal Cap Reinforcement:

Based on the research results from MSU, reinforcement in the cap is required to balance compressive forces of the pile/cap moment transfer. Note: deeper pile embedments reduce the required cap reinforcement in the following equations.

Design Parameters

$$f_y := 60000 \text{ psi} \quad \text{Reinforcing steel in cap}$$

$$s := 1.77 \text{ in} \quad \text{spacing of hoops, not exceeding 100 mm see LRFD 5.10.11.4.1d}$$

$$h := 18 \text{ in} \quad \text{depth of cap}$$

$$w := 18 \text{ in} \quad \text{width of cap}$$

$$h_c := 16 \text{ in} \quad \text{depth of cap minus cover}$$

$$w_c := 16 \text{ in} \quad \text{width of cap minus cover}$$

$$A_g := h \cdot w \quad \text{gross area of cap}$$

$$A_g = 0.21 \text{ m}^2$$

$$A_c := h_c \cdot w_c \quad \text{core dimension of cap. Cap width minus cover}$$

$$A_c = 0.17 \text{ m}^2$$

$$\phi_f := 0.9 \quad \text{LRFD 5.5.4.2 for tension of reinforced concrete}$$

Based on the Whitney stress block model tensile reinforcement in the bottom zone of the cap ($l_{emb}/2$) is required to transfer compression across pile. Add additional reinforcement in this zone. MSU research indicates U bars placed around the pile near the bottom mat of reinforcement are effective. Extending straight bars through the pile may also be effective in meeting this requirement. Develop additional U bars and straight bars $h/2$ beyond the face of the pile.

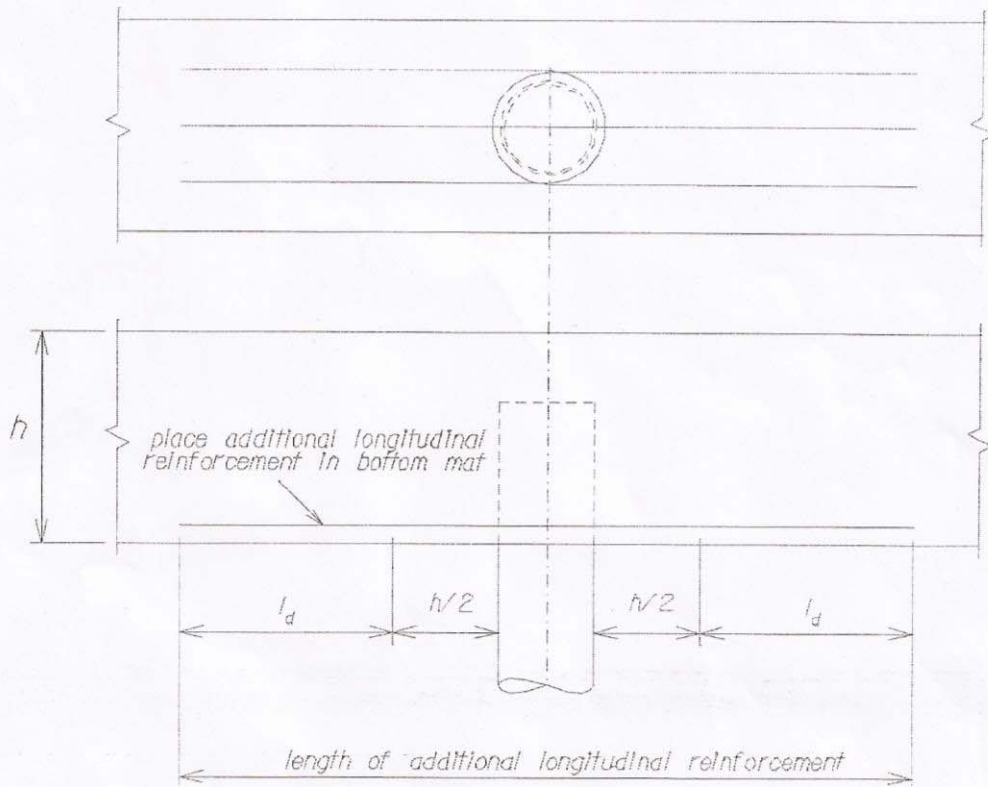
$$A_s := \frac{M_u}{\phi_f \cdot z \cdot f_y}$$

$$A_s = 3266 \text{ mm}^2$$

Provide additional longitudinal reinforcement equivalent to 25% of calculated A_s .

$$.25 \cdot A_s = 816 \text{ mm}^2$$

$$.25 \cdot A_s = 1.27 \text{ in}^2 \rightarrow \text{MSU test } \geq \#7 \text{ Bars } A_s = 1.2 \text{ in}^2 \text{ (U Bar)}$$



Des. by: _____ Date: 2/25/2005

Page

Cap Transverse Confinement:

Based on the research results from MSU, provide transverse confinement in cap. This confinement zone is located from the pile face to half the cap depth from the pile. This applies to interior bays only.

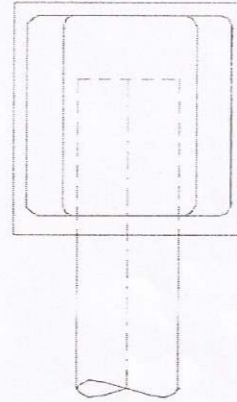
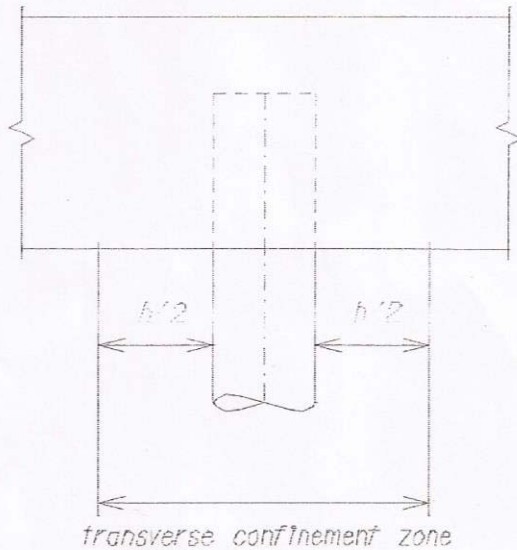
Ensure total amount of transverse reinforcement in the cap confinement zone satisfies the following equation.

$$A_{sh} := \begin{bmatrix} 0.3 \cdot s \cdot w_c \cdot \frac{P_c}{f_y} \cdot \left(\frac{A_g}{A_c} - 1 \right) \\ 0.12 \cdot s \cdot w_c \cdot \frac{P_c}{f_y} \end{bmatrix}$$

LRFD eqn 5.10.11.4.1d

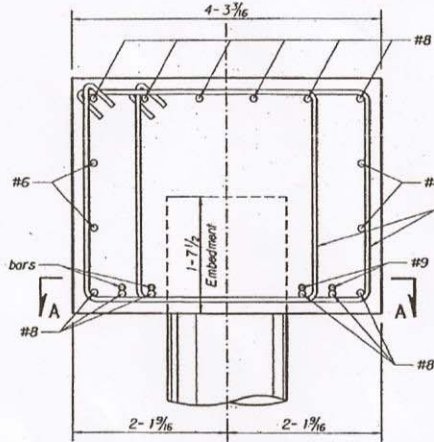
$$A_{sh} = \begin{pmatrix} 114 \\ 171 \end{pmatrix} \text{mm}^2$$

$$A_{sh} = \begin{pmatrix} 0.18 \\ 0.27 \end{pmatrix} \text{in}^2$$

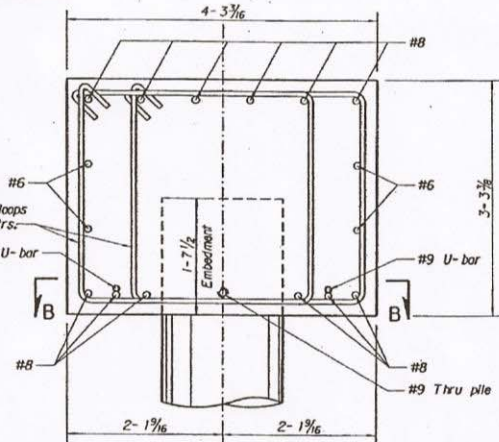


MSU test 2#3 bars @ 1.77in
 $A_s = .22 \text{in}^2$

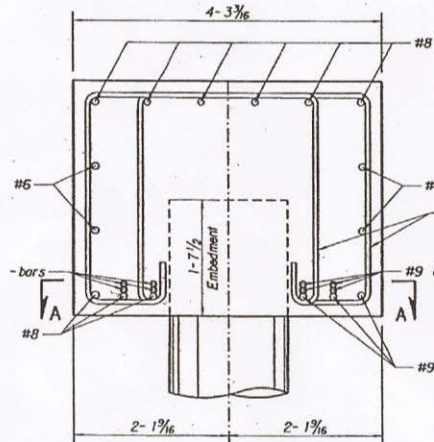
NOTE: The two options allow flexibility in providing the required additional longitudinal reinforcement. The choice is left to designers discretion.



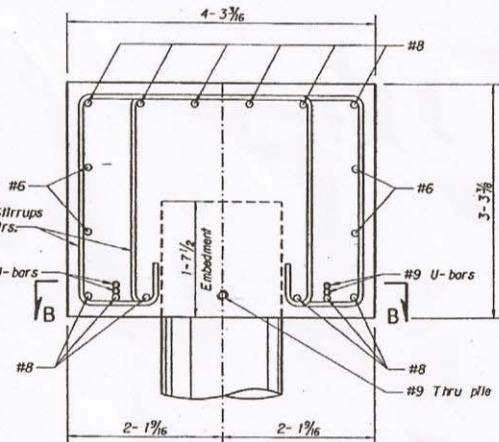
SECTION C-C
OPTION 1
Scale - 1" = 1'-0"



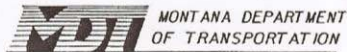
SECTION E-E
OPTION 2
Scale - 1" = 1'-0"



SECTION D-D
OPTION 1
Scale - 1" = 1'-0"

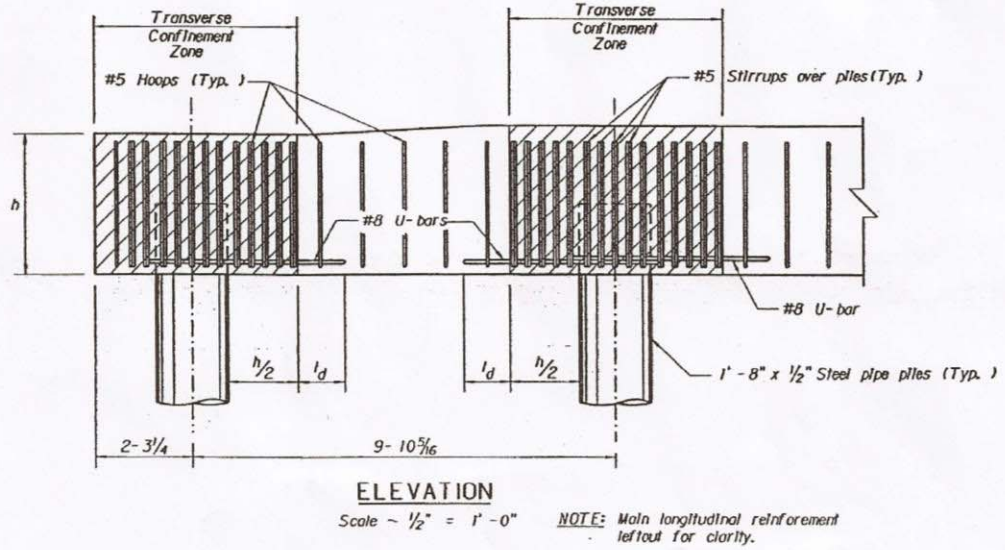
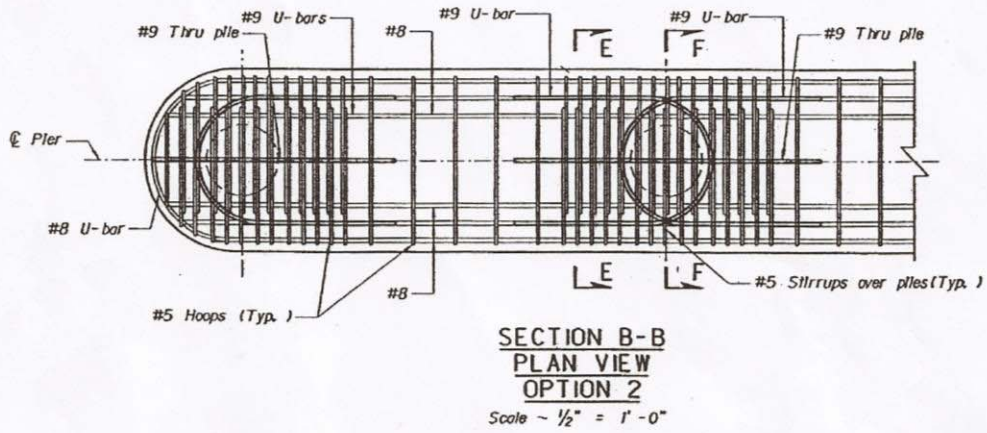
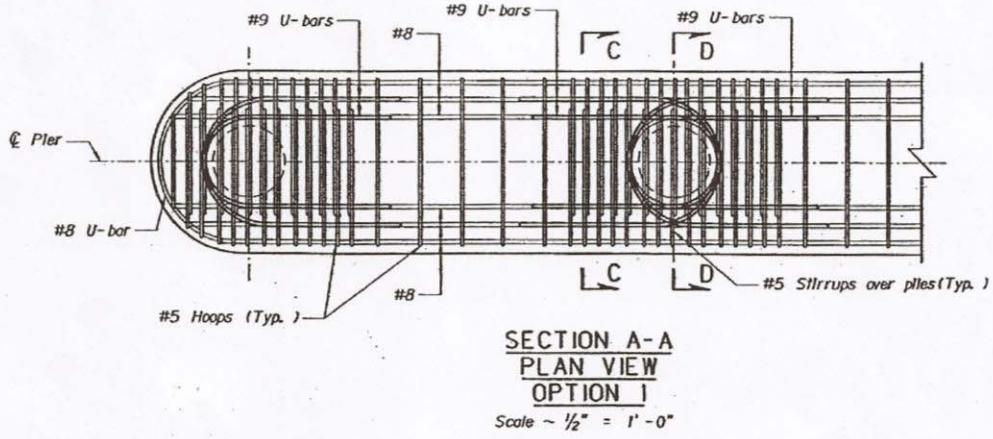


SECTION F-F
OPTION 2
Scale - 1" = 1'-0"



MONTANA DEPARTMENT
OF TRANSPORTATION

PILE CAP REINFORCEMENT
BASED ON
DESIGN EXAMPLE SAGER LANE - DEER LODGE



APPENDIX B – TEST SPECIMEN DESIGN CALCULATIONS

B.1 DESIGN OVERVIEW

Table 7 and Table 8 show summaries of the design parameters for the monotonic testing and the cycle testing, respectively. The actual calculations for each are shown in the following sections. Note that CT1 and CT2 are based on the same configuration and calculations completed for VT2.

Table 7: Summary of design parameters - monotonic tests

Verification Test:		VT1	VT2	VT2.5	VT3
Concrete Crushing and Pile Embedment Requirements	Concrete Compression Strength	Design: $f'c = 4$ ksi Actual: $f'c = 6.25$ ksi	Design = Actual: $f'c = 4$ ksi	Design = Actual: $f'c = 6.25$ ksi	Design = Actual: $f'c = 4$ ksi
	$\Phi_b = 0.7$ Applied?	No	Yes	Yes	No
	Design Moment Source	M_p of Pile	~25% increase of VT1	Same as VT1	Set from desired embedment length
	Design Moment	96.8 ft-kip	122.0 ft-kip	96.8 ft-kip	136.1 ft-kip
	Pile Wall Thickness	$t_p = 0.25$ in	$t_p = 0.50$ in (over-sized to ensure failure in cap)		
	Calculated M_p of Pile (MDT Design Guide Method)	$M_p = 96.8$ ft-kip	$M_p = 182.5$ ft-kip (oversized to ensure failure in cap)		
	Embedment	$L_{emb} = 9.0$ in	$L_{emb} = 11.75$ in	$L_{emb} = 9.0$ in	$L_{emb} = 10.375$ in
	Moment Arm	$z = 5.175$ in	$z = 6.756$ in	$z = 5.681$ in	$z = 5.966$ in
	Concrete Confinement Factor	$\alpha = 1.8$			
	Crushing Capacity: $\Phi_b \times f_n$	$1 \times f_n = 7.2$ ksi	$0.7 \times f_n = 5.0$ ksi	$0.7 \times f_n = 7.9$ ksi	$1 \times f_n = 7.2$ ksi
	Crushing Demand	$f_u = 6.8$ ksi	$f_u = 5.0$ ksi	$f_u = 7.1$ ksi	$f_u = 7.2$ ksi
Minimum Steel Requirements	Cracking Moment	$M_{cr} = 58.9$ ft-kip ($1.2 \times M_{cr} = 70.7$ ft-kip)			
	Minimum Required Steel based on $1.2 \times M_{cr}$	$A_{s_min} = 0.887$ in ²			
	Reinforcement Implemented for Cracking	2 #4s and 2 #5s $\rightarrow A_{s_min} = 1.0$ in ²			
Additional Steel Requirements	$\Phi_f = 0.9$ Applied?	Yes			No
	Additional Steel Required	$A_{s_Add} = 1.040$ in ²	$A_{s_Add} = 1.002$ in ²	$A_{s_Add} = 0.947$ in ²	$A_{s_Add} = 1.141$ in ²
	Additional Steel Description	1 #7 U-bar in each direction	1 #4 and 1 #5 in each direction	1 #7 U-bar in each direction	1 #7 U-bar in each direction
	Area of Additional Steel Implemented (U-bars)	$A_{s_Add} = 1.203$ in ²	$A_{s_Add} = 1.006$ in ²	$A_{s_Add} = 1.203$ in ²	$A_{s_Add} = 1.203$ in ²
Transverse Steel Requirements	Transverse Steel Required	$A_{s_trans} = 0.22$ in ²			
	Spacing of Transverse Steel	$s = 1.75$ in			
	Reinforcement Implemented for Transverse	#3 stirrups @ 1.75 in $\rightarrow A_{s_trans} = 0.22$ in ²			
Verification Test:		VT1	VT2	VT2.5	VT3

Table 8: Summary of design parameters – cyclic tests

Cycle Test:		CT1	CT2
Concrete Crushing and Pile Embedment Requirements	Concrete Compression Strength	Design = Actual: $f'_c = 4$ ksi	
	$\Phi_b = 0.7$ Applied?	Yes	
	Design Moment Source	~25% increase of VT1	
	Design Moment	122.0 ft-kip	
	Pile Wall Thickness	$t_p = 0.75$ in	
	Calculated M_p of Pile (MDT Design Guide Method)	$M_p > 182.5$ ft-kip (oversized to ensure failure in cap)	
	Embedment	$L_{emb} = 11.75$ in	
	Moment Arm	$z = 6.76$ in	$z = 6.75$ in
	Concrete Confinement Factor	$\alpha = 1.8$	
	Crushing Capacity: $\Phi_b \times f_n$	$0.7 \times f_n = 5.0$ ksi	
	Crushing Demand	$f_u = 5.0$ ksi	
Minimum Steel Requirements	Cracking Moment	$M_{cr} = 58.9$ ft-kip ($1.2 \times M_{cr} = 70.7$ ft-kip)	
	Minimum Required Steel based on $1.2 \times M_{cr}$	$A_{s_min} = 0.887$ in ²	
	Reinforcement Implemented for Cracking	2 #4s and 2 #5s $\rightarrow A_{s_min} = 1.0$ in ²	
Additional Steel Requirements	$\Phi_f = 0.9$ Applied?	Yes	
	Additional Steel Required	$A_{s_Add} = 1.002$ in ²	
	U-bar Steel Description	1 #4 and 1 #5 in each direction (double stacked)	
	U-bar Locations	Exterior Only	Interior and Exterior
	Area of Additional Steel Implemented (U-bars)	$A_{s_Add} = 1.006$ in ²	$A_{s_Add} = 2.012$ in ²
Transverse Steel Requ.	Transverse Steel Required	Same Confiruation as VT2	
	Reinforcement Implemented for Transverse	#3 stirrups @ 1.75 in $\rightarrow A_{s_trans} = 0.22$ in ²	
Cycle Test:		CT1	CT2

B.2 VT1 DESIGN CALCULATIONS

Pipe Pile to Cap (MDT) Design Method For VT1 :

Define overall design parameters

$D := 8.625\text{in}$	Outside diameter of pile
$F_y := 53000\text{psi}$	Pile steel yield strength, ASTM A-252, Grade 2 (35ksi)
$L_{\text{emb}} := 9.0\text{in}$	Nominal pile embedment length
$f_c := 4000\text{psi}$	Concrete cap strength - Class DD
$\phi_b := 1.0$	LRFD 5.5.4.2 for bearing on concrete
$t_p := 0.25\text{in}$	Thickness of pile wall
$\alpha := 1.8$	Factor for f_c constant in relation to how much steel confinement is in place

Step 1) Calculate the plastic moment capacity of the pile, M_p

$$Z := \frac{D^3}{6} - \frac{(D - 2 \cdot t_p)^3}{6} \quad Z = 17.54 \cdot \text{in}^3$$

$$M_{\text{npile}} := F_y \cdot Z \quad M_{\text{npile}} = 77.5 \cdot \text{ft} \cdot \text{kip}$$

$$M_p := 1.25 \cdot M_{\text{npile}} \quad \text{Apply MDT overstrength factor of 1.25} \quad M_p = 96.8 \cdot \text{ft} \cdot \text{kip}$$

Steps 2 and 3) Calculation of stress based on the Whitney Stress Block LRFD 5.7.2.2

$$\beta_1 := \begin{cases} 0.85 & \text{if } f_c \leq 4000\text{psi} \\ \left[0.85 - \frac{(f_c - 4000\text{psi})}{1000\text{psi}} \cdot 0.05 \right] & \text{if } 4000\text{psi} < f_c \leq 8000\text{psi} \\ 0.65 & \text{otherwise} \end{cases} \quad \beta_1 = 0.85$$

$$x := \frac{L_{\text{emb}}}{2} \quad x = 4.5 \cdot \text{in}$$

$$a := \beta_1 \cdot x \quad a = 3.825 \cdot \text{in}$$

$$z := L_{\text{emb}} - a \quad z = 5.175 \cdot \text{in}$$

Check the assumption of the alpha variable and embedment length:

$$f_n := \phi_b \cdot \alpha \cdot f_c \quad f_n = 7.200 \cdot \text{ksi}$$

$M_p = 96.837 \cdot \text{ft} \cdot \text{kip}$ From plastic moment calculation Therefore f_u is less than f_n for this case suggesting a suitable L_{emb} for the assumed α value.

$$f_u := \frac{M_p}{a \cdot D \cdot z} \quad f_u = 6.806 \cdot \text{ksi}$$

Step 4) Calculate the minimum cap flexural rein. to insure $M_n > 1.2 M_{cr}$ per the MDT design guide

Design Parameters:

$f_y := 60000\text{psi}$	Reinforcing steel in cap
cover := 1in	Desired amount of cover for reinforcement
h := 18in	Depth of cap
w := 18in	Width of cap
d := 16.376in	Distance from top of beam to steel in tension
$f_c := 4000\text{psi}$	Concrete Cap Strength
$\phi_f := 0.9$	Factor for flexure in concrete

Calculate the cracking moment, M_{cr} :

$$M_{cr} := \frac{11.5 \cdot \sqrt{1\text{psi}} \cdot \sqrt{f_c} \cdot w \cdot h^2}{6} \quad M_{cr} = 58.913\text{-ft}\cdot\text{kip}$$

Use a solve block to determine the minimum required area of reinforcing steel:

Guess a value for A_s : $A_s := 0.6\text{in}^2$

Given

$$1.2 \cdot M_{cr} = A_s \cdot f_y \cdot \left(d - 0.59 \cdot \frac{A_s \cdot f_y}{f_c \cdot w} \right)$$

$$A_{s\text{min}} := \text{Find}(A_s)$$

$$A_{s\text{min}} = 0.887\text{-in}^2$$

$$A_{s2\text{num}4\text{bars}} := 2 \cdot \frac{\pi}{4} \cdot \left(\frac{4}{8}\text{in} \right)^2$$

$$A_{s2\text{num}4\text{bars}} = 0.393\text{-in}^2$$

$$A_{s2\text{num}5\text{bars}} := 2 \cdot \frac{\pi}{4} \cdot \left(\frac{5}{8}\text{in} \right)^2$$

$$A_{s2\text{num}5\text{bars}} = 0.614\text{-in}^2$$

$$A_{s\text{Total}} := A_{s2\text{num}4\text{bars}} + A_{s2\text{num}5\text{bars}}$$

$$A_{s\text{Total}} = 1.006\text{-in}^2$$

Therefore, use two #4 bars and two #5 bars in the top and bottom of the cap to provide minimal reinforcement.

Step 5) Calculate the additional longitudinal and transverse rein. in the cap per the MDT design guide

If $M_u > 0.6 \cdot M_p$, then include additional cap reinforcement as specified by the MDT design guide:

Design Parameters:

$f_y := 60000 \text{psi}$	Reinforcing steel in cap
$h := 18 \text{in}$	Depth of cap
$h_c := 16 \text{in}$	Depth of cap minus the cover
$w := 18 \text{in}$	Width of cap
$w_c := 16 \text{in}$	Width of cap minus the cover
$\phi_f := 0.9$	
$A_g := h \cdot w$	Gross area of the cap
$A_c := h_c \cdot w_c$	Core area of the cap

Calculate the additional longitudinal reinforcement required based on the Whitney Stress Blocks:

$$A_s := \frac{M_p}{\phi_f \cdot (L_{\text{emb}} - a) \cdot f_y} \quad A_s = 4.158 \cdot \text{in}^2$$

Provide additional longitudinal reinforcement equivalent to 25% of calculated per the MDT specification:

$$0.25 \cdot A_s = 1.04 \cdot \text{in}^2 \quad \text{Amount of steel to add for additional steel in longitudinal direction.}$$

$$A_{2\text{num7bars}} := 2 \cdot \frac{\pi}{4} \left(\frac{7}{8} \text{in} \right)^2 \quad A_{2\text{num7bars}} = 1.203 \cdot \text{in}^2$$

Therefore, one additional #7 Ubars satisfies the additional reinforcement requirement

Step 6) Now calculate the cap transverse confinement:

This confinement zone is located from the pile face to half the cap depth from the pile. This applies to interior bays only.

Ensure the total amount of transverse reinforcement in the cap refinement zone satisfies the following equation:

Guess Values:

$$s_h := 1.75 \text{in} \quad A_{\text{sh_trial}} := 0.20 \text{in}^2 \cdot \begin{pmatrix} 1 \\ 1 \end{pmatrix}$$

Given

$$A_{\text{sh_trial}} = \left[\begin{array}{l} 0.3 \cdot s_h \cdot w_c \cdot \frac{f_c}{f_y} \cdot \left(\frac{A_g}{A_c} - 1 \right) \\ 0.12 \cdot s_h \cdot w_c \cdot \frac{f_c}{f_y} \end{array} \right] \quad \text{LRFD equ 5.10.11.4.1d}$$

$$A_{\text{sh}} := \text{Find}(A_{\text{sh_trial}}) \quad A_{\text{sh}} = \begin{pmatrix} 0.15 \\ 0.22 \end{pmatrix} \cdot \text{in}^2 \quad s_h = 1.75 \cdot \text{in}$$

$A_{2\text{num3bars}} := 0.22 \text{in}^2$ Therefore, two number 3 bars placed at 1.75in apart as specified by the MDT design guide.

B.3 VT2 DESIGN CALCULATIONS

Pipe Pile to Cap (MDT) Design Method For VT2b:

Define overall design parameters

$D := 8.625\text{in}$	Outside diameter of pile
$F_y := 53000\text{psi}$	Pile steel yield strength, ASTM A-252, Grade 2 (35ksi)
$L_{\text{emb}} := 11.75\text{in}$	Nominal pile embedment length
$f'_c := 4000\text{psi}$	Concrete cap strength - Class DD
$\phi_b := 0.7$	LRFD 5.5.4.2 for bearing on concrete
$t_p := 0.32\text{in}$	Thickness of pile wall
$\alpha := 1.8$	Factor for f'_c constant in relation to how much steel confinement is in place

Step 1) Calculate the plastic moment capacity of the pile, M_p

$$Z := \frac{D^3}{6} - \frac{(D - 2 \cdot t_p)^3}{6} \quad Z = 22.082 \cdot \text{in}^3$$

$$M_{\text{npile}} := F_y \cdot Z \quad M_{\text{npile}} = 97.5 \cdot \text{ft} \cdot \text{kip}$$

$$M_p := 1.25 \cdot M_{\text{npile}} \quad \text{Apply MDT overstrength factor of 1.25} \quad M_p = 121.9 \cdot \text{ft} \cdot \text{kip}$$

Steps 2 and 3) Calculation of stress based on the Whitney Stress Block LRFD 5.7.2.2

$$\beta_1 := \begin{cases} 0.85 & \text{if } f'_c \leq 4000\text{psi} \\ \left[0.85 - \frac{(f'_c - 4000\text{psi})}{1000\text{psi}} \cdot 0.05 \right] & \text{if } 4000\text{psi} < f'_c \leq 8000\text{psi} \\ 0.65 & \text{otherwise} \end{cases} \quad \beta_1 = 0.85$$

$$x := \frac{L_{\text{emb}}}{2} \quad x = 5.875 \cdot \text{in}$$

$$a := \beta_1 \cdot x \quad a = 4.994 \cdot \text{in}$$

$$z := L_{\text{emb}} - a \quad z = 6.756 \cdot \text{in}$$

Check the assumption of the alpha variable and embedment length:

$$f_n := \phi_b \cdot \alpha \cdot f'_c \quad f_n = 5.040 \cdot \text{ksi}$$

$M_p = 121.913 \cdot \text{ft} \cdot \text{kip}$ From plastic moment calculation

$$f_u := \frac{M_p}{a \cdot D \cdot z} \quad f_u = 5.027 \cdot \text{ksi}$$

Therefore f_u is less than f_n for this case suggesting a suitable L_{emb} for the assumed α value.

Step 4) Calculate the minimum cap flexural rein. to insure $M_n > 1.2 M_{cr}$ per the MDT design guide

Design Parameters:

$f_y := 60000\text{psi}$	Reinforcing steel in cap
cover := 1in	Desired amount of cover for reinforcement
$h := 18\text{in}$	Depth of cap
$w := 18\text{in}$	Width of cap
$d := 16.376\text{in}$	Distance from top of beam to steel in tension
$f_c := 4000\text{psi}$	Concrete Cap Strength
$\phi_f := 0.9$	Factor for flexure in concrete

Calculate the cracking moment, M_{cr} :

$$M_{cr} := \frac{11.5 \cdot \sqrt{1\text{psi}} \cdot \sqrt{f_c} \cdot w \cdot h^2}{6} \quad M_{cr} = 58.913 \cdot \text{ft} \cdot \text{kip}$$

Use a solve block to determine the minimum required area of reinforcing steel:

Guess a value for A_s : $A_s := 0.6\text{in}^2$

Given

$$1.2 \cdot M_{cr} = A_s \cdot f_y \cdot \left(d - 0.59 \cdot \frac{A_s \cdot f_y}{f_c \cdot w} \right)$$

$$A_{s\text{min}} := \text{Find}(A_s)$$

$$A_{s\text{min}} = 0.887 \cdot \text{in}^2$$

$$A_{s2\text{num}4\text{bars}} := 2 \cdot \frac{\pi}{4} \cdot \left(\frac{4}{8} \text{in} \right)^2$$

$$A_{s2\text{num}4\text{bars}} = 0.393 \cdot \text{in}^2$$

$$A_{s2\text{num}5\text{bars}} := 2 \cdot \frac{\pi}{4} \cdot \left(\frac{5}{8} \text{in} \right)^2$$

$$A_{s2\text{num}5\text{bars}} = 0.614 \cdot \text{in}^2$$

$$A_{s\text{Total}} := A_{s2\text{num}4\text{bars}} + A_{s2\text{num}5\text{bars}}$$

$$A_{s\text{Total}} = 1.006 \cdot \text{in}^2$$

Therefore, use two #4 bars and two #5 bars in the top and bottom of the cap to provide minimal reinforcement.

Step 5) Calculate the additional longitudinal and transverse rein. in the cap per the MDT design guide

If $M_u > 0.6 \cdot M_p$, then include additional cap reinforcement as specified by the MDT design guide:

Design Parameters:

$f_y := 60000 \text{ psi}$	Reinforcing steel in cap
$h := 18 \text{ in}$	Depth of cap
$h_c := 16 \text{ in}$	Depth of cap minus the cover
$w := 18 \text{ in}$	Width of cap
$w_c := 16 \text{ in}$	Width of cap minus the cover
$\phi_f := 0.9$	
$A_g := h \cdot w$	Gross area of the cap
$A_c := h_c \cdot w_c$	Core area of the cap

Calculate the additional longitudinal reinforcement required based on the Whitney Stress Blocks:

$$A_s := \frac{M_p}{\phi_f \cdot (L_{\text{emb}} - a) \cdot f_y} \quad A_s = 4.01 \cdot \text{in}^2$$

Provide additional longitudinal reinforcement equivalent to 25% of calculated per the MDT specification:

$$0.25 \cdot A_s = 1.002 \cdot \text{in}^2 \quad \text{Amount of steel to add for additional steel in longitudinal direction.}$$

Recall from above:

$$A_{s2\text{num}4\text{bars}} + A_{s2\text{num}5\text{bars}} = 1.006 \text{ in}^2$$

Therefore, one additional #4 and #5 Ubar satisfies the additional reinforcement requirement

Step 6) Now calculate the cap transverse confinement:

This confinement zone is located from the pile face to half the cap depth from the pile. This applies to interior bays only.

Ensure the total amount of transverse reinforcement in the cap refinement zone satisfies the following equation:

Guess Values:

$$s_h := 1.75 \text{ in} \quad A_{sh_trial} := 0.20 \text{ in}^2 \cdot \begin{pmatrix} 1 \\ 1 \end{pmatrix}$$

Given

$$A_{sh_trial} = \left[\begin{array}{l} 0.3 \cdot s_h \cdot w_c \cdot \frac{f_c}{f_y} \cdot \left(\frac{A_g}{A_c} - 1 \right) \\ 0.12 \cdot s_h \cdot w_c \cdot \frac{f_c}{f_y} \end{array} \right] \quad \text{LRFD equ 5.10.11.4.1d}$$

$$A_{sh} := \text{Find}(A_{sh_trial}) \quad A_{sh} = \begin{pmatrix} 0.15 \\ 0.22 \end{pmatrix} \cdot \text{in}^2 \quad s_h = 1.75 \cdot \text{in}$$

$A_{2\text{num}3\text{bars}} := 0.22 \text{ in}^2$ Therefore, two number 3 bars placed at 1.75in apart as specified by the MDT design guide.

B.4 VT2.5 DESIGN CALCULATIONS

Pipe Pile to Cap (MDT) Design Method For VT2.5:

Define overall design parameters

$D := 8.625\text{in}$	Outside diameter of pile
$F_y := 53000\text{psi}$	Pile steel yield strength, ASTM A-252, Grade 2 (35ksi)
$L_{\text{emb}} := 9.0\text{in}$	Nominal pile embedment length
$f'_c := 6250\text{psi}$	Concrete cap strength - Class DD
$\phi_b := 0.7$	LRFD 5.5.4.2 for bearing on concrete
$t_p := 0.25\text{in}$	Thickness of pile wall
$\alpha := 1.8$	Factor for f'_c constant in relation to how much steel confinement is in place

Step 1) Calculate the plastic moment capacity of the pile, M_p

$$Z := \frac{D^3}{6} - \frac{(D - 2 \cdot t_p)^3}{6} \quad Z = 17.54 \cdot \text{in}^3$$

$$M_{\text{npile}} := F_y \cdot Z \quad M_{\text{npile}} = 77.5 \cdot \text{ft} \cdot \text{kip}$$

$$M_p := 1.25 \cdot M_{\text{npile}} \quad \text{Apply MDT overstrength factor of 1.25} \quad M_p = 96.8 \cdot \text{ft} \cdot \text{kip}$$

Steps 2 and 3) Calculation of stress based on the Whitney Stress Block LRFD 5.7.2.2

$$\beta_1 := \begin{cases} 0.85 & \text{if } f'_c \leq 4000\text{psi} \\ \left[0.85 - \frac{(f'_c - 4000\text{psi})}{1000\text{psi}} \cdot 0.05 \right] & \text{if } 4000\text{psi} < f'_c \leq 8000\text{psi} \\ 0.65 & \text{otherwise} \end{cases} \quad \beta_1 = 0.737$$

$$x := \frac{L_{\text{emb}}}{2} \quad x = 4.5 \cdot \text{in}$$

$$a := \beta_1 \cdot x \quad a = 3.319 \cdot \text{in}$$

$$z := L_{\text{emb}} - a \quad z = 5.681 \cdot \text{in}$$

Check the assumption of the alpha variable and embedment length:

$$f_n := \phi_b \cdot \alpha \cdot f'_c \quad f_n = 7.875 \cdot \text{ksi}$$

$$M_p = 96.837 \cdot \text{ft} \cdot \text{kip} \quad \text{From plastic moment calculation} \quad \text{Therefore } f_u \text{ is less than } f_n \text{ for this case suggesting a suitable } L_{\text{emb}} \text{ for the assumed } \alpha \text{ value.}$$

$$f_u := \frac{M_p}{a \cdot D \cdot z} \quad f_u = 7.146 \cdot \text{ksi}$$

Step 4) Calculate the minimum cap flexural rein. to insure $M_n > 1.2 M_{cr}$ per the MDT design guide

Design Parameters:

$f_y := 60000\text{psi}$	Reinforcing steel in cap
$\text{cover} := 1\text{in}$	Desired amount of cover for reinforcement
$h := 18\text{in}$	Depth of cap
$w := 18\text{in}$	Width of cap
$d := 16.376\text{in}$	Distance from top of beam to steel in tension
$f'_c := 4000\text{psi}$	Concrete Cap Strength
$\phi_f := 0.9$	Factor for flexure in concrete

Calculate the cracking moment, M_{cr} :

$$M_{cr} := \frac{11.5 \cdot \sqrt{1\text{psi}} \cdot \sqrt{f'_c} \cdot w \cdot h^2}{6} \quad M_{cr} = 58.913 \cdot \text{ft} \cdot \text{kip}$$

Use a solve block to determine the minimum required area of reinforcing steel:

Guess a value for A_s : $A_s := 0.6\text{in}^2$

Given

$$1.2 \cdot M_{cr} = A_s \cdot f_y \cdot \left(d - 0.59 \cdot \frac{A_s \cdot f_y}{f'_c \cdot w} \right)$$

$$A_{s\text{min}} := \text{Find}(A_s)$$

$$A_{s\text{min}} = 0.887 \cdot \text{in}^2$$

$$A_{s2\text{num}4\text{bars}} := 2 \cdot \frac{\pi}{4} \cdot \left(\frac{4}{8} \text{in} \right)^2$$

$$A_{s2\text{num}4\text{bars}} = 0.393 \cdot \text{in}^2$$

$$A_{s2\text{num}5\text{bars}} := 2 \cdot \frac{\pi}{4} \cdot \left(\frac{5}{8} \text{in} \right)^2$$

$$A_{s2\text{num}5\text{bars}} = 0.614 \cdot \text{in}^2$$

$$A_{s\text{Total}} := A_{s2\text{num}4\text{bars}} + A_{s2\text{num}5\text{bars}}$$

$$A_{s\text{Total}} = 1.006 \cdot \text{in}^2$$

Therefore, use two #4 bars and two #5 bars in the top and bottom of the cap to provide minimal reinforcement.

Step 5) Calculate the additional longitudinal and transverse rein. in the cap per the MDT design guide

If $M_u > 0.6 \cdot M_p$, then include additional cap reinforcement as specified by the MDT design guide:

Design Parameters:

- $f_y := 60000 \text{psi}$ Reinforcing steel in cap
- $h := 18 \text{in}$ Depth of cap
- $h_c := 16 \text{in}$ Depth of cap minus the cover
- $w := 18 \text{in}$ Width of cap
- $w_c := 16 \text{in}$ Width of cap minus the cover
- $\phi_f := 0.9$
- $A_g := h \cdot w$ Gross area of the cap
- $A_c := h_c \cdot w_c$ Core area of the cap

Calculate the additional longitudinal reinforcement required based on the Whitney Stress Blocks:

$$A_s := \frac{M_p}{\phi_f \cdot (L_{\text{emb}} - a) \cdot f_y} \qquad A_s = 3.788 \cdot \text{in}^2$$

Provide additional longitudinal reinforcement equivalent to 25% of calculated per the MDT specification:

$$0.25 \cdot A_s = 0.947 \cdot \text{in}^2 \qquad \text{Amount of steel to add for additional steel in longitudinal direction.}$$

$$A_{2\text{num}7\text{bars}} := 2 \cdot \frac{\pi}{4} \left(\frac{7}{8} \text{in} \right)^2 \qquad A_{2\text{num}7\text{bars}} = 1.203 \cdot \text{in}^2$$

Therefore, one additional #7 Ubar satisfies the additional reinforcement requirement

Step 6) Now calculate the cap transverse confinement:

This confinement zone is located from the pile face to half the cap depth from the pile. This applies to interior bays only.

Ensure the total amount of transverse reinforcement in the cap refinement zone satisfies the following equation:

Guess Values:

$$s_h := 1.75 \text{in} \qquad A_{\text{sh_trial}} := 0.20 \text{in}^2 \cdot \begin{pmatrix} 1 \\ 1 \end{pmatrix}$$

Given

$$A_{\text{sh_trial}} = \begin{bmatrix} 0.3 \cdot s_h \cdot w_c \cdot \frac{f_c}{f_y} \cdot \left(\frac{A_g}{A_c} - 1 \right) \\ 0.12 \cdot s_h \cdot w_c \cdot \frac{f_c}{f_y} \end{bmatrix} \qquad \text{LRFD equ 5.10.11.4.1d}$$

$$A_{\text{sh}} := \text{Find}(A_{\text{sh_trial}}) \qquad A_{\text{sh}} = \begin{pmatrix} 0.15 \\ 0.22 \end{pmatrix} \cdot \text{in}^2 \qquad s_h = 1.75 \cdot \text{in}$$

$A_{2\text{num}3\text{bars}} := 0.22 \text{in}^2$ Therefore, two number 3 bars placed at 1.75in apart as specified by the MDT design guide.

B.5 VT3 DESIGN CALCULATIONS

Pipe Pile to Cap (MDT) Design Method For VT3:

Define overall design parameters

$D := 8.625\text{in}$	Outside diameter of pile
$F_y := 53000\text{psi}$	Pile steel yield strength, ASTM A-252, Grade 2 (35ksi)
$L_{\text{emb}} := 10.375\text{in}$	Nominal pile embedment length
$f'_c := 4000\text{psi}$	Concrete cap strength - Class DD
$\phi_b := 1.0$	LRFD 5.5.4.2 for bearing on concrete
$t_p := 0.3608\text{in}$	Thickness of pile wall; Picked theoretical thickness to match crushing capacity below
$\alpha := 1.8$	Factor for f'_c constant in relation to how much steel confinement is in place

Step 1) Calculate the plastic moment capacity of the pile, M_p

$$Z := \frac{D^3}{6} - \frac{(D - 2 \cdot t_p)^3}{6} \quad Z = 24.657 \cdot \text{in}^3$$

$$M_{\text{npile}} := F_y \cdot Z \quad M_{\text{npile}} = 108.9 \cdot \text{ft} \cdot \text{kip}$$

$$M_p := 1.25 \cdot M_{\text{npile}} \quad \text{Apply MDT overstrength factor of 1.25} \quad M_p = 136.1 \cdot \text{ft} \cdot \text{kip}$$

Steps 2 and 3) Calculation of stress based on the Whitney Stress Block LRFD 5.7.2.2

$$\beta_1 := \begin{cases} 0.85 & \text{if } f'_c \leq 4000\text{psi} \\ \left[0.85 - \frac{(f'_c - 4000\text{psi})}{1000\text{psi}} \cdot 0.05 \right] & \text{if } 4000\text{psi} < f'_c \leq 8000\text{psi} \\ 0.65 & \text{otherwise} \end{cases} \quad \beta_1 = 0.85$$

$$x := \frac{L_{\text{emb}}}{2} \quad x = 5.188 \cdot \text{in}$$

$$a := \beta_1 \cdot x \quad a = 4.409 \cdot \text{in}$$

$$z := L_{\text{emb}} - a \quad z = 5.966 \cdot \text{in}$$

Check the assumption of the alpha variable and embedment length:

$$f_n := \phi_b \cdot \alpha \cdot f'_c \quad f_n = 7.200 \cdot \text{ksi}$$

$$M_p = 136.128 \cdot \text{ft} \cdot \text{kip} \quad \text{From plastic moment calculation} \quad \text{Therefore } f_u \text{ is approximately equal to } f_n \text{ for this case suggesting a suitable } L_{\text{emb}} \text{ for the assumed } \alpha \text{ value.}$$

$$f_u := \frac{M_p}{a \cdot D \cdot z} \quad f_u = 7.2 \cdot \text{ksi}$$

Step 4) Calculate the minimum cap flexural rein. to insure $M_n > 1.2 M_{cr}$ per the MDT design guide

Design Parameters:

$f_y := 60000\text{psi}$	Reinforcing steel in cap
cover := 1in	Desired amount of cover for reinforcement
h := 18in	Depth of cap
w := 18in	Width of cap
d := 16.376in	Distance from top of beam to steel in tension
$f_c := 4000\text{psi}$	Concrete Cap Strength
$\phi_f := 0.9$	Factor for flexure in concrete

Calculate the cracking moment, M_{cr} :

$$M_{cr} := \frac{11.5 \cdot \sqrt{1\text{psi}} \cdot \sqrt{f_c} \cdot w \cdot h^2}{6} \quad M_{cr} = 58.913 \cdot \text{ft} \cdot \text{kip}$$

Use a solve block to determine the minimum required area of reinforcing steel:

Guess a value for A_s : $A_s := 0.6\text{in}^2$

Given

$$1.2 \cdot M_{cr} = A_s \cdot f_y \cdot \left(d - 0.59 \cdot \frac{A_s \cdot f_y}{f_c \cdot w} \right)$$

$$A_{s\text{min}} := \text{Find}(A_s)$$

$$A_{s\text{min}} = 0.887 \cdot \text{in}^2$$

$$A_{s2\text{num}4\text{bars}} := 2 \cdot \frac{\pi}{4} \cdot \left(\frac{4}{8} \text{in} \right)^2$$

$$A_{s2\text{num}4\text{bars}} = 0.393 \cdot \text{in}^2$$

$$A_{s2\text{num}5\text{bars}} := 2 \cdot \frac{\pi}{4} \cdot \left(\frac{5}{8} \text{in} \right)^2$$

$$A_{s2\text{num}5\text{bars}} = 0.614 \cdot \text{in}^2$$

$$A_{s\text{Total}} := A_{s2\text{num}4\text{bars}} + A_{s2\text{num}5\text{bars}}$$

$$A_{s\text{Total}} = 1.006 \cdot \text{in}^2$$

Therefore, use two #4 bars and two #5 bars in the top and bottom of the cap to provide minimal reinforcement.

Step 5) Calculate the additional longitudinal and transverse rein. in the cap per the MDT design guide

If $M_u > 0.6 \cdot M_p$, then include additional cap reinforcement as specified by the MDT design guide:

Design Parameters:

$f_y := 60000 \text{ psi}$	Reinforcing steel in cap
$h := 18 \text{ in}$	Depth of cap
$h_c := 16 \text{ in}$	Depth of cap minus the cover
$w := 18 \text{ in}$	Width of cap
$w_c := 16 \text{ in}$	Width of cap minus the cover
$\phi_f := 1.0$	
$A_g := h \cdot w$	Gross area of the cap
$A_c := h_c \cdot w_c$	Core area of the cap

Calculate the additional longitudinal reinforcement required based on the Whitney Stress Blocks:

$$A_s := \frac{M_p}{\phi_f \cdot (L_{emb} - a) \cdot f_y} \qquad A_s = 4.564 \text{ in}^2$$

Provide additional longitudinal reinforcement equivalent to 25% of calculated per the MDT specification:

$$0.25 \cdot A_s = 1.141 \text{ in}^2 \qquad \text{Amount of steel to add for additional steel in longitudinal direction.}$$

$$A_{2num7bars} := 2 \cdot \frac{\pi}{4} \left(\frac{7}{8} \text{ in} \right)^2 \qquad A_{2num7bars} = 1.203 \text{ in}^2$$

Therefore, one additional #7 Ubars satisfies the additional reinforcement requirement

Step 6) Now calculate the cap transverse confinement:

This confinement zone is located from the pile face to half the cap depth from the pile. This applies to interior bays only.

Ensure the total amount of transverse reinforcement in the cap refinement zone satisfies the following equation:

Guess Values:

$$s_h := 1.75 \text{ in} \qquad A_{sh_trial} := 0.20 \text{ in}^2 \cdot \begin{pmatrix} 1 \\ 1 \end{pmatrix}$$

Given

$$A_{sh_trial} = \begin{bmatrix} 0.3 \cdot s_h \cdot w_c \cdot \frac{f_c}{f_y} \cdot \left(\frac{A_g}{A_c} - 1 \right) \\ 0.12 \cdot s_h \cdot w_c \cdot \frac{f_c}{f_y} \end{bmatrix} \qquad \text{LRFD equ 5.10.11.4.1d}$$

$$A_{sh} := \text{Find}(A_{sh_trial}) \qquad A_{sh} = \begin{pmatrix} 0.15 \\ 0.22 \end{pmatrix} \cdot \text{in}^2 \qquad s_h = 1.75 \cdot \text{in}$$

$A_{2num3bars} := 0.22 \text{ in}^2$ Therefore, two number 3 bars placed at 1.75in apart as specified by the MDT design guide.

Strain data is first shown for the monotonic tests (VT1, VT2, VT2.5, and VT3) and then for the two cyclic tests (CT1 and CT2). For all strain figures, tension is shown as a positive value and compression is shown as negative value. The location for each strain gage is shown graphically on each figure.

Typically, each strain gage location consisted of two strain gages placed on opposite sides of the reinforcing bar; hence, the strain plots shown in the following figures have two dashed lines showing the strain output for each strain gage, while the solid line represents the average of the two gages. This average strain value provides a sense of the global strain of the section at that point. Furthermore, by examining the strain response for each of the actual strain gages, the amount of bending behavior vs. the amount of tension behavior can be estimated. The strain response for a bar resisting a pure tensile action, will result in a plot with the two strain responses falling very close to each other for a given drift value at any specific time. If the strain response of the two gages differs greatly, and often times one gage may show a tensile behavior while the opposite gage shows a compressive behavior, then it is likely that the strain location is predominantly in bending. Strain plots in which there are no dashed lines and only one solid line indicates that there was only one strain gage placed at that location.

C.1 VT1 STRAIN GAGE DATA

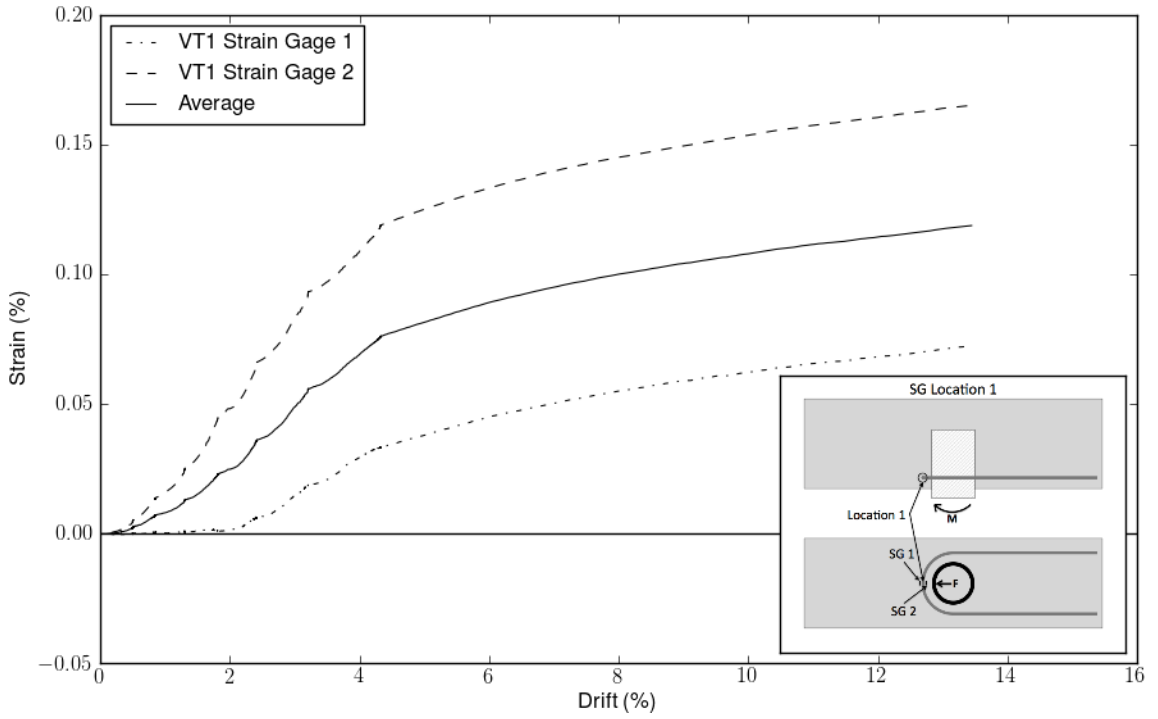


Figure 63: VT1 – Strain Gage Location 1

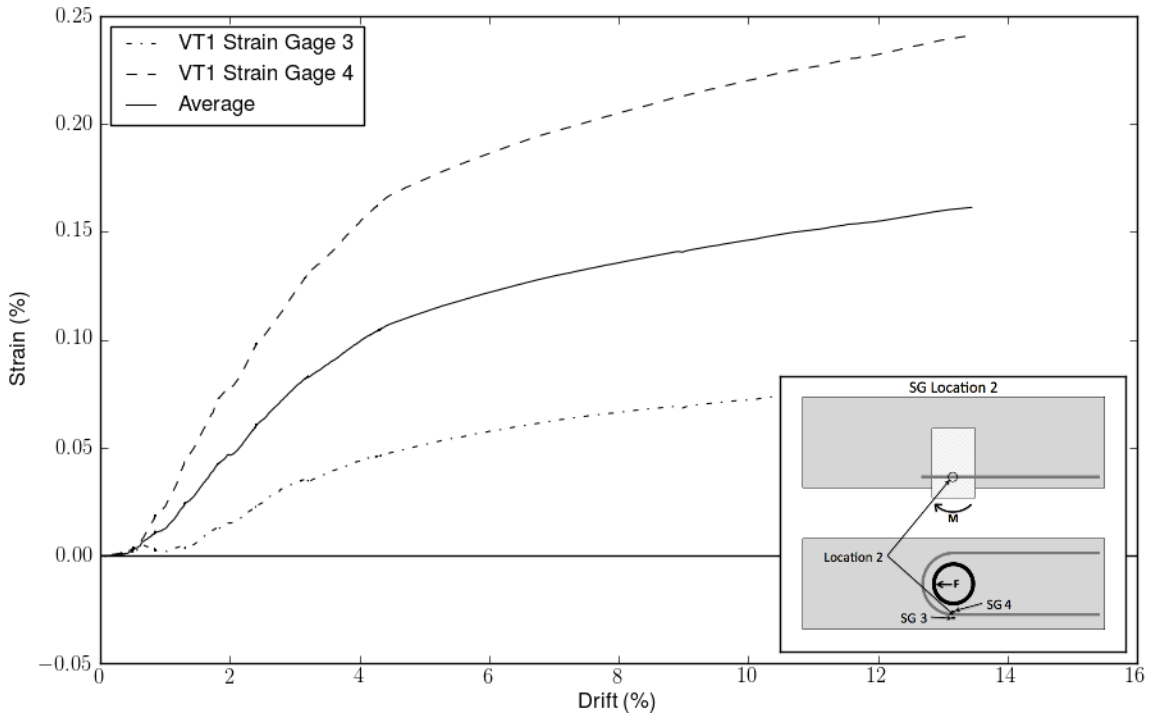


Figure 64: VT1 - Strain Location 2

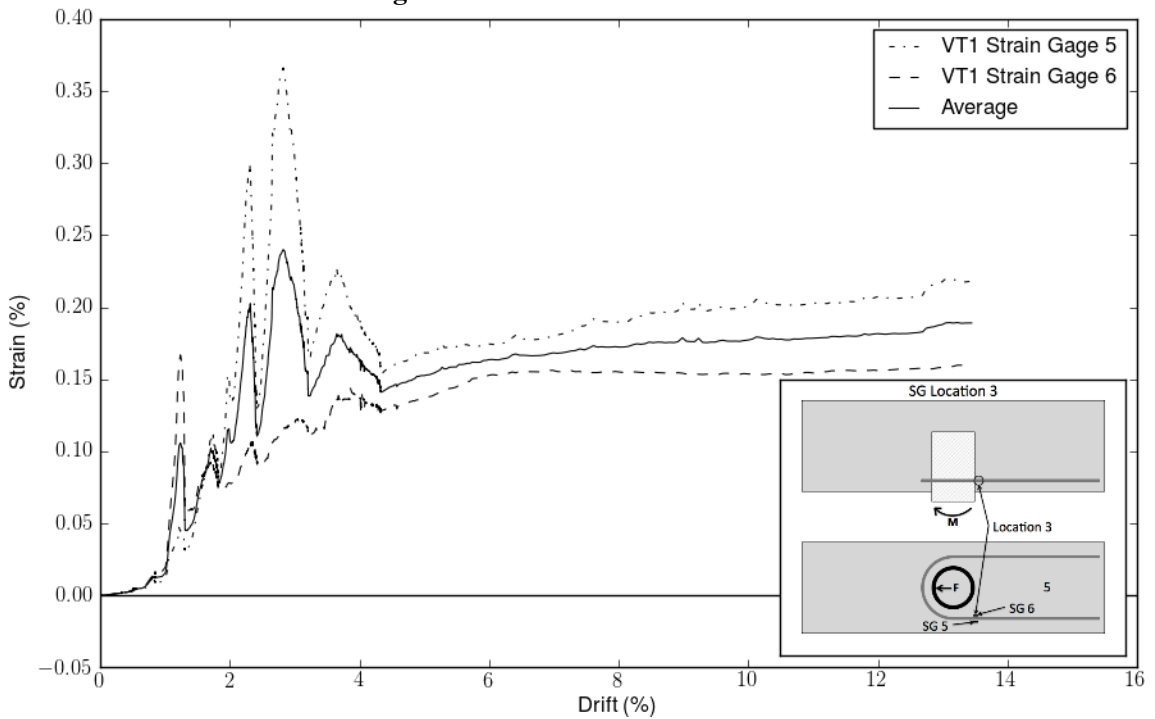


Figure 65: VT1 - Strain Gage Location 3

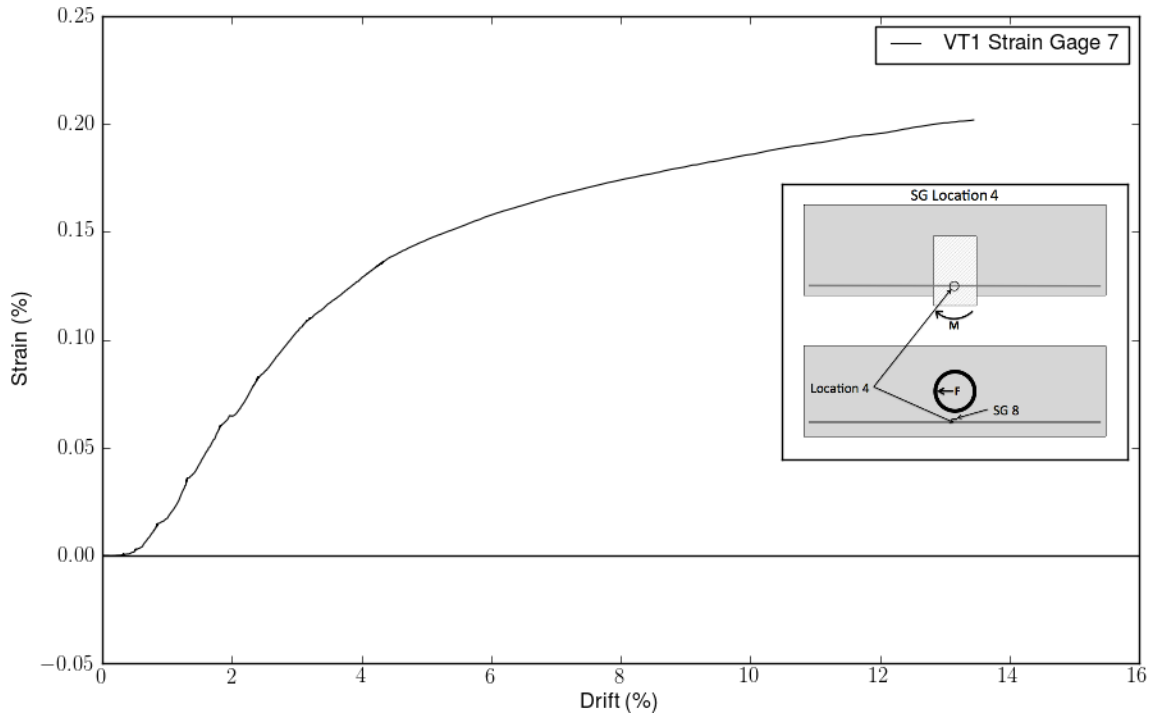


Figure 66: VT1 – Strain Gage Location 4

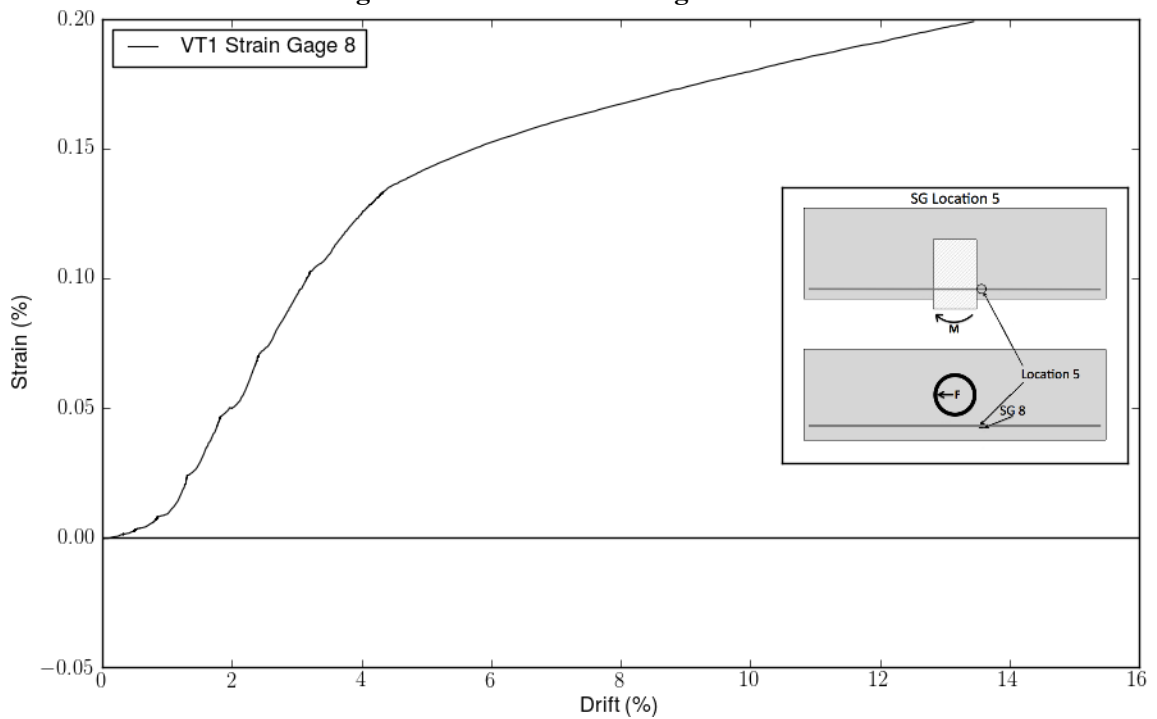


Figure 67: VT1 – Strain Gage Location 5

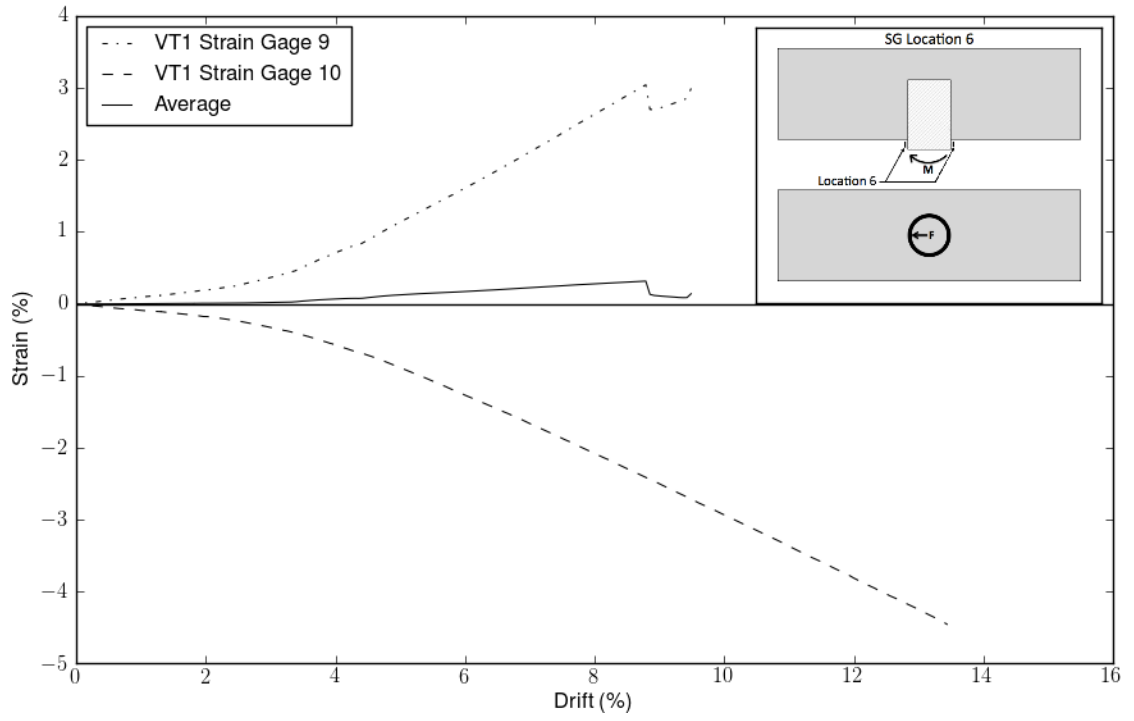


Figure 68: VT1 – Strain Gage Location 6

C.2 VT2 STRAIN GAGE DATA

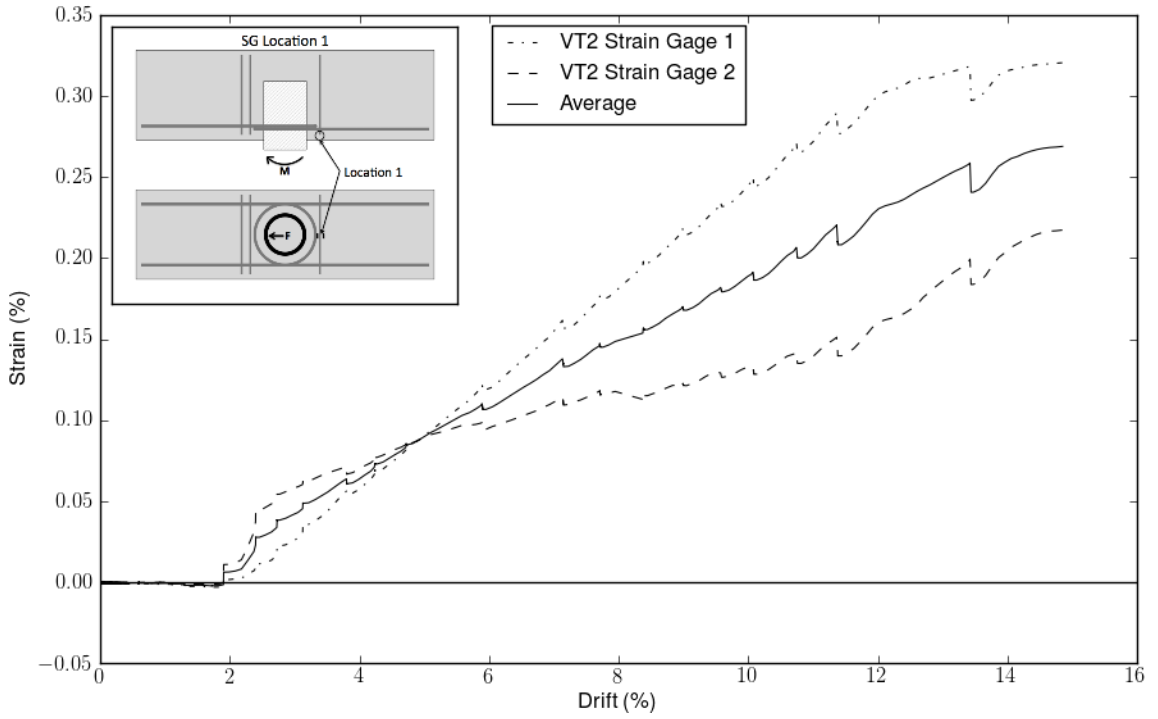


Figure 69: VT2 - Strain Gage Location 1

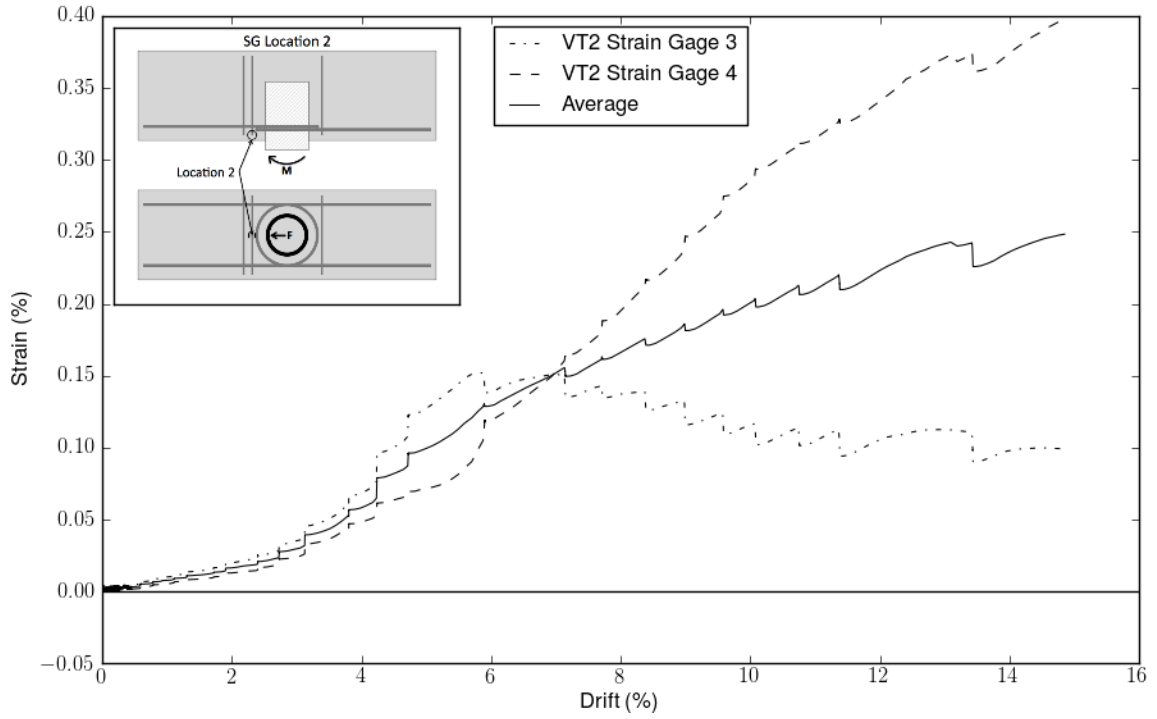


Figure 70: VT2 - Strain Gage Location 2

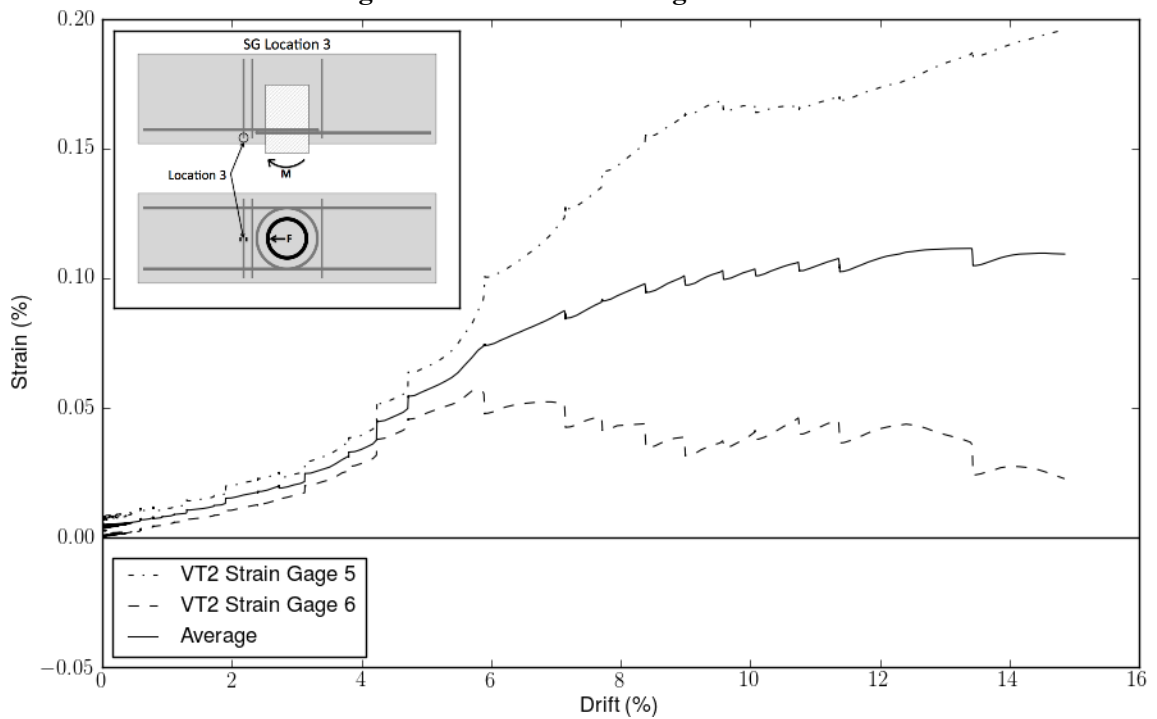


Figure 71: VT2 - Strain Gage Location 3

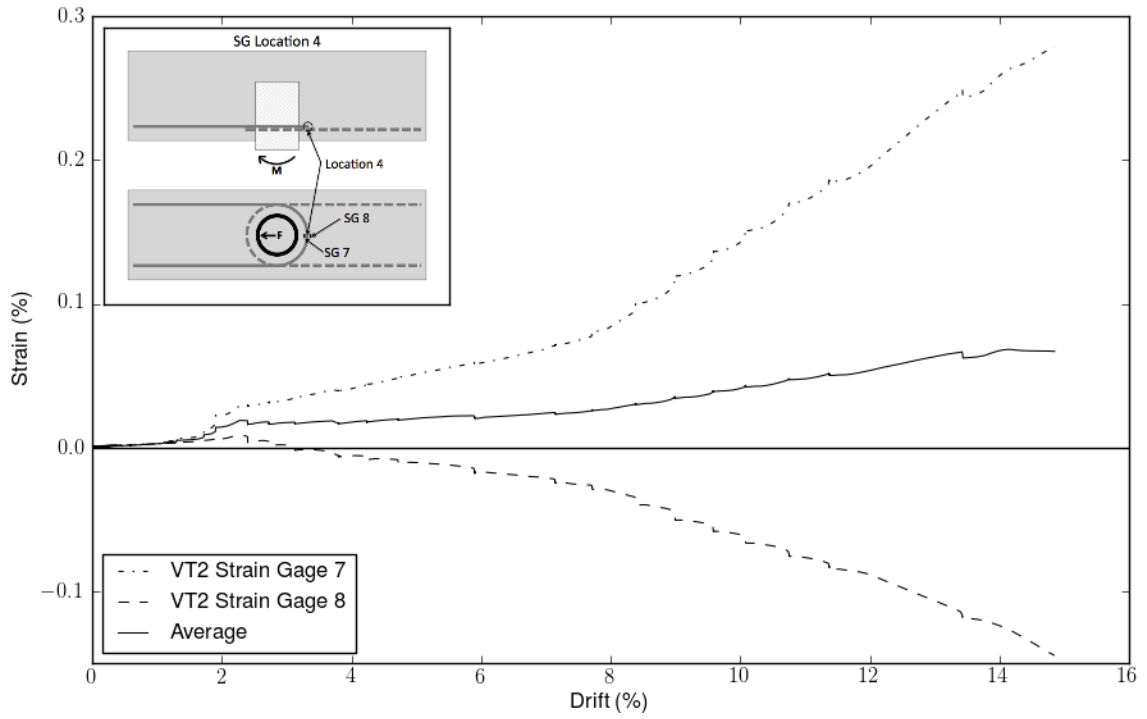


Figure 72: VT2 - Strain Gage Location 4

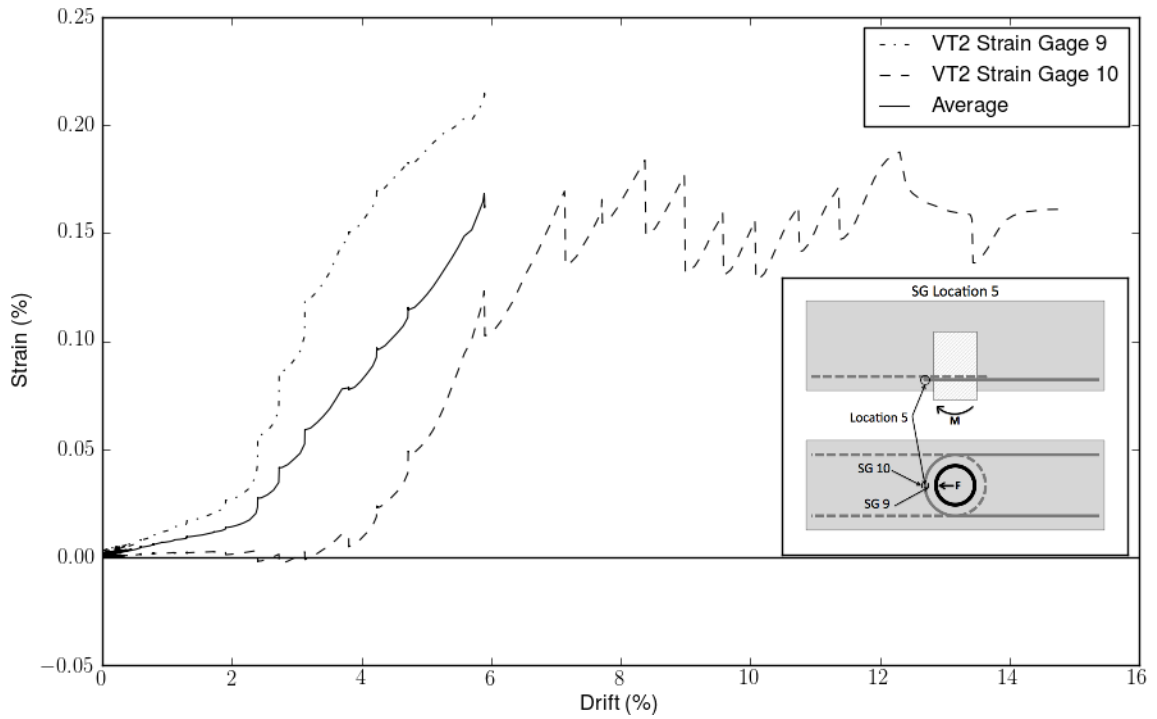


Figure 73: VT2 - Strain Gage Location 5

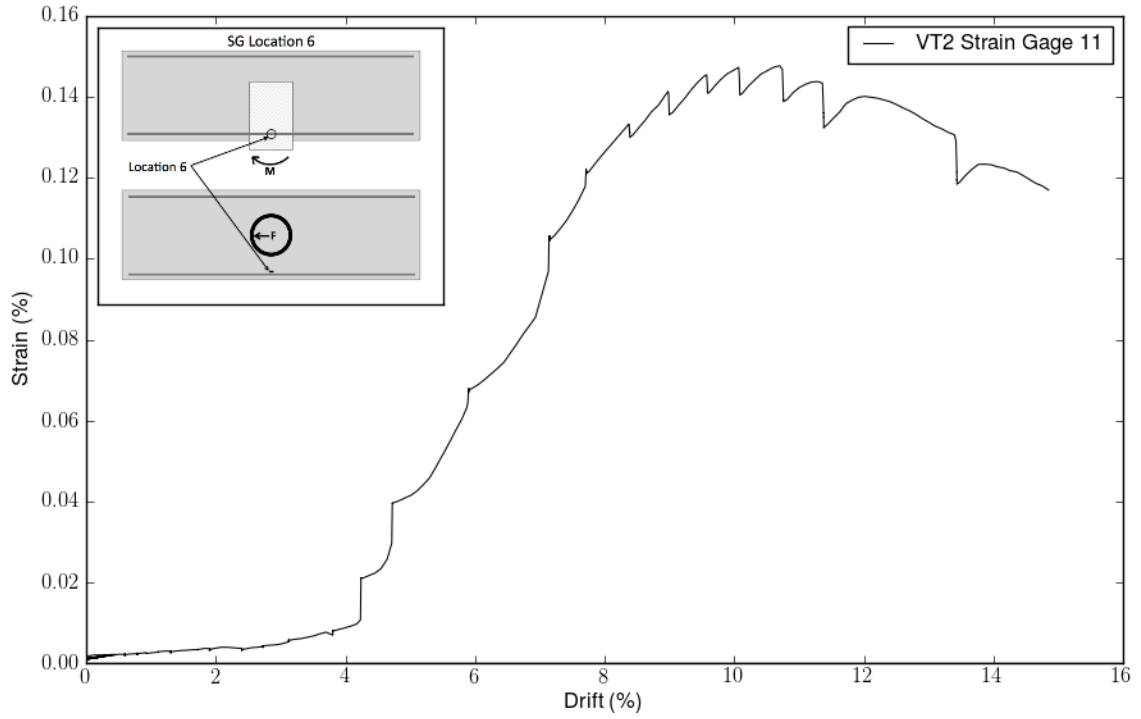


Figure 74: VT2 - Strain Gage Location 6

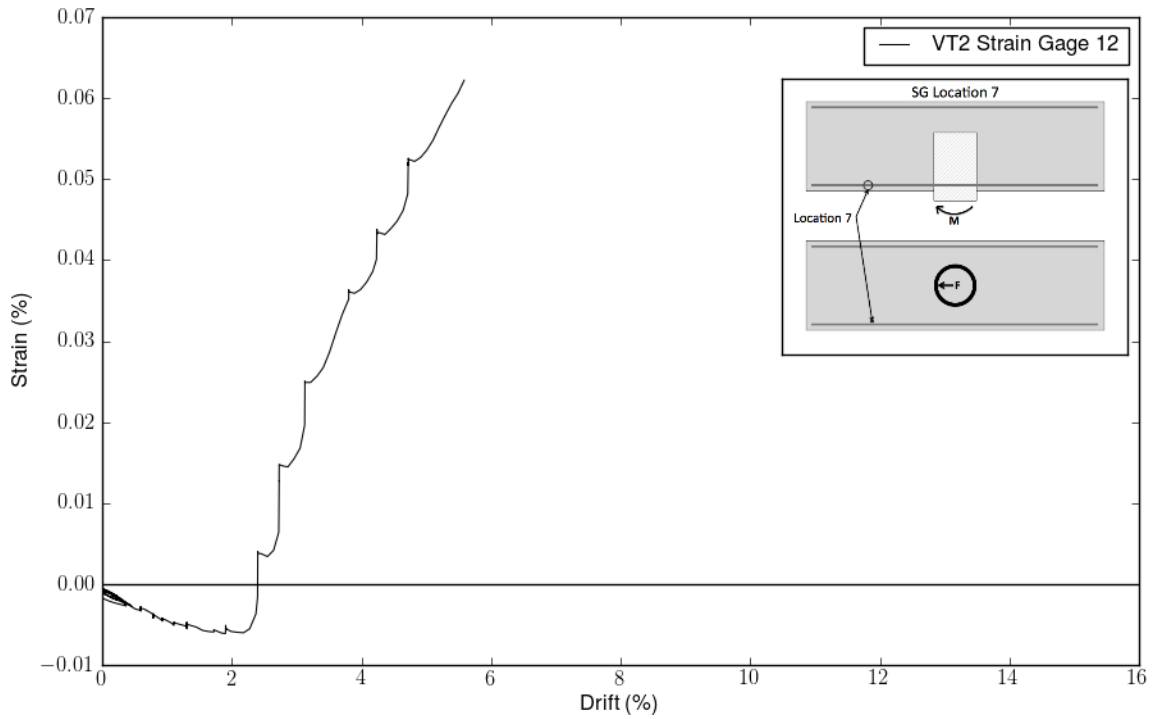


Figure 75: VT2 - Strain Gage Location 7

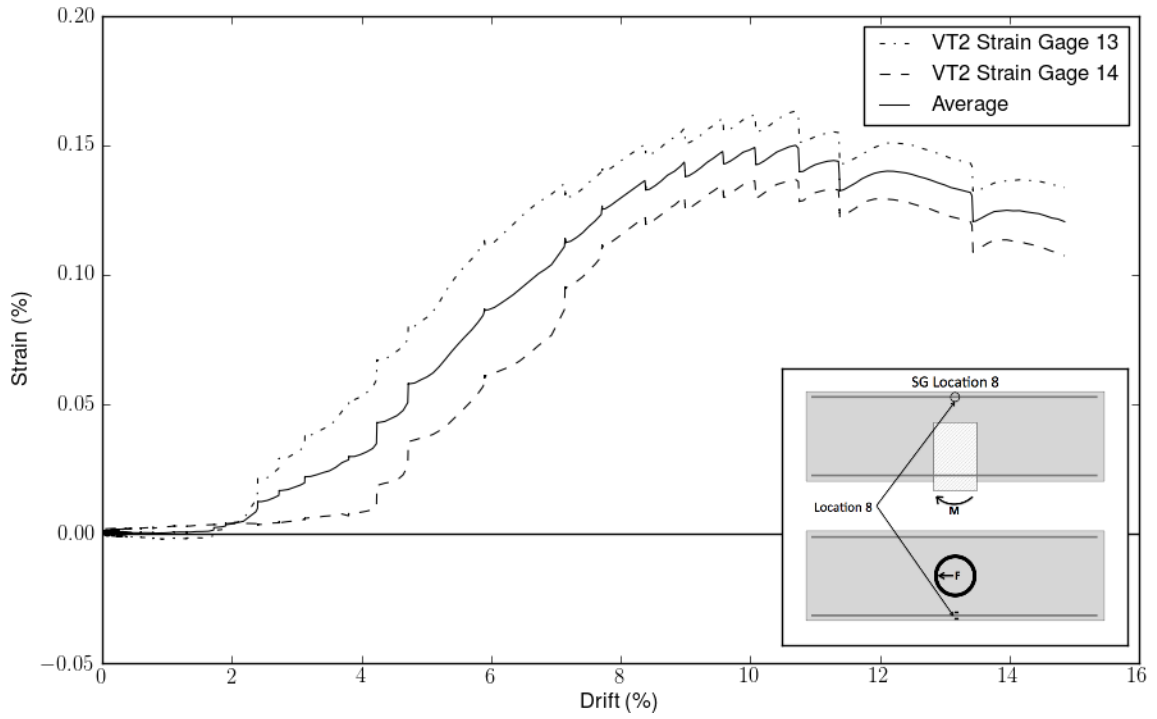


Figure 76: VT2 - Strain Gage Location 8

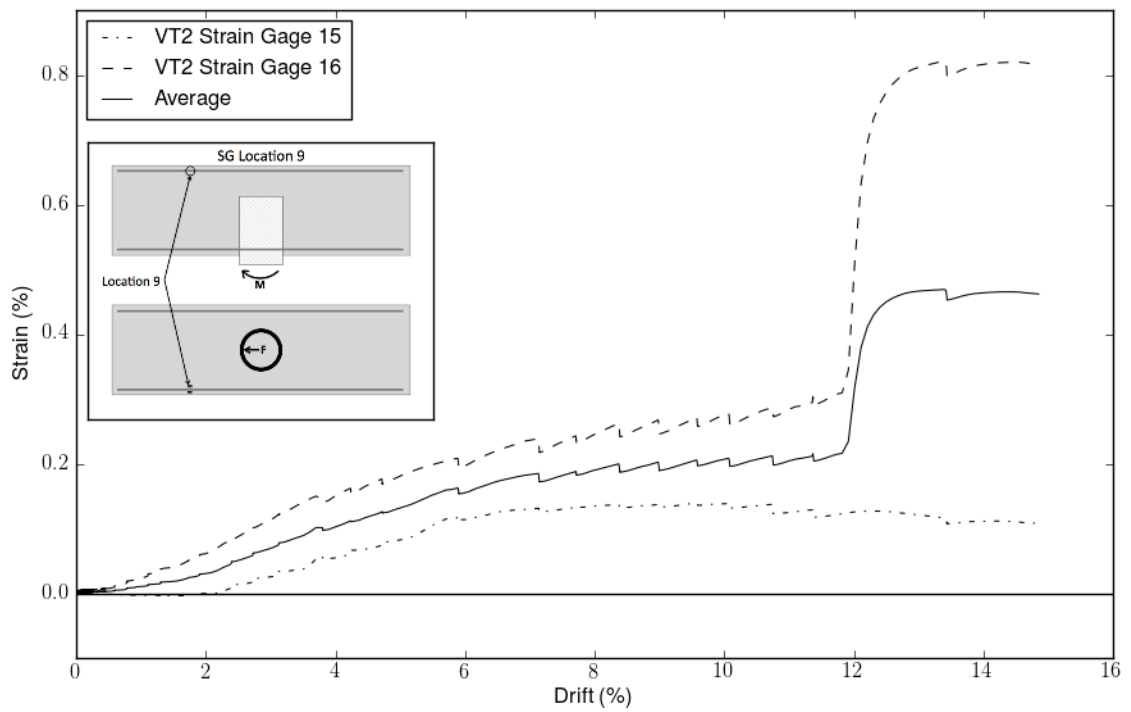


Figure 77: VT2 - Strain Gage Location 9

C.3 VT2.5 STRAIN GAGE DATA

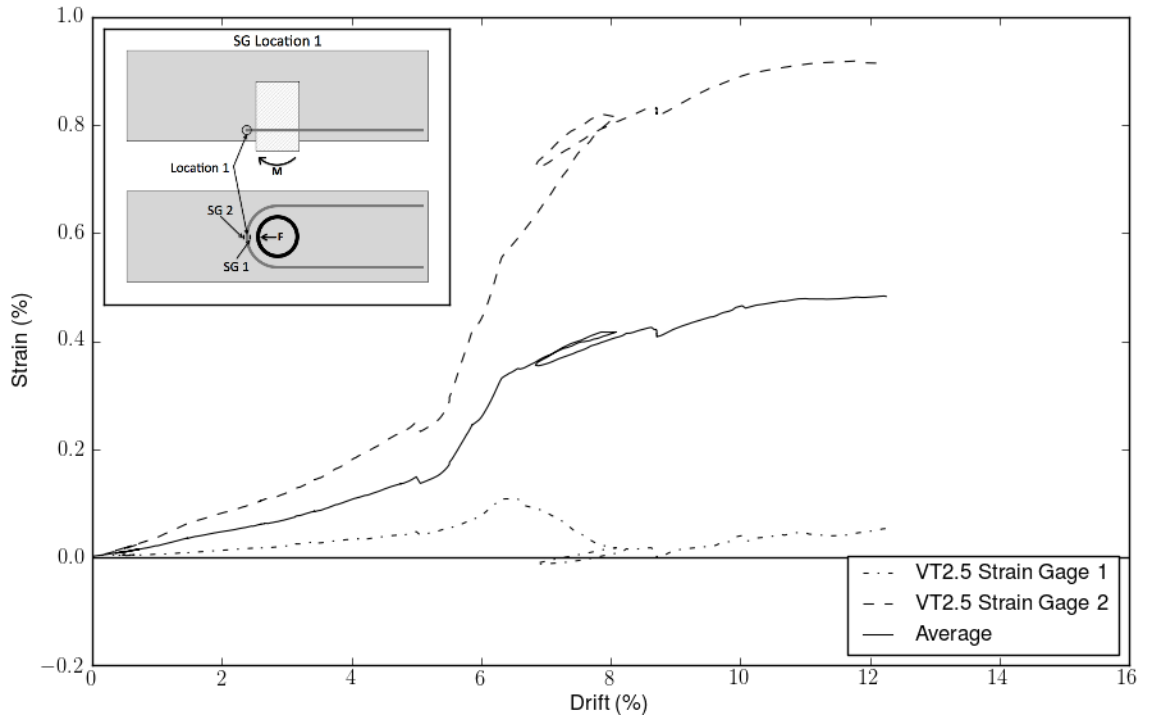


Figure 78: VT2.5 - Strain Gage Location 1

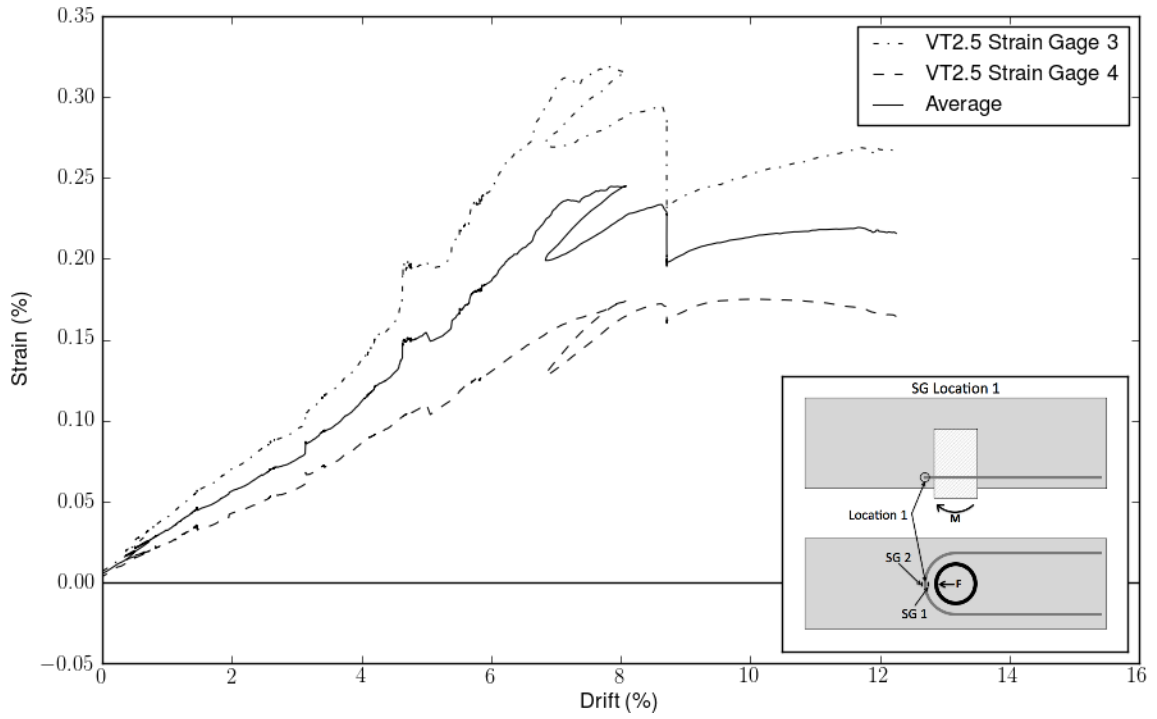


Figure 79: VT2.5 - Strain Gage Location 2

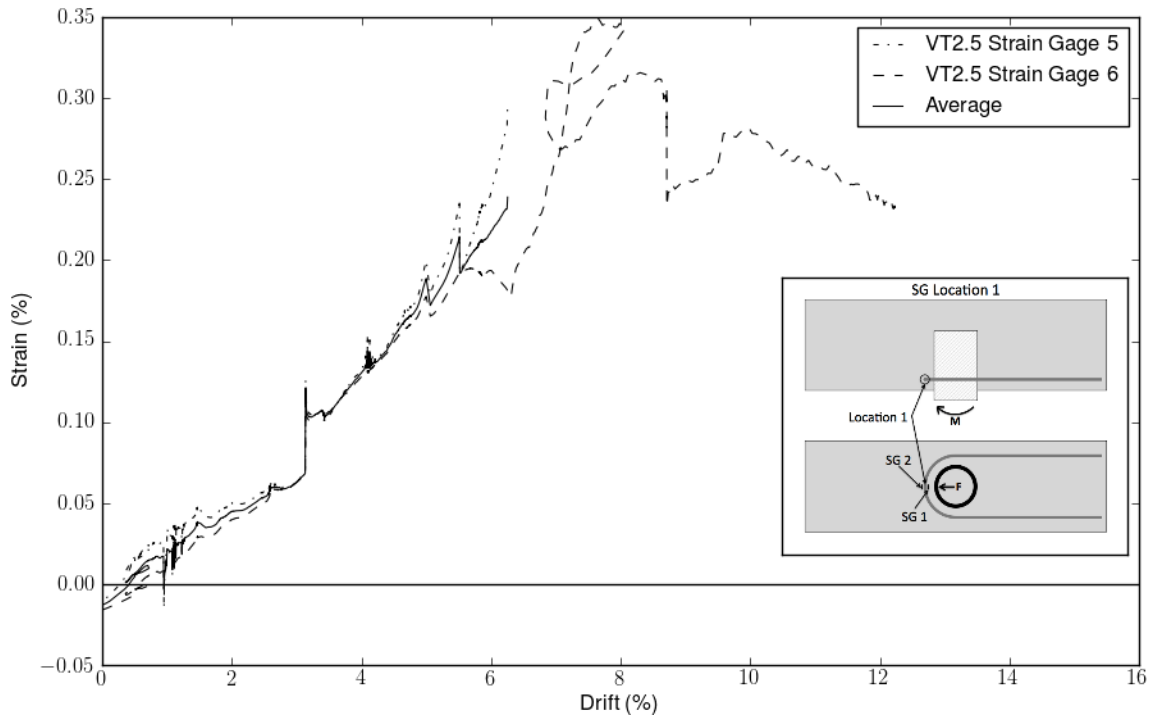


Figure 80: VT2.5 - Strain Gage Location 3

C.4 VT3 STRAIN GAGE DATA

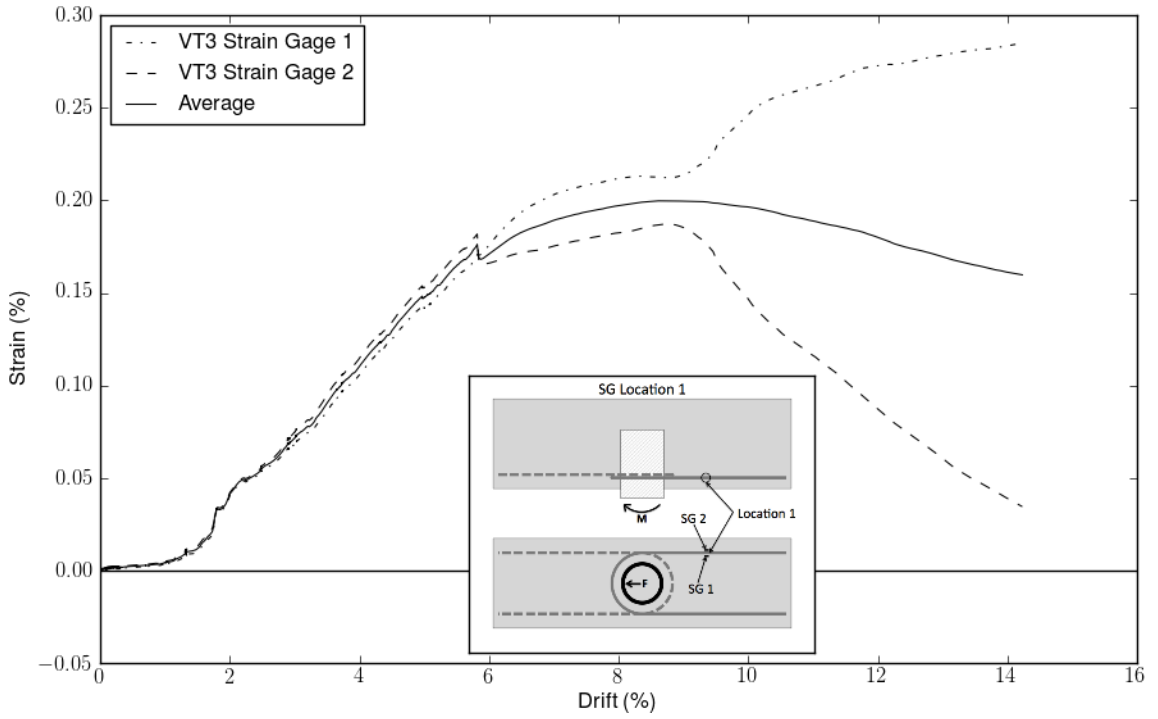


Figure 81: VT3 - Strain Gage Location 1

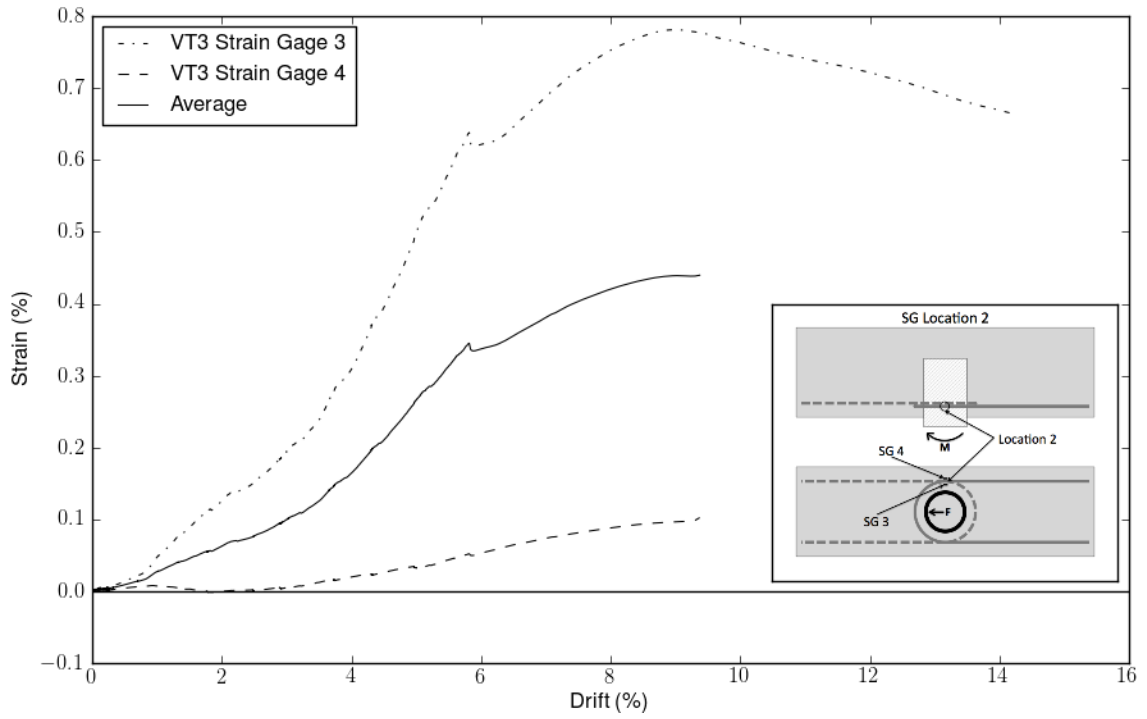


Figure 82: VT3 - Strain Gage Location 2

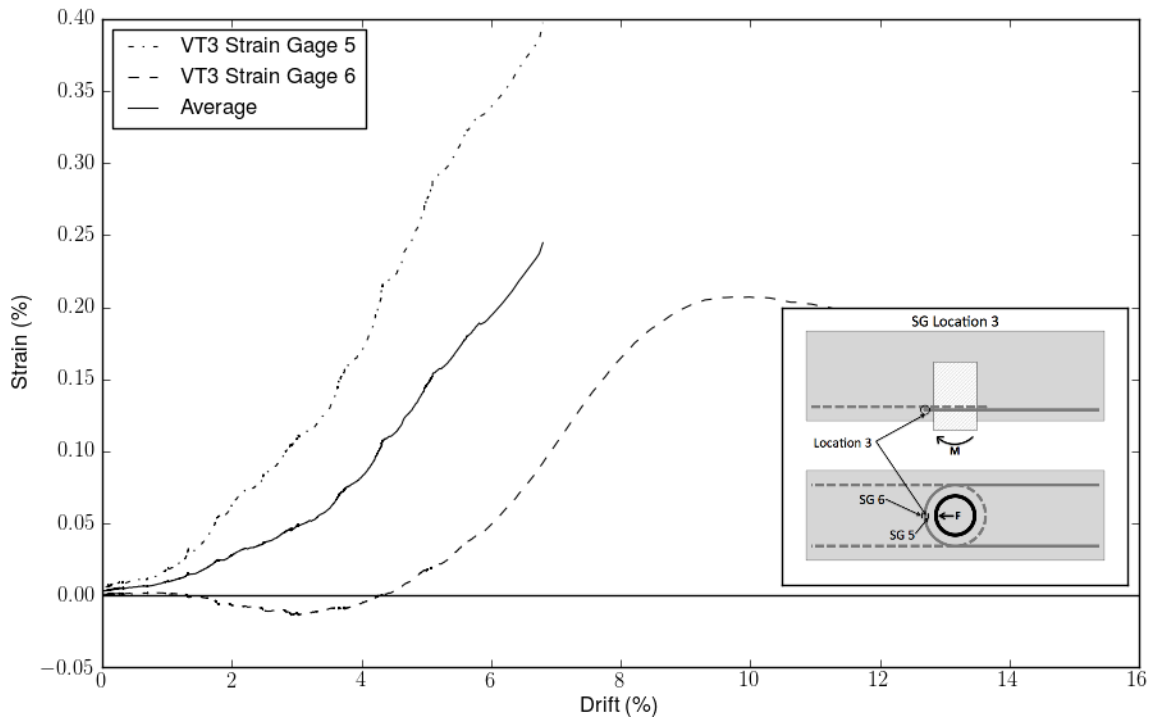


Figure 83: VT3 - Strain Gage Location 3

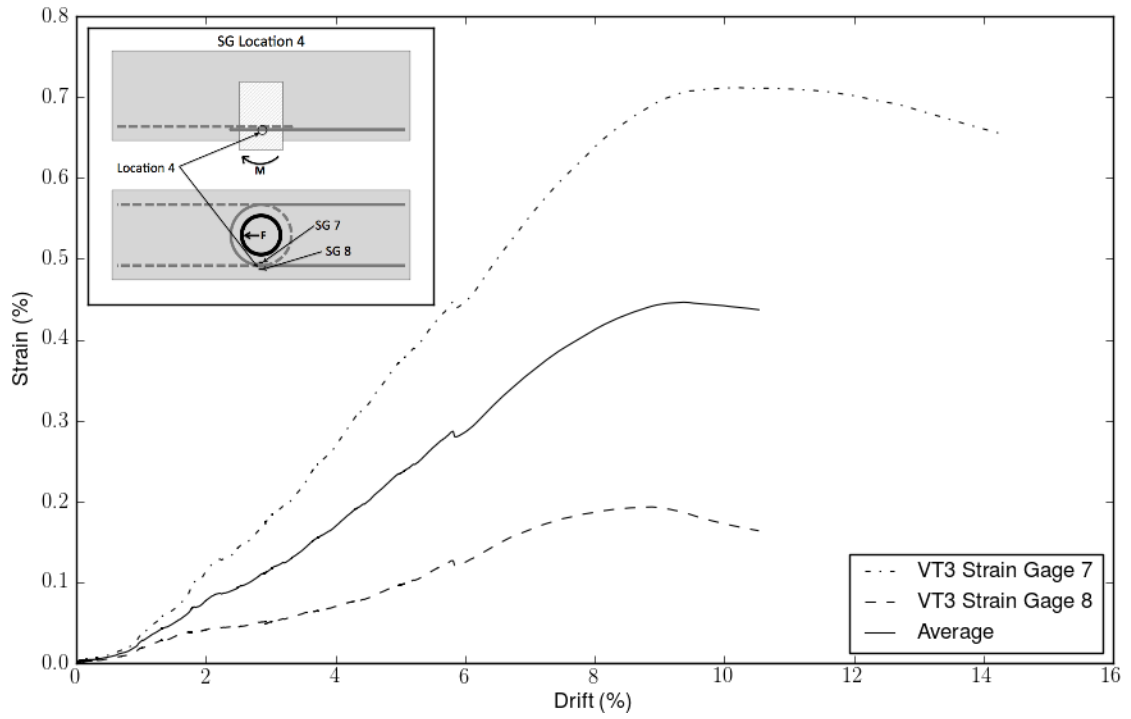


Figure 84: VT3 - Strain Gage Location 4

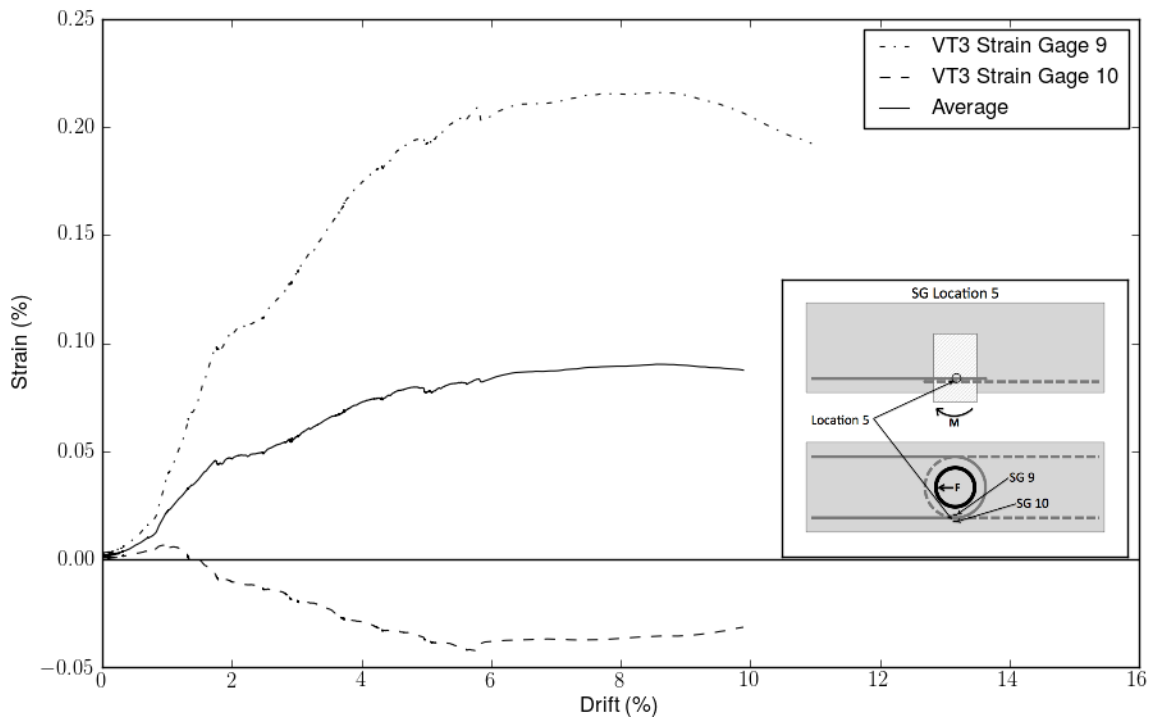


Figure 85: VT3 - Strain Gage Location 5

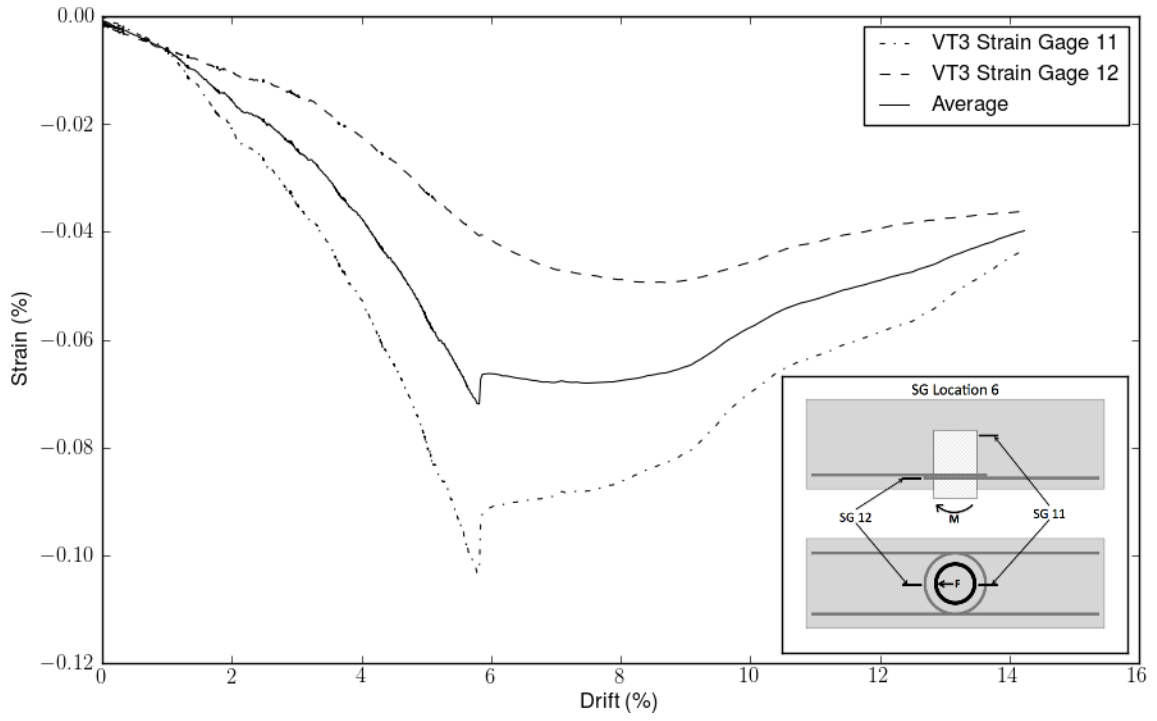


Figure 86: VT3 - Strain Gage Location 6

C.6 CT2 STRAIN GAGE DATA

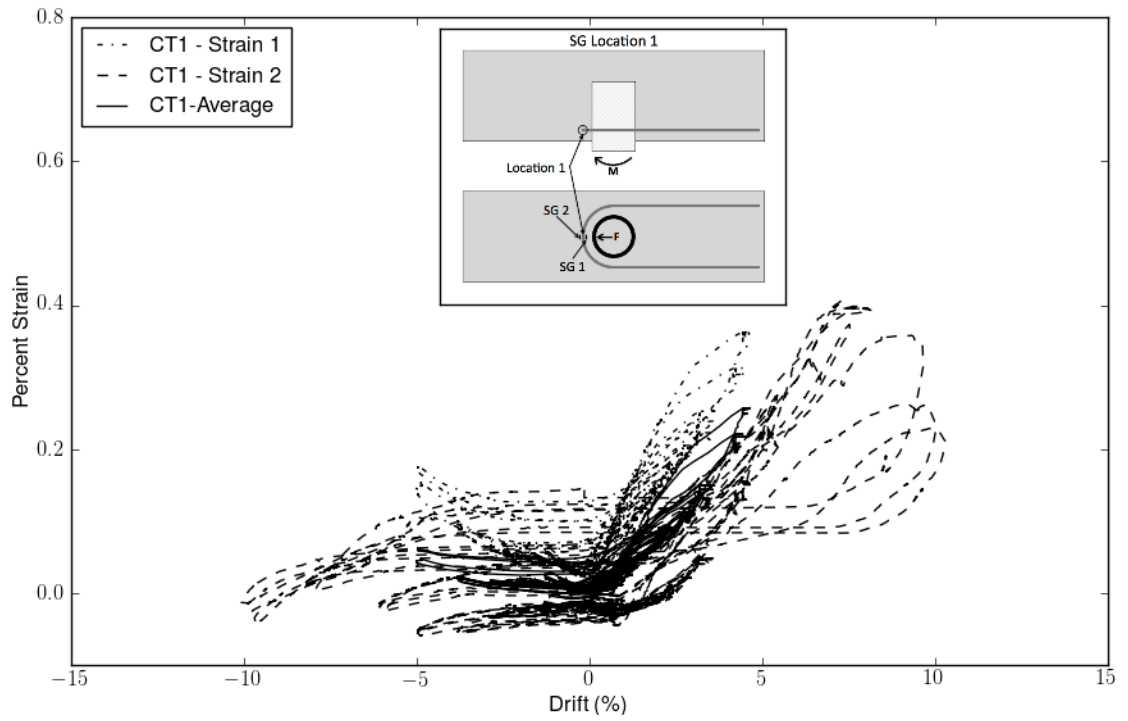


Figure 87: CT1 - Strain Gage Location 1

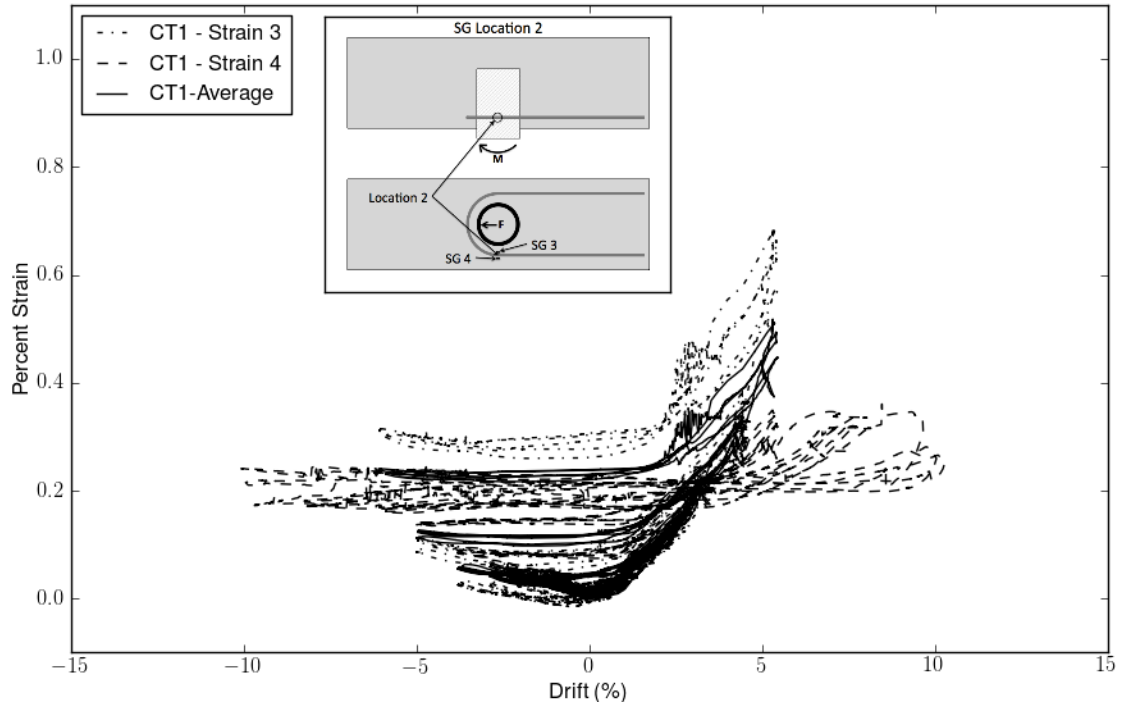


Figure 88: CT1 - Strain Gage Location 2

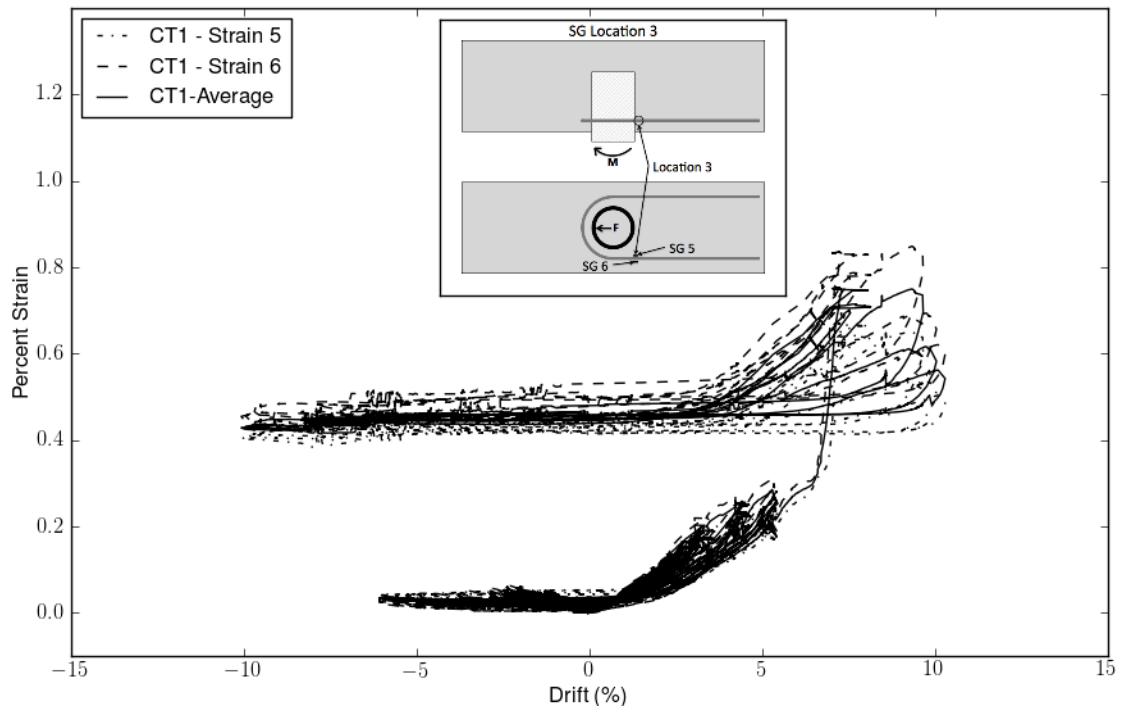


Figure 89: CT1 - Strain Gage Location 3

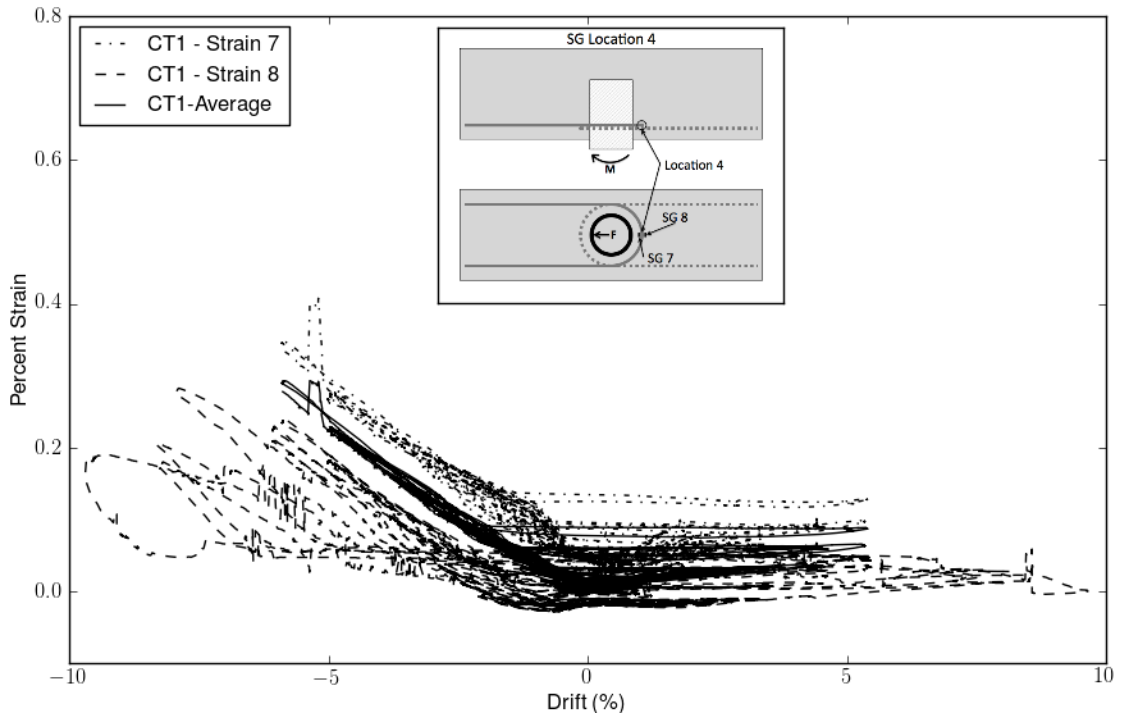


Figure 90: CT1 - Strain Gage Location 4

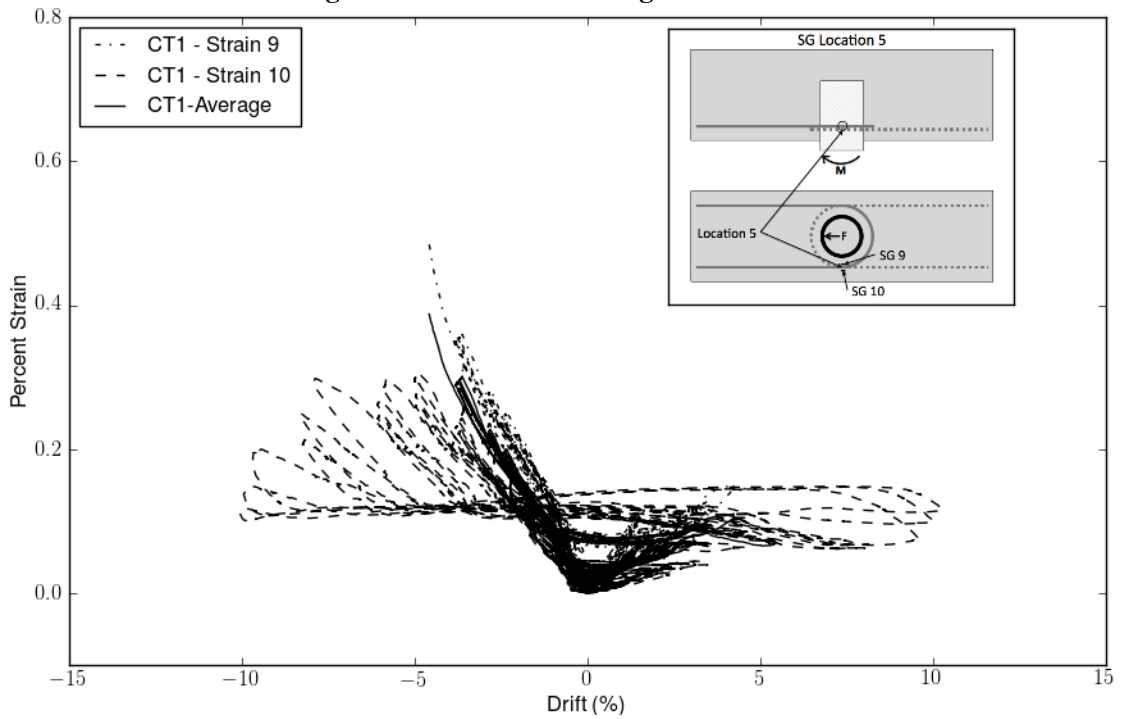


Figure 91: CT1 - Strain Gage Location 5

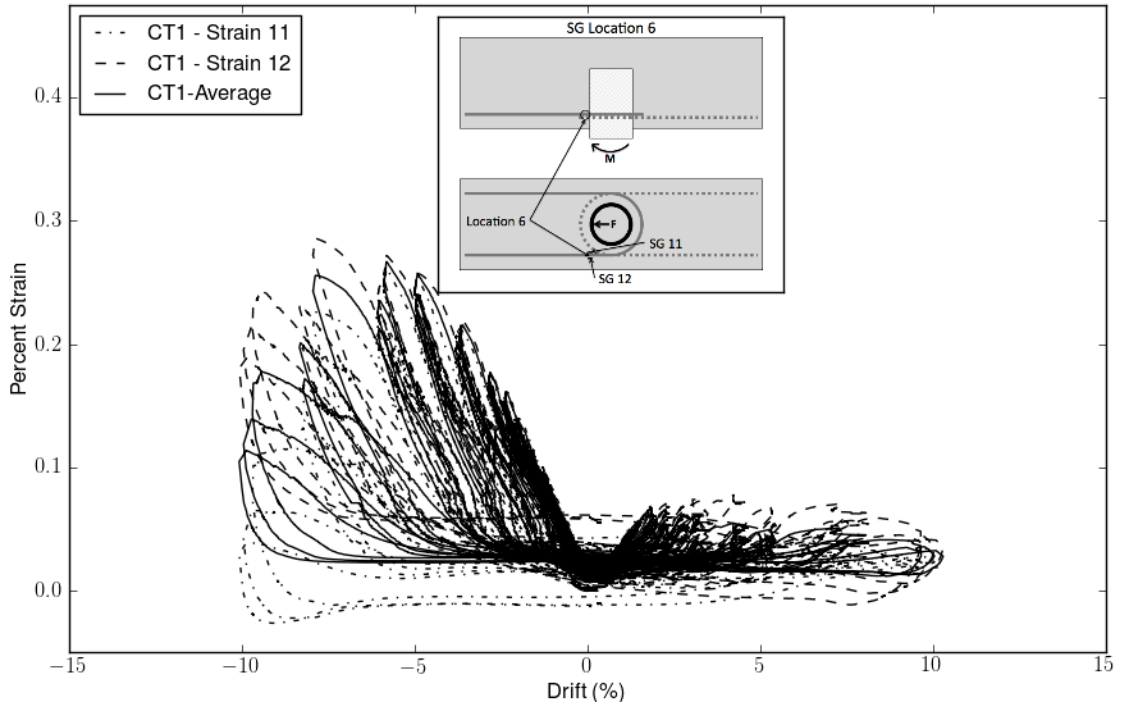


Figure 92: CT1 - Strain Gage Location 6

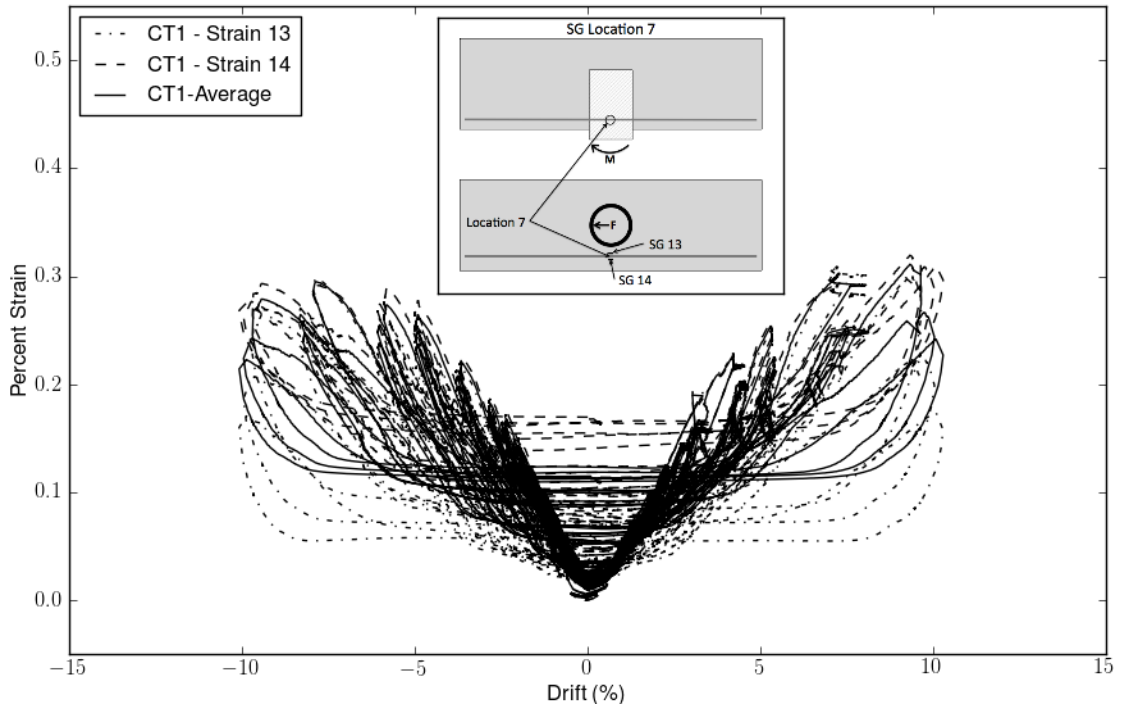


Figure 93: CT1 - Strain Gage Location 7

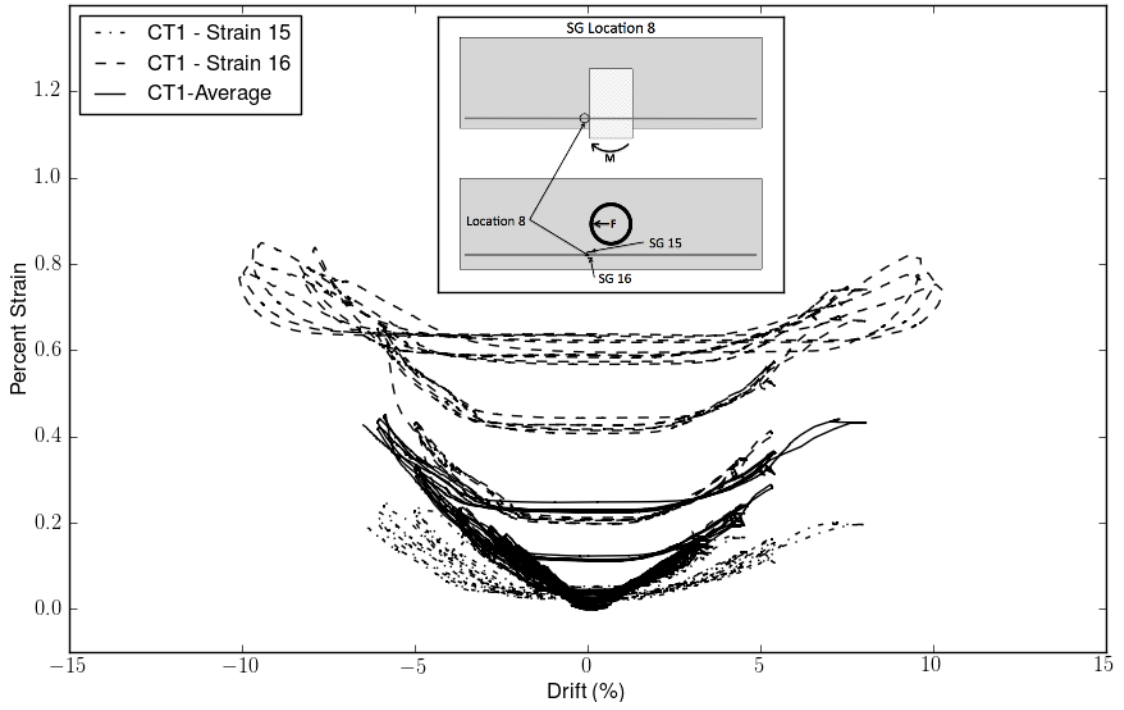


Figure 94: CT1 - Strain Gage Location 8

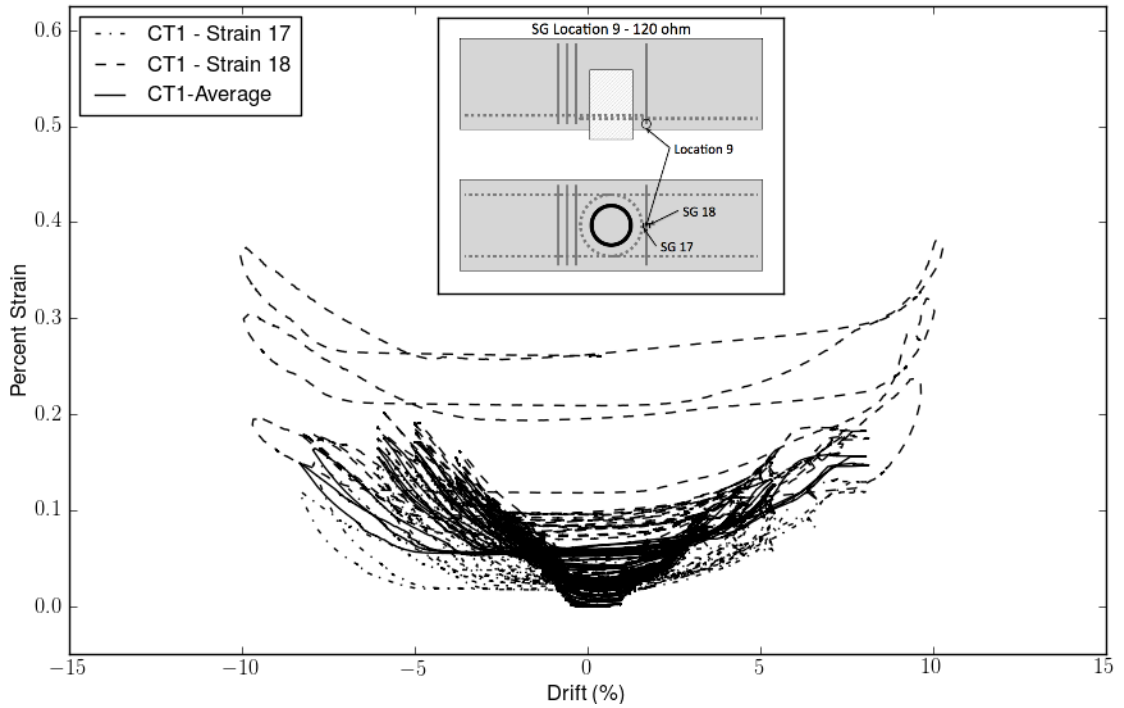


Figure 95: CT1 - Strain Gage Location 9

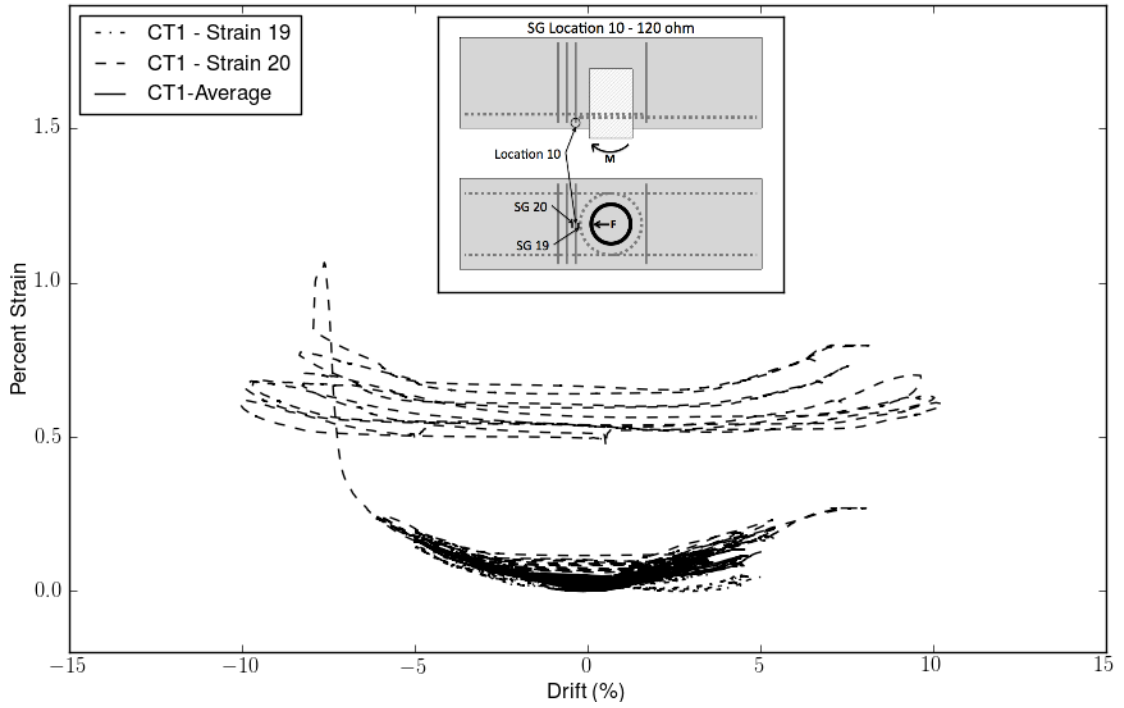


Figure 96: CT1 - Strain Gage Location 10

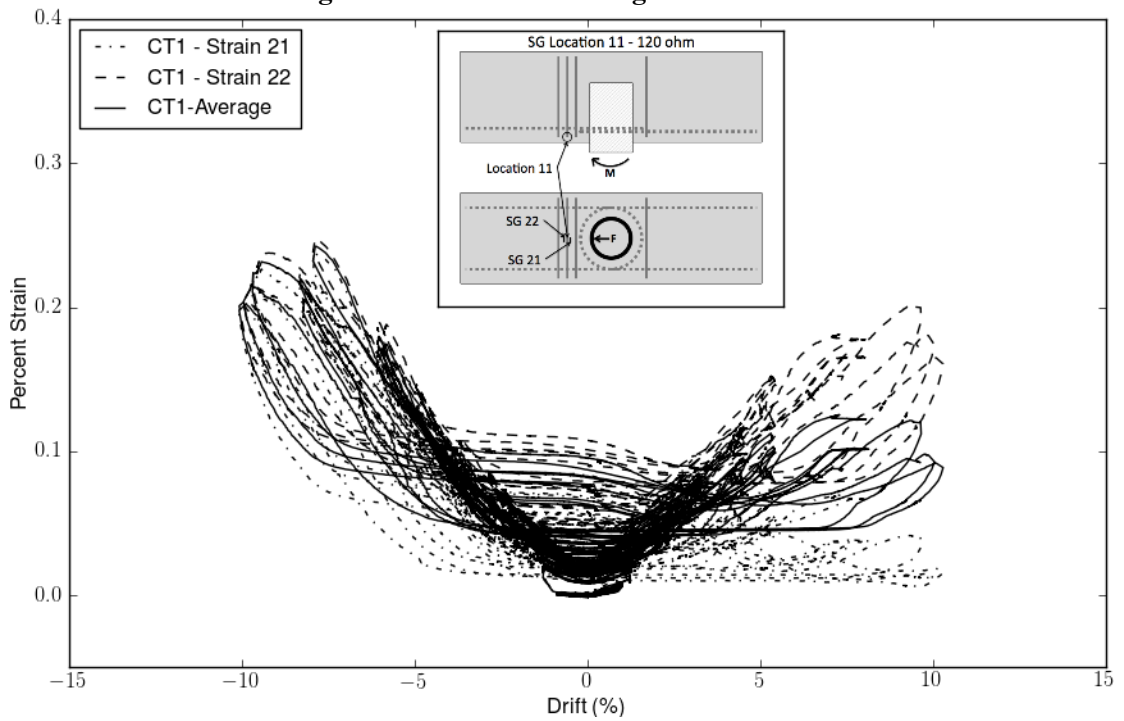


Figure 97: CT1 - Strain Gage Location 11

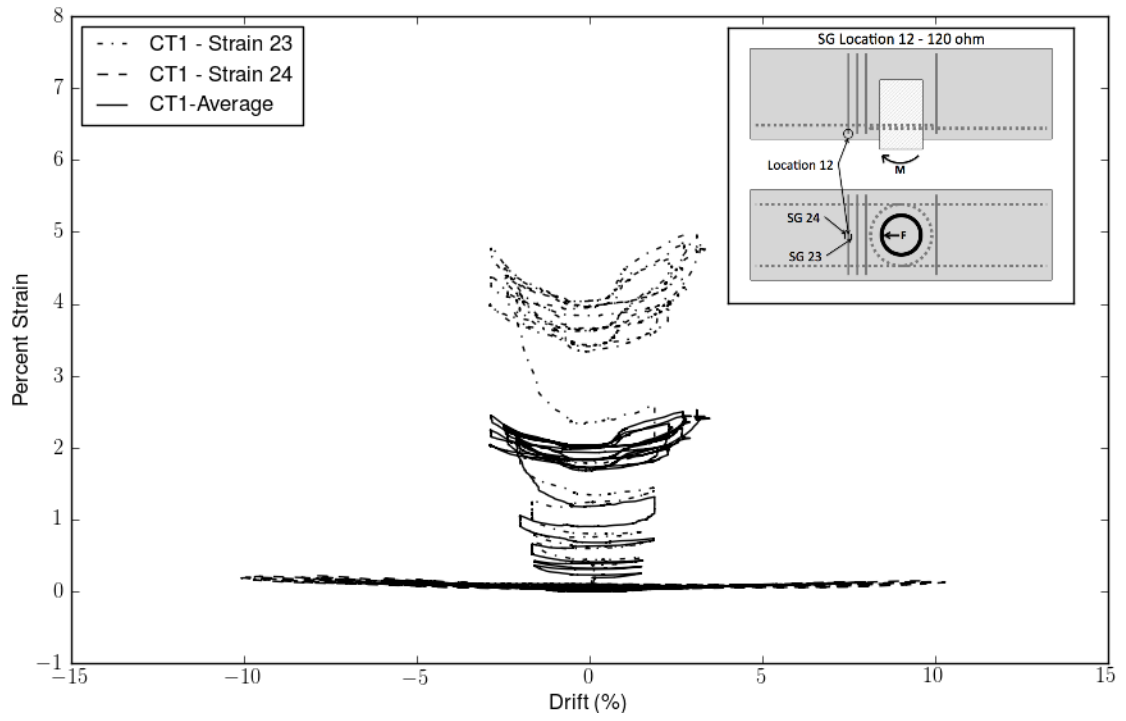


Figure 98: CT1 - Strain Gage Location 12

C.6 CT2 STRAIN GAGE DATA

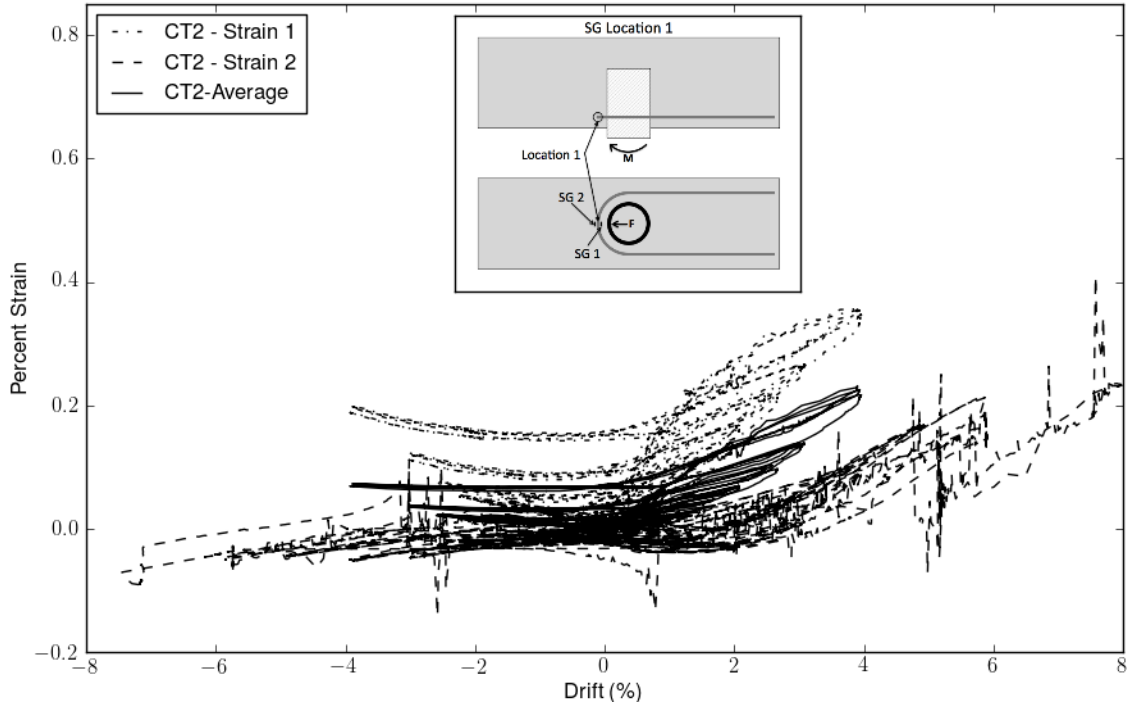


Figure 99: CT2 - Strain Gage Location 1

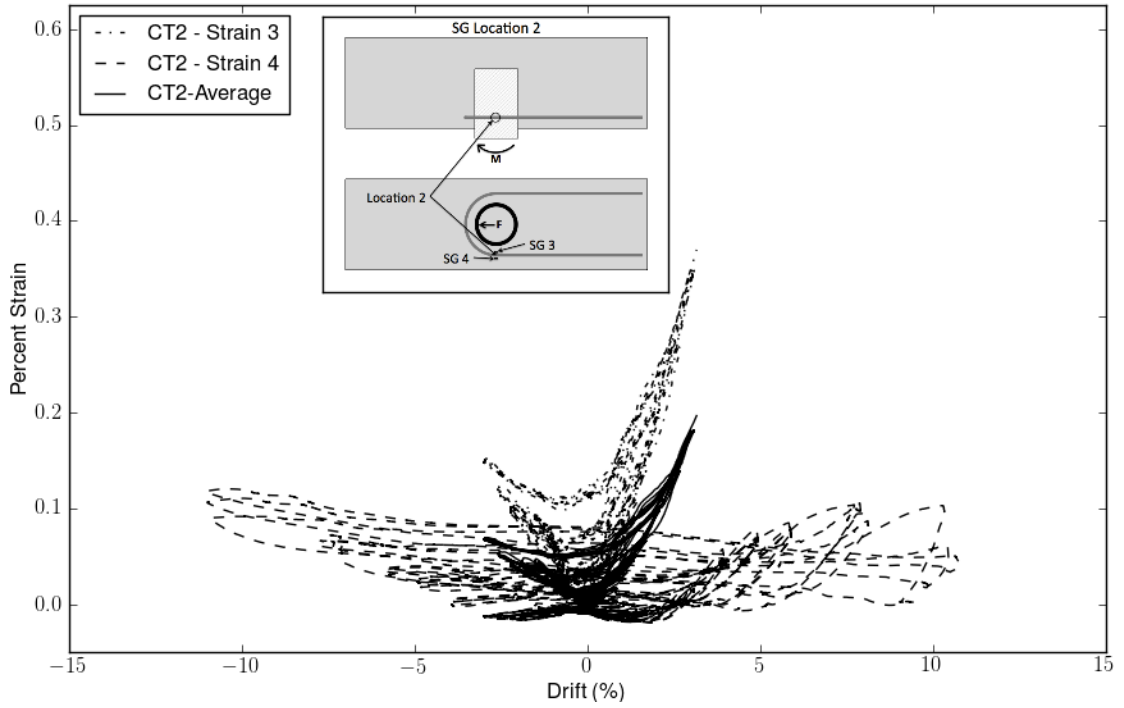


Figure 100: CT2 - Strain Gage Location 2

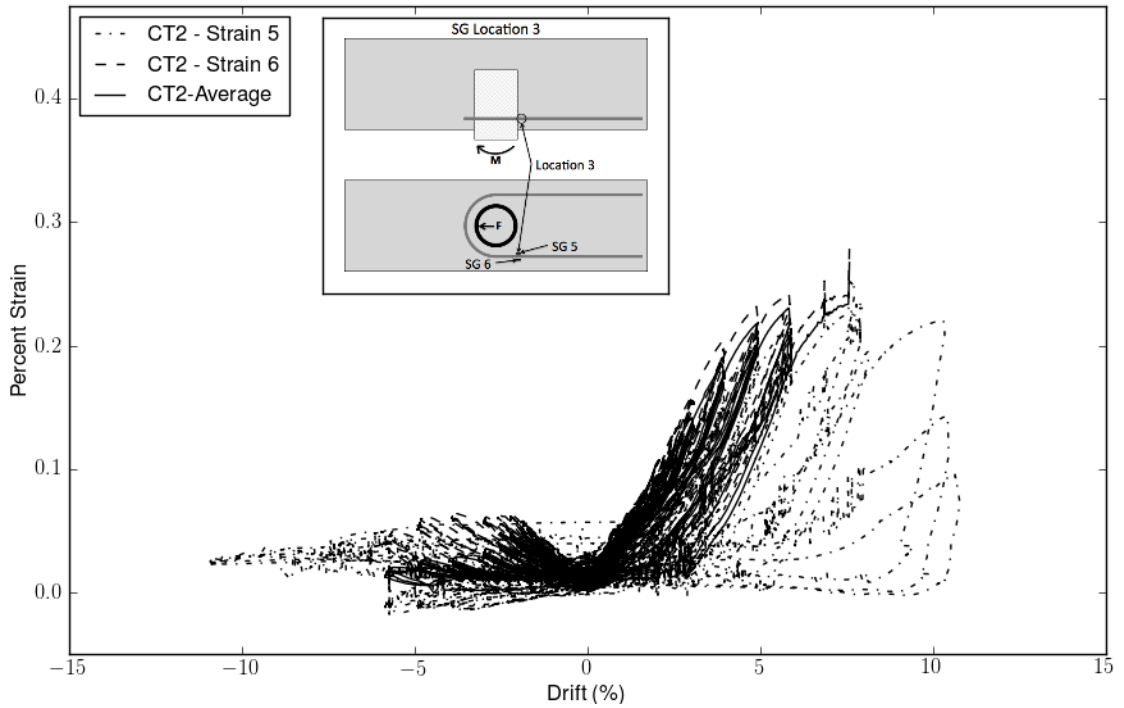


Figure 101: CT2 - Strain Gage Location 3

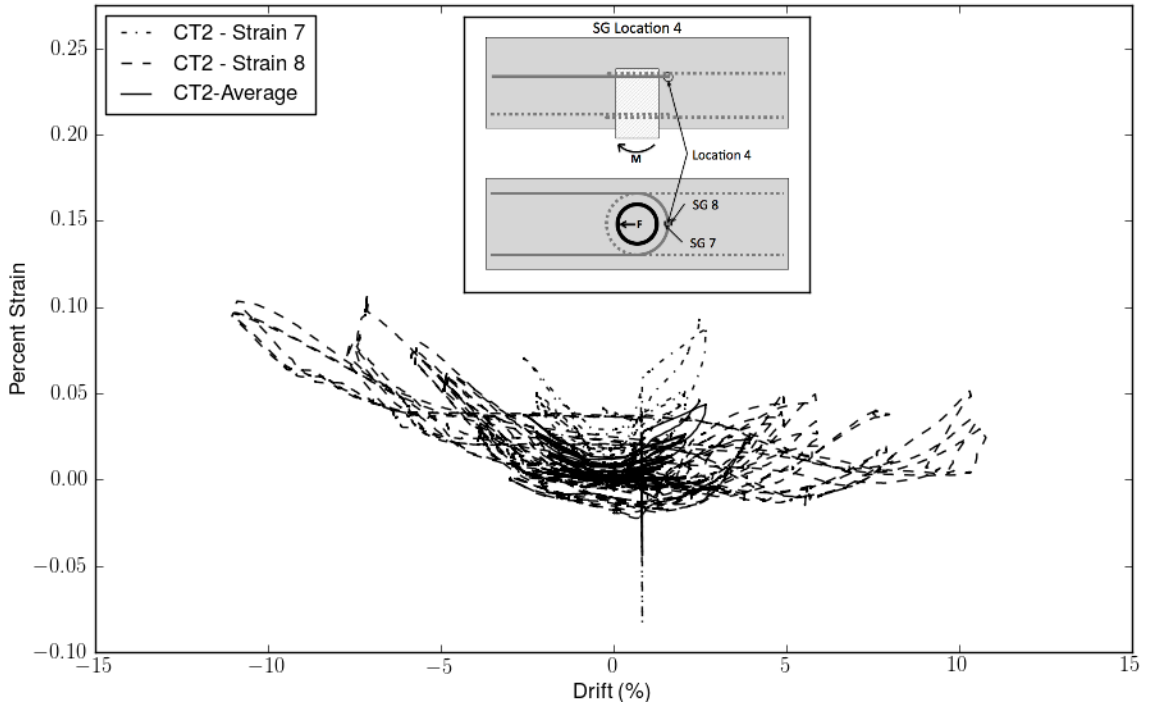


Figure 102: CT2 - Strain Gage Location 4

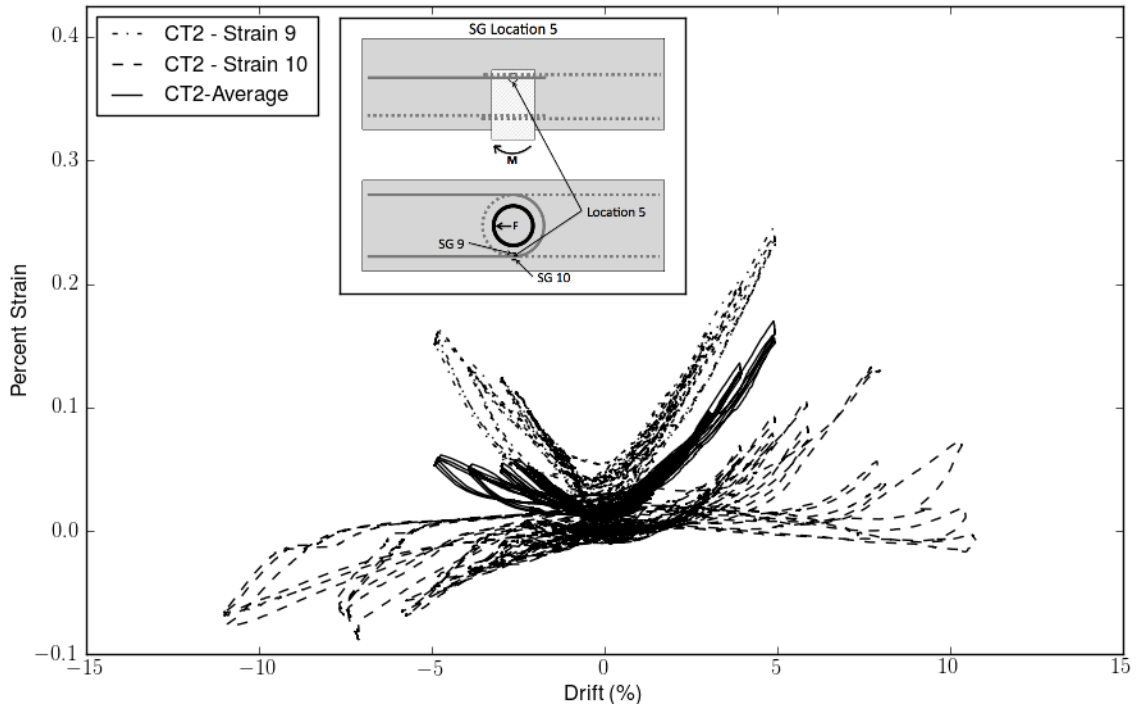


Figure 103: CT2 - Strain Gage Location 5

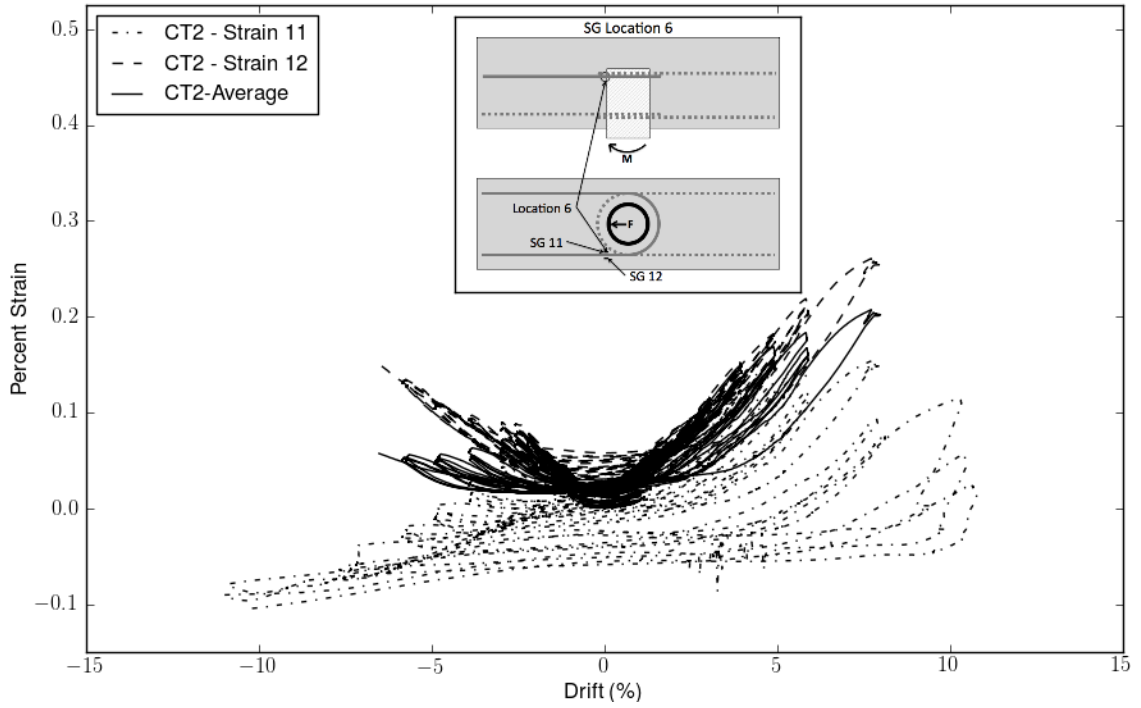


Figure 104: CT2 - Strain Gage Location 6

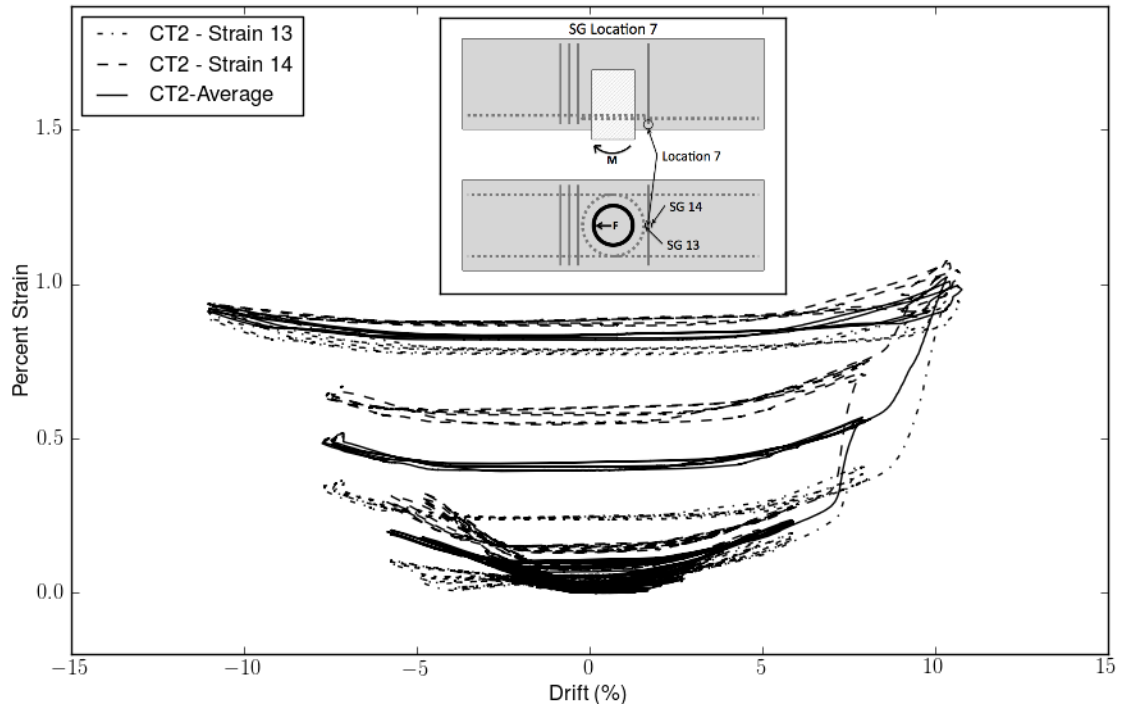


Figure 105: CT2 - Strain Gage Location 7

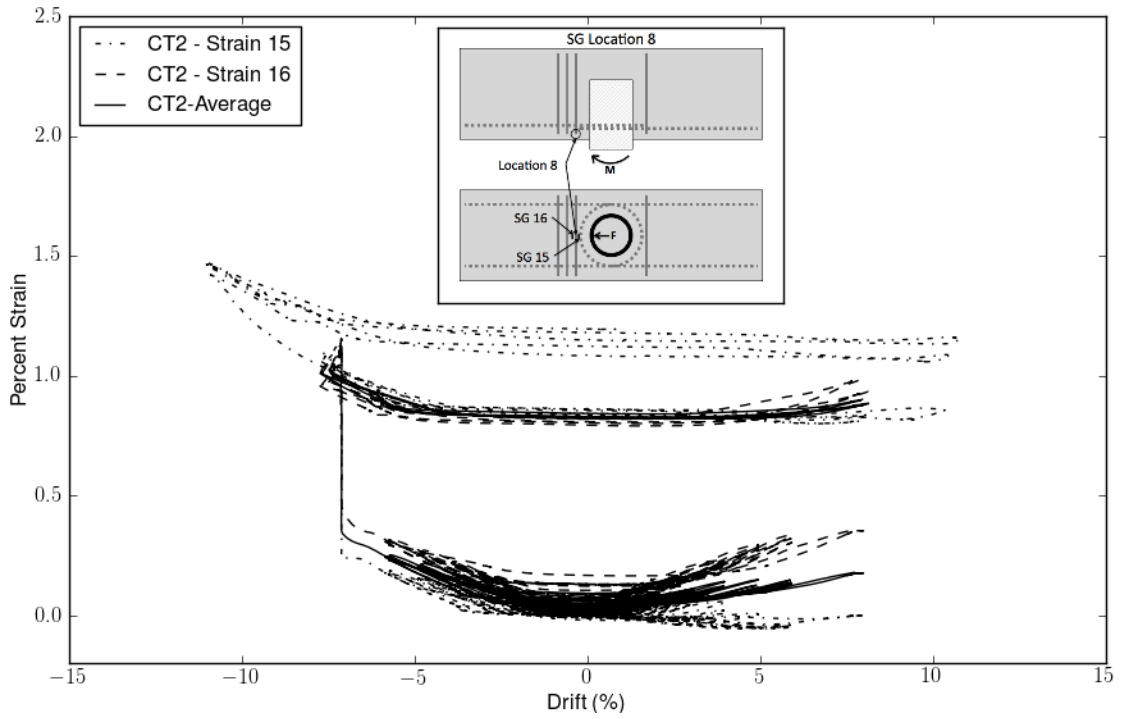


Figure 106: CT2 - Strain Gage Location 8

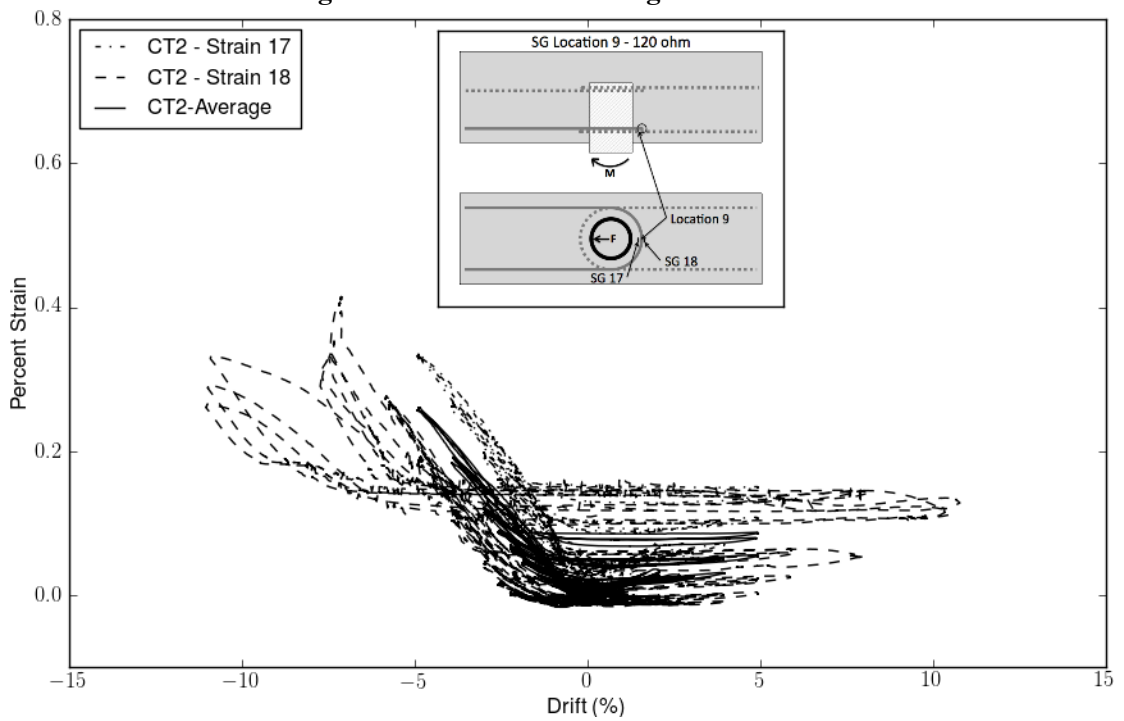


Figure 107: CT2 - Strain Gage Location 9

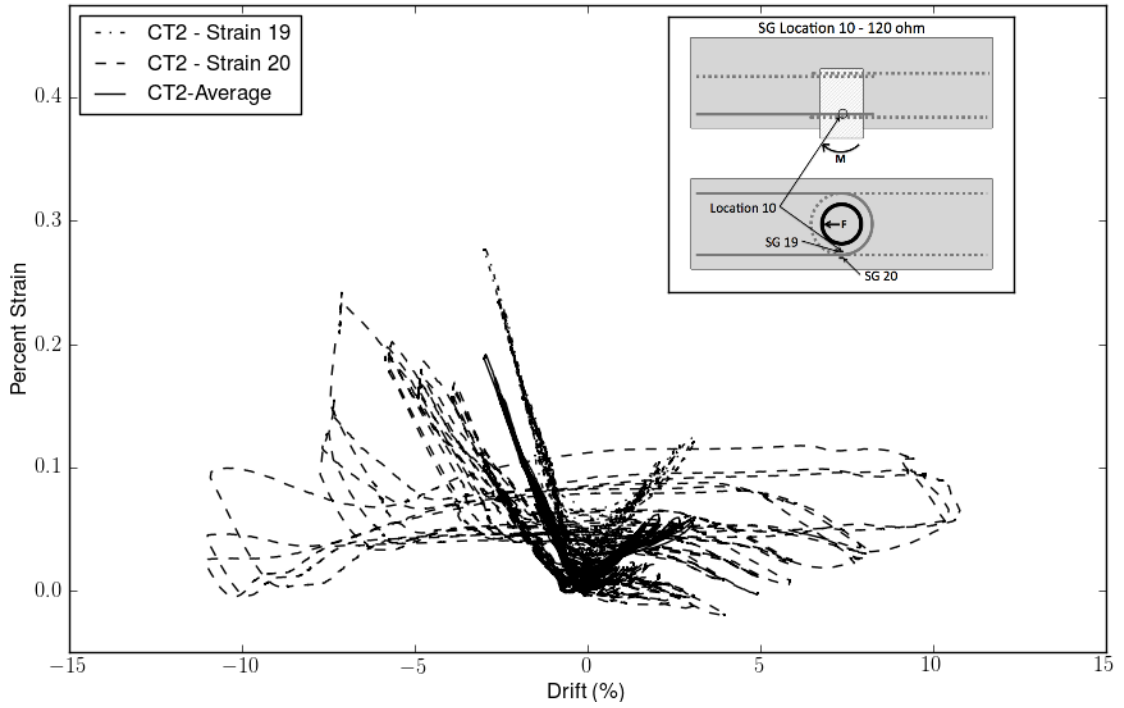


Figure 108: CT2 - Strain Gage Location 10

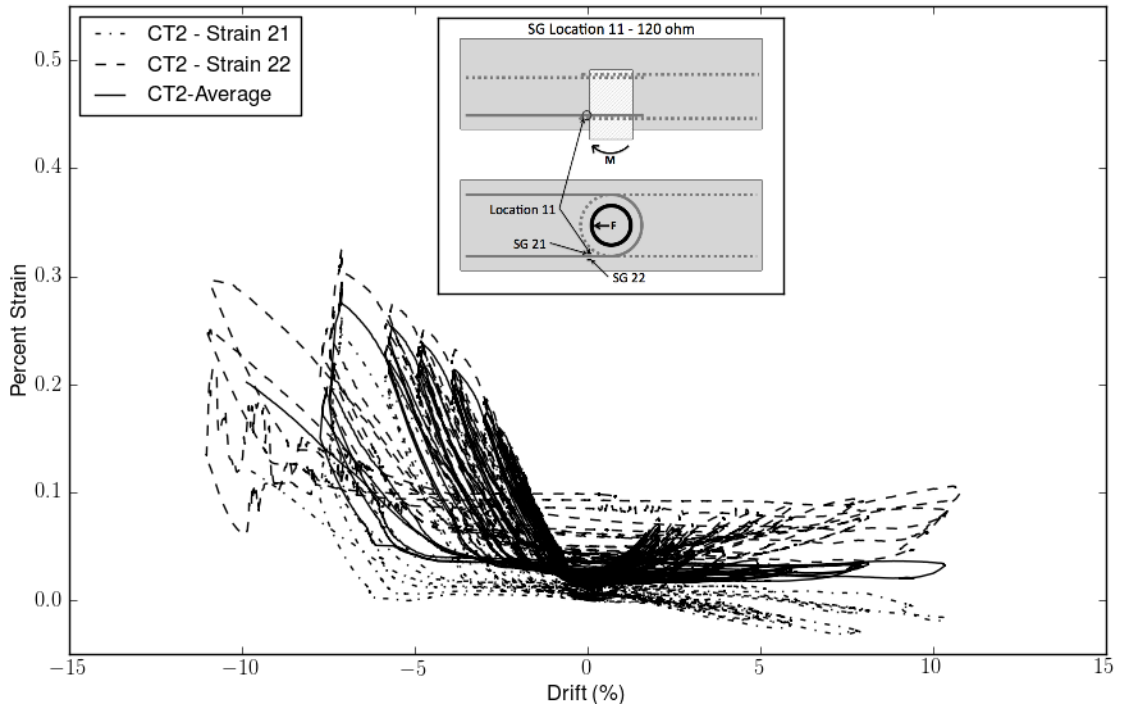


Figure 109: CT2 - Strain Gage Location 11

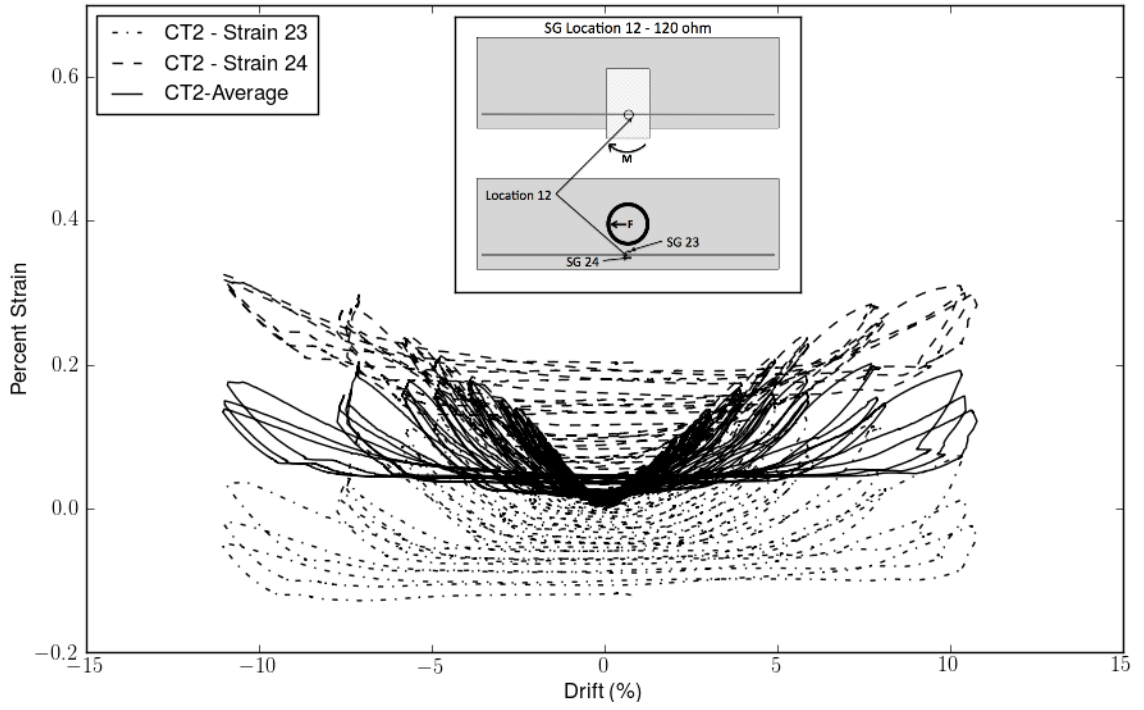


Figure 110: CT2 - Strain Gage Location 12